UNIVERSIDADE FEDERAL DO PARÁ
INSTITUTO DE GEOCIÊNCIAS
PROGRAMA DE PÓS-GRADUAÇÃO EM GEOLOGIA E GEOQUÍMICA

TESE DE DOUTORADO Nº 159

EFEITOS DAS MUDANÇAS CLIMÁTICAS NOS LIMITES AUSTRAL E BOREAL DOS MANGUEZAIS AMERICANOS DURANTE O HOLOCENO E ANTROPOCENO

Tese apresentada por:

ÉRIKA DO SOCORRO FERREIRA RODRIGUES
Orientador: Prof. Dr. Marcelo Cancela Lisboa Cohen (UFPA)

BELÉM- PARÁ
2021

Dados Internacionais de Catalogação na Publicação (CIP) de acordo com ISBD
Sistema de Bibliotecas da Universidade Federal do Pará
Gerada automaticamente pelo módulo Ficat, mediante os dados fornecidos pelo(a) autor(a)

R696e Rodrigues, Érika do Socorro Ferreira

Efeitos das mudanças climáticas nos limites austral e boreal dos manguezais americanos durante o Holoceno e Antropoceno / Érika do Socorro Ferreira Rodrigues. — 2021.
xix, 123 f.: il. color.

Orientador(a): Prof. Dr. Marcelo Cancela Lisboa Cohen

Coorientador(a): Prof. Dr. Kam-Biu Liu

Tese (Doutorado) - Programa de Pós-Graduação em Geologia e Geoquímica, Instituto de Geociências, Universidade Federal do Pará, Belém, 2021.

1. Aquecimento global. 2. Nível do mar. 3. Manguezais americanos. 4. Palinologia. 5. Holoceno e Antropoceno. I. Título.

CDD 551.9

Universidade Federal do Pará
Instituto de Geociências
Programa de Pós-Graduação em Geologia e Geoquímica

EFEITOS DAS MUDANÇAS CLIMÁTICAS NOS LIMITES AUSTRAL E BOREAL DOS MANGUEZAIS AMERICANOS DURANTE O HOLOCENO E ANTROPOCENO

TESE APRESENTADA POR:

ÉRIKA DO SOCORRO FERREIRA RODRIGUES

Como requisito parcial à obtenção do Grau de Doutora em Ciências na Área de GEOLOGIA e Linha de Pesquisa em GEOLOGIA MARINHA E COSTEIRA

Data de Aprovação: 08 / 09 / 2021

Banca examinadora:

Prof. Dr. Marcelo Cancela Lisboa Cohen
(Orientador-UFPA)

Prof. Dr. Paulo César Fonseca Giannini
(Membro – IG/USP)

Prof. Dr. Paulo Eduardo de Oliveira
(Membro – IG/USP)

Prof. Dr. José Augusto Martins Corrêa
(Membro-UFPA)

Prof. Dr. Nils Edvin Asp Neto
(Membro – UFPA)

Dedico aos meus queridos professores,
Marcelo Cohen e Luiz Pessenda

AGRADECIMENTOS

Ao Programa de Pós-Graduação do Instituto de Geociências e Universidade Federal do Pará (UFPA) pela infraestrutura disponível e apoio financeiro;

À Coordenação de Aperfeiçoamento de Pessoal de Nível Superior (CAPES, código de financiamento 001), e Conselho Nacional de Pesquisa (CNPq no.141968/2016-8) pela concessão da bolsa de doutorado (PDSE-CAPES);

À Louisiana State University (LSU- EUA) pela grande estrutura e apoio nos meus 7 meses de permanência de Doutorado Sanduíche (PDSE-CAPES);

Ao meu orientador no qual admiro muito, Prof. Dr. Marcelo Cancela Lisboa Cohen, agradeço sinceramente pela sua supervisão, apoio moral, incentivo, confiança, paciência, ensinamentos em trabalhos de campo e oportunidade de orientação em minha pesquisa de doutorado ao longo de quatro anos na Universidade Federal do Pará. Seus ensinamentos levarei para o resto de minha vida acadêmica;

Ao querido Prof. Dr. Luiz Carlos Ruiz Pessenda, agradeço a grande oportunidade e parceria nesse trabalho. Minha tese nunca poderia ter sido concluída sem todo apoio logístico durante os trabalhos de campo e atividades em seu laboratório (Centro de Energia Nuclear na Agricultura – CENA). Agradeço pela confiança e oportunidade relacionado ao trabalho da Baía de São Francisco do sul (SC). Sua abordagem ao ensino e à pesquisa tem me inspirado muito;

Agradeço ao Prof. Dr. Kam-biu Liu, o qual tive o privilégio de trabalhar em pesquisa relacionada a paleotempestologia e técnicas polínicas em seu laboratório na Universidade da Louisiana (LSU – EUA);

Ao Prof. Dr Marlon França (IFPA) pela paciência e conselhos na trajetória de conclusão da Tese;

À minha querida amiga, Cleida Freitas agradeço por me ensinar tudo sobre organização institucional assim como toda a paciência durante 7 anos de integra convivência;

Ao querido e especial amigo Dr. Qiang Yao agradeço a parceria nos artigos científicos.

Agradeço as minhas amigas Beatriz Luna e Luiza Reis pela parceria acadêmica. Amizades que levarei no coração;

Aos membros do laboratório de Paleoecologia global da LSU nas pessoas de Nicholas Culligan, Lance Riedlinger, Junghyung Ryu, Alex Moreno e Marianne Dietz. Agradeço a

atenção e auxílio nas análises polínicas e LOI-XRF;

Aos amigos e pesquisadores do CENA-USP: Beatriz Luna, Evandro Magalhães, Thiago Campos, Flávio Lorente. Elton Alves, Luiza Reis. Trabalho e foco na pesquisa sempre.

À amiga Dra. Camila Santos pela oportunidade de me aceitar no estágio docência do PPGG;

Às amigas Rose Caldas, Christiane Lucas e Laís Torres, pelos anos de convivência na sala de estudo 1- IG-PPGG-UFPA;

Aos colegas do Laboratório de Dinâmica Costeira PPGG- Geociências da Universidade Federal do Pará, - Vanessa Castelo, Sérgio Nunes, Sérgio Molano, Bettina Bozi, Fernando Borges e Neuza Freire. Agradecida pela amizade, críticas, sugestões e trocas de conhecimento durante esses anos;

Aos membros do GSED e ao Laboratório de Sedimentologia: Em especial aos amigos Renato Sol, Luiz Saturnino e Walmir Lima, além do querido Prof. Dr. Afonso Nogueira.

Agradeço aos revisores de meus manuscritos pelos comentários construtivos;

À Biblioteca Raimundo Montalvão e membros. Em especial Lúcia Imbiriba pela grande colaboração e atenção em relação as Normas acadêmicas;

Agradeço aos membros da secretaria do Programa de Pós-graduação em Geoquímica e Geologia nas pessoas de Joanicy Lopes, Cleida Freitas (Jozinha e Cleidoca) e ao coordenador Prof. Dr. Cláudio Nery Lamarão;

No final, agradeço aos meus irmãos e minha mãezinha Edna Ferreira. Em especial aos meus filhos: **Igor e Hannah** Rodrigues. Sem a existência de vocês dois em minha vida, nada, simplesmente nada teria acontecido. É um amor infinito, incondicional que me fortalece e me alimenta a seguir sempre em frente.

Raízes que serpenteiam em águas das costas americanas
Que agarram lamas nutridas por rios e oceano
Guardando filhos do carbono e protegendo gerações futuras das mazelas climáticas.

Érika Rodrigues

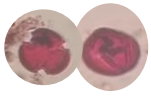

RESUMO

Durante o Holoceno a distribuições dos manguezais foi controlada em grande parte pelo clima e flutuações do nível do mar. O clima limitou essas florestas às latitudes 30°N e 28°S. Portanto, em resposta ao aquecimento global no Antropoceno, espera-se que os manguezais migrem para latitudes mais temperadas invadindo áreas úmidas colonizadas por marismas (*Spartina* sp.). O objetivo geral desta Tese é avaliar os efeitos das mudanças climáticas e flutuações do NRM na distribuição dos manguezais americanos ao longo do Holoceno e Antropoceno, baseado em imagens de satélite e drone, fácies sedimentares, diatomáceas, pólen, geoquímica (LOI, XRF, COT, NT, ST, C: N, C: S, $\delta^{13}C$ e $\delta^{15}N$) e datações por ^{210}Pb e ^{14}C. Para isto, foi escolhido um estuário do litoral sul do Espírito Santo como representante dos manguezais tropicais (20°41'S), além de regiões costeiras subtropicais situadas na costa norte (26° 6'S) e sul de Santa Catarina (28°29' S) e litoral da Louisiana (29°09'N). Os resultados desta pesquisa estão apresentados em quatro artigos científicos. O primeiro, (ver, capítulo II) trata sobre os efeitos do aquecimento global no estabelecimento dos manguezais na região costeira da Louisiana (29° 09' N) durante o Holoceno. O segundo artigo científico (ver, capítulo III) mostra a migração dos manguezais para o limite austral desse ecossistema no continente sul-americano, na região de Laguna, de acordo com o aumento nas temperaturas mínimas de inverno no Antropoceno (costa sul de Santa Catarina, 28°29' S). O terceiro manuscrito (ver, capítulo IV) avalia os impactos do aumento do nível do mar nos manguezais tropicais do sudeste brasileiro (costa sul Espírito Santo, 20°41'S) durante o Holoceno e Antropoceno, usando uma abordagem multi-proxy. O quarto artigo científico (ver, capítulo V) aborda o estabelecimento dos manguezais na Baía de São Francisco do Sul (costa norte de Santa Catarina, 26°6'S), em resposta ao aquecimento global nos últimos 1000 anos. Os resultados indicaram uma transgressão marinha na costa sul de Santa Catarina (28°29' S) e litoral da Louisiana (29° 09' N) no Holoceno inicial. Este processo natural converteu ambientes lacustres em lagunas colonizadas por ervas adaptadas a ambiente estuarino. Na costa tropical brasileira o aumento do NRM no Holoceno médio (2-5 m acima do nível atual) foi determinante para o estabelecimento dos manguezais. Este comportamento foi observado em um estuário localizado na costa sul do Espírito Santo (20°41'S) onde uma planície herbácea foi gradualmente substituída por uma laguna cercada por manguezais entre ~6300 anos cal AP e ~4650 anos cal AP. No entanto, entre ~4650 anos cal AP e 2700 anos cal AP a laguna colonizada por manguezais em suas margens foi convertida em uma planície de maré ocupada por ervas,

palmeiras e árvores/arbustos refletindo a redução da influência estuarina no Holoceno tardio, de acordo com a queda do NRM. A partir dos últimos mil anos ocorreu uma diminuição significativa na ocorrência de pólen de manguezal nos sedimentos das planícies de maré do sul do Espírito Santo (390 cal anos AP (1560 DC) e 77 cal anos AP (1873 DC), provavelmente causado por uma queda no NRM associada a Pequena Idade do Gelo (LIA). Estudos paleoclimáticos indicaram flutuações na temperatura durante LIA (380 a 50 anos cal AP) e MCA – Período Quente Medieval (950 a 750 anos cal AP) no Holoceno tardio e consequente mudança na vegetação no sul do Brasil. Estes eventos climáticos provavelmente influenciaram o aparecimento da sucessão de gêneros de manguezais na Baía de São Francisco do Sul (costa norte de Santa Catarina, 26°6' S). Os efeitos da queda e/ou estabilização do nível do mar no Holoceno tardio foram registrados na costa sul catarinense (Laguna, 28°29′S) através da mudança na geomorfologia costeira. Neste mesmo período no litoral de Louisiana (29°09′N), sedimentos arenosos (sedimentos *overwash*) foram depositados nesses estuários refletindo a migração gradual desses sedimentos em direção ao continente provavelmente resultado de eventos de tempestade. As tendências de NRM na costa sul brasileira (Laguna, 28°29′S) e norte americana (litoral da Louisiana, 29°09′N) a partir do Holoceno médio foram as mesmas apresentando condições físico-químicas apropriadas para o desenvolvimento de manguezais, como ocorreu no litoral do Espírito Santo (~6300 anos cal AP) e na Baía de São Francisco do sul (~1500 anos cal AP). Entretanto, não foram registrados grãos de pólen de manguezal nos sedimentos do atual limite austral (Laguna, 28°29′S) e boreal (litoral da Louisiana, 29°09′N) dos manguezais americanos durante o Holoceno. Neste intervalo de tempo ocorreu uma contribuição significativa de matéria orgânica de origem estuarina em planícies de maré ocupadas por *Spartina* sp. Em relação ao aquecimento global e aumento do NRM no Antropoceno um aumento de pólen de manguezal nos testemunhos sedimentares do Espírito Santo (20°40'S) refletiram a migração do mangue para planícies arenosas topograficamente mais elevadas anteriormente dominada por vegetação herbácea. Em relação aos manguezais de Laguna (atual limite austral dos manguezais americanos, 28°29′S), análises de pólen e datações de ^{14}C e ^{210}Pb indicaram que os manguezais foram estabelecidos sob influência estuarina entre ~ 1957 e 1986 DC, representados por árvores de *Laguncularia* sp. Análises espaço temporal com base em imagens de satélite e drone indicaram que os manguezais vêm se expandindo nas últimas décadas com introdução de novos gêneros de mangue. Em nossa área de estudo na Baía de São Francisco do Sul (costa norte de Santa Catarina, 26°6' S), análises palinológicas e datação ^{14}C revelaram que

os manguezais se estabeleceram em torno de ~ 1500 anos cal AP representados por *Laguncularia* sp. seguido por *Avicennia* sp. (~500 anos cal AP) e *Rhizophora* sp. apenas no último século. Provavelmente, essa sucessão de gêneros de manguezais foi causada por uma tendência de aquecimento na América do Sul durante o Holoceno tardio e as árvores *de Rhizophora* sp. pelo aquecimento durante o Antropoceno. Em relação aos manguezais localizados no litoral da Louisiana registros históricos indicaram a presença de pequenos arbustos de *Avicennia* sp. no início do século XX. Atualmente, estudos de sensoriamento remoto coordenado por Cohen (2021) indicam uma expansão latitudinal de *Avicennia* sp. colonizando áreas que eram anteriormente ocupadas por *Spartina* sp. após duas décadas de invernos quentes. Portanto, os manguezais migraram dos trópicos para zonas temperadas na medida que as temperaturas mínimas de inverno aumentaram durante o Holoceno. No entanto, os manguezais de Laguna e Louisiana (atual limite dos manguezais sul e norte americano) estabeleceram- se apenas no início e meado do século XXI, respectivamente. Tal dinâmica dos manguezais americanos estudados na presente tese foi causada provavelmente pelo aquecimento global natural do Holoceno e intensificado durante o Antropoceno. Esse processo também causou um aumento do nível do mar que resultou na migração dos manguezais de zonas baixas para novas planícies de maré mais elevadas.

.

Palavras-chave: Aquecimento global. Aumento nível do mar. Manguezais americanos. Palinologia. Holoceno e Antropoceno.

ABSTRACT

During the Holocene, mangrove distributions were primarily controlled by climate change and sea level fluctuations. In particular, low winter temperatures in the subtropical coastal areas limited these ecosystems to expand beyond 30°N and 28°S in the North and South Hemisphere. Therefore, under the continuous warming trend during the Anthropocene, mangroves are expected to migrate to more temperate regions previously occupied by saltmarshes (e.g., *Spartina* sp.). The purpose of this Thesis is evaluate the effects of climate changes and SLR fluctuations on the distribution of American mangroves along the Holocene and Anthropocene, based on satellite and drone images, sedimentary facies, diatoms, pollen, geochemistry (LOI, XRF, TOC , TN, TS, C: N, C: S, $\delta^{13}C$ and $\delta^{15}N$) as well ^{210}Pb and ^{14}C datings .To achieve the aforementioned objectives, studies were conducted on the tropical coast of southeastern Brazil - south of the Espírito Santo State (20°41'S), the subtropical coastal regions located on the north (26°6'S) and south (28°29’ S) coast of Santa Catarina, and Louisiana littoral (29° 09' N). The results of this research are presented in four scientific papers. The first one (see, chapter II) deals with the effects of global warming on the establishment of mangroves in the Louisiana littoral (29° 09’ N) during the Holocene. The second scientific paper (see, chapter III) shows southward migration of the austral limit mangroves in South America, according to the increase in minimum winter temperatures in the Anthropocene (southern Santa Catarina coast, 28°29' S). The third manuscript (see, chapter IV) assesses the impacts of sea level rise on tropical mangroves in southeastern Brazil (southern Espírito Santo coast, 20°41'S) during the Holocene and Anthropocene, using a multi-proxy approach. The fourth scientific paper (see, chapter V) addresses the establishment of mangroves in the São Francisco do Sul Bay (north Santa Catarina coast , 26° 6'S), in response to global warming in the last 1000 years. The results indicated a marine transgression off the southern coast of Santa Catarina (28°29’ S) and the Louisiana littoral (29°09’ N) during early Holocene. This natural process converted a lake into lagoons colonized by herbs adapted to an estuarine environment. On the Brazilian tropical coast, the middle Holocene high sea-level stand (2-5 m above the current level) was decisive for the establishment of mangroves. This comportment was observed in an estuary located on the south coast of Espírito Santo (20°41'S) where a herbaceous plain was gradually replaced by a lagoon surrounded by mangroves between ~6300 cal yr BP and ~4650 cal yr BP. However, between ~ 4650 cal yr BP and 2700 cal yr BP the lagoon colonized by mangroves on its margins was converted to a tidal flat occupied by herbs, palms and trees/shrubs reflecting the reduction of estuarine

influence in the late Holocene, according to with the fall and/or stabilization of the RSL. From the last thousand years there has been a significant decrease in the occurrence of mangrove pollen in the sediments of the tidal flats of southern Espirito Santo (390 cal yr BP (1560 AD) and 77 cal yr BP (1873 AD), probably caused by a RSL fall associated with Little Ice Age (LIA). Paleoclimatic studies have indicated temperature fluctuations during LIA (380 to 50 cal yr BP) and MCA – Medieval Warm Period (950 to 750 cal yr BP) in the late Holocene and consequent change in the Brazil southern vegetation. These climatic events probably influenced the appearance of the mangrove genera succession in the São Francisco do Sul Bay (north Santa Catarina coast, 26°6' S). The effects of the sea level fall and/or stabilization during late Holocene were recorded on the southern coast of Santa Catarina (Laguna, 28° 29 ′ S) through changes in coastal geomorphology. In this same period at the Louisiana coastline (29°09 ′ N), sandy sediments (*overwash* sediments) were deposited in these estuaries reflecting the gradual migration of these sediments towards land likely a result of storm events. The position of RSL on the southern Brazilian coast (Laguna, 28° 29 ′ S) and north american (Louisiana coast, 29° 09 ′ N) from the middle Holocene were the same presenting suitable physicochemical conditions for mangrove development, as occurred on the coast of Espírito Santo (~6300 cal yr BP) and São Francisco do Sul Bay (~1500 cal yr BP). However, no mangrove pollen grains were recorded in the sediments of the current austral (Laguna, 28° 29 ′ S) and boreal (Louisiana coast, 29° 09 ′ N) limit of American mangroves during the Holocene. During this time interval, there was a significant contribution of organic matter of estuarine source in tidal flats occupied by *Spartina* sp. Regarding to global warming and RSL rise during Anthropocene an increase mangrove pollen of Espírito Santo sedimentary cores (20° 40' S) reflected mangrove migration to topographically higher sandy plains previously dominated by herbaceous vegetation. Regarding Laguna mangroves (current southern limit of the American mangroves, 28° 29 ′ S), pollen analyzes, ^{14}C and ^{210}Pb datings indicated that the mangroves were established under estuarine influence between ~1957 and 1986 AD, represented by *Laguncularia* sp. trees. Spatio-temporal analyzes based on satellite and drone images indicated that mangroves have been expanding in recent decades with the introduction of new mangrove genera. In our study area in São Francisco do Sul Bay (north coast of Santa Catarina, 26°6' S), palynological analyzes and ^{14}C dating revealed that mangroves were established around ~ 1500 cal yr BP represented by *Laguncularia* sp. followed by *Avicennia* sp. (~500 cal yr BP) and *Rhizophora* sp. in the last century. This mangrove succession genera were likely caused by a warming trend in South

America during the late Holocene and *Rhizophora* sp. by warming during the Anthropocene. In relation to the mangroves located on the Louisiana littoral, historical records indicated the presence of small shrubs of *Avicennia* sp. at the beginning of the 20th century. Currently, remote sensing studies coordinated by Cohen (2021) indicate a latitudinal expansion of *Avicennia* sp. colonizing areas that were previously occupied by *Spartina* sp. after two decades of warm winters. Therefore, mangroves migrated from the tropics to temperate zones as winter minimum temperatures increased during the Holocene. The Laguna and Louisiana mangroves (currently South and North American mangroves limit) were only established in the early and mid-21st century, respectively. Such dynamics were likely caused by the natural global warming of the Holocene and intensified during the Anthropocene. This process also caused a RSL rise which resulted in the migration of mangrove from lowlands to new higher tidal flats.

Keywords: Global Warming. SL rise. American Mangroves. Palynology. Holocene and Anthropocene.

LISTA DE ILUSTRAÇÕES

CAPÍTULO I : EFEITOS DO AQUECIMENTO GLOBAL E AUMENTO DO NÍVEL RELATIVO DO MAR NA DISTRIBUIÇÃO DOS MANGUEZAIS AMERICANOS DURANTE O HOLOCENO E ANTROPOCENO

CAPÍTULO V: EXPANSION OF MANGROVES BRAZILIAN SOUTH COAST IN THE LAST 1000 YEARS LED BY WARMING HOLOCENE AND ANTHROPOCENE TIME

LISTA DE TABELAS

CAPÍTULO I: EFEITOS DO AQUECIMENTO GLOBAL E AUMENTO DO NÍVEL RELATIVO DO MAR NA DISTRIBUIÇÃO DOS MANGUEZAIS AMERICANOS DURANTE O HOLOCENO E ANTROPOCENO

CAPÍTULO V: EXPANSION OF MANGROVES BRAZILIAN SOUTH COAST IN THE LAST 1000 YEARS LED BY WARMING HOLOCENE AND ANTHROPOCENE TIME

LISTA DE ABREVIATURAS, SIGLAS E SÍMBOLOS

AP	Antes do presente
AMS	*Accelerator Mass Spectrometer* – Espectrômetro de Massa Acoplado ao Acelerador
CAM	Crassulacean and metabolism
COD	Carbono Orgânico Dissolvido
COP	Carbono Orgânico Particulado
CENA	Centro de Energia Nuclear na Agricultura
CWP	Current Warm Period
Cal yr. BP	Calibrated years Before Present - Anos calibrados Antes do Presente
COT	Carbono Orgânico Total
ºC	Grau (s) Celsius
%	por cento
‰	por mil
GOM	Golfo do México
ha	Hectare
Km^2	Quilômetros quadrados
IFPA	Instituto Federal do Pará
IES	Instituição de Ensino Superior
IG	Instituto de Geociências
LSU	Louisiana University
LACUFF	Laboratório de Radiocarbono da Universidade Federal Fluminense
LSU	Louisiana State University
LS	Louisiana State
LGP	Laboratório Global de Paleoecologia
LADIC	Laboratório de Dinâmica Costeira
LOQ	Laboratório de Oceanografia Química
LOI	Loss on ignition
LIA	Little Age Ice
m	metros
mm	milímetros

MPA	Massa Polar Atlântica
MTA	Massa Tropical Atlântica
Mgal/d–	1 milhão de galões por dia
MCA	Medieval Climate Anomaly
N	Norte
NOAA	National Oceanic and Atmospheric Administration
NRM	Nível Relativo do Mar
NT	Nitrogênio Total
pH	Potencial Hidrogeniônico
ppm	Parte por milhão
PPGG	Porgrama de Pós- Graduação em Geologia e Geoquímica
Port Fourchon	Porto marítimo (LA-EUA)
Pb-210	Chumbo 210
PVC	Policloreto de Vinila
SC	Santa Catarina
SF-Bay	Baia de São Francisco do Sul
XRF	X-ray fluorescence
USP	Universidade de São Paulo
UFPA	Universidade Federal do Pará
UGAMS	Centro de Estudos Aplicados a Isótopos da Universidade da Geórgia
VPDB	Vienna Pee Dee Belemnite

SUMÁRIO

CAPÍTULO I INTEGRADOR: EFEITOS DO AQUECIMENTO GLOBAL E AUMENTO DO NÍVEL RELATIVO DO MAR NA DISTRIBUIÇÃO DOS MANGUEZAIS AMERICANOS DURANTE O HOLOCENO E ANTROPOCENO

1 INTRODUÇÃO

Os manguezais são ecossistemas costeiros de transição entre os ambientes terrestres e marinhos, típicos de regiões tropicais e subtropicais ocorrendo entre as latitudes 30°N e 30°S com maior desenvolvimento próximo à linha do Equador (Giri *et al.* 2011). Esses bosques tropicais se desenvolvem em planícies lamosas, muitas vezes com alto conteúdo orgânico em áreas protegidas da ação de ondas. Desempenham diversas funções naturais de grande importância ecológica e econômica, tais como: barreiras naturais capazes de atenuar os efeitos de tempestades e aumento do nível do mar, retenção de sedimentos carreados pelos rios, ação de filtro biológico, concentração de nutrientes e renovação da biomassa costeira (França *et al.* 2019, Yao *et al.* 2020). Denominados "carbono azul" podem atuar como sumidouros, armazenando uma quantidade significativa de carbono, além de nutrientes e metais em seus sedimentos (Debrot *et al.* 2020, Taillardat *et al.* 2018). Os manguezais também são altamente susceptibilidade às mudanças na temperatura, subsidência, frequência de inundação das marés e aumento da precipitação nas bacias hidrográficas (Cohen *et al.* 2012, Liu *et al.* 2014, Alongi 2015, Yao & Liu 2017). É importante salientar que a distribuição dos manguezais está relacionada com a variação da temperatura ocorrendo em regiões onde a média mensal mais fria está acima de 20°C e sua mortalidade ocorre em temperatura próximo a 0°C (Duke 1992). Tais restrições ambientais impostas aos manguezais torna-o um importante indicador das mudanças do nível do mar e clima (Blasco *et al.* 1996), e uma ferramenta útil para mitigar essas mudanças na zona costeira de regiões tropicais e subtropicais. No entanto, dependendo da latitude e proximidade de grandes estuários, alguns fatores ambientais podem operar mais intensamente no controle da dinâmica dos manguezais, como as temperaturas de inverno em zonas subtropicais.

As mudanças na distribuição espacial dos manguezais ocorreram proporcionalmente às mudanças climáticas e flutuação do nível do mar (Ellison 2008, Quisthoudt *et al.* 2012). Por exemplo, no final do Quaternário, devido ao clima mais frio e grandes oscilações do nível do mar palino-estudos forneceram evidências de contração em larga escala nas áreas dos manguezais na América do Sul (Van der Hammen *et al.* 1994). Neste período os manguezais

devem ter sobrevivido em vários refúgios onde o clima mais aquecido permitisse sua colonização (Woodroffe & Grindrod 1991). No Hemisfério Norte os manguezais se expandiram de acordo com as mudanças do clima no Holoceno (Sandoval-Castro *et al.* 2012b). A partir do Holoceno inicial as baixas temperaturas (Toomey *et al.* 1993) e posição do nível do mar (-8m abaixo do nível atual) impossibilitaram o desenvolvimento dos manguezais na costa do Golfo do México - GOM (Donoghue *et al.* 2011, Van Soelen *et al.* 2010, Nordt *et al.* 2004). Entretanto, entre o Holoceno médio e o tardio o nível do mar se estabilizou favorecendo um aumento na extensão destas florestas em ambos os hemisférios, permitindo que se expandissem para áreas no interior dos continentes (Osland *et al.* 2017). Amplos estudos paleoclimáticos registraram manguezais expandindo na Flórida (Yao & Liu 2017a), Texas (Sherrod & McMillan 1985a) e Louisiana (McKee & Vervaeke 2018), em diferentes intervalos de tempo. Do mesmo modo, em torno de ~ 7000 anos cal AP os manguezais tropicais da costa brasileira foram estabelecidos no Espírito Santo (19º S), Bahia (17º S), Rio Grande do Norte (5º S), Pará (1º S) e Amapá (2º N) (Cohen *et al.* 2012, 2014, 2020a, Pessenda *et al.* 2012, França *et al.* 2013, 2015, Fontes *et al.* 2017, Ribeiro *et al.* 2018). Nos últimos séculos, as concentrações de gases de efeito estufa de origem antrópica vem aumentando gradualmente (Marengo 2006), intensificando ondas de calor e causando degelo das calotas polares da Groenlândia e a Antártida (Shepherd *et al.* 2021) no qual tornou-se a predominante causa para a aceleração do aumento do nível do mar nos dias atuais (Oppenheimer *et al.* 2019). Essas florestas dificilmente persistirão se a taxa de elevação do nível do mar for > 5 mm ano^{-1} (Mckee *et al.* 2007), podendo sofrer submersão ao longo da zona mais baixa das planícies de maré e\ou migrarem em direção ao continente (Cohen *et al.* 2018b, 2020a).

Até o final do século XXI espera-se que as frequências de calor elevem o nível do mar (98cm) e os manguezais migrem para planícies topograficamente mais elevadas anteriormente ocupadas por vegetação herbácea. Além disso, a maior parte do aquecimento previsto globalmente está concentrado em zonas temperadas, permitindo que os manguezais migrem para zonas mais ao norte, substituindo pântanos salgados (Gilman *et al.* 2008).

Nesse contexto, o objetivo deste estudo foi comparar os efeitos do aquecimento global e aumento NRM, durante o Holoceno e Antropoceno em manguezais tropicais (Espírito Santo, 20°40'S) e subtropicais do litoral sul brasileiro (costa norte e sul de Santa Catarina,

26°6'S/28°29'S) e norte americano (Louisiana, 29°09’ N). Para alcançar tal objetivo, este trabalho utilizou a integração de dados multi-proxy baseado em imagens de satélite e drone, fácies sedimentares, diatomáceas, pólen, geoquímica (LOI, XRF, COT, NT, ST, C: N, C: S, $\delta^{13}C$ e $\delta^{15}N$) e datações por ^{210}Pb e ^{14}C em treze (13) testemunhos sedimentares extraídos do litoral da Louisiana (Capítulo II), costa norte e sul de Santa Catarina (capítulos V e III) e Espírito Santo (Capítulo IV).

2 ÁREA DE ESTUDO

Os locais de estudo compreendem os estuários do litoral sudeste (Espírito Santo, 20°40' S) e sul brasileiro (Baía de São Francisco do Sul, 26° 6' S e Lagoa de Santo Antônio, 28°29' S) e norte americano (Bay Champagne, 29° 09’ N) (**Figura 1**). Vale ressaltar que a Lagoa de Santo Antônio em Laguna e Bay Champagne na Louisiana representam os atuais limites austral e boreal dos manguezais americanos, respectivamente.

A primeira área de estudo (ver, capítulo II) se localiza no promontório de Caminada-Moreau, sul de Nova Orleans (litoral do Estado da Louisiana, EUA). Este estuário apresenta uma das maiores taxas de retração costeira da América do Norte. A área é predominantemente influenciada pela precipitação local e o Bayou Lafourche (Dietz *et al.* 2018). Dois (2) testemunhos sedimentares (BC81, 200cm e BC82, 400cm) foram coletados nas margens de uma laguna semi-circular (**Tabela 1**) chamada de Bay Champagne com 2 metros de profundidade e cercada por marismas (*Spartina* sp.) e manguezais (*Avicennia germinans*).

A segunda área estudada, encontra-se na costa sul do Estado de Santa Catarina e está inserida na lagoa de Santo Antônio no qual faz parte de um complexo lagunar posicionado entre as cidades de Imbituba e Laguna, ocupando cerca de 40 km de extensão (Lagoa de Imaruí e Lagoa Mirim). Um total de seis (6) testemunhos sedimentares (LAG-3, LAG-4, LAG-5, LAG-6, RP-3 e RP-4) foram amostrados nesta lagoa cercada por manguezais representados por *Laguncularia racemosa* e *Avicennia schaueriana*. Informações sobre método de coleta e localização estão inseridos na **Tabela 1** (ver, capítulo III).

A terceira área em destaque se localiza na costa norte de Santa Catarina. A Baía de São Francisco do Sul, abrange uma área estimada de 160 km² com 20 km de comprimento, 5 km de largura e 28 m de profundidade (Kilca *et al.* 2011). A coleta do testemunho sedimentar SF05 (**Tabela 1**) foi realizada na parte sudeste da Baía de São Francisco do Sul (ver, capítulo V). É um estuário que inclui 60 Km^2 de áreas de manguezais bem preservadas além de ser fortemente influenciado por rios (ex., rio Palmital) e córregos (Barros *et al.* 2010)

A última área de estudo está localizada na costa sul do Espírito Santo, sudeste do Brasil, em dois estuários sob influência dos rios Jabuti, Aldeia Velha e Benevente próximos aos municípios de Guarapari e Anchieta. São considerados os mais extensos e conservados do Espírito Santo, com uma área de aproximadamente 4,6 km^2 (Vale & Ferreira 1998). Espécies importantes de mangue, como *Rhizophora mangle*, ocorrem próximas às margens

do canal, enquanto *Avicennia germinans* estão localizadas em planícies de maré mais elevadas topograficamente. Quatro (4) testemunhos sedimentares (G-3, G-4, RBN-2 e RBN-1) foram coletados (**Tabela 1**) a partir de uma área transicional manguezal e vegetação herbácea. (ver, capítulo IV).

Tabela 1- Vegetação, método de amostragem e localização dos testemunhos

Código testemunhos	Unidade de vegetação	Método de coleta	Coordenadas	Localização
BC81	Manguezal	TR	N 29º6"53,10"/O 90º10'33,38"	Louisiana
BC82	Manguezal	TR	N 29º 6" 48,88' /O 90º 10' 0,83"	Louisiana
LAG- 3	Manguezal	TR	28°29'42.9"S /48°47'43.1"O	Laguna
LAG-4	Manguezal	TR	28°29'38.0"S/ 48°47'49.6"O	Laguna
LAG- 5	Manguezal	TR	28°29'34.9"S /48°47'49.7"O	Laguna
LAG- 6	Manguezal	TR	28°29'37.5"S/ 48°47'57.2"O	Laguna
RP03	Manguezal	TR	28°29′35.2333″S/48°50′52.9254"O	Laguna
RP04	Manguezal	TR	28°29′14.6022″S/48°50′31.4710"O	Laguna
G-3	Manguezal/herbácea	TR	20°41' 4.03" S/40°31' 22.57"O	Espírito Santo
G-4	Manguezal/herbácea	TR	20°41' 4.47" S/40°31' 22.97" O	Espírito Santo
RBN2	Manguezal/ herbácea	TR	20°40'21.24"S/ 0°31'57.61"O	Espírito Santo
RBN1	Manguezal	TR	20°47′1.42″S/40°38′34.06"O	Espírito Santo
SF05	Mangrove	TR	26°6'48.10"S /48°47'17.00"O	Baía de São Francisco do Sul.

TR- Trado Russo

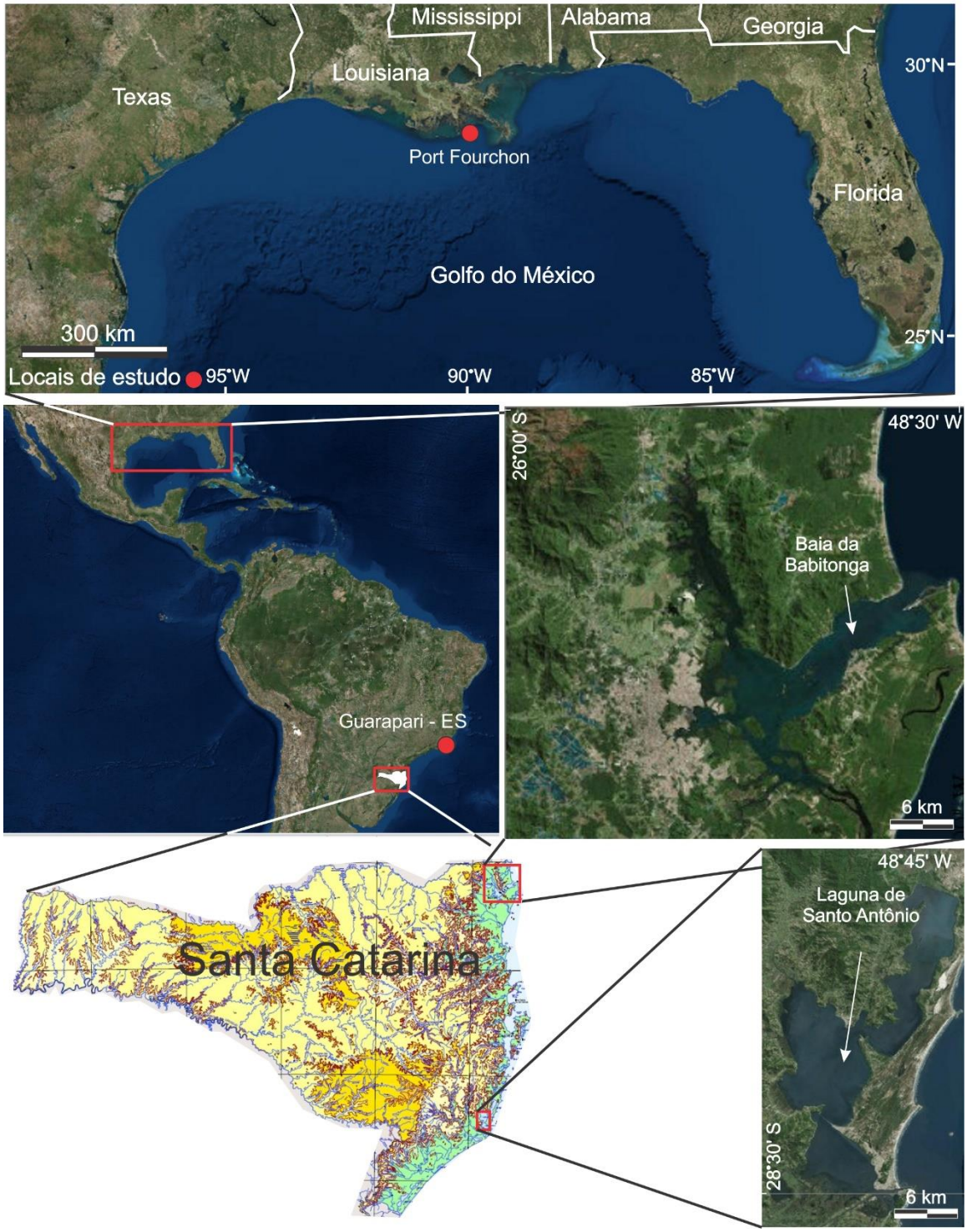

Figura 1 - Setores da costa norte e sul americana onde foram amostrados testemunhos.

2.1 BAY CHAMPAGNE - LOUISIANA (29 ° 09 ′ N)

2.1.1 Contexto geológico e geomorfológico

A laguna de Bay Champagne faz parte de um complexo deltaico formado há ~ 3500 anos cal AP e permaneceu ativo até 1600 anos cal AP. Esta planície costeira é coberta por depósitos sedimentares do Quaternário e Terciário (Meyer & Turcan 1955). As formas de relevo formados por depósitos holocênicos têm elevações relativamente baixas e estão sujeitos às inundações provocadas por furacões e tempestades. Os depósitos sedimentares pleistocênicos estão localizados abaixo dos depósitos holocênicos onde estão localizados os ecossistemas de pradarias. Esses sedimentos foram depositados durante a última glaciação quando o desgelo das calotas resultaram no transporte e deposição de grandes quantidades de sedimentos. Atualmente, esses depósitos formam uma espessa camada cobrindo a área em direção ao litoral (Fisk 1952). O tipo de morfologia costeira de Bay Champagne faz com que seja particularmente vulnerável às inundações causadas por furacões (Ritchie & Penland 1988).

2.1.2 Clima

Ao longo da costa da Louisiana as temperaturas do ar no inverno são tipicamente mais frias no interior e mais quentes ao longo da costa. O clima é subtropical úmido, com temperatura anual mensal variando entre 6°C e 30°C. Projeções climáticas indicam um aumento na intensidade e no número de furacões em resposta ao aquecimento global, uma vez que essas tempestades mais fortes são normalmente responsáveis pela maioria dos danos às áreas costeiras (Dietz *et al.* 2018, Zimmerman *et al.* 2001). As interações entre a elevação do nível do mar e o aquecimento do ar e do oceano no inverno na Louisiana tem influenciado na dinâmica da vegetação costeira, inclusive nos manguezais (Krauss *et al.* 2011).

2.1.3 Vegetação

O sul da Louisiana apresenta 40 a 45 % de sua vegetação na forma de pântanos, pois a Louisiana é a porta de drenagem da Bacia Hidrográfica do Baixo Mississippi. Seus wetlands (zonas úmidas) são muito expressivas, abrangendo um gradiente climático que vai desde manguezais, pântanos salinos, pântanos salobros (saltmarshes) e de água “doce” (swamp) seguidos por florestas periodicamente alagadas (bottomland hardwood swamps) com predominância de ervas, vegetação arbórea e arbustiva variada (Field 1991). A maioria das zonas úmidas costeiras da Louisiana são classificadas como pântanos intermarés. Os

manguezais são representados pela espécie *Avicennia germinans* (Acanthaceae - black mangrove), o qual tem se expandido ao longo da região costeira da Louisiana devido a ocorrência de invernos menos rigorosos (Osland *et al.* 2017, Snyder *et al.* 2021). Estes ecossistemas são encontrados nos limites das planícies deltaicas margeando lagunas e ilhas barreira em um total de 2.400 ha.

2.2 LAGUNA - SUL DE SANTA CATARINA (28° 29 ′ S)

2.2.1 Contexto geológico- geomorfológico

A lagoa de Santo Antônio está inserida na unidade geomorfológica de planícies litorâneas que correspondem a uma estreita faixa situada na porção oriental do estado junto ao Oceano Atlântico, no qual existem praias arenosas e dunas que mostram a predominância de processos marinhos e eólicos. (Santa Catarina 1986). Os ambientes deposicionais encontrados na região são: ilhas barreira, planícies costeiras com cordões litorâneos (strand plains), lagunares e eólicos (Giannini 1993).

O canal de entrada da lagoa atua como um filtro dinâmico, em consequência disso, os efeitos da ação da maré e das correntes são bastante atenuados no interior da lagoa (Miranda *et al.* 2002). Outra singularidade desta região, do ponto de vista geomorfológico, é a desembocadura do Rio Tubarão com o maior exemplo de delta lagunar ativo da costa brasileira (Santa Catarina 1986).

2.2.2 Clima

O clima de Santa Catarina é Cfa e Cfb (segundo a classificação de Köppen) ou seja, subtropical úmido com verão quente e temperado (Alvares *et al.* 2013). A temperatura do ar possui uma média anual de 19°C apresentando 15°C nos meses mais frios. A umidade é em torno de 85%, e a precipitação média anual está entre 1250 mm (Imbituba) e 1400 mm (Laguna) (INMET 2017). O clima é controlado pelo Anticiclone Tropical do Atlântico Sul e Anticiclone Migratório Polar.

2.2.3 Vegetação

As florestas de mangue da Lagoa de Santo Antônio são bastante homogêneas em termos de desenvolvimento estrutural e composição de espécies. A vegetação no local consiste quase inteiramente de *Laguncularia racemosa* e pequenos arbustos de *Avicennia schaueriana*, além de *Spartina densiflora*, uma espécie de pântano salino. A pteridófita *Acrostichum*

aurum, típica de pântano, também vivem associadas às florestas de mangue (Soares *et al.* 2012, Tomlinson 1994).

2.3 SÃO FRANCISCO DO SUL- COSTA NORTE DE SANTA CATARINA (26°6' S)

2.3.1 Contexto geológico- geomorfológico

A característica geomorfológica mais proeminente da Baía de São Francisco do Sul é a faixa costeira escarpada que, ao cruzar a costa cria embainhamentos costeiros onde várzeas e, com menos frequência, sistemas estuarinos são encontrados (Angulo *et al.* 2009). A geologia do quaternário da área de estudo é caracterizada por barreiras do Pleistoceno e Holoceno e planícies de maré com sedimentos lamosos, praias, sucessão de cristas de praia e dunas (Angulo *et al.* 2009). Dunas parabólicas são facilmente notadas colonizadas por diferentes tipos de vegetação adaptadas a substratos com baixo teor de matéria orgânica. Cristas de praia apresentam uma elevação de até 6 m acima do nível relativo do mar atual.

2.3.2 Clima

A área do estuário da Baía de São Francisco do Sul apresenta clima subtropical (Cfa, de acordo com a classificação de Koppen) apresentando verão úmido e inverno moderadamente seco, sendo que a precipitação média anual varia entre 1000 e 1500 mm e a temperatura média é de 18ºC. Segundo Berger (2008), os meses mais quentes na área da Baía de São Francisco do Sul são janeiro e fevereiro, com temperatura de 24,5°C, já os meses mais frios são julho e agosto, com temperatura média de 16,5° e 17,3°, respectivamente.

2.3.3 Vegetação

A vegetação que circunda a Baía de São Francisco do Sul é caracterizada pelo ecossistema de restinga onde as mais representativas famílias de plantas são Asteraceae (ex., *Baccharis singularis*), Bromeliaceae (ex., *Aechmea gamosepala*), Dryopteridaceae (ex., *Rumohra adiantiformis*), Fabaceae (ex., *Dalbergia ecastaphyllum*), Mytaceae (ex., Marlierea *tomentosa*), Rubiaceae (ex., *Psychotria*) e Poaceae (ex., *Lasiacis ligulata*). Além disso, florestas de mangue ocorrem na planície costeira, caracterizada *por Rhizophora mangle* (1,5-7 m de altura), *Laguncularia racemosa* (1–9 m de altura) e *Avicennia germinans* (3–4 m de altura) (Cunha *et al.* 2006).

2.4 LITORAL SUL DO ESPÍRITO SANTO (20° 40' S)

2.4.1 Contexto geológico- geomorfológico

O Estado do Espírito Santo apresenta um quadro morfológico que permite divisão esquemática do estado em três regiões: 1) Litoral – formações Quaternárias constituídas por planícies litorâneas, praias, restingas e aluviões continentais depositados pelo Rio Doce e outros cursos d'água menores; 2) Tabuleiros – correspondendo a chapadões areníticos paleogênicos pouco alterados pela erosão fluvial; e 3) Áreas Elevadas Interiores – correspondendo a terrenos pré-cambrianos bastante acidentados, onde são comuns ocorrências de picos isolados, denominados de pontões ou pães-de-açúcar. Tal divisão reflete diretamente sua evolução tectônica e disposição litológica, somada às ações de ordem climáticas atuantes na região (CPRM 2014).

2.4.2 Clima

A região é caracterizada por um clima tropical quente e úmido, com precipitação média anual de 1400 milímetros (Peixoto & Gentry 1990), que está concentrada no verão, entre novembro e janeiro. A temporada seca (outono-inverno) ocorre entre maio e setembro e é regulada pela posição da Zona de Convergência Intertropical (ZCIT) e a Zona de Convergência do Atlântico Sul (ZCAS) (Tomaziello *et al.* 2016).

2.4.3 Vegetação

As áreas úmidas cobrem uma parte significativa da área de estudo, com manguezais que variam de 3 a 15 m de altura. Espécies importantes de mangue, como *Rhizophora mangle*, ocorrem próximas às margens do canal, enquanto *Avicennia germinans* cresce principalmente em áreas topograficamente mais altas. Nas planícies herbáceas, existem arbustos e ervas ao longo das planícies arenosas em áreas topográficas mais altas que os manguezais. As espécies predominantes são Euphorbiaceae, Poaceae, Asteraceae, Cyperaceae e Fabaceae. Além da floresta ombrófila densa, com espécies de Arecaceae, Myrtaceae, Euphorbiaceae, Poaceae, Fabaceae e Rubiaceae. Essas unidades são distribuídas dentro de regimes específicos de inundação, tipos de sedimentos e salinidades da água intersticial (Cohen & Lara 2003, Cohen *et al.* 2019).

3 MÉTODOS

3.1 TRABALHO DE CAMPO E PROCESSAMENTO DE AMOSTRA

Para este estudo, nove (9) testemunhos de sedimentos foram coletados em planícies de marés ocupadas por manguezais e quatro (4) testemunhos coletados a partir de planícies de inundação em uma área transicional colonizada por manguezal e vegetação herbácea, em diferentes níveis topográficos: “manguezal” (BC81, BC82, LAG-3, LAG-4, LAG-5, LAG-6, RP03 e RP04) “manguezal/vegetação herbácea” (G-3, G-4, RBN-1e RBN-2) (ver, **Tabela 1**).

Os treze (13) testemunhos analisados seguiram a mesma metodologia de coleta (Cohen *et al.* 2003). Dois testemunhos sedimentares foram coletados nas margens de Bay Champagne, litoral da Louisiana (BC81 e BC82, 29 ° 09 ′ N). Na costa sul de Santa Catarina (28° 29 ′ S), seis (6) testemunhos foram amostrados na Lagoa de Santo Antônio (LAG-3, LAG-4, LAG-5, LAG-6, RP03 e RP04) e na costa norte de Santa Catarina (26°6' S), um (1) testemunho (SF05) na extremidade sudeste da Baía de São Francisco do sul. O trabalho de campo do litoral sul do Espírito Santo (20° 40' S) ocorreu ao longo de dois vales estuarinos e foram coletados quatro (4) testemunhos sedimentares: G-3, G-4, RBN-2 e RBN-1.

O total de dez (10) testemunhos foram radiografados para identificação de estruturas sedimentares. Os testemunhos amostrados no litoral da Louisiana (BC81 e BC82) não foram radiografados (ver, capítulo II). Esses testemunhos foram amostrados por vibração e armazenados em tubos de alumínio que dificultam a remoção das colunas de sedimentos para uma adequada radiografia em uma clínica.

As amostras para análise granulométrica foram coletadas em um intervalo de 5cm ao longo dos testemunhos sedimentares estudados e levadas ao Laboratório de Oceanografia Química / UFPA. Grão e tamanho foram determinados por meio de um analisador de partículas à laser (*Laser Particle Size*, SHIMADZU SALD 3101). As distribuições do tamanho de grão do sedimento seguiram o método de Wentworth (1922) e os gráficos foram elaborados no software SYSGRAN (Camargo 1999), com frações areia (2-0,0625 mm), silte (62,5-3,9 μm) e argila (3,9-0,12 μm). A análise das fácies incluiu descrições de cor (Color 2009), litologia, textura e estrutura (Walker 1992) e foram codificadas de acordo com Miall (1978).

3.2 PALINOLOGIA

Para análise palinológica os treze (13) testemunhos foram sub-amostrados ($1cm^3$) com total de 482 amostras em diferentes intervalos. Todas as amostras foram preparadas usando técnicas analíticas padrão para pólen, incluindo acetólise (Faegri & Iversen 1989). Os resíduos das amostras foram colocados em microtubos (Eppendorf) e mantidos em gelatina glicerinada. Os resíduos das amostras foram montados em lâminas com glicerina. Manuais para descrição morfológica de pólen e esporos foram consultados (Roubik & Moreno 1991, Colinvaux *et al.* 1999, Lorente *et al.* 2017), juntamente com a coleção de referência do Laboratório de Dinâmica Costeira da Universidade Federal do Pará (UFPA- BR) e Laboratório de Paleoecologia Global da Universidade da Louisiana (LSU-EUA), a fim de identificar grãos de pólen e esporos. O total de 300 a 400 grãos de pólen foram contados em cada amostra. Programas como TILIA e TILIAGRAPH foram usados para calcular e traçar diagramas polínicos (Grimm 1990).

3.3 DIATOMÁCEAS

As diatomáceas há muito são elogiadas por serem usadas como indicadores ambientais confiáveis (Harding & Taylor 2005). O aumento da relevância desse indicador ambiental pode ser atribuído a sua alta abundância e diversidade de espécies, que é distribuída entre os ambientes aquáticos. Além disso, as estruturas são altamente duráveis e bem preservadas nos sedimentos (Barker *et al.* 2005). A análise para diatomáceas foi realizada no testemunho coletado na Baía de São Francisco do Sul, 26°6' S (costa norte de Santa Catarina) (ver, capítulo V).

A metodologia aplicada seguiu (Battarbee 1986), utilizando amostras de $1cm^3$ coletadas em intervalos de 20 cm ao longo de testemunho sedimentar (SF5, 100cm). Cada amostra foi pré-tratada com 30% de H_2O_2 e 10% de HCl. Em seguida foram preparadas um total de cinco (5) lâminas, montadas com a resina Naphrax como meio de inclusão. A identificação das diatomáceas foi baseada na análise microestrutural da parede celular silicificada, como camada externa, tamanho dos poros, formas e volume (Lorente *et al.* 2020, Tremarin *et al.* 2008). Para caracterização quantitativa pelo menos 500 válvulas para cada amostra foram contadas e os diagramas foram produzidos pelo software Tilia graph e CONISS (Grimm & Troostheide 1994).

3.4 δ13C, δ15N, C/N e C/S

Um total de 800 amostras (6-50 mg) foram coletadas no intervalo de 5cm ao longo de treze (13) testemunhos sedimentares para realização das análises geoquímica (Pessenda *et al.* 2010). Valores isotópicos de $\delta^{13}C$, $\delta^{15}N$ e elementares C, N e S (C/N-C/S) foram analisados no Laboratório de Isótopos Estáveis do Centro de Energia Nuclear na Agricultura (CENA). Neste laboratório as amostras foram analisadas em um Espectrômetro de Massas ANCA SL 2020, da Europe Scienfic, que contém um analisador elementar acoplado. Os resultados elementares (C, N e S) foram expressos em porcentagem por peso seco, e os isotópicos ($\delta^{13}C$ e $\delta^{15}N$) são expressos em delta por notação de milhar com uma precisão analítica maior que 0,2‰, em relação ao VPDB (molusco fóssil *Belemnitella americana* da Formação Peedee da Carolina do Sul, USA), sendo o desvio padrão de 0,1‰ para a matéria orgânica. A partir dos resultados elementares (C, N e S) foi possível calcular as razões C/N e C/S para as amostras sedimentares.

A relação entre $\delta^{13}C$, $\delta^{15}N$ e C/N foi usada para fornecer informações sobre a origem da matéria orgânica preservada no ambiente costeiro (Meyer 1997, 2003). Os valores de $\delta^{13}C$ têm valores médios diferentes entre plantas terrestres, de água doce e fontes marinhas (Meyers 1997). Algumas classes de plantas também têm diferentes fontes de CO_2 (ar vs. água) ou diferentes fracionamentos isotópicos de carbono (C3 vs. C4 vias fotossintéticas). O nitrogênio atmosférico tem um valor $\delta^{15}N$ de zero, e as plantas terrestres tendem a ter valores $\delta^{15}N$ próximo a 0‰. Marismas (*Spartina* sp.) tem valores de $\delta^{15}N$ em torno de + 6‰ e plâncton tem valores entre +6 a + 10 ‰ (McCarthy 1985).

A análise elementar de ST foi aplicada nas amostras do testemunho sedimentar SF5 (100 cm), amostrado na Baía de São Francisco do Sul, 26°6' S (costa norte de Santa Catarina) (ver, capítulo VI). Um total de vinte (20) amostras foram maceradas e homogeneizadas e enviadas para o Laboratório de Ciclagem de Nutrientes do CENA-USP, onde foram pesadas (~100 mg) em recipientes de cerâmica e submetidas à combustão. A quantidade de enxofre (S) por peso seco da amostra foi obtida através de detecção infravermelha pelo equipamento SC 144DRLECO. Em relação a razão entre C e S (C/S), pode ser utilizada para distinguir sedimentos de origem marinha ou de água doce (Lorente *et al.* 2020). É possível essa razão ser calculada levando em consideração a quantidade de sulfato dissolvido disponível e a formação de pirita nas amostras. Sedimentos orgânicos que apresentam valores de C/S

maiores que 10 indicam a influência de água doce, enquanto valores de C/S entre 0,5 e 5 correspondem a amostras com influência marinha (Berner & Raiswell 1984).

3.5 LOI (LOSS-ON-IGNITION) - XRF (FLUORESCÊNCIA DE RAIOS-X)

Os testemunhos sedimentares (BC81, 400cm e BC82, 200cm) coletados em Bay Champagne, (litoral da Louisiana, 29 ° 09 ′ N) foram levadas ao Laboratório de Paleoecologia Global da Universidade da Louisiana (LSU- EUA) para determinação das análises de XRF e LOI. Os valores de XRF foram determinados a partir das concentrações de elementos mais encontrados em ambientes terrestres e costeiros (Cl, K, Ca, Ti, Mn, Fe, Br, Sr, Zn e Zr, ppm) analisados em um Innov-X Delta Premium DP-4000 (Dispositivo portátil de fluorescência raios - X). Este dispositivo registra as concentrações iniciais em contagens por segundo (cps) para > 30 elementos, convertendo cps em concentrações (partes por milhões) usando uma calibração interna para padrões sólidos NIST 2710a e 2711a. Após a abertura dos testemunhos a análise foi conduzida através de três frequências para 30 segundos cada em intervalos de 2 cm. Para as determinações com base em "loss on ignition" (LOI), as amostras sedimentares (BC81, 200cm e BC82, 400cm) de Bay Champagne (litoral da Louisiana, 29 ° 09 ′ N) seguiram o procedimento de Liu & Fearn (2000). Um total de 600 amostras foram coletadas para análise de LOI. As amostras foram retiradas ao longo do testemunho sedimentar com intervalo de 1cm e queimadas a uma temperatura entre 105°, 550°, e 1000°C em um forno de Barnstead. Os valores de LOI foram expressos em percentagem (%) de água, matéria orgânica, carbonatos e residuais (ver, capítulo II)

Em relação aos testemunhos sedimentares (G-3-100 cm, G-4-100 cm, RBN-2-170 cm e RBN-1- 400cm) coletados no litoral sul do Espírito Santo (20° 40' S), as análises de XRF foram realizadas no Laboratório de ^{14}C do Centro de Energia Nuclear na Agricultura (CENA/USP). A análise de XRF foi realizada escaneando quatro (4) testemunhos sedimentares em intervalos de 2 cm usando um espectrômetro de energia dispersiva de fluorescência de raio-X portátil (pED-XRF-modelo Tracer III-SD, Bruker AXS, Madison, EUA). Apenas os principais elementos químicos em sedimentos costeiros representativos de origens marinhas (Yao *et al.* 2015a, Br, Ca, Cl, K e Sr) foram selecionadas para esta análise (ver, capítulo IV)

3.6 DATAÇÃO POR ^{14}C e ^{210}Pb

Trinta e sete (37) amostras ~ 10g cada foram usadas para datação por radiocarbono (**Tabela 2**). As amostras foram verificadas e fisicamente limpas (sem raízes) sob o microscópio estereoscópico. O material residual para cada amostra foi extraído com 2% de HCl a 60°C por 4 horas, lavado com água destilada até pH neutro (Pessenda *et al.* 2010, 2012). A matéria orgânica do sedimento foi analisada por Accelerator Mass Espectrometria (AMS) no Centro de Estudos Aplicados a Isótopos (Athens, Georgia, EUA) e LACUFF -BR (Universidade Federal Fluminense). As idades do radiocarbono são relatadas em anos antes do presente 1950 (ano AP) normalizado para $\delta^{13}C$ de –25 ‰ VPDB, ano cal AP, 2σ (Reimer *et al.* 2009).

As datações de Pb-210 foram realizadas em dois (2) testemunhos sedimentares amostrado na costa sul de Santa Catarina, 28° 29 ′ S – Lagoa de Santo Antônio. Testemunhos LAG-3 e LAG-6 (**Tabela 2**)

As análises para datação com Pb-210 foram realizadas no Departamento de Petrologia e Metalogenia, do Instituto de Geociências e Ciências da Terra, Universidade Estadual Paulista Júlio de Mesquista Filho (UNESP/Rio Claro). As amostras de sedimentos foram analisadas utilizando as atividades de Po-209 (traçador) e Po-210 (natural). Após várias etapas de separação, os isótopos de Po-209 e Po-210 foram removidos por deposição espontânea, e, então, contados usando um sistema de espectrometria alfa. O método do Pb-210 é apropriado para determinar a idade dos sedimentos modernos na faixa de até 100-150 anos de idade. Quantificando as atividades de Pb-210 e Ra-226 nos sedimentos, foi possível determinar o excesso de Pb-210 atmosférico e estimar a idade de deposição, a partir da taxa de sedimentação.

No Capítulo III, o uso de datação múltipla permitiu uma corroboração entre métodos que se apoiariam no fornecimento de cronologias precisas (Piotrowska *et al.* 2010b).

Deve ser destacado que a datação ^{14}C do LAG-6 (40 cm) indicou uma idade de 1922–1876 DC, enquanto o 210Pb (42cm) revelou uma idade por volta de 1943 DC, então 21 anos mais jovem do que a margem de erro da datação ^{14}C (**Tabela 2 e 3**). Esta diferença cronológica entre os dois métodos pode ser considerada aceitável porque a bioturbação causada pela fauna do solo pode misturar matéria orgânica local em diferentes níveis estratigráficos (Boulet *et al.* 1995, Gouveia & Pessenda 2000) (ver, capítulo III).

Tabela 2- Profundidade estratigráfica selecionada para identificação de taxas de sedimentação com base em datação de ^{210}Pb.

Testemunhos/profundidade (cm)	^{210}Pb (AD) anos	^{210}Pb (AD) anos sedimentation
LAG3/ 0 cm	2015	
LAG3/10 cm	2012	(5,3 mm / ano (0–60 cm)
LAG3/20 cm	2008	
LAG3/30 cm	2004	
LAG3/40 cm	2000	
LAG3/50 cm	1996	
LAG3/58 cm	1993	
LAG6/ 0 cm	2015	(16,13 mm / ano (0–50 cm)
LAG 6/7 cm	2009	
LAG 6/14 cm	1998	
LAG 6/21 cm	1986	
LAG 6/28 cm	1974	
LAG 6/35 cm	1961	
LAG 6/42 cm	1943	
LAG 6/ 50 cm	1921	

Tabela - 3 Amostras de matéria orgânica sedimentar selecionadas para datação por radiocarbono com: local de código (profundidade), número do laboratório, porcentagem de carbono moderno (pMC), idade ^{14}C, idades calibradas (cal- Calib 6.0; Reimer *et al.*2009) e mediana das idades do Litoral da Louisiana (Capítulo II), Laguna (SC) (Capítulo III) litoral sul do Espírito Santo (Capítulo IV) e Baía São Francisco do sul (SC) (Capítulo V)

Laboratório (UGAMS)	Amostra profundidade (cm)	^{14}C ano AP	pMC (± error)	média (cal ano AP)
UGAMS 27,333	LAG3\60–65	361 ± 23		~385
UGAMS 34,672	LAG3\90–95	960 ± 26		~840
UGAMS 34,673	LAG4\20–25		103.819 (0.322)	1957 AD
UGAMS 34,674	LAG4\60–65	589 ± 23		~540
UGAMS 34,675	LAG5\52–55		104.329 (0.302)	1957 AD
UGAMS 26,627	LAG5\90–95	1019 ± 24		~940
UGAMS 34,676	LAG6\35–40	51 ± 23		~50
UGAMS 34,680	RP4\30–32		100.036 (0.298)	1956 AD
UGAMS 34,681	RP4\60–65	359 ± 23		~380
UGAMS 34,682	RP4\170–175	8130 ± 30		~9050
UGAMS 34,677	RP3\32–35		104.64 (0.302)	1957 AD
UGAMS 34,679	RP3\ 100–105			~585
UGAMS-34381	BC81\ 170	2150 ± 20		~2128
UGAMS-34379	BC82 \170	1580 ± 20		~1470
LAC 190456	BC82 \300	5766 ± 48		~6525
LAC 190457	BC82\ 350	5621 ± 48		~6370
UGAMS-34380	BC82\ 400	7330 ± 30		~8113
LAC190419	G-3 \ 28		104,5	1958 AD
LAC190690	G-3 \ 40	3274	66,529	~3500
LAC190691	G-3 \ 75	5497	50,442	~6300
LAC190692	G-4 \ 35	117	98,551	~77
LAC190693	G-4 \ 82	2585	72,487	~2704
LAC190420	RBN2 \53-55		106,441 ±0.689	2007 AD
LAC190421	RBN2\ 95-97		100,802 ±0,617	1955 AD
LAC190422	RBN2 \141-143	314	93,902	~390
LAC190423	RBN2 \168-170	505	96,169	~515
LAC190410	RBN1\ 50-52	103.669 ±0.555	Moderno	~1957AD
LAC 190412	RBN1\ 104-106		1261–1423	~1342
LAC190413	RBN1\ 155-157		1343–1570	~1457
LAC 190414	RBN1\ 203-205		2745–2930	~2838
LAC 190415	RBN1\ 253-255		4137–4317	~4227
LAC 190416	RBN1\ 303-305		4498–4651	~4575
LAC 190417	RBN1\ 353-355		4569–4831	~4700
LAC 190418	RBN1\ 394–396		4840–4974	~4907
LAC180247	SF05\ 15-20	100.88 ± 0.340*	424-496	1958-1957AD
UGAMS34683	SF05\ 40-45	360 ±23		~429
LACUFF180246	SF05\ 60-65	1540 ± 20		~1462

4 RESULTADOS E DISCURSÃO

4.1 HOLOCENO

Após o Último Máximo Glacial, o aumento gradual da temperatura global provocou o derretimento dos mantos de gelo causando transgressões marinhas em muitas áreas da costa americana, mudando a morfologia costeira e a distribuição da vegetação (Yao & Liu 2017, França *et al.* 2018). Isto foi evidenciado ao longo dos testemunhos sedimentares coletados no litoral da Louisiana, 29 ° 09 ′ N e costa sul brasileira (Laguna, 28° 29 ′ S). No litoral da Louisiana este processo natural mudou um lago de água doce (~ 8100 - ~ 6500 anos cal AP) cercada por ervas, samambaias e uma floresta boreal (*Pinus* sp., *Betula* sp., *Quercus* sp.) para uma laguna (~ 6500 - ~ 1500 anos cal AP) ocupada por herbáceas e macrófitas adaptadas a água salobra (*Bolboschoenus* sp., *Spartina* sp, *Typha angustifolia* e *Typha latifolia*). O enriquecimento nos valores isotópicos $\delta^{13}C$ (-24 a -22 ‰) e diminuição da razão C/N (25 para 9), sugerem uma maior contribuição da matéria orgânica marinha neste intervalo de tempo. Além disso, as análises de XRF indicaram um maior aporte de elementos típicos de ambiente estuarino (> Cl e Br) e menor de elementos de origem terrestre (< Fe e Ti). Essa lagoa provavelmente foi estabelecida no Holoceno inicial quando o nível do mar no Golfo do México estava ~ 8 m abaixo do nível moderno (Donoghue 2011) e substituída por uma laguna de acordo com o aumento do nível do mar no Holoceno médio (Blum *et al.* 2002, ~2 m acima do atual) (ver, capítulo II).

Uma situação semelhante ocorreu em Laguna, (costa sul de Santa Catarina, 28º 29´ S). Uma tendência de aumento no percentual de grãos de pólen de ervas associado ao enriquecimento isotópico $\delta^{13}C$ e a diminuição nos valores de C/N sugerem uma transição de uma planície fluvial ocupadas por gramíneas, arbustos e samambaias para uma planície de maré dominado por ervas e com uma contribuição substancial de matéria orgânica de origem estuarina no Holoceno inicial-médio (ver, capítulo III).

Em Laguna (costa sul de Santa Catarina) e litoral da Louisiana (Bay Champagne) a elevação do NRM no Holoceno foi determinante para o estabelecimento de planícies de marés lamosas ocupadas por vegetação e espécies adaptada a ambientes estuarinos (ex. *Spartina* sp.; bivalve *Rangia cuneata*). Neste intervalo de tempo não houve registro de pólen de manguezal nos sedimentos de planícies de maré destas áreas de estudo (ver, capítulo III e II)

Na costa tropical brasileira o aumento do NRM no Holoceno médio (2-5 m acima do nível atual) foi determinante para a migração dos manguezais para o interior de estuários e lagunas (Angulo *et al.* 2006, Suguio *et al.* 2013, Toniolo *et al.* 2020, Cohen *et al.* 2020).

Em nossa área de estudo no Espírito Santo (20° 40' S) os efeitos do aumento NRM foram registrados em dois testemunhos posicionados em diferentes níveis topográficos (G-3; 0,7 m e RBN-1; 0,1 m acima do NRM). Em relação ao testemunho G-3, os resultados revelaram a conversão de uma planície de inundação ocupada por palmeiras e ervas em uma laguna cercada por manguezais, caracterizado por uma tendência de aumento nos grãos de pólen de mangue de 5% para 60% e indicadores marinhos (ex. dinoflagelados) entre ~ 6300 anos cal AP e ~ 4650 anos cal AP. A análise XRF também indicou uma tendência de aumento nas concentrações de Ca, Sr, Cl, Br e K (ver, capítulo IV). No testemunho RBN-1, localizado a 17 km distante do testemunho G-3 em uma planície de maré mais baixa os dados indicaram uma laguna com matéria orgânica sedimentar proveniente de plantas terrestres C3 e carbono orgânico marinho e manguezais (5-15% pólen do mangue) presente ao longo de sua margem entre ~ 4900 anos cal AP e ~ 4230 anos cal AP. A análise de XRF também indicou maiores concentrações Ca e Sr.

Da mesma forma durante o Holoceno médio uma forte influência marinha foi registrada na base do testemunho sedimentar SF5 (100-70 cm) coletado na Baía de São Francisco do sul (costa norte de Santa Catarina, 26°6' S) situada 300 km de Laguna (28° 29 ′ S) (ver, capítulo V). A assembleia de pólen indicou a presença de vegetação de restinga e plantas aquáticas. Essa vegetação geralmente está associada a um substrato sob influência de água salobra além de ocorrerem perto da costa (Korte *et al.* 2013). O diagrama binário $\delta^{13}C$ ($\overline{x}$ = - 26,3 ‰) e os valores C: N ($\overline{x}$ = ~ 16) indicaram contribuições de plantas terrestres C3 e matéria orgânica de ambiente estuarino. Além disso, indicadores marinhos abundantes (ex. foraminíferos, diatomáceas marinhas, *Acritarcas* e outros dinoflagelados) também estavam presentes. Os cistos de *Acritarca* normalmente habitam em águas costeiras rasas (Félix & Souza 2012). Tal assinatura de pólen e microfósseis confirmam a influência marinha. Não ouve registro de pólen de manguezal na Baía de São Francisco do Sul neste intervalo de tempo (Capítulo V).

Em torno do Holoceno médio e tardio ocorreu uma gradual queda de NRM (Angulo *et al.* 2006, Toniolo *et al.* 2020), o que facilitou a construção de deltas. As florestas de mangue

migraram para o mar durante este período (Cohen *et al.* 2014, França *et al.* 2015, Cohen *et al.* 2020a, 2020b).

No Espírito Santo (20° 40' S) os efeitos da queda do NRM foram registrados ao longo de dois (2) testemunhos sedimentares: G-4 e G-3 (0,1 m, 0,45m e 0,7 m acima do NRM). Este processo favoreceu a expansão de ervas e palmeiras nas planícies mais altas, e a migração dos manguezais para as planícies de maré mais baixas entre ~4650 cal anos AP e 2700 cal anos AP. Os valores da razão C/N aumentaram e os isotópicos ($\delta^{15}N$) diminuíram, indicando uma tendência de diminuição da matéria orgânica sedimentar proveniente de algas. Concentrações de Ca, Sr, e Br diminuíram durante este tempo. No entanto, em um testemunho (RBN-1, 0,1 m acima do NRM) amostrado em planície de maré inferior ao testemunho G-3 e cuja assembleia polínica era dominada por *Rhizophora*, apresentou um aumento de pólen de mangue de 10 a 20% em torno de ~ 4230 e ~ 1450 cal anos AP. A tendência de diminuição isotópica de $\delta^{13}C$ e $\delta^{15}N$, provavelmente reflete um aumento de plantas terrestres C3 e influência terrestre. Esta zona topograficamente mais baixa favoreceu a expansão dos manguezais apresentando menores taxas de sedimentação (~ 0,35 mm /ano), indicando uma diminuição do espaço disponível para acúmulo de sedimentos causado pela queda do NRM.

Durante os últimos 1000 anos o nível do mar global atingiu o nível máximo, entre 12 e 21 cm, e o mínimo, entre -19 e -26 cm ocorridos em ~ 1150 DC e ~ 1730 DC, respectivamente (Grinsted *et al.* 2009). Esta queda no NRM foi atribuída à Pequena Idade do Gelo (LIA) que ocorreu durante os últimos seis ou sete séculos (Lean & Rind 1999), tendo terminado entre 1850 e 1890 DC (Bradley & Jones 1992).

No litoral do Espírito Santo (20° 40' S) um testemunho (RBN-2, 100 cm acima NRM)) coletado no ecótono floresta de manguezais e vegetação herbácea, registrou os impactos do LIA no Holoceno tardio. Entre 390 anos cal AP (1560 DC) e 1955 DC, o pólen de mangue estava quase totalmente ausente com aumento de pólen de ervas em comparação com a fase anterior (515 - 390 cal anos AP). Indicadores marinhos (foraminíferos e dinoflagelados) não foram encontrados. Essa fase também foi caracterizada por uma tendência de aumento da razão C/N, sugerindo uma diminuição da influência aquática na matéria orgânica sedimentar. As concentrações de elementos típicos de ambiente estuarino (Br, Ca, Cl e K) diminuíram durante esse intervalo de tempo, provavelmente como consequência de uma queda do NRM atribuída a Pequena Idade do Gelo - LIA (ver, capítulo IV).

Estudos paleoclimáticos indicaram flutuações na temperatura durante LIA (380 a 50 anos cal AP) e MCA – Período Quente Medieval (950 a 750 anos cal AP) e consequente mudança na vegetação no sul do Brasil (Behling *et al.* 2004, França *et al.* 2018). Estes eventos climáticos provavelmente influenciaram o aparecimento da sucessão de gêneros de manguezais na Baía de São Francisco do Sul (costa norte de Santa Catarina, 26°6' S) com a colonização pioneira de *Laguncularia* sp. (~ 1400 anos cal AP) seguido pelo estabelecimento de *Avicennia* sp. (~500 anos cal AP) e o aparecimento tardio de *Rhizophora* sp., apenas no final século XX (ver, capítulo V).

Os efeitos da queda seguido da estabilização do nível do mar no Holoceno tardio foram registrados na costa sul catarinense (Laguna, 28° 29 ′ S) através da mudança na geomorfologia costeira. Depósitos arenosos foram acumulados entre ~ 940 e ~ 385 anos cal BP nas profundidades 120 e 100 cm, 100 e 65 cm, 100 e 60 cm, 70 e 43 cm e 100 e 55 cm dos testemunhos RP-3, RP-4, LAG-3, LAG-4 e LAG-5, respectivamente. Provavelmente, após a queda e estabilização do NRM, ilhas barreiras surgiram isolando a laguna e permitindo o estabelecimento de planícies de maré lamosas (ver, capítulo III).

No litoral de Louisiana (29 ° 09 ′ N), sedimentos arenosos (sedimentos *overwash*) foram depositados no interior de uma laguna nos últimos ~ 1470 cal anos AP e ~ 2100 cal anos AP indicados nas profundidades 170 - 0 cm dos testemunhos BC82 e BC81. Esses depósitos arenosos refletem a migração gradual desses sedimentos em direção à terra provavelmente resultado de eventos de tempestade neste intervalo de tempo. Estudos mostram que o litoral da Louisiana foi afetado por intensos furacões e tempestades tropicais em torno do Holoceno (Dietz *et al.* 2018). Os valores de XRF mostram aumento nas concentrações de Zn e Zr, tais valores estão relacionados a fração areia e provavelmente indicam fases de intemperismo da rocha levado pela ação das correntes e marés e depositada como areia de praia. (Johnson *et al.* 2020) (ver, capítulo II)

A posição do NRM na costa sul brasileira (Laguna, 28° 29 ′ S) e norte americana (litoral da Louisiana, 29 ° 09 ′ N) no Holoceno médio criou ambientes deposicionais e condições físico-químicas apropriadas para o desenvolvimento de manguezais, como constatado também no litoral do Espírito Santo com o desenvolvimento de manguezais tropicais desde o Holoceno médio. Entretanto, não foram registrados grãos de pólen de manguezais nos atuais limites austrais e boreais dos manguezais americanos durante o

Holoceno médio-tardio. Provavelmente, apesar dos ambientes deposicionais apropriados para o desenvolvimento dos manguezais nessas latitudes subtropicais no Holoceno médio, os impactos das temperaturas frias do inverno nas planícies de marés ocupadas por marismas (*Spartina* sp.) e posicionadas no atual limite austral e boreal dos manguezais americanos inibiram o desenvolvimento dessas florestas costeiras (ver, capítulo II e III).

Nossos estudos, a partir de uma análise comparativa de dados multi-proxy indicam que os manguezais foram estabelecidos no litoral Espírito Santo (20° 40' S) de acordo com a elevação do NRM no Holoceno médio (~ 6300 e ~ 4200 anos cal AP). Os manguezais da Baía de São Francisco do sul (26°6' S) foram estabelecidos em torno ~1500 anos cal AP associado ao aumento da temperatura no Holoceno tardio, impulsionando a migração dos manguezais para latitudes temperadas ao longo da costa sul brasileira (ver, capítulo IV e V). Essa tendência revela uma gradual expansão dos manguezais tropicais para costas subtropicais brasileiras associado ao aquecimento global natural e o aumento NRM do Holoceno (Kaufman *et al.* 2020). Os manguezais de Laguna e Louisiana foram estabelecidos apenas em meados e início do século XX, provavelmente influenciados pelo aquecimento global pós era industrial.

4.2 ANTROPOCENO

O Antropoceno descreve o período no qual a humanidade impactou a atmosfera e oceanos mudando a dinâmica dos ecossistemas costeiros (Zalasiewicz *et al.* 2018). Para os manguezais, isso significa lidar com uma composição diferente de gases atmosféricos, aumento do nível do mar, aquecimento da temperatura, e mudanças na frequência e intensidade de eventos climáticos (furacões e tempestades de inverno) (Allen *et al*. 2018). Nosso trabalho revelou que não ouve registro de pólen de mangue nos sedimentos de planícies de maré situadas no limite austral (Laguna, 28° 29 ′ S) e boreal (litoral da Louisiana, 29 ° 09 ′ N) do continente americano durante o Holoceno, mesmo apresentando condições adequadas para seu estabelecimento promovido pela elevação do NRM no Holoceno. Nesse período ocorreu uma contribuição significativa de matéria orgânica de origem estuarina em planícies de maré ocupadas por *Spartina* sp. No entanto os manguezais americanos posicionado em Laguna (28° 29 ′ S) e litoral da Louisiana (29 ° 09 ′ N) apareceram apenas em meados e início do século XX (ver, capítulo II e III).

Em relação ao aumento NRM no Antropoceno os testemunhos do Espírito Santo (20° 40' S) indicaram a migração dos manguezais situados em planícies de maré mais baixas para

as mais altas, ocupando planícies arenosas anteriormente dominada por vegetação herbácea (ver, capítulo IV). Análise espaço temporal baseado em imagens de satélite e drone revelou um aumento na área de mangue de 458 ha em 1985 para 470 ha em 2003 e para 479 ha em 2017, com um ganho de 4,6% entre 1985 e 2017. Isto foi registrado no testemunho RBN-2 onde apresentou uma tendência de aumento de pólen de mangue (0 a 60%) e uma tendência decrescente de pólen de ervas (70 a 40%) desde ~ 1955 DC. A razão C/N diminuiu de 27 para 15, enquanto os valores isotópicos de $\delta^{15}N$ aumentaram de 2,6 para 3,7‰, revelando um aumento da influência da matéria orgânica aquática durante o Antropoceno. As análises de XRF indicaram maiores concentrações de elementos típicos de ambiente costeiro (Br, Cl e K). A mesma tendência foi vista no testemunho G-3 no qual apresentou um aumento significativo de pólen de mangue (5 a 60%) e a ausência de pólen de palmeiras desde 1958 DC. Os valores da razão C/N diminuíram de 22,5 para 15 enquanto os valores isotópicos do $\delta^{15}N$ aumentaram de 1,7 para 4,4‰. O testemunho G-4 também apresentou uma tendência de aumento de pólen de mangue (15 a 65%) desde ~ 77 anos cal AP (~ 1870 DC). Os valores da razão C/N e $\delta^{15}N$ apresentaram uma diminuição de 24 para 16 e um aumento de 1,6 para 3,6‰, respectivamente, sugerindo um aumento na influência aquática nos últimos 77 anos cal AP. Essas tendências observadas nos manguezais do Espírito Santo (20° 40' S) devem estar relacionadas ao aumento NRM desde o final da Pequena Idade do Gelo (LIA) e intensificado nas últimas décadas. O aumento da porcentagem e concentração de pólen sugere uma incursão da zona de mangue de planícies de maré mais baixas para mais altas nas últimas décadas (ver, capítulo IV).

Considerando o limite austral dos manguezais americanos, com base nas análises de pólen e datações de ^{14}C e ^{210}Pb, os manguezais de Laguna (28° 29 ′ S) foram estabelecidos sob influência estuarina entre ~ 1957 e 1986 DC, representados por árvores de *Laguncularia* sp. Nas últimas décadas as áreas de manguezais vem se expandindo e sendo ocupadas por árvores/arbustos de *Laguncularia* sp. e *Avicennia* sp. com estatura entre 2 e 11 m. (ver, capítulo III). Essas diferenças na estatura da vegetação de mangue entre os setores da lagoa de Santo Antônio (Laguna, 28° 29 ′ S) podem ser atribuídas às variações de temperatura através de um gradiente de impacto da borda para o interior dessas florestas. As partes internas da lagoa com árvores de mangue mais altas oferecem alguma proteção contra os ventos do inverno. Em contraste, setores mais expostos aos ventos de inverno apresentam baixas

estaturas de arvores de mangue. Estas características geomorfológicas da lagoa controlam o desenvolvimento dos manguezais. Outro fator importante para explicar a diferença de estatura dos manguezais entre os setores da Lagoa de Santo Antônio (Laguna, 28° 29 ′ S) seria diferentes graus de tolerância a temperatura entre as espécies de mangue. Diante disso, plantas de *Spartina* sp. colonizam grande parte do litoral de Santa Catarina e substituem os manguezais nas regiões onde as temperaturas são mais baixas que 5°C (Soares *et al.* 2012). Na Baía de São Francisco do sul (costa norte de Santa Catarina, 26°6' S), os manguezais exibem árvores de *Rhizophora* sp., *Avicennia* sp. e *Laguncularia* sp. (ver, capítulo V) enquanto os manguezais da costa sul de Santa Catarina são representados apenas por *Laguncularia* e com pontuais arbustos de *Avicennia* sp. (ver, capítulo III). Esta distribuição do gênero manguezal ao longo do litoral sul brasileiro deve revelar sua intolerância às baixas temperaturas de inverno, onde *Laguncularia* sp. e *Avicennia* sp. são mais tolerantes às baixas temperaturas do que *Rhizophora* sp. (Duke *et al.* 1998). Em nossa área de estudo na Baía de São Francisco do Sul (costa norte de Santa Catarina) estudos de pólen e datação ^{14}C revelaram que os manguezais se estabeleceram em torno de ~ 1500 anos cal AP representados por *Laguncularia* sp. seguido por *Avicennia* sp. (~500 anos cal AP) e *Rhizophora* sp. apenas no último século. Provavelmente, essa sucessão de gêneros de manguezais foi causada por uma tendência de aquecimento na América do Sul durante o Holoceno tardio e as árvores *de Rhizophora* sp. pelo aquecimento durante o Antropoceno. (ver, capítulo V).

Em relação aos manguezais localizados no litoral da Louisiana registros históricos indicaram a presença de pequenos arbustos de *Avicennia* sp. no início do século XX. A primeira evidência de manguezais no Litoral da Louisiana data o ano de 1900 DC, representados por plantas de *Avicennia* sp. com estatura menor que 0,6 m (Lloyd & Tracy 1901). Atualmente, estudos no litoral da Louisiana reportam a expansão latitudinal de *Avicennia* sp. colonizando áreas que eram anteriormente ocupadas por *Spartina* sp. após duas décadas de invernos quentes (Perry & Mendelssohn 2009). Da mesma forma o trabalho de sensoriamento remoto coordenado por Cohen (2021) indicou um aumento significativo nas áreas (3 ha) e estatura dos manguezais nas últimas décadas (ver, capítulo II).

Portanto, esta tendência em escala continental da migração dos manguezais para zonas temperadas e para planícies de maré mais elevadas desde o século XX pode ser considerada um fenômeno global no qual está relacionada com o aquecimento global e aumento do NRM.

5 CONCLUSÃO

A análise comparativa entre os manguezais tropicais situados no litoral do Espírito Santo (20° 37' S) e subtropicais localizados na costa norte e sul de Santa Catarina (26°6' S e 28° 29 ′ S) e litoral da Louisiana (29 ° 09 ′ N) revelou que esses ecossistemas foram estabelecidos em zonas tropicais no Holoceno médio por conta do aumento do nível do mar. Durante o Holoceno inicial nos atuais limites austrais e boreais dos manguezais americanos, a transgressão marinha transformou ambientes lacustres em lagunas ocupadas por vegetações adaptadas aos ambientes de água salobra no atual limite austral (sul de Santa Catarina, 28° 29 ′ S) e boreal (litoral da Louisiana, 29 ° 09 ′ N) do continente americano. No entanto, não foram identificados grãos de pólen do mangue durante o Holoceno mesmo apresentando condições físico-químicas e hidrodinâmicas adequadas para os manguezais nos seus atuais limites norte e sul. Neste intervalo de tempo os manguezais subtropicais do sul de Santa Catarina e Louisiana tiveram suas planícies de marés ocupadas apenas por marismas representadas principalmente por *Spartina* sp.

Nos últimos 1000 anos oscilações na temperatura associados a eventos climáticos no Holoceno tardio (LIA e MCA) influenciaram na sucessão de gêneros de manguezais na Baía de São Francisco do Sul (costa norte de Santa Catarina, 26°6' S). O aparecimento tardio do gênero de *Rhizophora* sp. no último século em planícies de maré localizada na Baía de São Francisco do sul sugere uma maior intolerância às baixas temperaturas desde gênero quando comparada à *Laguncularia* sp. e *Avicennia* sp., que são mais tolerantes às baixas temperaturas.

Portanto, nossos dados indicam que a elevação do NRM durante o Holoceno inicial e médio no litoral do Espírito Santo foi a principal força que impulsionou o estabelecimento e migração dos manguezais para planícies mais elevadas anteriormente ocupadas por vegetação herbácea. No entanto, embora a tendências de aumento do NRM ser a mesma para a costa tropical e subtropical brasileira, os manguezais subtropicais da Baía de São Francisco do Sul foram estabelecidos apenas em ~1500 anos cal AP sugerindo que o aquecimento global natural do Holoceno causou a expansão do mangue de áreas tropicais para subtropicais no Holoceno tardio. Assim, os manguezais migraram dos trópicos para zonas temperadas na medida que as temperaturas mínimas de inverno aumentaram durante o Holoceno tardio. Os manguezais se estabeleceram no atual limite sul e norte americano apenas início e meado do século XXI, respectivamente. Tal dinâmica foi causada provavelmente pelo aquecimento

global natural do Holoceno e intensificado durante o Antropoceno. Esse processo também causou um aumento do nível do mar que resultou na migração dos manguezais de zonas baixas para novas planícies de maré mais elevadas.

CAPÍTULO II: THE EFFECT OF GLOBAL WARMING ON THE ESTABLISHMENT OF MANGROVES IN COASTAL LOUISIANA DURING THE HOLOCENE

Erika Rodrigues[a]; Marcelo C. L. Cohen[a], Kam-biu Liu[b], Luiz C.R. Pessenda[c], Dilce Rossetti[d], Qiang Yao[b], Junghyung Ryu[b], Adriana de Souza[a]

[a] Laboratory of Coastal Dynamics, Graduate Program of Geology and Geochemistry, Federal University of Pará, Brazil Federal University of Pará. Rua Augusto Corrêa, 01 - Guamá. CEP 66075-110, Belém (PA), Brazil.

[b] Department of Oceanography and Coastal Sciences, Louisiana State University, Baton Rouge, Louisiana 70803, U.S.A

[c] University of São Paulo, CENA/1413 C Laboratory, Av. Centenário 303, 13400-000, Piracicaba, São Paulo, Brazil.

[d] Nacional Space Research Institute (INPE), Rua dos Astronautas 1758-CP 515, CEP: 12245-970, São José dos Campos (SP), Brazil.

* Accepted for publication in Geomorphology

Geomorphology 381 (2021) 107648

Contents lists available at ScienceDirect

Geomorphology

journal homepage: www.elsevier.com/locate/geomorph

The effect of global warming on the establishment of mangroves in coastal Louisiana during the Holocene

Erika Rodrigues [a], Marcelo C.L. Cohen [a,*], Kam-biu Liu [b], Luiz C.R. Pessenda [c], Qiang Yao [b], Junghyung Ryu [b], Dilce Rossetti [d], Adriana de Souza [a], Marianne Dietz [b]

[a] Laboratory of Coastal Dynamics, Graduate Program of Geology and Geochemistry, Federal University of Pará, Brazil Federal University of Pará, Rua Augusto Corrêa, 01 - Guamá, CEP 66075-110 Belém, PA, Brazil
[b] Department of Oceanography and Coastal Sciences, Louisiana State University, Baton Rouge, LA 70803, USA
[c] University of São Paulo, CENA/^{14}C Laboratory, Av. Centenário 303, 13400-000 Piracicaba, São Paulo, Brazil
[d] National Space Research Institute (INPE), Rua dos Astronautas 1758-CP 515, CEP: 12245-970 São José dos Campos, SP, Brazil

ARTICLE INFO

Article history:
Received 15 July 2020
Received in revised form 26 January 2021
Accepted 28 January 2021
Available online 10 February 2021

Keywords:
Anthropocene
Avicennia
Isotopes
Palynology
Port Fourchon

ABSTRACT

Winter temperature and sea-level position are critical factors affecting the global distribution of mangroves and saltmarshes. The replacement of saltmarshes by mangroves is expected due to global warming, reflecting the long-term natural trends in the Holocene and anthropogenic impacts since the 20th century. We documented the Holocene history of wetlands dynamics in the boreal limits of the American mangroves, located at Bay Champagne, Louisiana (USA), by integrating sedimentological, palynological, geochemical (δ^{13}C and C\N), X-ray fluorescence (XRF) data, and radiocarbon chronology from two sediment cores. The results indicated a freshwater lake environment with herbs and wetland ferns, as well as C_3 terrestrial plants, between ~8100 and ~6500 cal yr BP. This environment shifted into a lagoon and saltmarshes having sedimentary organic matter sourced from marine algae between ~6500 and ~1500 cal yr BP. In the final stage, washover sediments were deposited in the lagoon during the last ~1500 cal yr BP. Despite the increased marine influence over the last ~6500 cal yr BP, mangrove pollen were not recorded between ~8100 and ~1500 cal yr BP, suggesting that mangroves were absent in the study area during that time interval. Historical evidence and a comparative analysis of our multi-proxy data with other mangrove studies from the Gulf of Mexico, Caribbean, and eastern South America revealed a gradual mangrove expansion from tropical to subtropical coasts of South and North America during the mid-late Holocene. The mangrove colonies at their current boreal (29° 09′ N) and austral (28° 29′ S) limits were established in the early and mid-20th century, respectively. This mangrove dynamics on a continental scale suggests that the poleward mangrove migration was likely caused by the warming climate during the Holocene. More importantly, the industrial-era warming has likely accelerated the mangrove expansion, but it was not the primary force that drove the mangrove migration into temperate zones.

1. Introduction

Mangroves are perhaps some of the most typical ecosystems of tropical coasts, consisting of valuable and productive intertidal forests (Food and Agriculture Organization of the United Nations, 2007; Ribeiro et al., 2019). The main products and services of mangroves include protection from storms and sea-level rise (Alongi, 2008); plant and animal productivity (Ewel et al., 1998); sources of organic matter for coastal ecosystems (Walsh and Nittrouer, 2004; Dittmar et al., 2006); and sequestration and storage of atmospheric and oceanic carbon, thereby mitigating climate change effects (Fisher and Huo, 2012; Taillardat et al., 2018).

Mangroves are also very useful indicators of climate and sea-level changes (Blasco et al., 1996; Fromard et al., 2004; Alongi, 2008) due to the high susceptibility to variations in air/water temperatures, subsidence, tidal flooding frequency, river discharge, estuarine salinity, and nutrient flux, as well as tropical cyclones intensified by climate changes (Amaral et al., 2006; McLeod and Salm, 2006; Cohen et al., 2012; Krauss et al., 2014; Liu et al., 2014; Alongi, 2015; Yao and Liu, 2017). However, depending on the latitude and proximity of large estuaries, some environmental drivers may operate more intensely in controlling the mangrove dynamics, such as winter temperatures on subtropical zones (Cohen et al., 2020b), and fluvial discharge, for instance, near the Amazon River (Cohen et al., 2012). Regarding the northern and southern limits of American mangroves, the air/water temperature becomes the most critical factor in controlling the establishment, expansion, and contraction of mangroves (Cavanaugh et al., 2018, 2019). This ecosystem cannot develop under low temperatures, and then they occur mainly between latitudes 25° N and 25° S (Giri et al., 2011). Its distribution is limited to zones where the coldest-monthly temperature average is above 20 °C and the annual temperature range is <5 °C (Walsh, 1974;

* Corresponding author at: Federal University of Pará - Brazil, Rua Augusto Corrêa, 01 - Guamá, CEP 66075-110 Belém, PA, Brazil.
E-mail address: mcohen@ufpa.br (M.C.L. Cohen).

https://doi.org/10.1016/j.geomorph.2021.107648
0169-555X/

Chapman, 1975; Duke, 1992). This restriction is associated with mangrove's low tolerance to low air temperature, usually inhibiting at around 5 °C (Tomlinsom, 1986; Stuart et al., 2007; Krauss et al., 2014). A consequence of global warming is that mangroves can expand into temperate zones. Some studies have documented the influence of changes in air temperature in the latitudinal distribution of mangroves (Everitt et al., 1996; Stevens et al., 2006; Perry and Mendelssohn, 2009; Stokes et al., 2010; Osland et al., 2015, 2017, 2018, 2019).

Records of mangrove species on Earth during the Tertiary (Sherrod and McMillan, 1985) and Quaternary (Cannon et al., 2009) revealed that the climate controlled their establishment and extinction in the northern hemisphere (Sun and Li, 1999). Mangrove dynamics is generally associated with global climate and sea-level changes since the Last Glacial Maximum (LGM) (Alongi, 2008). In North America, there were alternations of mangrove expansion and contraction in response to pronounced changes in temperatures over the late Quaternary (Sherrod and McMillan, 1985; Woodroffe and Grindrod, 1991; Sandoval-Castro et al., 2012; Saintilan et al., 2014; Osland et al., 2017), and they were restricted to regions equatorward of their modern limits during the LGM. During this period, mangroves also decreased in Asia and Europe (Woodroffe and Grindrod, 1991; Cannon et al., 2009), being restricted to refuge areas with less impact of cold air temperature (Cannon et al., 2009). However, a poleward expansion was recorded in the Northern Hemisphere after 19,000 years ago (Sandoval-Castro et al., 2012; Kennedy et al., 2016). In the Caribbean, mangrove northern limit retreated to more equatorial zones during the Pleistocene (Sherrod and McMillan, 1985). As a result of warmer climates and higher sea levels during the Holocene, mangroves expanded poleward, reaching Florida (Yao and Liu, 2017), Texas (Sherrod and McMillan, 1985), and Louisiana (McKee and Vervaeke, 2018) at different times.

According to pollen and isotopic studies from the South China Sea, mangroves would have replaced boreal forests and temperate grasslands due to a slight increase in air temperature and slow marine transgression at ~14,000 cal yr BP (Sun and Li, 1999). Meanwhile, mangroves were not recorded in North America or Europe, probably due to the low temperatures (Sherrod and McMillan, 1985).

The increased winter temperatures during the last century (IPCC, 2014), mainly in boreal and temperate regions (Solomon et al., 2007), caused a mangrove expansion in the Gulf of Mexico (Cavanaugh et al., 2014), resulting in the replacement of salt marsh vegetation dominated by *Spartina alterniflora* (Sherrod and McMillan, 1985).

The ecological implications of global warming to the new biogeography of ecosystems adapted to tropical areas in the near future can be studied by reconstructing the long-term dynamics of mangroves, mainly along the northern and southern mangrove limits in the Americas. As such, a stratigraphic analysis of mangroves relative to sea-level and climate changes during the Holocene must be provided from various coastal environments to permit an inter-regional comparison. This work aims to discuss the influence of sea-level changes and global warming on American mangroves during the Holocene. We studied the Holocene changes in coastal depositional paleoenvironments, and the dynamics of temperate vegetation and mangroves in southern Louisiana, USA, representing the modern boreal limit of the American mangroves, by the integration of sedimentological, palynological, geochemical ($\delta^{13}C$ and C\N), X-ray fluorescence (XRF) data, and radiocarbon chronology. These data are essential to evaluate and calibrate models that predict the fate of mangroves as the minimum winter temperatures continue to increase (Cavanaugh et al., 2014, 2015, 2018).

2. Study area

2.1. Geomorphology

The Caminada-Moreau Headland is a complex mosaic of barrier islands formed by the transport of sediments by wind, waves, and tidal and longshore currents (Kulp et al., 2005). The study area in Bay

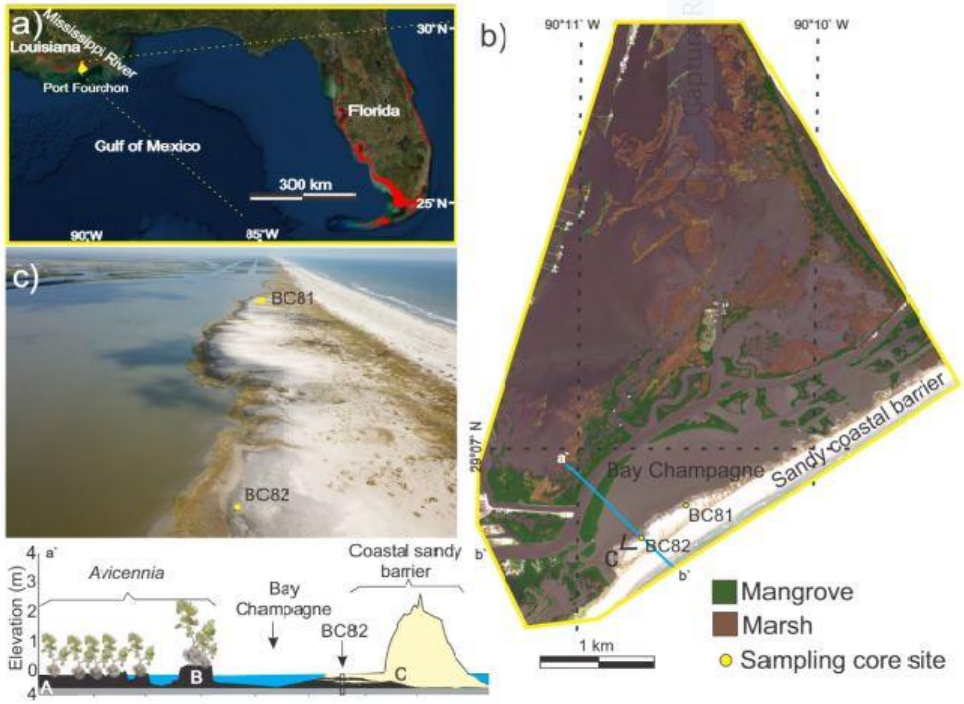

Fig. 1. a) Location of the study area, b) vegetation map with a stratigraphic profile (a'–b') exhibiting vegetation, geomorphology, and the facies associations, c) drone image showing the coring sites along a sandy coastal barrier.

Champagne (29° 6′ 53, 10″ N/90° 10′ 33, 38″W, Fig. 1) is located in the southwestern end of this headland, near Port Fourchon in the State of Louisiana. This site is part of the Lafourche complex delta lobes, formed ~3500 years ago, and remained active until 1600 to 600 cal yr BP. During this time, nutrient-rich sediments were deposited in floodplains along tributaries, contributing to establishing wetland systems across subdeltas (Blum and Roberts, 2012).

Bay Champagne (BC) is a semi-circular brackish lagoon (salinity: 32‰) (Fig. 1b, and c), with a maximum depth of 2.5 m (Liu et al., 2011). The lagoon is surrounded by cordgrass (*Spartina alterniflora*) and black mangrove (*Avicennia germinans*) vegetation (Naquin et al., 2014). A sandy barrier, standing ~2 m above the mean relative sea-level, partially protects the backbarrier tidal flat wetlands from the impact of high energy waves and storm-forced winds (Dietz et al., 2018). Local barrier islands, including the Timbalier Island and Grand Isle (Shea Penland, 1988), are strongly affected by erosion due to overwashing (Liu et al., 2011; Dietz et al., 2018). In addition, the decadal historical record from Bay Champaign indicates rapid shoreline retreat and coastal erosion in this area, especially during active periods of hurricanes, exacerbating the long-term trend of coastal subsidence and land loss (Dietz et al., 2018). A re-nourishment project was initiated in 2012 and completed in 2014 (Coastal Engineering Consultants, 2015), attempting to interrupt the rapid shoreline retreat process and sustain barrier beaches along the Caminada-Moreau headland (Jafari et al., 2018).

The coastal region in southern Louisiana is especially vulnerable to global climate change (Dietz et al., 2018; Johnson et al., 2020), resulting from the Holocene sea-level rise (Kjerfve, 1994). Traditional models have indicated a sea-level 3 to 4 m below present at 6000 years BP, followed by a rise to 1.5 m below present at 5000 BP (Saucier, 1994).

2.2. Physiography

The climate in the study area is humid subtropical, with mean monthly temperatures between 6 °C and 30 °C. The mean precipitation is about 1600 mm/year, with the wetter season from June to September and the drier season from September to June (National Climatic Data Center, 2018). During the last two centuries, the Louisiana coast has been subjected to climatic anomalies (Mock et al., 2007; Perry and Mendelssohn, 2009). The Louisiana coast is frequently affected by severe weather phenomena, including hurricanes, heavy rainfall, flooding, drought, heatwaves, and freezing events (Vega, 2012). Beach fronts and dunes along the Caminada coast support salinity tolerant vegetation, especially graminoid such as cordgrass (*Spartina alterniflora*), sea oats (*Uniola paniculata*), and bitter panicum (*Panicum amarum* var. *amarum* '*Fourchon*'). Cordgrass is found on active overwash deposits (Brantley et al., 2014). Trees and shrubs are mainly represented by wax myrtle (*Myrica cerifera*), iva (*Iva imbricate*), vine (*Lycium barbarum*), eastern baccharis (*Baccharis halimifolia*), and black mangroves (*Avicennia germinans* L.) (Henry and Twilley, 2013). After the restoration project (Coastal Engineering Consultants Inc., 2015), the Caminda coastline has been used for vegetative plantations, including various native dune grass species. Data about the modern American mangrove distribution were obtained at http://data.unep-wcmc.org/datasets/4.

3. Materials and methods

3.1. Remote sensing

The spatial analysis was developed with high-resolution images obtained by the drone Phantom 4 Advanced DJI. This drone had a FC 6310 digital 4K/20MP (RGB), which provided images of high spatial resolution (2.6 cm) of the study area. The drone images were processed using the Agisoft Metashape Professional version 1.6.2 software. The vegetation was visually classified by photointerpretation using various tools in the Global Mapper Software 19. Details about the image processing may be obtained in Cohen et al. (2020a, 2020b).

3.2. Sampling and facies description

Two sediment cores (BC81 - 2,75 m, 29° 6″ 53,10″ N/90° 10′ 33,38″W and BC82 - 4 m, 29° 6″ 48,88′ N/90° 10′ 40,83″ W) were acquired via an aluminum push corer at the southern margin of the BC lagoon (Fig. 1b and c). The cores were measured and photographed in the field and kept in a cold room (4 °C) at Louisiana State University. Grain size analysis (5 cm intervals) was determined by laser diffraction in the Laboratory of Chemical Oceanography of the Federal University of Pará UFPA (Brazil).

Sedimentary features, such as color, texture, lithology, and structure, were used to characterize the facies (Harper, 1984; Walker, 1992). The code of sedimentary facies was based on Miall (1978). The facies, pollen, isotopes, and elemental analyses were grouped into facies associations to determine a sedimentary environment (Reading, 1996). Cluster analysis of pollen grains supported the grouping of the facies associations.

3.3. LOI and XRF data

Loss-on-ignition (LOI) analysis was performed at 1 cm intervals. It involved heating sediment samples at 105°, 550°, and 1000 °C to determine the contents of water, organic matter, and carbonates, respectively. XRF analysis was performed by scanning the core at 2 cm intervals using a handheld Innov-X Delta XRF. Only the major chemical elements in coastal sediments (ppm) representative of marine (e.g. Br, Ca, Cl, and Sr) and terrestrial (e.g. Fe, Ti, and Mn) origins were selected for this analysis (Yao et al., 2015).

3.4. Palynological analysis

The cores were sub-sampled at intervals of 5 cm, whereby 1 cm^3 of sediment was removed for pollen analysis. Before the sediment processing, one tablet of exotic *Lycopodium* spores was inserted into each sample to calculate the pollen concentration (grains/cm^3) and pollen accumulation rates (grains/cm^2/year). Sediment samples were treated following traditional pollen analytical procedures, using hydrochloric acid, hydrofluoric acid, and acetic anhydride/sulfuric acid (Faegri and Iversen, 1989). The product of this treatment was fixed on slides in a glycerin gelatin medium. Pollen and spore morphology books were used as references (McAndrews et al., 1973; Willard et al., 2004), as well as the collections of the LSU Global Paleoecology Lab. A minimum of 300 pollen grains were counted for each sample. The total pollen sum did not include fern spores, algae, and foraminifers. Pollen diagrams are presented as percentages of the total pollen sum. The taxa were categorized into: herbs, trees and shrubs, and aquatics. Cluster analysis and pollen diagram plotting were processed by the software TILIA (Version 1.7.16) (Grimm, 1990).

3.5. Isotopic analysis and radiocarbon dating

The isotopic composition ($\delta^{13}C$) of modern organic matter was analyzed from 134 samples (6–50 mg) taken at 5 cm intervals along the two cores. The stable carbon isotopes were determined at the Stable Isotopes Laboratory of the Center for Nuclear Energy in Agriculture (CENA/USP), using an ANCA SL2020 mass spectrometer (see further details in Pessenda et al. (2004)). Five sediment samples (~2 g each) were used for radiocarbon dating. The samples were physically cleaned using a microscope to prevent natural contamination at ^{14}C Laboratory of CENA (Pessenda et al., 2004). The organic matter was chemically processed by treating with 2% HCl at 60 °C over 4 h, washed with distilled water, and dried (50 °C) to eliminate young organic fractions (fulvic and/or humic acids) and carbonates (Pessenda et al., 2010, 2012). The sediment organic matter was analyzed by Accelerator Mass Spectrometry (AMS) at the ^{14}C Laboratory of CENA/USP, LACUFF (Fluminense Federal University, Brazil), and Center for Applied Isotope Studies (UGAMS) of the University of Georgia. Radiocarbon ages are reported in years before

Table 1
Samples of sedimentary organic matter selected for radiocarbon dating and results with code site, laboratory number, depth (m), ^{14}C ages (yr BP, 1σ), calibrated ages (cal. yr BP, 2σ deviation), sedimentation rate and median of calibrated ages (cal. yr BP).

Sediment core	Code site and laboratory number	Depth (m)	Ages (^{14}C yr BP, 1σ)	Ages (cal. yr BP, 2σ deviation)	Sedimentation rate (mm/yr)	Median of calibrated ages (cal. yr BP)
BC81	UGAMS-34381	170	2150 ± 20	2096–2160	0.76	2128
BC82	UGAMS-34379	170	1580 ± 20	1412–1528	1.1	1470
BC82	LAC 190456	300	5766 ± 48	6406–6645	0.26	6525
BC82	LAC 190457	350	5621 ± 48	6286–6454-		6370
BC82	UGAMS-34380	400	7330 ± 30	8035–8191	0.6	8113

1950 CE (yr BP). The radiocarbon ages were normalized to $\delta^{13}C$ of −25‰VPDB, and are presented in cal yr BP, with a precision of 2σ (Reimer et al., 2013).

4. Results

4.1. Radiocarbon ages and sedimentation rates

Radiocarbon ages and sedimentation rates are provided in Table 1. The ages recorded ranged from 8113 to 1470 cal yr BP (Figs. 2 and 3). Partial age inversions were observed between 350 (6286–6454 cal yr BP) and 300 cm (6406–6645 cal yr BP) (Fig. 3). It can be attributed to high sedimentation rates and/or reworking of organic remains by storms or bioturbation by benthic organisms (Pessenda et al., 2012). The sedimentation rates (0.2 to 1 mm/yr) were within the range recorded in other cores sampled from tidal flats in the Gulf of Mexico (Naquin et al., 2014; Yao et al., 2015). The sedimentation rates in the muddy segment (400–170 cm) of core BC82 were lower (0.6 and 0.26 mm/y) than in the sandy intervals (170–0 cm) of this core (1.11 mm/yr) and core BC81 (0.77 mm/yr) (Figs. 2 and 3).

4.2. Facies description

Three facies associations were recognized in the studied cores (Figs. 4, 5, and Table 2). Facies association A consisted of massive sand (facies Sm) and massive mud (facies Mm), related to a lacustrine environment. Facies association B consisted of lenticular and flaser heterolithic bedded deposits of facies Hl and Hf, respectively, related to a lagoonal environment. Facies association C, which included massive sand (Sm), and flaser heterolithic deposits (Hf), was attributed to washovers. These environments were interpreted based on the integration of sedimentary features with pollen, isotopic, C/N, LOI, and XRF data, as described in the following.

4.2.1. Facies association A (lacustrine)

This facies association was represented by the 400–310 cm interval of core BC82, accumulated between ~8100 and ~6500 cal yr BP. It was characterized by massive mud (Mm) and lenticular heterolithic bedded deposits (Hl; 40–80% silt, 20–60% clay), ranging in color from dark brown (2.5/110Y) to dark gray (3/1 10Y). This facies association contained ~4% of carbonate and ~7% of organic matter. Two ecological groups characterized by herbaceous (25–65%) and tree and shrub pollen (30–55%) were present. The herbaceous taxa were predominantly composed of Amaranthaceae (0–20%), Asteraceae (0–18%), Poaceae (0–12%), *Amaranthus* (0–5%), and *Artemisia* (0–4%). Arboreal taxa were mainly represented by *Pinus* (0–35%), Fagaceae (0–3%), *Betula* (0–1%), and *Quercus* (0–1%). Fern pollen mainly consisted of Polypodiaceae (Fig. 3). XRF analysis indicated the highest concentration of Fe (14 k–20 k ppm), K (8 k–13 k ppm), Ti (1.5 k–2 k ppm), and Mn (370–800 ppm), while the values for Cl (3.5 k–12 k ppm), Ca (5.3 k–8.6 k ppm), Br (184–248 ppm), and Sr (63–98 ppm) were the lowest.

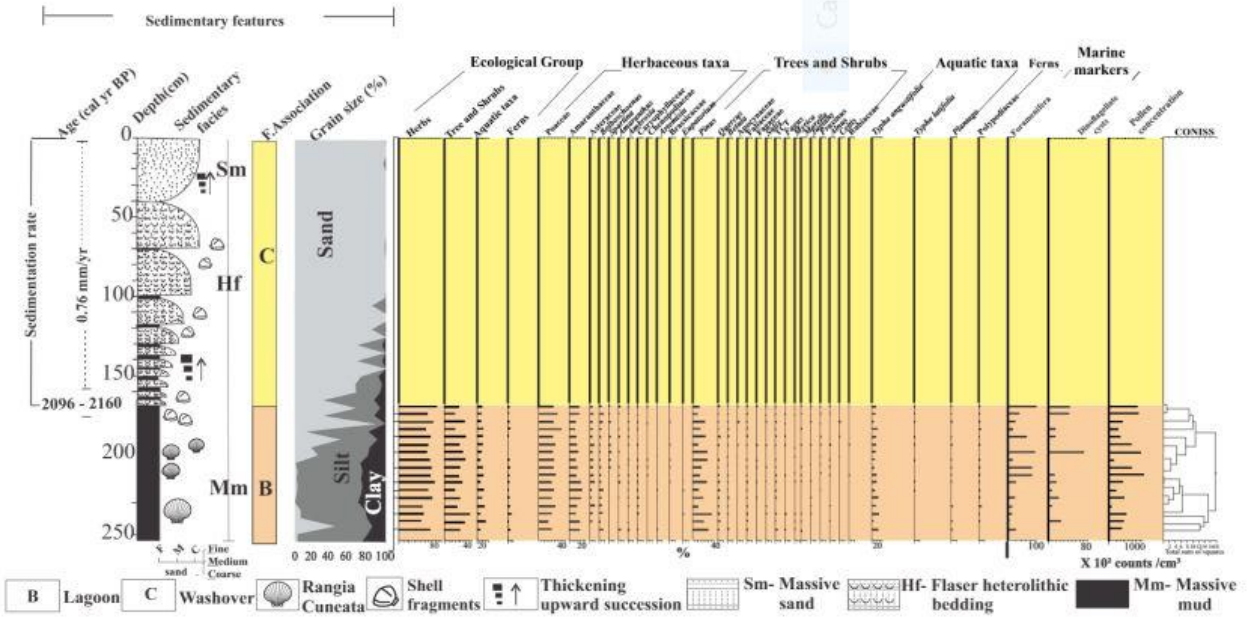

Fig. 2. Stratigraphy of core BC81 exhibiting sedimentary characteristics, facies associations, and pollen data with percentages of the ecological groups. Pollen diagrams are presented as percentages of the total pollen sum.

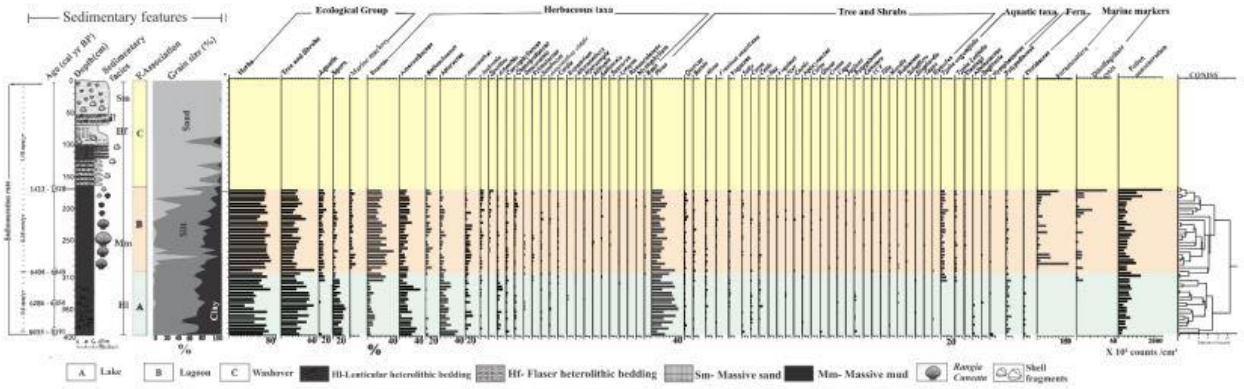

Fig. 3. Stratigraphy of core BC82 exhibiting sedimentary characteristics, facies associations, and pollen data with percentages of the ecological groups. Pollen diagrams are presented as percentages of the total pollen sum.

$\delta^{13}C$ values oscillated between −24.4‰ and −22.02‰ ($\bar{x} = -24$‰), while the C/N ratio alternated between 12 and 52 ($\bar{x} = 25$) (Fig. 5).

4.2.2. Facies association B (lagoonal)

This facies association was evidenced in cores BC81 (270–170 cm) (Figs. 2 and 4), and BC82 (300–170 cm) (Figs. 3 and 5). The sediments were accumulated between ~6525 and ~1470 cal yr BP in core BC82 and up to ~2128 cal yr BP in core BC81. They consisted of dark gray (4/1 10Y) massive mud (Mm) and lenticular heterolithic bedded deposits (Hl; 0–80% sand, 15–80% silt, 5–60% clay). This facies association contained ~4% of carbonate and ~7% of organic matter. The bivalve *Rangia cuneata* was present in life position. The palynological analysis permitted the identification of three ecological groups, represented by pollen of herbs (50–70%), trees and shrubs (20–55%) and aquatic plants (2–10%), in addition to marine markers, such as dinoflagellate cysts and foraminifera. Herbs were mainly represented by Poaceae (0–25%), Amaranthaceae (0–14%), Asteraceae (0–6%), *Amaranthus* (0–4%), *Ambrosia* (0–4%), *Bolboschoenus* (5%), Caryophyllaceae (2%), *Spartina* (0–3%) and Chenopodiaceae (0–2%). Arboreal pollen included mainly *Pinus* (0–20%), *Quercus* (0–3%), *Betula* (0–3%), and *Alnus* (0–2%). The group of aquatic plants was predominantly composed of *Typha angustifolia* (0–14%) and *Typha latifolia* (0–3%) (Figs. 2 and 3). *Typha angustifolia* disperses as a reticulate, monoporate monad pollen (22.7 ± 2.6 μm) (Fig. 1a and b, supplementary material), and *Typha latifolia* is reliably represented in the pollen record as perforate-reticulate, tetrads pollen (25.70 ± 1.58) (Finkelstein, 2003; Hamdi et al., 2010; Skvarla and Larson, 1963) (Fig. 1c and d, supplementary material). XRF results revealed an increasing trend in Cl (3 k–20 k ppm) and Br (190–950 ppm) and a decreasing trend in Fe (7 k–17.5 k ppm) and Mn (186–500 ppm) compared to facies association A. Facies association B presented more enriched $\delta^{13}C$ values (~ −22‰) than the facies association A (~−24‰). C/N values decreased upward from ~25 to ~11 within this association (Figs. 4 and 5).

4.2.3. Facies association C (washover)

These deposits were identified in both studied cores in the interval 170–0 cm, formed during the last ~1470 cal yr BP (170–0 cm) and ~2100 cal yr BP in the cores BC82 and BC81, respectively. The cores consisted of dark gray (4/1 10Y) flaser heterolithic bedded deposits (facies Hf; 60–100% sand, 0–40% silt, 0–10% clay); sandy layers were cross laminated. The upper part of facies association A was characterized by massive sand (Sm; 14% coarse, 73% medium, 13% fine); grain size increased gradually upward in this sandy facies. Shell fragments were frequent in this association. The carbonate concentration oscillated between 4 and 20%, while the organic matter decreased upward from 4 to 2%. A wide range of variation was recorded for the concentrations of Ca (2.7 k–130 k ppm), Sr (100–572 ppm), Zn (0–46 ppm), and Zr (44–422 ppm). The concentration of Ti (270–1134 ppm), and Fe (2100–7200 ppm) also varied largely, but with values that were lower than in facies associations A and B. $\delta^{13}C$ and C/N values oscillated between −20 and −27‰ and 3 and 28, respectively. No pollen grain was found in this facies association (Figs. 4 and 5).

5. Discussion

The sampling sites are accumulating washover sediments at present (Fig. 1b and c). These sites were chosen due to their position in the central

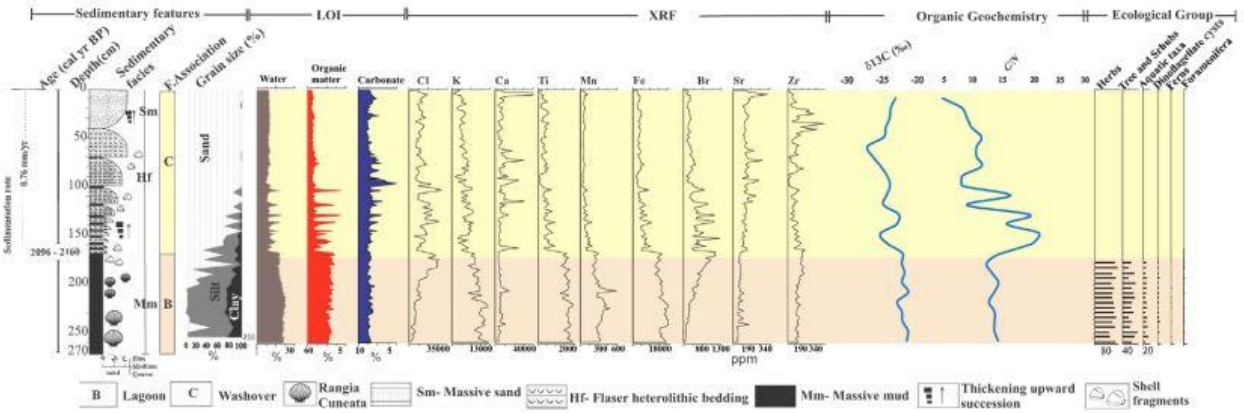

Fig. 4. Summary of core BC81, presenting sedimentary characteristics, pollen ecological groups, and geochemical data.

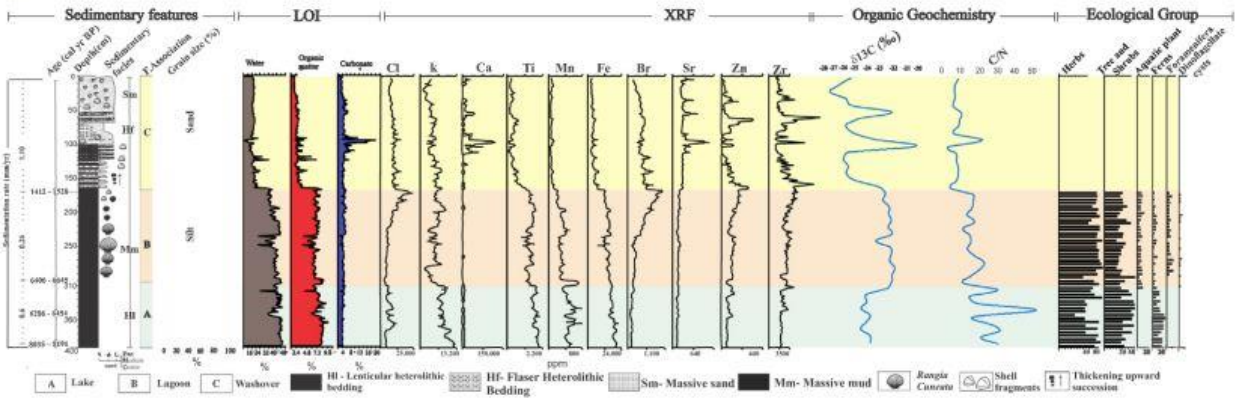

Fig. 5. Summary of core BC82, presenting sedimentary characteristics, pollen ecological groups, and geochemical data.

portion of an old lake (Fig. 7), with the potential to preserve the oldest lacustrine records. Depositional environments with a predominance of sandy sediments are not suitable for preserving pollen grains (Havinga, 1967). However, such environment may have evolved from an environment with low hydrodynamic flow that was favorable for the muddy (silt and clay) sedimentation (Reineck and Singh, 1980; Reading, 1996) and suitable for pollen preservation, as indicated by several pollen studies in tidal flats (Behling et al., 2001, 2004; Cohen et al., 2005a, 2005b, 2012, 2020b; Guimarães et al., 2013; Moraes et al., 2017; Ribeiro et al., 2018), fluvial flood plains (Cohen et al., 2014a, 2014b, 2014c, 2020a; Fontes et al., 2017; Lima et al., 2017; Silva et al., 2018), lagoons (Cohen et al., 2020b, 2016; França et al., 2016), and lakes (Lara and Cohen, 2009; Smith et al., 2011; Buso Junior et al., 2013). For example, oxbow lakes, developed after a channel abandonment, can be filled by muddy sediments and converted into a fluvial terrace or an active channel with sandy deposition (Cohen et al., 2014c; Rossetti et al., 2014). In the case of the study area, evidence based on facies association indicated the development of a lake (~8100 to ~6500 cal yr BP), which subsequently evolved into a lagoon (6500–1470 cal yr BP). Relatively high pollen concentrations (50 k–200 k pollen grains/cm^3, Figs. 2 and 3) in the sediments from this period suggested that the land around the lake and lagoon was well-vegetated. Gradually over the last ~1470 cal yr BP, this coastal lake and lagoon at the coring site has been filled by washover sandy sediment, which was not conducive to retention and preservation of pollen.

5.1. Depositional phases

5.1.1. Early Holocene (~8100 to ~6500 cal yr BP): lacustrine

The prevalence of muddy deposits in facies association A (i.e., basis of core BC82, 400–310 cm) indicates a low energy depositional environment, most likely a freshwater lake. The $\delta^{13}C$ and C/N, ranging from −24.4 to −22.02‰ and 12 to 52 respectively, recorded in these deposits support that C3 terrestrial plants were the source for the sedimentary organic matter (C3 plants $\delta^{13}C$: −32‰ to −21‰ and C/N: >12; Deines, 1980; Meyers, 1994; Tyson, 1995). The concentrations of K, Ti, Fe, and Mn in facies association A were compatible with values recorded in environments with a high input of terrestrial sourced sediment (Cuven et al., 2013; Yao et al., 2018). The presence of arboreal pollen from *Pinus*, *Quercus*, Fagaceae, and *Betula*, as well as herbs (mainly represented by Asteraceae and Amaranthaceae) and wetland ferns (represented by Polypodiaceae), conforms with a freshwater, terrestrial setting. Altogether, these characteristics are taken as evidence of a lacustrine environment for facies association A. The inferred lake developed in the study area during the early Holocene when the sea-level was ~8 m below the modern sea-level (Donoghue, 2011) (Fig. 7).

5.1.2. Mid-late Holocene (~6500 to ~1470 cal yr BP): lagoonal

This phase is recorded by facies association B, which is lithologically similar to the lacustrine deposits characterized by the prevalence of muddy components (facies Mm and Hl) indicating low energy environments. However, the presence of the bivalve *Rangia cuneata* attests to a connection to marine waters, as this species is typical of brackish water environments (Tarver, 1972; Warzocha et al., 2016). This bivalve, native to the Gulf of Mexico (Benson, 2010), has often been used to indicate marine influence during the Holocene (Rodriguez et al., 2004; Wakida-Kusunoki and MacKenzie, 2004). Accordingly, we interpret facies association B to represent a lagoon. The slight enrichment of $\delta^{13}C$ values in facies association B (~−22‰) compared to the lacustrine deposits (−24‰), and the decreasing C/N values from ~25 to ~9, suggest the contribution of marine organic matter ($\delta^{13}C$: −24‰ to −16‰ and

Table 2
Characteristics of the three facies association.

Facies association	Facies description	Ecological group	Geochemical data	Elements predominance (ppm)	Interpretation
A	Lenticular heterolithic bedding (facies Hl)	Herbs, tree/shrubs, and ferns	$\delta^{13}C = -24.4$ to −22‰ C/N = 12–2	Fe: 14 k–20 k K: 8 k–13 k Ti: 1.5 k–2 k Mn: 370–800	Lake
B	Massive mud (facies Mm) with *Rangia cuneata*	Herbs and aquatic plants from brackishwater. Foraminifera/dinoflagellate	$\delta^{13}C = -23$ to −21‰ C/N = 6–22	Cl: 3 k–20 k Br: 190–950 Fe: 7 k–17.5 k Mn: 186–500	Lagoon
C	Flaser heterolithic bedding (Hf), massive sand (Sm) with shell fragments	No pollen/ferns	$\delta^{13}C = -27$ to −20‰ C/N = 5–20	Cl: 6 k–24 k Ca: 2.7 k–130 k Br: 230–1200 Sr: 100–572 Zr: 44–422	Washover

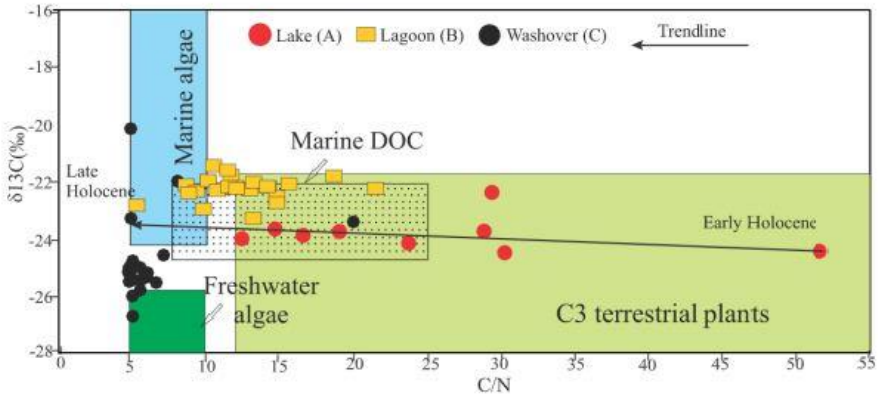

Fig. 6. Binary diagram showing the source of the sedimentary organic matter for each sedimentary facies associations based on the relationship between $\delta^{13}C$ and C/N.

C/N: <10; Deines, 1980; Meyers, 1994; Tyson, 1995) (Fig. 6), as expected in a lagoon. The upward increase of Cl (from 4 k to 13 k ppm) and Br (from 264 to 950 ppm) and decrease of Fe (from 16 k to 11 k ppm) and Mn (from 400 to 200 ppm) are also indications of a coastal environment with marine influence and lower input of terrestrial sediments. The pollen assemblage, marked by the increased abundance of brackishwater herbaceaous (*Bolboschoenus*, *Spartina*) and brackishwater aquatic (*Typha angustifolia* and *Typha latifolia*) plants, is further consistent with the inferred lagoon environment. The aquatic macrophyte cattail (*Typha*) can tolerate environments with high salinity (Hameed et al., 2012; Akhtar et al., 2017) and variation in water level (Ladislas et al., 2012). Paleoecological studies in brackish lagoonal deposits from Mexico also indicated the establishment of *Typha* ~6000cal yr BP (Caballero et al., 2005). In addition, the occurrence of foraminifera and dinoflagellate cysts in this stratigraphic unit is further evidence for a marine-influenced environment, such as a lagoon.

5.1.3. Late Holocene (last ~1470 cal yr BP): shoreline retreat

This phase is recorded by facies association C, whereby the muddy deposits changed abruptly upward into heterolithic mud/sand and massive sand. It represents the modern washover sediments that are deposited inland of a beach by overwash. Overwash is the flow of water and sediment over the beach's crest that does not return to the water body. Coastal overwash is mainly caused by hurricanes and winter storms along the Atlantic and Gulf Coasts of the United States (Liu, 2004; Donnelly et al., 2006). This sedimentary succession may reflect the gradual landward migration of sandy coastal barriers due to marine transgression (Fig. 7). This interpretation is based on the increased marine influence with respect to the lagoon deposits of the previous phase. This is evidenced by the lower input of terrestrially-sourced sediments evidenced by the decreasing trend of Ti (1700 to 400 ppm), Fe (from 12 k to 2 k ppm), and Mn (from 230 to 75 ppm) and strong oscillations of Ca (2 k–129 k ppm), Cl (5.6 k–24 k ppm), Sr (100–572 ppm), Br (230–1200 ppm), Zn (0–46 ppm), and Zr (44–422 ppm). High Zn and Zr values are found in the sand fraction. Then, probably, oscillations of Zn and Zr values indicated phases of rock weathering carried by the action of the currents and tides and deposited as beach sand. Ca, Cl, Br, and Sr are constituents of biogeochemical cycling in marine systems (Yao and Liu, 2017; Joe-Wong et al., 2019). The significant decrease in C/N values, from ~10 to ~6, with respect to the lagoonal phase, and the $\delta^{13}C$ values, between −20‰ and −27‰, are consistent with this interpretation (marine algae, $\delta^{13}C$: −24‰ to −16‰ and C/N: <10) (Deines, 1980; Meyers, 1994; Tyson, 1995) (Fig. 6). Local oscillations of these values that were synchronized with Ca, Sr, Zn, and Zr peak concentrations are probably a result of storm events, since this coastline is notably affected by intense hurricanes and tropical storms (Dietz et al., 2018; Johnson et al., 2020).

5.2. Absence of mangrove pollen along the cores

The analyzed cores did not contain mangrove pollen grains, despite the dense occupation of *Avicennia* trees around the lagoon nowadays. Noteworthy is that lakes, lagoons, tidal flats, and fluvial floodplains present suitable hydrodynamic conditions for muddy sedimentation with pollen derived from plants that lived at the times the sediments were deposited. Under this situation, lagoonal and lacustrine sediments preserve pollen grains transported by wind and from the flora surrounding the lake or lagoon. The spatial representation of lagoonal or lacustrine pollen records changes according to the wind intensities and the watershed area influencing the lake or lagoon (Cohen et al., 2008, 2014c). In addition, the pollen percentage of each vegetation unit is distance-weighted, where the closer to the source, the greater the pollen signal from that plant (Davis, 2000; Xu et al., 2012). Thus, pollen accumulated in lagoon or lake sediments presents a wider spatial representation of the regional flora than tidal flats sediments. Pollen rain in tidal flats, mainly occupied by dense mangrove forests, should indicate local vegetation, while open canopy tends to present a higher proportion of long distance transport pollen rain (Weng et al., 2004; Gosling et al., 2009).

Considering the pollen grains can be transported by wind and currents mainly in open areas (Brush and Brush, 1972; Solomon et al., 1982; Weng et al., 2004), it is common to record <1% pollen grains that do not represent the local vegetation during the sediment accumulation. For instance, a core taken from a marsh in southwestern Louisiana revealed one or two *Avicennia* pollen grains in the 0, 210, and 280 cm depth, probably transported by currents or hurricanes (Yao et al., 2020). By contrast, cores taken from tidal flats occupied by mixed mangroves with *Rhizophora*, *Laguncularia*, and *Avicennia* in Florida contained pollen percentages of 30–60% of *Rhizophora*, 5–20% of *Avicennia*, and 5–15% of *Laguncularia* (Yao et al., 2015; Yao and Liu, 2017). The lagoon and tidal flat sediments covered by *Avicennia* trees in Bay Champagne, the study area, accumulate between 6 and 9% of *Avicennia* pollen (Ryu, 2020). In Amazonian mangroves, pollen traps installed on tidal flats occupied only by *Avicennia* trees present ~15% (~540 grains/cm^2/yr) of *Avicennia* pollen (Behling et al., 2001). Accumulation rates of *Avicennia* pollen are also relatively elevated in a mangrove with *Rhizophora* and *Avicennia* trees (average 450 grains/cm^2/yr). Even in mangroves dominated by *Rhizophora*, pollen grains of *Avicennia* may be found (average 120 grains/cm^2/yr) (Behling et al., 2001). In addition, *Avicennia* pollen grains have been found in thousands of stratigraphic pollen spectra obtained from cores sampled from the American coasts with *Avicennia* trees (e.g. Cohen et al., 2005a, b, 2009, 2012, 2014a, b, c, 2015, 2016; Vedel et al., 2006; Peros et al., 2007; Guimarães et al., 2011, 2013; Smith et al., 2011, 2012; França et al., 2014, 2016, 2019; Yao et al.,

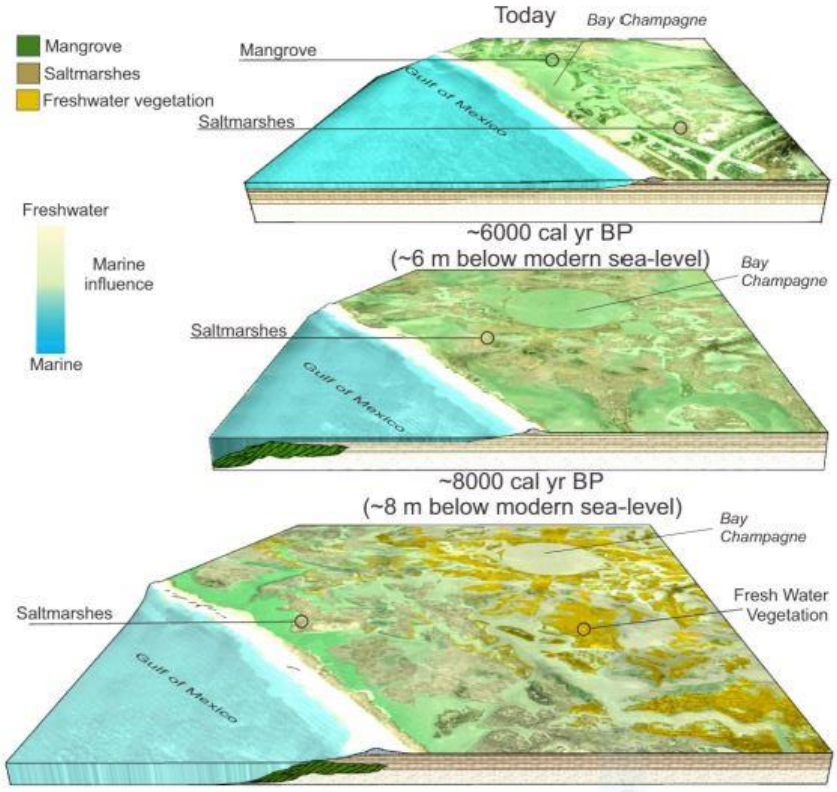

Fig. 7. Model of the geomorphology and vegetation development under the Holocene relative sea-level rise.

2015; Yao and Liu, 2017; Moraes et al., 2017; Ribeiro et al., 2018; Cordero-Oviedo et al., 2019; Jones et al., 2019).

These data suggest that sediments accumulated in tidal flats or lagoons with *Avicennia* or near *Avicennia* trees tend to have a significant *Avicennia* pollen representation. Therefore, the absence of *Avicennia* pollen grains in the sedimentary sequences formed during the lake (8100–6500 cal yr BP) and lagoon (6500–1470 cal yr BP) phases in our cores (Figs. 2 and 3) suggests that mangroves with *Avicennia* trees were absent at or near our study site during the Holocene.

The absence of mangroves in the modern northern limit of American mangroves between ~8100 and ~1470 cal yr BP is an important finding that contributes significantly to the discussions about the main forces driving the mangrove establishment on the American continent during the Holocene, as well as its poleward expansion in the Anthropocene (since the mid-twentieth century (Zalasiewicz et al., 2018)). Nevertheless, it is necessary to assess the effects of sea-level rise on the studied coastal vegetation and morphology, since the salinity gradients along the zones under marine or estuarine influence need to be conducive to mangrove development (Lara and Cohen, 2006).

5.3. American mangrove establishment controlled by sea-level

Mangroves colonized the distal portion of the continental shelf during the Last Glacial Maximum (LGM) (~27 and ~20 k cal yr BP) due to the worldwide lowering of the eustatic sea-level (Murray-Wallace, 2007; Cohen et al., 2014a, 2014b, 2014c). The continental shelf emerged almost completely, positioning the coastline at some sites ~100 km of its current location (Nittrouer et al., 1996; Clark et al., 2009; Harris et al., 2013). After the LGM low sea-level, melting ice sheets caused transgression between 16 and 4 ka in many areas of southern North America (Gischler, 2015) and, probably, a landward mangrove migration along the continental shelf (Cohen et al., 2012, 2014b). A rapid relative sea-level rise was recorded on the eastern coast of South America during the early-middle Holocene. The sea-level in southeastern and northeastern Brazilian coast was between 5 and 1 m above the modern sea-level, at approximately 5500 cal yr BP, with a gradual fall during the middle to late Holocene (Angulo et al., 2006, 2016; Caldas et al., 2006; Lorente et al., 2013; Cohen et al., 2020a). Sea-levels comparable to the modern one were already reached between 6000 and 5000 cal yrs BP in the northern Brazilian coast (Cohen et al., 2005b, 2012). Several works have attributed the mangrove establishment in the middle Holocene along the tropical coasts to the lower rates of sea-level rise or a stable sea-level in the middle Holocene (Woodroffe et al., 1985, 2015; Toscano and Macintyre, 2003; Khan et al., 2017; Ribeiro et al., 2018; Cohen et al., 2020a) (Fig. 8). Then, mangroves were established in the tropical Brazilian littoral at ~7000 cal yr BP: Espírito Santo (19° S), Bahia (17° S), Rio Grande do Norte (5° S), Pará (1° S), and Amapá (2° N) (Cohen et al., 2012, 2014a, 2014b, 2020a; Pessenda et al., 2012; França et al., 2013, 2015; Fontes et al., 2017; Ribeiro et al., 2018).

Similarly, transgressive events were also recorded in the northern Gulf of Mexico (Anderson and Fillon, 2004), with a high sea-level rise rate of 7.4 ± 0.7 m/ka in the early Holocene, and a reduced rate of 2.3 mm/yr in the middle to late Holocene (Wanless et al., 1994; Khan et al., 2017). The relative stability of modern coastal systems along the Gulf of Mexico is primarily due to the stabilization of sea-level approximately 6000 years ago (Donoghue, 2011). Blum et al. (2002) proposed that the middle Holocene sea-level along the Texas Gulf coast was at −9 m at ca. 7.8 ka, then rose rapidly to +2 m by ca. 6.8 ka. However, according to Khan et al. (2017), the relative sea-level did not exceed the present height during the Holocene, and around ~6.5 ka, sea-level was at 6.2 m below the modern sea-level (Willard and Bernhardt, 2011). The sea-

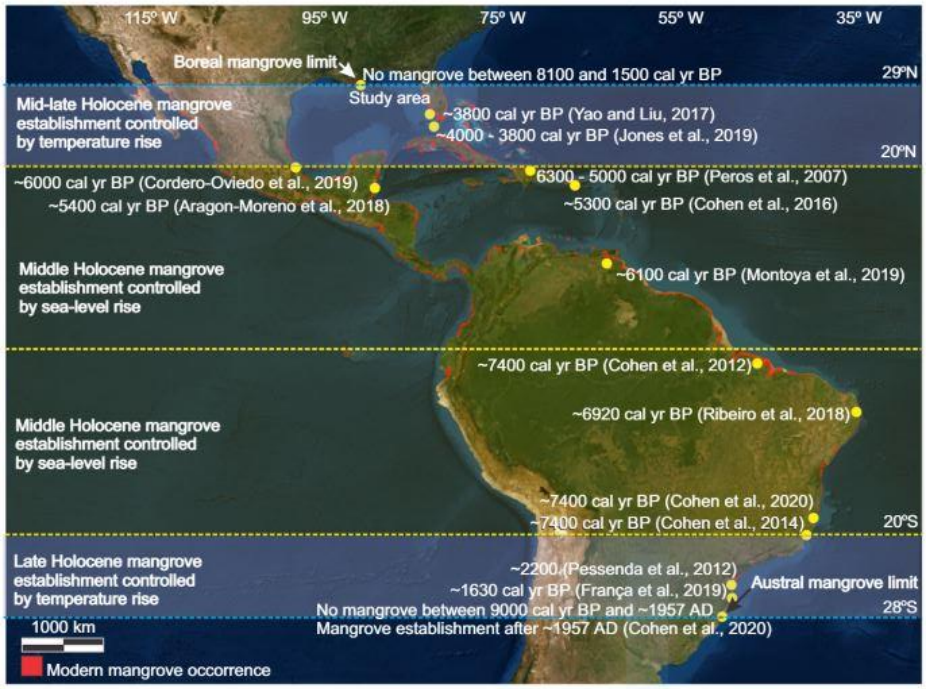

Fig. 8. American mangrove distribution in the tropical and subtropical zones and time of the mangrove establishment during the Holocene. The modern American mangrove distribution was obtained at http://data.unep-wcmc.org/datasets/4.

level, which was near the modern level during the middle Holocene, allowed mangrove establishment in the Caribbean and Gulf of Mexico coast, a tropical zone, at ~6100, ~5400, ~5300, and ~5500 cal yr BP, in Venezuela (9° N), Puerto Rico (18° N), Yucatan Peninsula-Mexico (18°–21° N) and Cuba (22° N), respectively (Peros et al., 2007; Cohen et al., 2016; Aragón-Moreno et al., 2018; Montoya et al., 2019). In addition, mangroves were recorded in the western Gulf of Mexico coast (20° N) at ~6000 cal yr BP (Cordero-Oviedo et al., 2019).

In the study area (29° N), marine transgression caused the development of lagoons and saltmarshes with a strong contribution of marine organic matter after ~6500 cal yr BP (Figs. 4, 5, 6, and 7). This sedimentary environment associated with vegetation and sedimentary organic matter suggests favorable physical-chemical conditions for mangrove establishment. Therefore, of the sea-level dependent factors, mangroves could have been established in the study area since ~6500 cal yr BP. However, contrasting with the tropical coasts, there was no evidence of mangrove presence around the Bay Champagne lagoon, the current northern mangrove limit, between 6500 and 1470 cal yr BP. A similar situation occurred at the southern limit of American mangroves at Laguna, southern Brazilian coast (28° 29′ S), where pollen studies also indicate the absence of mangroves during the Holocene. Mangroves were established at their current southern limit of South America only in the Anthropocene (Cohen et al., 2020b). Probably, despite the physical-chemical conditions suitable for mangrove establishment promoted by the sea-level rise, the temperature may not yet have been high enough to allow the growth of mangroves at their current northern and southern limits of American mangroves during the middle-late Holocene. In addition, biogeographic studies indicated that modern global distribution of mangroves is mainly controlled by temperature, hence being limited to tropical and subtropical regions (Lugo and Patterson-zucca, 1977; Sherrod and McMillan, 1985; Duke et al., 1998; Stevens et al., 2006; Stuart et al., 2007).

5.4. Mangrove establishment controlled by climate

Considering that mangroves are susceptible to changes in sea-level and climate in a millennial timescale (Chapman, 1975; Duke, 1992; Blasco, 1996; Fromard et al., 2004; Alongi, 2008), and to local factors in a secular/decadal time scale (Moraes et al., 2017; Ribeiro et al., 2018) the (1) presence or (2) absence of mangroves along their current northern and southern limits during the Holocene is essential to identify the reasons for the mangrove expansion to more temperate zones during the recent decades. Regarding the hypothesis of the (1) continuous presence of mangroves in the current northern (29° N) and southern (28° S) boundaries of the American continent (North and South America) during the middle-late Holocene, it would indicate relative stability of relative sea-level and climate during that period. In this case, studies that show the poleward mangrove expansion during the most recent decades (e.g. Cavanaugh et al., 2014; Saintilan et al., 2014; Osland and Feher, 2020) could be incorrectly attributing such mangrove dynamics to allogeneic processes, for instance, global warming. Alternatively, it may be caused by autogenic mechanisms, for instance, related to the action of tides, storms, dynamics of beach-barrier, delta switching, and lateral migration of meandering fluvial channels, then creating and destroying mangrove substrates in a cyclical process with expansion and contraction phases of mangrove areas in a decadal time scale (Moraes et al., 2017). In this context, such mangrove expansion would be related to processes operated locally and intrinsic to the depositional system (Beebower, 1964; Cecil, 2013).

By contrast, the (2) absence of mangroves in their current northern and southern limits in the Holocene indicates an allogeneic process driving the mangrove expansion from tropical into temperate latitudes in a millennial time scale. In general, the geological record suggests equatorward contraction of mangroves during the LGM (Woodroffe and Grindrod, 1991; Cannon et al., 2009), when these forests occurred

only in refuge areas more protected from the impact of cold air temperature (Cannon et al., 2009). In contrast, a poleward mangrove expansion occurred after the LGM (Sandoval-Castro et al., 2012; Kennedy et al., 2016). During the early and middle Holocene, this trend may have been favored in tropical to subtropical areas by increasing the global mean surface temperature (O'ishi and Abe-Ouchi, 2011; Fig. 8).

There is a consensus about global warming between the LGM and early Holocene (Kaufman et al., 2020). However, less well understood is the climate between the mid and late Holocene (Sundqvist et al., 2014). The Antarctic Peninsula underwent an early-Holocene warm phase and stable temperatures between 9200 and 2500 years ago (Mulvaney et al., 2012). Studies over land north of 40°N have indicated warming during the middle Holocene (O'ishi and Abe-Ouchi, 2011). Other proxy records indicated global cooling during the late Holocene (Marcott et al., 2013). However, with no direct net contribution from the orbitally-driven insolation, the global annual mean radiative forcing in the Holocene should be dominated by the retreating ice sheets and rising atmospheric greenhouse gases, with both favoring a globally averaged warming (Liu et al., 2014). Climate models simulate a robust global annual mean warming along the Holocene, mainly in response to rising CO_2 and the retreat of ice sheets (Liu et al., 2014). Other climate models suggest no change or warming during the mid-late Holocene (Braconnot et al., 2007; Timm and Timmermann, 2007; Lohmann et al., 2013). The increase of CO_2 and CH_4 concentrations after 7000 and 5000 years ago contributed to the late Holocene warmth, prolonging the natural interglacial warmth initiated by orbital variations. These mid-late Holocene greenhouse gas increases may be natural or anthropogenic in origin (Ruddiman, 2003; Broecker and Stocker, 2006; Kaplan et al., 2011; Ruddiman et al., 2016). A stable isotope record from ice wedges from the Arctic indicated a long-term winter warming trend during the mid-late Holocene (Meyer et al., 2015). $\delta^{18}O$ of planktonic foraminifera from the western tropical South Atlantic Ocean on the northeast Brazilian margin showed a progressive warming trend of slightly >1 °C during the transition from the mid- to late-Holocene (Santos et al., 2013). A record of Holocene sea-surface temperatures and sea-ice presence from the Polar Front of the East Atlantic Southern Ocean showed late Holocene warming and no abrupt Neoglacial cooling (Nielsen et al., 2004). Jomelli et al. (2011) proposed Holocene warming for the eastern tropical Pacific with increased atmospheric temperature and retreat of glaciers in the southern tropics in response to enhanced austral summer insolation. This Holocene climate trend indicated by the climate models and proxy records is consistent with the hypothesis that climate warming permitted mangroves to expand from the tropics to subtropics during the mid-late Holocene (Fig. 8).

Although the coastal stabilization or low rates of sea-level change around the middle Holocene may have played a role in the establishment of northern and southern American mangroves in areas located between the latitude of 20°N and 20°S, the subtropical mangroves were established only in the mid-late Holocene in both hemispheres, probably as a result of global warming that caused a poleward mangrove expansion from the latitude of 20° to 29°. The mangroves in the subtropical Brazilian coast were established between ~2200 cal yr BP (São Paulo, 25° S) and ~1630 cal yr BP (Santa Catarina-Brazil, 26° S) (Pessenda et al., 2012; França et al., 2019), and the subtropical mangroves in North America appeared after ~4000 cal yr BP in the Everglades-Florida (25° N) (Willard and Bernhardt, 2011; Yao et al., 2015; Yao and Liu, 2017; Jones et al., 2019) (Fig. 8). Regional-scale droughts may have some influence in delaying the mangrove establishment in the subtropical mangroves of the Everglades (Willard and Bernhardt, 2011), but global warming in the mid-late Holocene must be considered as the main force favoring the mangrove expansion from tropical to subtropical areas in both hemispheres.

Our study shows the absence of mangroves between ~8100 and ~1500 cal yr BP in Port Fourchon (29° 09′ N), USA. The first evidence of black mangroves in Louisiana was dated at approximately 1900 CE (Lloyd and Tracy, 1901). These authors described early mangrove stands short in stature (<0.6 m) growing on offshore islands, mainly in Breton Sound. In addition, a historical video of the U.S. Library of Congress (http://www.loc.gov/item/mp76000363) also exhibited black mangroves at the Breton National Wildlife Refuge in Louisiana in 1915. Similarly, in the southern limit of the American mangroves at Laguna, Brazil (28° 29′ S), even though physicochemical and hydrodynamic conditions were favorable for the establishment and expansion of mangroves since the middle Holocene, mangrove establishment occurred only between ~1957 and ~1986 CE (Cohen et al., 2020b). It is noteworthy that a subtropical Brazilian mangrove stand (26° S), established since ~1630 cal yr BP, contained *Rhizophora* trees only during the last decades (França et al., 2019). *Rhizophora* is less tolerant to low temperatures than *Laguncularia* and *Avicennia* (Duke et al., 1998; Quisthoudt et al., 2012). The presence of mangroves in Louisiana, even incipient and restricted to some islands since the beginning of the 20th century, suggests that this ecosystem was established only after appropriate climatic conditions were present since that time.

We propose that the establishment of *Avicennia* trees in the study area was related to the natural warming trend after the Little Ice Age (LIA). This cold climatic episode was attributed to solar activity fluctuations during the last six or seven centuries (Lean and Rind, 1999), ending between 1850 and 1890 CE (Bradley and Jones, 1992). Ongoing remote sensing work (unpublished) by Cohen and co-workers indicates a significant increase in the area and stature of Louisiana mangroves in recent decades, especially in the 21st century. Therefore, while our data suggest that a poleward mangrove migration occurred due to natural global warming during the late Holocene, the industrial-era warming must have intensified the mangrove expansion during the last few decades, when temperature increased at a higher rate in the boreal and temperate regions than in the tropics (Solomon et al., 2007).

6. Conclusions

Our integrated multi-proxy investigation based on sedimentology, ^{14}C radiocarbon dating, pollen analysis, as well as X-ray fluorescence, isotope ($\delta^{13}C$), and C\N data indicate a marine transgression at Bay Champagne, Louisiana-USA during the Holocene. This natural process changed the environment from a freshwater lake (~8100 to ~6500 cal yr BP) to a brackish water lagoon (~6500 to ~1500 cal yr BP). During the last ~1500 cal yr BP, washover sand was deposited into the lagoon due to the relative sea-level rise and hurricanes. Physicochemical and hydrodynamic conditions suitable for mangrove development occurred in the study site over the last ~6500 cal yr BP. However, mangrove pollen were not recorded in sediments between ~8100 and ~1500 cal yr BP, suggesting that mangroves were absent during the entire period. A comparative analysis of these multi-proxy data and historical records of mangrove establishment phases in the Gulf of Mexico, Caribbean, and eastern South America indicated that mangroves expanded gradually from the tropical to subtropical South and North American coasts during the mid and late Holocene. The modern boreal (29° 09′ N) and austral (28° 29′ S) mangrove limits were established in the early and mid-20th century, respectively. This mangrove dynamics on a continental scale suggests that poleward mangrove migration was caused by natural Holocene global warming. The industrial-era warming must have intensified the mangrove expansion. However, the Anthropocene global warming was not a direct forcing that initiated the mangrove migration into temperate zones.

Supplementary data to this article can be found online at https://doi.org/10.1016/j.geomorph.2021.107648.

Declaration of competing interest

The authors declare that they have no known competing financial interests or personal relationships that could have appeared to influence the work reported in this paper.

Acknowledgments

The authors thank the Graduate Program in Geology and Geochemistry of the Federal University of Pará. We also acknowledge the logistic support provided by the College of the Coastal and Environment of the Louisiana State University. This study was financed by the Brazilian Council for Technology and Science-CNPq (Project # 307497/2018-6), FAPESP 2017/03304-1, the U.S. National Science Foundation (NSF Project # 1759715), the Ministry of Science and Technology of the People's Republic of China (Project # 2017YFE0107400), and NOAA through the Louisiana Sea Grant (Project #2013-39).

References

Akhtar, N., Hameed, M., Nawaz, F., Ahmad, K.S., Hamid, A., Segovia-Salcedo, C., Shahnaz, M.M., 2017. Leaf anatomical and biochemical adaptations in *Typha domingensis* Pers. ecotypes for salinity tolerance. Bot. Sci. 95, 807–821. https://doi.org/10.17129/botsci.886.

Alongi, Daniel M., 2008. Mangrove forests: resilience, protection from tsunamis, and responses to global climate change. Estuar. Coast. Shelf Sci. 76, 1–13. https://doi.org/10.1016/j.ecss.2007.08.024.

Alongi, D.M., 2015. The Impact of climate change on mangrove forests. Curr. Clim. Chang. Rep. 1, 30–39. https://doi.org/10.1007/s40641-015-0002-x.

Amaral, P.G.C., Ledru, M.-P., Branco, F.R., Giannini, P.C.F., 2006. Late Holocene development of a mangrove ecosystem in southeastern Brazil (Itanhaém, state of São Paulo). Palaeogeogr. Palaeoclimatol. Palaeoecol. 241, 608–620. https://doi.org/10.1016/j.palaeo.2006.04.010.

Anderson, J.B., Fillon, R.H., 2004. Late Quaternary stratigraphic evolution of the northern Gulf of Mexico margin. SEPM (Soc. Sedimen. Geol.) 79, 311.

Angulo, R., Lessa, G., Souza, M., 2006. A critical review of mid- to late-Holocene sea-level fluctuations on the eastern Brazilian coastline. Quat. Sci. Rev. 25, 486–506. https://doi.org/10.1016/j.quascirev.2005.03.008.

Angulo, R.J., Giannini, P.C.F., Souza, M.C. De, Lessa, G.C., Angulo, R.J., Giannini, P.C.F., Souza, M.C. De, Lessa, G.C., 2016. Holocene paleo-sea level changes along the coast of Rio de Janeiro, southern Brazil: comment on Castro et al. (2014). An. Acad. Bras. Cienc. 88, 2105–2111. https://doi.org/10.1590/0001-3765201620140641.

Aragón-Moreno, A.A., Islebe, G.A., Torrescano-Valle, N., Arellano-Verdejo, J., 2018. Middle and late Holocene mangrove dynamics of the Yucatan Peninsula, Mexico. J. South Am. Earth Sci. 85, 307–311. https://doi.org/10.1016/j.jsames.2018.05.015.

Beebower, J.R., 1964. Cyclothems and cyclic depositional mechanism in alluvial plain sedimentation. Bull. Kans. Univ. Geol. Surv. 169, 35–42.

Behling, H., Cohen, M.C.L., Lara, R.J., 2001. Studies on Holocene mangrove ecosystem dynamics of the Bragança Peninsula in north-eastern Pará, Brazil. Bosque 167, 225–242.

Behling, H., Cohen, M.L., Lara, R., 2004. Late Holocene mangrove dynamics of Marajó Island in Amazonia, northern Brazil. Veg. Hist. Archaeobot. 13, 73–80. https://doi.org/10.1007/s00334-004-0031-1.

Benson, A., 2010. *Rangia cuneata*. USGS Nonindigenous Aquatic Species Database, Gainesville, FL. [online] Available from. https://www.fws.gov/fisheries/ans/erss/uncertainrisk/Rangia-cuneata-WEB-10-01-12.pdf. (Accessed 12 April 2020).

Blasco, F., 1996. Mangroves as indicators of coastal change. Catena 27, 167–178.

Blasco, F., Saenger, P., Janodet, E., 1996. Mangroves as indicators of coastal change. CATENA 27, 167–178. https://doi.org/10.1016/0341-8162(96)00013-6.

Blum, M.D., Roberts, H.H., 2012. The Mississippi Delta Region: past, present, and future. Annu. Rev. Earth Planet. Sci. 40, 655–683. https://doi.org/10.1146/annurev-earth-042711-105248.

Blum, M.D., Carter, A.E., Zayac, T., Goble, R., 2002. Middle Holocene sea-level and evolution of the Gulf of Mexico Coast (USA). J. Coast. Res. 36, 65–80. https://doi.org/10.2112/1551-5036-36.sp1.65.

Braconnot, P., Otto-Bliesner, B., Harrison, S., Joussaume, S., Peterchmitt, J.Y., Abe-Ouchi, A., Crucifix, M., Driesschaert, E., Fichefet, T., Hewitt, C.D., Kageyama, M., Kitoh, A., Laîné, A., Loutre, M.F., Marti, O., Merkel, U., Ramstein, G., Valdes, P., Weber, S.L., Yu, Y., Zhao, Y., 2007. Results of PMIP2 coupled simulations of the Mid-Holocene and last glacial maximum - part 1: experiments and large-scale features. Clim. Past 3, 261–277. https://doi.org/10.5194/cp-3-261-2007.

Bradley, R.S., Jones, P.D., 1992. When was the "Little Ice Age"? In: Mikami, T. (Ed.), Proceedings of the International Symposium on the "Little Ice Age" Climate. Department of Geography, Tokyo Metropolitan University, pp. 1–4

Brantley, S.T., Bissett, S.N., Young, D.R., Wolner, C.W.V., Moore, L.J., 2014. Barrier Island morphology and sediment characteristics affect the recovery of dune building grasses following storm-induced overwash. PLoS One 9, e104747. https://doi.org/10.1371/journal.pone.0104747.

Broecker, W.S., Stocker, T.F., 2006. The Holocene CO_2 rise: anthropogenic or natural? Eos (Washington. DC) 87, 27. https://doi.org/10.1029/2006EO030002.

Brush, G.S., Brush, L.M., 1972. Transport of pollen in a sediment-laden channel; a laboratory study. Am. J. Sci. 272, 359–381. https://doi.org/10.2475/ajs.272.4.359.

Buso Junior, A.A., Pessenda, L.C.R., Oliveira, P.E., Giannini, P.C., Cohen, M.C.L., Volkmer-Ribeiro, C., Barros de Oliveira, S.M., Favaro, D.I.T., Rossetti, D.F., Lorente, F., Borotti Filho, M.A., Schiavo, J.A., Bendassolli, J.A., França, M.C., Guimaraes, J.F., Siqueira, G., 2013. From an estuary to a freshwater lake: a paleo-estuary evolution in the context of Holocene sea-level fluctuations, Southeastern Brazil. Radiocarbon 55, 1735–1746. https://doi.org/10.2458/azu_js_rc.55.16210.

Caballero, M., Peinalba, M.C., Martinez, M., Ortega-Guerrerol, B., Vazquez, L., 2005. A Holocene record from a former coastal lagoon in Bahia Kino, Gulf of California, Mexico. The Holocene 15, 1236–1244. https://doi.org/10.1191/0959683605hl896rr.

Caldas, L.H. de O., Oliveira, J.G. de M., Stattegger, W.E. de, Stattegger, K., Vital, H., 2006. Geometry and evolution of Holocene transgressive and regressive barriers on the semi-arid coast of NE Brazil. Geo-Mar. Lett. 26, 249–263. https://doi.org/10.1007/s00367-006-0034-2.

Cannon, C.H., Morley, R.J., Bush, A.B.G., 2009. The current refugial rainforests of Sundaland are unrepresentative of their biogeographic past and highly vulnerable to disturbance. Proc. Natl. Acad. Sci. U. S. A. 106, 11188–11193. https://doi.org/10.1073/pnas.0809865106.

Cavanaugh, K.C., Kellner, J.R., Forde, A.J., Gruner, D.S., Parker, J.D., Rodriguez, W., Feller, I.C., 2014. Poleward expansion of mangroves is a threshold response to decreased frequency of extreme cold events. Proc. Natl. Acad. Sci. 111, 723–727. https://doi.org/10.1073/pnas.1315800111.

Cavanaugh, K.C., Parker, J.D., Cook-Patton, S.C., Feller, I.C., Williams, A.P., Kellner, J.R., 2015. Integrating physiological threshold experiments with climate modeling to project mangrove species' range expansion. Glob. Chang. Biol. 21, 1928–1938. https://doi.org/10.1111/gcb.12843.

Cavanaugh, K.C., Osland, M.J., Bardou, R., Hinojosa-Arango, G., López-Vivas, J.M., Parker, J.D., Rovai, A.S., 2018. Sensitivity of mangrove range limits to climate variability. Glob. Ecol. Biogeogr. 27, 925–935. https://doi.org/10.1111/geb.12751.

Cavanaugh, K.C., Dangremond, E.M., Doughty, C.L., Park Williams, A., Parker, J.D., Hayes, M.A., Rodriguez, W., Feller, I.C., 2019. Climate-driven regime shifts in a mangrove–salt marsh ecotone over the past 250 years. Proc. Natl. Acad. Sci. U. S. A. 116, 21602–21608. https://doi.org/10.1073/pnas.1902181116.

Cecil, C.B., 2013. An overview and interpretation of autocyclic and allocyclic processes and the accumulation of strata during the Pennsylvanian–Permian transition in the central Appalachian Basin, USA. Int. J. Coal Geol. 119, 21–31. https://doi.org/10.1016/j.coal.2013.07.012.

Chapman, V.J., 1975. Mangrove biogeography. In: Walsh, G.E., Snedaker, S.C., Teas, H.J. (Eds.), International Symposium on Biology and Management of Mangroves. University of Florida Press, Miami, pp. 179–212.

Clark, P.U., Dyke, A.S., Shakun, J.D., Carlson, A.E., Clark, J., Wohlfarth, B., Mitrovica, J.X., Hostetler, S.W., McCabe, A.M., 2009. The Last Glacial Maximum. Science 325, 710–714. https://doi.org/10.1126/science.1172873.

Coastal Engineering Consultants, 2015. Caminada headland beach and dune restoration (BA-45) completion report; Coastal protection and restoration authority. Baton Rouge, LA, USA.

Cohen, M.C.L., Behling, H., Lara, R.J., 2005a. Amazonian mangrove dynamics during the last millennium: the relative sea-level and the Little Ice Age. Rev. Palaeobot. Palynol. 136, 93–108. https://doi.org/10.1016/j.revpalbo.2005.05.002.

Cohen, M.C.L., Souza Filho, P.W.M., Lara, R.J., Behling, H., Angulo, R.J., 2005b. A model of Holocene mangrove development and relative sea-level changes on the Bragança Peninsula (northern Brazil). Wetl. Ecol. Manag. 13, 433–443. https://doi.org/10.1007/s11273-004-0413-2.

Cohen, M.C.L., Lara, R.J., Smith, C.B., Angélica, R.S., Dias, B.S., Pequeno, T., 2008. Wetland dynamics of Marajó Island, northern Brazil, during the last 1000 years. CATENA 76, 70–77.

Cohen, M.C.L., Behling, H., Lara, R.J., Smith, C.B., Matos, H.R.S., Vedel, V., 2009. Impact of sea-level and climatic changes on the Amazon coastal wetlands during the late Holocene. Veg. Hist. Archaeobot. 18, 425–439. https://doi.org/10.1007/s00334-008-0208-0.

Cohen, M.C.L., Pessenda, L.C.R., Behling, H., de Fátima Rossetti, D., França, M.C., Guimarães, J.T.F., Friaes, Y., Smith, C.B., 2012. Holocene palaeoenvironmental history of the Amazonian mangrove belt. Quat. Sci. Rev. 55, 50–58.

Cohen, M.C.L., França, M.C., Rossetti, D., Pessenda, L.C.R., Giannini, P.C.F., Lorente, F.L., Junior, A.Â.B., Castro, D., Macario, K., 2014a. Landscape evolution during the late Quaternary at the Doce River mouth, Espírito Santo State, Southeastern Brazil. Palaeogeogr. Palaeoclimatol. Palaeoecol. 415, 48–58. https://doi.org/10.1016/j.palaeo.2013.12.001.

Cohen, M.C.L., Pessenda, L.C.R., Smith, C.B., Guimarães, J.T.F., França, M.C., 2014b. Amazonian mangroves during the Late Pleistocene and Holocene. In: Carvalho, I. de S., Garcia, M., Lana, C.C., Strohschoen, O. (Eds.), Paleontologia: Cenários de Vida - Paleoclimas. Interciência, Rio de Janeiro, pp. 387–402.

Cohen, M.C.L., Rossetti, D.F., Pessenda, L.C.R., Friaes, Y.S., Oliveira, P.E., 2014c. Late Pleistocene glacial forest of Humaitá-Western Amazonia. Palaeogeogr. Palaeoclimatol. Palaeoecol. 415, 37–47. https://doi.org/10.1016/j.palaeo.2013.12.025.

Cohen, M.C.L., Alves, I.C.C., França, M.C., Pessenda, L.C.R., Rossetti, D. de F., 2015. Relative sea-level and climatic changes in the Amazon littoral during the last 500 years. CATENA 133, 441–451. https://doi.org/10.1016/j.catena.2015.06.012.

Cohen, M.C.L., Lara, R.J., Cuevas, E., Oliveras, E.M., Da Silveira Sternberg, L., 2016. Effects of sea-level rise and climatic changes on mangroves from southwestern littoral of Puerto Rico during the middle and late Holocene. Catena 143. https://doi.org/10.1016/j.catena.2016.03.041.

Cohen, M.C.L., Figueiredo, B.L., Oliveira, N.N., Fontes, N.A., França, M.C., Pessenda, L.C.R., de Souza, A.V., Macario, K., Giannini, P.C.F., Bendassolli, J.A., Lima, P., 2020a. Impacts of Holocene and modern sea-level changes on estuarine mangroves from northeastern Brazil. Earth Surf. Process. Landforms 45, 375–392. https://doi.org/10.1002/esp.4737.

Cohen, M.C.L., Rodrigues, E., Rocha, D.O.S., Freitas, J., Fontes, N.A., Pessenda, L.C.R., de Souza, A.V., Gomes, V.L.P., França, M.C., Bonotto, D.M., Bendassolli, J.A., 2020b. Southward migration of the austral limit of mangroves in South America. Catena 195, 104775. https://doi.org/10.1016/j.catena.2020.104775.

Cordero-Oviedo, C., Correa-Metrio, A., Urrego, L.E., Vázquez, G., Blaauw, M., Escobar, J., Curtis, J.H., 2019. Holocene establishment of mangrove forests in the western coast of the Gulf of Mexico. Catena 180, 212–223. https://doi.org/10.1016/j.catena.2019.04.025.

Cuven, S., Paris, R., Falvard, S., Miot-Noirault, E., Benbakkar, M., Schneider, J.L., Billy, I., 2013. High-resolution analysis of a tsunami deposit: case-study from the 1755 Lisbon tsunami in southwestern Spain. Mar. Geol. 337, 98–111. https://doi.org/10.1016/j.margeo.2013.02.002.

Davis, M.B., 2000. Palynology after Y2K — understanding the source area of pollen in sediments. Annu. Rev. Earth Planet. Sci. 28, 1–18.

Deines, P., 1980. The isotopic composition of reduced organic carbon. In: Fritz, P., Fontes, J.C. (Eds.), Handbook of Environmental Isotope Geochemistry. The Terrestrial Environments. Elsevier, Amsterdam, pp. 329–406.

Dietz, M., Liu, K., Bianchette, T., Dietz, M.E., Liu, K., Bianchette, T.A., 2018. Hurricanes as a major driver of coastal erosion in the Mississippi River Delta: a multi-decadal analysis of shoreline retreat rates at Bay Champagne, Louisiana (USA). Water 10, 1480. https://doi.org/10.3390/w10101480.

Dittmar, T., Hertkorn, N., Kattner, G., Lara, R.J., 2006. Mangroves, a major source of dissolved organic carbon to the oceans. Glob. Biogeochem. Cycles 20. https://doi.org/10.1029/2005GB002570 n/a-n/a.

Donnelly, C., Kraus, N., Larson, M., 2006. State of knowledge on measurement and modeling of coastal overwash. J. Coast. Res. 22, 965–991. https://doi.org/10.2112/04-0431.1.

Donoghue, J.F., 2011. Sea level history of the northern Gulf of Mexico coast and sea level rise scenarios for the near future. Clim. Chang. 107, 17–33. https://doi.org/10.1007/s10584-011-0077-x.

Duke, N.C., 1992. Mangrove floristics and biogeography. American Geophysical Union (AGU), pp. 63–100 https://doi.org/10.1029/CE041p0063.

Duke, N.C., Ball, M.C., Ellison, J.C., 1998. Factors influencing biodiversity and distributional gradients in mangroves. Glob. Ecol. Biogeogr. Lett. 7, 27–47. https://doi.org/10.2307/2997695.

Everitt, J.H., Judd, F.W., Escobar, D.E., Davis, M.R., 1996. Integration of remote sensing and spatial information technologies for mapping black mangrove on the Texas gulf coast. J. Coast. Res. 12, 64–69.

Ewel, K.C., Twilley, R.R., Ong, J.E., 1998. Different kinds of mangrove forests provide different goods and services. Glob. Ecol. Biogeogr. Lett. 7, 83–94.

Faegri, K., Iversen, J., 1989. Textbook of Pollen Analyses. John Wiley and Sons, New York 328 p.

Finkelstein, S.A., 2003. Identifying pollen grains of *Typha latifolia*, *Typha angustifolia*, and Typha xglauca. Can. J. Bot. 81, 985–990. https://doi.org/10.1139/b03-084

Fisher, R., Huo, J., 2012. A Business Plan for Blue Carbon Offsets at Duke University (Master of Environmental Management degree in the Nicholas School of the Environment of Duke University).

Fontes, N.A., Moraes, C.A., Cohen, M.C.L., Alves, I.C.C., França, M.C., Pessenda, L.C.R., Francisquini, M.I., Bendassolli, J.A., Macario, K., Mayle, F., 2017. The impacts of the Middle Holocene high sea-level stand and climatic changes on mangroves of the Jucuruçu River, Southern Bahia – Northeastern Brazil. Radiocarbon 59, 215–230. https://doi.org/10.1017/RDC.2017.6.

Food and Agriculture Organization of the United Nations, 2007. The World's Mangroves, 1980–2005: A Thematic Study in the Framework of the Global Forest Resources Assessment 2005. Food and Agriculture Organization of the United Nations.

França, M.C., Cohen, M.C.L., Pessenda, L.C.R., Rossetti, D.F., Lorente, F.L., Buso Junior, A.Á., Guimarães, J.T.F., Friaes, Y., Macario, K., 2013. Mangrove vegetation changes on Holocene terraces of the Doce River, southeastern Brazil. Catena 110, 59–69.

França, M.C., Francisquini, M.I., Cohen, M.C.L., Pessenda, L.C.R., 2014. Inter-proxy evidence for the development of the Amazonian mangroves during the Holocene. Veg. Hist. Archaeobot. 23, 527–542. https://doi.org/10.1007/s00334-013-0420-4.

França, M.C., Alves, I.C.C., Castro, D.F., Cohen, M.C.L., Rossetti, D.F., Pessenda, L.C.R., Lorente, F.L., Fontes, N.A., Junior, A.Á.B., Giannini, P.C.F., Francisquini, M.I., 2015. A multi-proxy evidence for the transition from estuarine mangroves to deltaic freshwater marshes, Southeastern Brazil, due to climatic and sea-level changes during the late Holocene. Catena 128, 155–166. https://doi.org/10.1016/j.catena.2015.02.005.

França, M.C., Alves, I.C.C., Cohen, M.C., Rossetti, D.F., Pessenda, L.C., Giannini, P.C., Lorente, F.L., Buso Junior, A.A., Bendassolli, J.A., Macario, K., 2016. Millennial to secular timescale impacts of climate and sea-level changes on mangroves from the Doce River delta, Southeastern Brazil. The Holocene 26, 1733–1749. https://doi.org/10.1177/0959683616645938.

França, M.C., Pessenda, L.C., Cohen, M.C., de Azevedo, A.Q., Fontes, N.A., Silva, F.B., de Melo, J.C., Piccolo, M. de C., Bendassolli, J.A., Macario, K., 2019. Late-Holocene subtropical mangrove dynamics in response to climate change during the last millennium. The Holocene 29, 445–456. https://doi.org/10.1177/0959683618816438.

Fromard, F., Vega, C., Proisy, C., 2004. Half a century of dynamic coastal change affecting mangrove shorelines of French Guiana. A case study based on remote sensing data analyses and field surveys. Mar. Geol. 208, 265–280. https://doi.org/10.1016/j.margeo.2004.04.018.

Giri, C., Ochieng, E., Tieszen, L.L., Zhu, Z., Singh, A., Loveland, T., Masek, J., Duke, N., 2011. Status and distribution of mangrove forests of the world using earth observation satellite data. Glob. Ecol. Biogeogr. 20, 154–159. https://doi.org/10.1111/j.1466-8238.2010.00584.x.

Gischler, E., 2015. Quaternary reef response to sea-level and environmental change in the western Atlantic. Sedimentology 62, 429–465. https://doi.org/10.1111/sed.12174.

Gosling, W.D., Mayle, F.E., Tate, N.J., Killeen, T.J., 2009. Differentiation between Neotropical rainforest, dry forest, and savannah ecosystems by their modern pollen spectra and implications for the fossil pollen record. Rev. Palaeobot. Palynol. 153, 70–85. https://doi.org/10.1016/j.revpalbo.2008.06.007.

Grimm, E., 1990. TILIA and TILIAGRAPH: PC spreadsheet and graphic software for pollen data. INQUA Sub-Commission on Data-Handling Methods Newsletter.

Guimarães, J.T.F., Cohen, M.C.L., Pessenda, L.C.R., Franca, M.C., Smith, C.B., Nogueira, A.C.R., 2011. Mid- and late-Holocene sedimentary process and palaeovegetation changes near the mouth of the Amazon River. The Holocene 22, 359–370. https://doi.org/10.1177/0959683611423693.

Guimarães, J.T.F., Cohen, M.C.L., Franca, M.C., Pessenda, L.C.R., Behling, H., 2013. Morphological and vegetation changes on tidal flats of the Amazon Coast during the last 5000 cal. yr BP. The Holocene 23, 528–543. https://doi.org/10.1177/0959683612463097.

Hamdi, S.M.M., Assadi, M., Segarra-Moragues, J.G., 2010. Pollen morphology of Iranian species of Typha L. (Typhaceae) and its taxonomic significance. Feddes Repert. 121, 85–96. https://doi.org/10.1002/fedr.200911130.

Hameed, M., Nawaz, T., Ashraf, M., Tufail, A., Kanwal, H., Sajid Aqeel Ahmad, M., Ahmad, I., 2012. Leaf Anatomical Adaptations of Some Halophytic and Xerophytic Sedges of the Punjab.

Harper, C., 1984. Improved methods of facies sequence analysis. Facies Model.

Harris, M.S., Sautter, L.R., Johnson, K.L., Luciano, K.E., Sedberry, G.R., Wright, E.E., Siuda, A.N.S., 2013. Continental shelf landscapes of the southeastern United States since the last interglacial. Geomorphology 203, 6–24. https://doi.org/10.1016/j.geomorph.2013.02.014.

Havinga, A.J., 1967. Palynology and pollen preservation. Rev. Paleobot. Palynol. 2, 81–98.

Henry, K.M., Twilley, R.R., 2013. Soil development in a coastal Louisiana wetland during a climate-induced vegetation shift from salt marsh to mangrove. J. Coast. Res. 292, 1273–1283. https://doi.org/10.2112/JCOASTRES-D-12-00184.1.

IPCC, 2014. Contribution of working groups I, II and III to the fifth assessment report of the intergovernmental panel on climate change. In: Pachauri, R.K., Meyer, L.A. (Eds.), Climate Change 2014: Synthesis Report. Geneva, p. 151.

Jafari, N.H., Harris, B.D., Stark, T.D., 2018. Geotechnical investigations at the caminada headlands beach and dune in coastal Louisiana. Coast. Eng. 142, 82–94. https://doi.org/10.1016/j.coastaleng.2018.04.014.

Joe-Wong, C., Schlesinger, D.R., Chow, A.T., Myneni, S.C.B., 2019. Sea level rise produces abundant organobromines in salt-affected coastal wetlands. Geochem. Persp. Lett. 10, 31–35. https://doi.org/10.7185/geochemlet.1911.

Johnson, C.L., Chen, Q., Ozdemir, C.E., 2020. Lidar time-series analysis of a rapidly transgressing low-lying mainland barrier (Caminada Headlands, Louisiana, USA). Geomorphology 352, 106979. https://doi.org/10.1016/j.geomorph.2019.106979.

Jomelli, V., Khodri, M., Favier, V., Brunstein, D., Ledru, M.-P., Wagnon, P., Blard, P.-H., Sicart, J.-E., Braucher, R., Grancher, D., Bourlès, L., Braconnot, P., Vuille, M., 2011. Irregular tropical glacier retreat over the Holocene epoch driven by progressive warming. Nature. https://doi.org/10.1038/nature10150.

Jones, M.C., Wingard, G.L., Stackhouse, B., Keller, K., Willard, D., Marot, M., Landacre, B.E., Bernhardt, C., 2019. Rapid inundation of southern Florida coastline despite low relative sea-level rise rates during the late-Holocene. Nat. Commun. 10, 1–13. https://doi.org/10.1038/s41467-019-11138-4.

Kaplan, J.O., Krumhardt, K.M., Ellis, E.C., Ruddiman, W.F., Lemmen, C., Goldewijk, K.K., 2011. Holocene carbon emissions as a result of anthropogenic land cover change. Holocene 21, 775–791. https://doi.org/10.1177/0959683610386983.

Kaufman, D., McKay, N., Routson, C., Erb, M., Davis, B., Heiri, O., Jaccard, S., Tierney, J., Dätwyler, C., Axford, Y., Brussel, T., Cartapanis O., Chase, B., Dawson, A., de Vernal, A., Engels, S., Jonkers, L., Marsicek, J., Moffa-Sánchez, P., Morrill, C., Orsi, A., Rehfeld, K., Saunders, K., Sommer, P.S., Thomas, E., Tonello, M., Tóth, M., Vachula, R., Andreev, A., Bertrand, S., Biskaborn, B., Bringué, M., Brooks, S., Caniupán, M., Chevalier, M., Cwynar, L., Emile-Geay, J., Fegyveresi, J., Feurdean, A., Finsinger, W., Fortin, M.C., Foster, L., Fox, M., Gajewski, K., Grosjean, M., Hausmann, S., Heinrichs, M., Holmes, N., Ilyashuk, B., Ilyashuk, E., Juggins, S., Khider, D., Koinig, K., Langdon, P., Larocque-Tobler, I., Li, J., Lotter, A., Luoto, T., Mackay, A., Magyari, E., Malevich, S., Mark, B., Massaferro, J., Montade, V., Nazarova, L., Novenko, E., Parfil, P., Pearson, E., Peros, M., Pienitz, R., Płóciennik, M., Porinchu, D., Potito, A. Rees, A., Reinemann, S., Roberts, S., Rolland, N., Salonen, S., Self, A., Seppä, H., Shala, S., St-Jacques, J.M., Stenni, B., Syrykh, L., Tarrats, P., Taylor, K., van den Bos, V., Velle, G., Wahl, E., Walker, I., Wilmshurst, J., Zhang, E., Zhilich, S., 2020. A global database of Holocene paleotemperature records. Sci. Data 7, 1–34. https://doi.org/10.1038/s41597-020-0445-3.

Kennedy, J.P., Pil, M.W., Proffitt, C.E., Boeger, W.A., Stanford, A.M., Devlin, D.J., 2016. Postglacial expansion pathways of red mangrove, *Rhizophora mangle*, in the Caribbean Basin and Florida. Am. J. Bot. 103, 260–276. https://doi.org/10.3732/ajb.1500183.

Khan, N.S., Ashe, E., Horton, B.P., Dutton, A., Kopp, R.E., Brocard, G., Engelhart, S.E., Hill, D.F., Peltier, W.R., Vane, C.H., Scatena, F.N., 2017. Drivers of Holocene sea-level change in the Caribbean. Quat. Sci. Rev. https://doi.org/10.1016/j.quascirev.2016.08.032.

Kjerfve, B., 1994. Coastal Lagoons. Elsevier Oceanogr. Ser. 60, pp. 1–8. https://doi.org/10.1016/S0422-9894(08)70006-0.

Krauss, K.W., McKee, K.L., Lovelock, C.E., Cahoon, D.R., Saintilan, N., Reef, R., Chen, L., 2014. How mangrove forests adjust to rising sea level. New Phytol. 202, 19–34. https://doi.org/10.1111/nph.12605.

Kulp, M., Penland, S., Williams, S.J., Jenkins, C., Flocks, J., Kindinger, J., 2005. Geologic framework, evolution, and sediment resources for restoration of the Louisiana coastal zone. J. Coast. Res. https://doi.org/10.2307/25737049.

Ladislas, S., El-Mufleh, A., Gérente, C., Chazarenc, F., Andrès, Y., Béchet, B., 2012. Potential of aquatic macrophytes as bioindicators of heavy metal pollution in urban stormwater runoff. Water Air Soil Pollut. 223, 877–888. https://doi.org/10.1007/s11270-011-0909-3.

Lara, R.J., Cohen, M.C.L., 2006. Sediment porewater salinity, inundation frequency and mangrove vegetation height in Bragança, North Brazil: an ecohydrology-based empirical model. Wetl. Ecol. Manag. 14, 349–358. https://doi.org/10.1007/s11273-005-4991-4.

Lara, R.J., Cohen, M.C.L., 2009. Palaeolimnological studies and ancient maps confirm secular climate fluctuations in Amazonia. Clim. Chang. 94, 399–408. https://doi.org/10.1007/s10584-008-9507-9.

Lean, J., Rind, D., 1999. Evaluating sun-climate relationships since the Little Ice Age. J. Atmos. Solar Terrest. Phys. 61, 25–36.

Lima, W.J.S., Cohen, M.C.L., Rossetti, D.F., França, M.C., 2017. Late Pleistocene glacial forest elements of Brazilian Amazonia. Palaeogeogr. Palaeoclimatol. Palaeoecol. https://doi.org/10.1016/j.palaeo.2017.11.050.

Liu, K., 2004. Paleotempestology: principles, methods, and examples from Gulf coast lake-sediments. In: Murnane, R., Liu, K.B. (Eds.), Hurricanes and Typhoons: Past, Present, and Future. Columbia University, New York, pp. 13–57.

Liu, K., Li, C., Bianchette, T., McCloskey, T., 2011. Storm deposition in a coastal backbarrier lake in Louisiana caused by hurricanes Gustav and Ike. J. Coast. Res. 64, 1866–1870.

Liu, Z., Zhu, J., Rosenthal, Y., Zhang, X., Otto-Bliesner, B.L., Timmermann, A., Smith, R.S., Lohmann, G., Zheng, W., Timm, O.E., 2014. The Holocene temperature conundrum. Proc. Natl. Acad. Sci. U. S. A. 111, E3501–E3505. https://doi.org/10.1073/pnas.1407229111.

Lloyd, F.E., Tracy, S.M., 1901. The insular flora of Mississippi and Louisiana. Bull. Torrey Bot. Club 28, 61. https://doi.org/10.2307/2477884.

Lohmann, G., Pfeiffer, M., Laepple, T., Leduc, G., Kim, J.H., 2013. A model-data comparison of the Holocene global sea surface temperature evolution. Clim. Past 9, 1807–1839. https://doi.org/10.5194/cp-9-1807-2013.

Lorente, F.L., Pessenda, L.C.R., Oboh-Ikuenobe, F., Buso Jr., A.A., Cohen, M.C.L., Meyer, K.E.B., Giannini, P.C.F., de Oliveira, P.E., Rossetti, D. de F., Borotti Filho, M.A., França, M.C., de Castro, D.F., Bendassolli, J.A., Macario, K., 2013. Palynofacies and stable C and N isotopes of Holocene sediments from Lake Macuco (Linhares, Espírito Santo, southeastern Brazil): depositional settings and palaeonvironmental evolution. Palaeogeogr. Palaeoclimatol. Palaeoecol. 55, 325–330. https://doi.org/10.1016/j.palaeo.2013.12.004.

Lugo, A.E., Patterson-zucca, C., 1977. The Impact of Low Temperature Stress on Mangrove Structure and Growth.

Marcott, S.A., Shakun, J.D., Clark, P.U., Mix, A.C., 2013. A reconstruction of regional and global temperature for the past 11,300 years. Science 339 (80), 1198–1201. https://doi.org/10.1126/science.1228026.

McAndrews, J.H., McAndrews, J.H., Berti, A.A., Norris, G., Museum, R.O., 1973. Key to the Quaternary pollen and spores of the Great Lakes region. Royal Ontario Museum, Toronto 72 p.

McKee, K.L., Vervaeke, W.C., 2018. Will fluctuations in salt marsh–mangrove dominance alter vulnerability of a subtropical wetland to sea-level rise? Glob. Chang. Biol. 24, 1224–1238. https://doi.org/10.1111/gcb.13945.

McLeod, E., Salm, R.V., 2006. Managing Mangroves for Resilience to Climate Change. IUCN, Gland, Switzerland.

Meyer, H., Opel, T., Laepple, T., Dereviagin, A.Y., Hoffmann, K., Werner, M., 2015. Long-term winter warming trend in the Siberian Arctic during the mid- to late Holocene. Nat. Geosci. 8, 122–125. https://doi.org/10.1038/ngeo2349.

Meyers, Philip A., 1994. Preservation of elemental and isotopic source identification of sedimentary organic matter. Chem. Geol. 114, 289–302. https://doi.org/10.1016/0009-2541(94)90059-0.

Miall, A.D., 1978. Lithofacies types and vertical profile models in braided river deposits: a summary. Fluv. Sedimentol. 5, 597–600.

Mock, C.J., Mojzisek, J., McWaters, M., Chenoweth, M., Stahle, D.W., 2007. The winter of 1827–1828 over eastern North America: a season of extraordinary climatic anomalies, societal impacts, and false spring. Clim. Chang. 83, 87–115. https://doi.org/10.1007/s10584-006-9126-2.

Montoya, E., Pedra-Méndez, J., García-Falcó, E., Gómez-Paccard, M., Giralt, S., Vegas-Vilarrúbia, T., Stauffer, F.W., Rull, V., 2019. Long-term vegetation dynamics of a tropical megadelta: Mid-Holocene palaeoecology of the Orinoco Delta (NE Venezuela). Quat. Sci. Rev. https://doi.org/10.1016/j.quascirev.2019.105874.

Moraes, C.A., Fontes, N.A., Cohen, M.C., França, M.C., Pessenda, L.C., Rossetti, D.F., Francisquini, M.I., Bendassolli, J.A., Macario, K., 2017. Late Holocene mangrove dynamics dominated by autogenic processes. Earth Surf. Process. Landforms. https://doi.org/10.1002/esp.4167.

Mulvaney, R., Abram, N.J., Hindmarsh, R.C.A., Arrowsmith, C., Fleet, L., Triest, J., Sime, L.C., Alemany, O., Foord, S., 2012. Recent Antarctic Peninsula warming relative to Holocene climate and ice-shelf history. Nature 489, 141–144. https://doi.org/10.1038/nature11391.

Murray-Wallace, C.V., 2007. Eustatic sea-level changes since the last glaciation. In: Elias, S.A. (Ed.), Encyclopedia of Quaternary Science. Elsevier, Amsterdam, pp. 3034–3043.

Naquin, J.D., Liu, K., McCloskey, T.A., Bianchette, T.A., 2014. Storm deposition induced by hurricanes in a rapidly subsiding coastal zone. J. Coast. Res. 70, 308–313. https://doi.org/10.2112/si70-052.1.

National Climatic Data Center, 2018. NOAA Baseline Climatological Dataset - Monthly Weather Station Temperature and Precipitation Data. www.ncdc.noaa.gov.

Nielsen, S.H.H., Koç, N., Crosta, X., 2004. Holocene climate in the Atlantic sector of the Southern Ocean: controlled by insolation or oceanic circulation? Geology 32, 317–320. https://doi.org/10.1130/G20334.1.

Nittrouer, C.A., Kuehl, S.A., Figueiredo, G., Allison, M.A., K, I.I.C., Rine, J.M., Faria, T.L.E.C., Silveira, O.M., 1996. The Geological Record Preserved by Amazon Shelf Sedimentation. p. 16.

O'ishi, R., Abe-Ouchi, A., 2011. Polar amplification in the mid-Holocene derived from dynamical vegetation change with a GCM. Geophys. Res. Lett. 38. https://doi.org/10.1029/2011GL048001 n/a-n/a.

Osland, M.J., Feher, L.C., 2020. Winter climate change and the poleward range expansion of a tropical invasive tree (Brazilian pepper—Schinus terebinthifolius). Glob. Chang. Biol. 26, 607–615. https://doi.org/10.1111/gcb.14842.

Osland, M.J., Day, R.H., From, A.S., McCoy, M.L., McLeod, J.L., Kelleway, J.J., 2015. Life stage influences the resistance and resilience of black mangrove forests to winter climate extremes. Ecosphere 6, art160. https://doi.org/10.1890/ES15-00042.1.

Osland, M.J., Day, R.H., Hall, C.T., Brumfield, M.D., Dugas, J.L., Jones, W.R., 2017. Mangrove expansion and contraction at a poleward range limit: climate extremes and land-ocean temperature gradients. Ecology 98, 125–137. https://doi.org/10.1002/ecy.1625.

Osland, M.J., Feher, L.C., López-Portillo, J., Day, R.H., Suman, D.O., Guzmán Menéndez, J.M., Rivera-Monroy, V.H., 2018. Mangrove forests in a rapidly changing world: Global change impacts and conservation opportunities along the Gulf of Mexico coast. Estuar. Coast. Shelf Sci. 214, 120–140. https://doi.org/10.1016/j.ecss.2018.09.006.

Osland, M.J., Hartmann, A.M., Day, R.H., Ross, M.S., Hall, C.T., Feher, L.C., Vervaeke, W.C., 2019. Microclimate influences mangrove freeze damage: implications for range expansion in response to changing macroclimate. Estuar. Coasts 42, 1084–1096. https://doi.org/10.1007/s12237-019-00533-1.

Peros, M.C., Reinhardt, E.G., Davis, A.M., 2007. A 6000-year record of ecological and hydrological changes from Laguna de la Leche, north coastal Cuba. Quat. Res. 67, 69–82. https://doi.org/10.1016/j.yqres.2006.08.004.

Perry, C.L., Mendelssohn, I.A., 2009. Ecosystem effects of expanding populations of *Avicennia germinans* in a Louisiana salt marsh. Wetlands 29, 396–406. https://doi.org/10.1672/08-100.1.

Pessenda, L.C.R., Ribeiro, A.D.S., Gouveia, S.E.M., Aravena, R., Boulet, R., Bendassolli, J.A., 2004. Vegetation dynamics during the late Pleistocene in the Barreirinhas region, Maranhão State, northeastern Brazil, based on carbon isotopes in soil organic matter. Quat. Res. 62, 183–193. https://doi.org/10.1016/j.yqres.2004.06.003.

Pessenda, L.C.R., Gouveia, S.E.M., Ribeiro, A. de S., De Oliveira, P.E., Aravena, R., 2010. Late Pleistocene and Holocene vegetation changes in northeastern Brazil determined from carbon isotopes and charcoal records in soils. Palaeogeogr. Palaeoclimatol. Palaeoecol. 297, 597–608. https://doi.org/10.1016/j.palaeo.2010.09.008.

Pessenda, L.C.R., Vidotto, E., De Oliveira, P.E., Buso, A.A., Cohen, M.C.L., Rossetti, D. de F., Ricardi-Branco, F., Bendassolli, J.A., 2012. Late Quaternary vegetation and coastal environmental changes at Ilha do Cardoso mangrove, southeastern Brazil. Palaeogeogr. Palaeoclimatol. Palaeoecol. 363, 57–68.

Quisthoudt, K., Schmitz, N., Randin, C.F., Dahdouh-Guebas, F., Robert, E.M.R., Koedam, N., 2012. Temperature variation among mangrove latitudinal range limits worldwide. Trees Struct. Funct. 26, 1919–1931. https://doi.org/10.1007/s00468-012-0760-1.

Reading, H.G., 1996. Sedimentary Environments: Processes, Facies and Stratigraphy. 3a ed. Blackwell Science.

Reimer, P.J., Bard, E., Bayliss, A., Beck, J.W., Blackwell, P.G., Ramsey, C.B., Buck, C.E., Cheng, H., Edwards, R.L., Friedrich, M., Grootes, P.M., Guilderson, T.P., Haflidason, H., Hajdas, I., Hatté, C., Heaton, T.J., Hoffmann, D.L., Hogg, A.G., Hughen, K.A., Kaiser, K.F., Kromer, B., Manning, S.W., Niu, M., Reimer, R.W., Richards, D.A., Scott, E.M., Southon, J.R., Staff, R.A, Turney, C.S.M., van der Plicht, J., 2013. IntCal13 and Marine13 radiocarbon age calibration curves 0–50,000 years cal BP. Radiocarbon 55, 1869–1887. https://doi.org/10.2458/azu_js_rc.55.16947.

Reineck, H.E., Singh, I.B., 1980. Depositional Sedimentary Environments, With Reference to Terrigenous Clastics. Second edition. Depos. Sediment. Environ. With Ref. to Terrigenous Clastics Textbook. (Second Ed. (Textb.).

Ribeiro, S.R., Batista, E.J.L., Cohen, M.C., França, M.C., Pessenda, L.C., Fontes, N.A., Alves, I.C., Bendassolli, J.A., 2018. Allogenic and autogenic effects on mangrove dynamics from the Ceará Mirim River, north-eastern Brazil, during the middle and late Holocene. Earth Surf. Process. Landforms. https://doi.org/10.1002/esp.4342.

Ribeiro, R. de A., Rovai, A.S., Twilley, R.R., Castañeda-Moya, E., 2019. Spatial variability of mangrove primary productivity in the neotropics. Ecosphere 10. https://doi.org/10.1002/ecs2.2841.

Rodriguez, A.B., Anderson, J.B., Siringan, F.P., Taviani, M., 2004. Holocene evolution of the East Texas coast and inner continental shelf: along-strike variability in coastal retreat rates. J. Sediment. Res. 74, 405–421. https://doi.org/10.1306/092403740405.

Rossetti, D.F., Cohen, M.C.L., Bertani, T.C., Hayakawa, E.H., Paz, J.D.S., Castro, D.F., Friaes, Y., 2014. Late Quaternary fluvial terrace evolution in the main southern Amazonian tributary. Catena 116. https://doi.org/10.1016/j.catena.2013.11.021.

Ruddiman, W.F., 2003. The anthropogenic greenhouse era began thousands of years ago. Clim. Chang. https://doi.org/10.1023/B:CLIM.0000004577.17928.fa.

Ruddiman, W.F., Fuller, D.Q., Kutzbach, J.E., Tzedakis, P.C., Kaplan, J.O., Ellis, E.C., Vavrus, S. J., Roberts, C.N., Fyfe, R., He, F., Lemmen, C., Woodbridge, J., 2016. Late Holocene climate: natural or anthropogenic? Rev. Geophys. https://doi.org/10.1002/2015RG000503.

Ryu, J., 2020. Late Holocene Environmental Changes and Ecosystem Dynamics in Louisiana's Coastal Wetlands: A Multi-Site, Multi-Proxy Investigation. Louisiana State University.

Saintilan, N., Wilson, N.C., Rogers, K., Rajkaran, A., Krauss, K.W., 2014. Mangrove expansion and salt marsh decline at mangrove poleward limits. Glob. Chang. Biol. 20, 147–157. https://doi.org/10.1111/gcb.12341.

Sandoval-Castro, E., Muñiz-Salazar, R., Enríquez-Paredes, L.M., Riosmena-Rodríguez, R., Dodd, R.S., Tovilla-Hernández, C., Arredondo-García, M.C., 2012. Genetic population structure of red mangrove (*Rhizophora mangle* L.) along the northwestern coast of Mexico. Aquat. Bot. 99, 20–26. https://doi.org/10.1016/J.AQUABOT.2012.01.002.

Santos, T.P., Franco, D.R., Barbosa, C.F., Belem, A.L., Dokken, T., Albuquerque, A.L.S., 2013. Millennial- to centennial-scale changes in sea surface temperature in the tropical South Atlantic throughout the Holocene. Palaeogeogr. Palaeoclimatol. Palaeoecol. 392, 1–8. https://doi.org/10.1016/j.palaeo.2013.08.019.

Saucier, R.T., 1994. Geomorphology and Quaternary Geologic History of the Lower Mississippi Valley. volume 1. U. S. Army Corps of Engineers, Vicksburg ed.

Shea Penland, J.R.S., 1988. Barrier Island Erosion and Protection in Louisiana: A Coastal Geomorphological Perspective. p. 38.

Sherrod, C.L., McMillan, C., 1985. The distributional history and ecology of mangrove vegetation along the northern Gulf of Mexico coastal region. Contrib. Mar. Sci. 28, 129–140.

Silva, M.N.A., Cohen, M.C.L., Rossetti, D.F., Pessenda, L.C.R., 2018. Did sea-level changes affect the Brazilian Amazon Forest during the Holocene? Radiocarbon 60, 91–112. https://doi.org/10.1017/RDC.2017.62.

Skvarla, J.J., Larson, D.A., 1963. Nature of cohesion within pollen tetrads of *Typha latifolia*. Science (80-) 140, 173–175. https://doi.org/10.1126/science.140.3563.173.

Smith, C.B., Cohen, M.C.L., Pessenda, L.C.R., França, M.C., Guimarães, J.T.F., Rossetti, D. de F., Lara, R.J., 2011. Holocene coastal vegetation changes at the mouth of the Amazon River. Rev. Palaeobot. Palynol. 168, 21–30.

Smith, C.B., Cohen, M.C.L., Pessenda, L.C.R., França, M.C., Guimarães, J.T.F., 2012. Holocenic proxies of sedimentary organic matter and the evolution of Lake Arari-Amazon Region. Catena 90, 26–38.

Solomon, A.M., Blasing, T.J., Solomon, J.A., 1982. Interpretation of floodplain pollen in alluvial sediments from an Arid Region. Quat. Res. 18, 52–71.

Solomon, S., Qin, D., Manning, M., Chen, Z., Marquis, M., Averyl, K.B., Tignor, M., Miller, H.L., 2007. Climate Change 2007: The Physical Science Basis. Contribution of Working Group I to the Fourth Assessment Report of the Intergovernmental Panel on Climate Change. Cambridge University Press.

Stevens, P.W., Fox, S.L., Montague, C.L., 2006. The interplay between mangroves and saltmarshes at the transition between temperate and subtropical climate in Florida. Wetl. Ecol. Manag. 14, 435–444. https://doi.org/10.1007/s11273-006-0006-3.

Stokes, D.J., Healy, T.R., Cooke, P.J., 2010. Expansion dynamics of monospecific, temperate mangroves and sedimentation in two embayments of a barrier-enclosed lagoon, Tauranga Harbour, New Zealand. J. Coast. Res. 261, 113–122. https://doi.org/10.2112/08-1043.1.

Stuart, S.A., Choat, B., Martin, K.C., Holbrook, N.M., Ball, M.C., 2007. The role of freezing in setting the latitudinal limits of mangrove forests. New Phytol. 173, 576–583. https://doi.org/10.1111/j.1469-8137.2006.01938.x.

Sun, X., Li, X., 1999. A pollen record of the last 37 ka in deep sea core 17940 from the northern slope of the South China Sea. Mar. Geol. 156, 227–244. https://doi.org/10.1016/S0025-3227(98)00181-9.

Sundqvist, H.S., Kaufman, D.S., McKay, N.P., Balascio, N.L., Briner, J.P., Cwynar, L.C., Sejrup, H.P., Seppä, H., Subetto, D.A., Andrews, J.T., Axford, Y., Bakke, J., Birks, H.J.B., Brooks, S. J., De Vernal, A., Jennings, A.E., Ljungqvist, F.C., Rühland, K.M., Saenger, C., Smol, J.P., Viau, A.E., 2014. Arctic Holocene proxy climate database - new approaches to assessing geochronological accuracy and encoding climate variables. Clim. Past 10, 1605–1631. https://doi.org/10.5194/cp-10-1605-2014.

Taillardat, P., Friess, D.A., Lupascu, M., 2018. Mangrove blue carbon strategies for climate change mitigation are most effective at the national scale. Biol. Lett. 14, 20180251. https://doi.org/10.1098/rsbl.2018.0251.

Tarver, J., 1972. Occurrence, distribution, and density of Rangia cuneata in Lakes Pontchartrain and Maurepas, Louisiana, (Louisiana Wild Life and Fisheries Commission. Technical bulletin no. 1) [WWW Document]. URL https://www.amazon.com/Occurrence-distribution-Pontchartrain-Louisiana-Commission/dp/B0006CD1SA (accessed 5.18.20).

Timm, O., Timmermann, A., 2007. Simulation of the last 21,000 years using accelerated transient boundary conditions. J. Clim. 20, 4377–4401. https://doi.org/10.1175/JCLI4237.1.

Tomlinsom, P.B., 1986. The Botany of Mangroves. Cambridge University Press, Cambridge.

Toscano, M.A., Macintyre, I.G., 2003. Corrected western Atlantic sea-level curve for the last 11,000 years based on calibrated 14C dates from *Acropora palmata* framework and intertidal mangrove peat. Coral Reefs 22, 257–270. https://doi.org/10.1007/s00338-003-0315-4.

Tyson, R.V., 1995. Sedimentary Organic Matter: Organic Facies and Palynofacies. Chapman and Hall, London.

Vedel, V., Behling, H., Cohen, M., Lara, R., 2006. Holocene mangrove dynamics and sea-level changes in northern Brazil, inferences from the Taperebal core in northeastern Pará State. Veg. Hist. Archaeobot. 15, 115–123. https://doi.org/10.1007/s00334-005-0023-9.

Vega, A.J., 2012. Louisiana Weather and Climate - Louisiana State University Baton Rouge [WWW Document] (URL https://books.google.com.br/books?id=0wglj5alm9oC&printsec=frontcover&hl=pt-BR#v=onepage&q&f=false (accessed 5.17.20)).

Wakida-Kusunoki, A.T., MacKenzie, C.L., 2004. Rangia and marsh clams, *Rangia cuneata*, *R. flexuosa*, and *Polymesoda caroliniana*, in Eastern México: distribution, biology and ecology, and historical fisheries. Mar. Fish. Rev. 66, 13–20.

Walker, R.G., 1992. Facies, facies models and modern stratigrahic concepts. In: Walker, R.G., James, N.P. (Eds.), Facies Models - Response to Sea Level Change. Geological Association of Canada, Ontario, pp. 1–14.

Walsh, G.E., 1974. Mangroves: a review. In: Reinold, R.J., Queen, W.H. (Eds.), Ecology of Halophytes. Academic Press, New York, pp. 51–174.

Walsh, J., Nittrouer, C., 2004. Mangrove-bank sedimentation in a mesotidal environment with large sediment supply, Gulf of Papua. Mar. Geol. 208, 225–248. https://doi.org/10.1016/j.margeo.2004.04.010.

Wanless, H.R., Parkinson, R.W., Tedesco, L.P., 1994. Sea level control on stability of Everglades wetlands. In: Davis, S.M., Ogden, J.C. (Eds.), Everglades: The Ecosystem and Its Restoration. St. Lucie Press, pp. 199–222.

Warzocha, J., Szymanek, L., Witalis, B., Wodzinowski, T., 2016. The first report on the establishment and spread of the alien clam *Rangia cuneata* (Mactridae) in the Polish part of the Vistula Lagoon (southern Baltic). Oceanologia 58, 54–58. https://doi.org/10.1016/j.oceano.2015.10.001.

Weng, C., Bush, M.B., Silman, M.R., 2004. An analysis of modern pollen rain on an elevational gradient in southern Peru. J. Trop. Ecol. 20, 113–124. https://doi.org/10.1017/S0266467403001068.

Willard, D.A., Bernhardt, C.E., 2011. Impacts of past climate and sea level change on Everglades wetlands: placing a century of anthropogenic change into a late-Holocene context. Clim. Chang. 107, 59–80. https://doi.org/10.1007/s10584-011-0078-9.

Willard, D.A., Bernhardt, C.E., Weimer, L., Cooper, S.R., Gamez, D., Jensen, J., 2004. Atlas of pollen and spores of the Florida everglades. Palynology 28, 175–227.

Woodroffe, C.D., Grindrod, J., 1991. Mangrove biogeography: the role of quaternary environmental and sea-level change. J. Biogeogr. 18, 479–492. https://doi.org/10.2307/2845685.

Woodroffe, C.D., Thom, B.G., Chappell, J., 1985. Development of widespread mangrove swamps in mid-Holocene times in northern Australia. Nature 317, 711–713. https://doi.org/10.1038/317711a0.

Woodroffe, S.A., Long, A.J., Punwong, P., Selby, K., Bryant, C.L., Marchant, R., Bronk Ramsey, C., Buck, C.E., Burr, G.S., Edwards, R.L., Friedrich, M., Grootes, P.M., Guilderson, T.P., Hajdas, I., Heaton, T.J., Hogg, A.G., Hughen, K.A., Kaiser, K.F., Kromer, B., McCormac, F.G., Manning, S.W., Reimer, R.W., Richards, D.A., Southon, J.R., Talamo, S., Turney, C.S.M., van der Plicht, J., Weyhenmeyer, C.E., 2015. Radiocarbon dating of mangrove sediments to constrain Holocene relative sea-level change on Zanzibar in the southwest Indian Ocean. The Holocene 25, 820–831. https://doi.org/10.1177/0959683615571422.

Xu, Q., Tian, F., Bunting, M.J., Li, Y., Ding, W., Cao, X., He, Z., 2012. Pollen source areas of lakes with inflowing rivers: modern pollen influx data from Lake Baiyangdian, China. Quat. Sci. Rev. 37, 81–91. https://doi.org/10.1016/j.quascirev.2012.01.019.

Yao, Q., Liu, K., 2017. Dynamics of marsh-mangrove ecotone since the mid-Holocene: a palynological study of mangrove encroachment and sea level rise in the Shark River Estuary, Florida. PLoS One 12, e0173670. https://doi.org/10.1371/journal.pone.0173670.

Yao, Q., Liu, K., Platt, W.J., Rivera-Monroy, V.H., 2015. Palynological reconstruction of environmental changes in coastal wetlands of the Florida Everglades since the mid-Holocene. Quat. Res. 83, 449–458. https://doi.org/10.1016/j.yqres.2015.03.005.

Yao, Q., Liu, K., Ryu, J., 2018. Multi-proxy characterization of hurricanes Rita and Ike storm deposits in the Rockefeller Wildlife Refuge, Southwestern Louisiana. J. Coast. Res. 85, 841–845. https://doi.org/10.2112/si85-169.1.

Yao, Q., Liu, K. Biu, Aragón-Moreno, A.A., Rodrigues, E., Xu, Y.J., Lam, N.S., 2020. A 5200-year paleoecological and geochemical record of coastal environmental changes and shoreline fluctuations in southwestern Louisiana: implications for coastal sustainability. Geomorphology 365, 107284. https://doi.org/10.1016/j.geomorph.2020.107284.

Zalasiewicz, J., Waters, C.N., Williams, M., Summerhayes, C., 2018. The Anthropocene as a Geological Time Unit: A Guide to the Scientific Evidence and Current Debate. Cambridge University Press.

CAPÍTULO III: SOUTHWARD MIGRATION OF THE AUSTRAL LIMIT OF MANGROVES IN SOUTH AMERICA

Marcelo C.L. Cohen [a,*] , Erika Rodrigues[a] , Denise O.S. Rocha[a] , Jaine Freitas[a] , Neuza A. Fontes[a] , Luiz C.R. Pessenda[b] , Adriana V. de Souza[a] , Vivian L.P. Gomes[a] , Marlon Carlos França[c] , Daniel M. Bonotto[d] , José A. Bendassolli[e]

a Graduate Program of Geology and Geochemistry, Federal University of Pará, Av. Perimentral 2651, Terra Firme, 66077-530 Belém, PA, Brazil

b University of São Paulo, CENA/14C Laboratory, Av. Centenário 303, 13400-000 Piracicaba, São Paulo, Brazil

c Federal Institute of Pará, Av. Alm. Barroso, 1155, Marco, 66090-020 Belém, PA, Brazil

d Instituto de Geociências e Ciências da Terra, Universidade Estadual Paulista Júlio de Mesquita Filho-UNESP, Rio Claro, São Paulo, Brazil

e University of São Paulo, CENA/Stable Isotopes Laboratory, São Paulo, Brazil

Catena 195 (2020) 104775

Contents lists available at ScienceDirect

Catena

journal homepage: www.elsevier.com/locate/catena

Southward migration of the austral limit of mangroves in South America

Marcelo C.L. Cohen[a,*], Erika Rodrigues[a], Denise O.S. Rocha[a], Jaine Freitas[a], Neuza A. Fontes[a], Luiz C.R. Pessenda[b], Adriana V. de Souza[a], Vivian L.P. Gomes[a], Marlon Carlos França[c], Daniel M. Bonotto[d], José A. Bendassolli[e]

[a] Graduate Program of Geology and Geochemistry, Federal University of Pará, Av. Perimentral 2651, Terra Firme, 66077-530 Belém, PA, Brazil
[b] University of São Paulo, CENA/^{14}C Laboratory, Av. Centenário 303, 13400-000 Piracicaba, São Paulo, Brazil
[c] Federal Institute of Pará, Av. Alm. Barroso, 1155, Marco, 66090-020 Belém, PA, Brazil
[d] Instituto de Geociências e Ciências da Terra, Universidade Estadual Paulista Júlio de Mesquita Filho-UNESP, Rio Claro, São Paulo, Brazil
[e] University of São Paulo, CENA/Stable Isotopes Laboratory, São Paulo, Brazil

ARTICLE INFO

Keywords:
Anthropocene
Drone
Global warming
Laguncularia

ABSTRACT

Temperature influences the global distribution of mangroves, and global warming may be causing a poleward mangrove expansion. Sedimentary features, pollen, and isotopes data from six sediment cores, as well as ^{14}C datings, indicated a marine transgression during the Holocene, and it contributed to the expansion of tidal flats occupied by saltmarshes. Environmental conditions suitable for mangroves development occurred on the study site during the Holocene, but, according to ^{210}Pb and ^{14}C dating, the establishment of mangroves mainly represented by *Laguncularia* trees only began between ~1957 and ~1986 (AD) on the studied tidal flats. Spatial-temporal analysis, based on satellite and drone images, revealed a mangrove expansion of ~10 ha in the study area between 2003 (96.1 ha) and 2019 (106.1 ha). Nowadays, in the study area, saltmarshes, mainly characterized by *Spartina* and *Acrostichum*, are sharing tidal flats with mangroves, represented by *Laguncularia* (≤5 m tall) and *Avicennia* (≤11 m tall). Probably, the absence of mangroves during the Holocene, followed by their establishment and expansion during the Anthropocene in the subtropical zone, is associated with a migration of the austral mangrove limit into the temperate zone, caused by the gradual increase in winter temperatures. This process may be related to a poleward mangrove migration since the late Holocene, caused by a natural Holocene global warming. However, the industrial-era warming must have intensified the mangrove expansion into temperate zones.

1. Introduction

Global warming has been controversial during the last decades, mainly about human influence on climate (Keller, 2003). However, stronger recent warming trends indicated that human influence is dominant in long-term warming (Medhaug et al., 2017). For instance, human-induced warming reached approximately 1 °C above pre-industrial levels in 2017, increasing at 0.2 °C per decade (Allen et al., 2018), and minimum temperatures globally are rising at twice the rate of maximum temperatures (Easterling et al., 2000; Walther et al., 2002). Global warming is causing a poleward migration of isotherms at rates averaging 27 km/decade (Burrows et al., 2011), and pushing tropical species to become more abundant in temperate areas (Parmesan and Yohe, 2003; Poloczanska et al., 2013), for instance, plants (Sturm et al., 2001; Van Grunsven et al., 2010), butterfly species (Parmesan et al., 1999), birds (Thomas and Lennon, 1999) and modern corals (Yamano et al., 2011) have advanced poleward.

In this context, mangroves may also be used as indicators of climate change (Alongi, 2008; Blasco et al., 1996; Fromard et al., 2004), since they are strongly susceptible to cold temperatures. For this reason, mangroves are restricted to latitudes where the coldest monthly mean temperature is above 20 °C, and the annual thermal amplitude is less than 5 °C (Chapman, 1976; Giri et al., 2011; Walsh, 1974). Then, cold temperatures have limited the northern and southern limits for mangroves to around 30°N (Kangas et al., 1961) and 28°S (França et al., 2019; Soares et al., 2012). However, saltmarshes are dominated by freeze-tolerant herbs that are most abundant along temperate and arctic coasts (Ibáñez et al., 2012). Probably, under global warming influence, mangroves will migrate to higher latitudes, replacing salt marsh (Field, 1995; Gilman et al., 2008; Woodroffe and Grindrod, 1991).

Mangrove contraction and expansion in North America occurred during the Quaternary in response to changes in temperatures (Osland

* Corresponding author at: Federal University of Pará – Brazil, Rua Augusto Corrêa, 01 – Guamá, CEP 66075-110 Belém, PA, Brazil.
E-mail address: mcohen@ufpa.br (M.C.L. Cohen).

https://doi.org/10.1016/j.catena.2020.104775
Received 13 February 2020; Received in revised form 8 June 2020; Accepted 28 June 2020
Available online 11 July 2020

et al., 2017; Saintilan et al., 2014; Sandoval-Castro et al., 2012; Sherrod and McMillan, 1985; Woodroffe and Grindrod, 1991). Mangroves occupied areas north of their current limits in Texas, Louisiana, Mississippi, Alabama, and Georgia before the Quaternary (Gee, 2001; Sherrod and McMillan, 1985; Westgate and Gee, 1990). In contrast, during the Pleistocene, the northern limit of mangroves retreated to more equatorial zones in the Caribbean (Sherrod and McMillan, 1985). Regarding the Last Glacial Maximum (LGM), mangrove limits migrated to more tropical zones, followed by an expansion poleward after the LGM (Kennedy et al., 2016; Sandoval-Castro et al., 2012). During the early and mid Holocene, the global mean surface temperature increased (Kaufman et al., 2020), causing a sea-level rise (Angulo et al., 2016; Cohen et al., 2020), and the establishment of tropical mangroves along the Brazilian coast at ~7000 cal yrs BP (Cohen et al., 2020, 2014, 2012; Fontes et al., 2017; França et al., 2015, 2013; Ribeiro et al., 2018). This Holocene warming may have caused a mangrove expansion from tropical to subtropical zones during the late Holocene (França et al., 2019; Pessenda et al., 2012). According to Alongi (2008), the mangrove dynamics in the northern hemisphere is related to global climate and sea-level changes since the LGM.

Regarding the industrial-era warming, some studies have indicated a tropicalization of coastal wetlands ecosystems, for instance, by the poleward mangrove expansion along Mexico (Saintilan et al., 2014) and United States (Cavanaugh et al., 2014; Osland et al., 2018; Perry and Mendelssohn, 2009). In the hypothesis of the poleward expansion of mangroves in North America is being caused by the modern global warming, the southern boundary of the Southern American mangroves must also be migrating poleward. In this context, the warming for Southern Brazil between 1960 and 2002 was stronger in the minimum temperature range at annual timescales (+0.5 °C per decade) and in winter (+0.4 °C per decade) as compared to the smaller warming trends in maximum temperatures at annual and summer timescales (+0.2 °C per decade) (Marengo and Camargo, 2008). Marengo (2006) estimated an increase between 3 and 5 °C by 2080 for the Brazilian territory. If this recent rise in temperature is inducing such poleward mangrove migration, this ecosystem should be absent along its modern austral limit during the Holocene, since the industrial-era warming has led to a modern climate that is unprecedented in the Holocene context (Porter et al., 2019). Then, to test the relationship between latitudinal mangrove expansion and global warming, this work aims to develop a paleoenvironmental reconstruction on a millennial and decadal-scale based on satellite/drone images and pollen, geochemical ($\delta^{13}C$, $\delta^{15}N$ and C\N) and sedimentary data, as well as ^{14}C and ^{210}Pb datings along six cores sampled from tidal flats occupied by mangroves in their austral limit.

2. Study site

2.1. Geomorphological settings

The study site is at Santo Antônio Lagoon, near the city of Laguna in the State of Santa Catarina (Fig. 1). The lagoon complex, formed by the Imaruí, Mirim, and Santo Antônio lagoon, has approximately 40 km in length (Eichler et al., 2006). The Santa Catarina coastal plain is subdivided mainly into four depositional systems: Holocene regressive barrier, strand-plain, dune fields, and Holocene lagoonal system. The Holocene regressive barrier system occurs in the south of Laguna and is associated with back-barrier lagoonal and paleo-lagoonal deposits. The strand plain system is composed of, at least, a late Pleistocene and a Holocene section. The strand plain is distinguished from the barrier system by the absence of a contiguous back-barrier lagoon. The Imaruí and Mirim lagoons, which occur behind the Pleistocene strand plains, are drowned river valleys (Angulo et al., 1999).

2.2. Climate

The climate is subtropical humid without a dry season. In the state of Santa Catarina, the highest temperature in summer at Laguna reaches 30 °C, and the minimum in winter is 6 °C. The humidity is around 85%, and the annual average precipitation is between 1250 mm (Imbituba) and 1400 mm (Laguna) (INMET, 2017). The climate is controlled by South Atlantic Tropical Anticyclone, related to trade winds from the NE, and Polar Migratory Anticyclone (PMA). The migration of the PMA to the north can generate cold fronts with increases in precipitation rates (Carvalho do Amaral et al., 2013).

2.3. Vegetation

The native vegetation of east Santa Catarina is subdivided into five main zones: The Coastal vegetation, Atlantic pluvial forest, Cloud forest zone, Araucaria forest, and the Grassland. Coastal vegetation consists of mangrove, and plants communities occupying beaches and dunes directly or indirectly influenced by the ocean (Behling, 1995). The foredune vegetation is mainly characterized by a low diversity of herbaceous species that occurs under variable temperature, with low soil humidity and constant sand movements (Cordazzo and Seeliger, 1995). The dominant families are Poaceae, Amaranthaceae, Asteraceae, and Apiaceae. The vegetation surrounding the lagoons, swamps, and peat bogs are mainly represented by Lentibulariaceae, Cyperaceae, and Poaceae families. The lowland forest is characterized by a high diversity of species, with a large number of epiphytes, lianes, and several types of ferns. The dominant trees are Euphorbiaceae, Moraceae, Fabaceae, Malpighiaceae, Aquifoliaceae, Urticaceae, and Myrtaceae families (Carvalho do Amaral et al., 2013).

3. Material and methods

The materials used involved spatial–temporal analysis based on satellite/drone images and digital elevation models obtained by drone data. Field investigation allowed validation of the results through the acquisition of topographic data, vegetation height, and vegetation types. Sedimentary features, isotopic and elemental laboratory analysis on six sediment cores, with temporal control obtained by ^{14}C (AMS) and ^{210}Pb dating, were developed, following a pre-designed methodology flow chart (Fig. 2).

3.1. Data sources

3.1.1. Satellite data

According to the availability and quality of QuickBird satellite images obtained from Google Earth Pro, seven dates (Aug/2003, Jun/2009, Jan/2012, Jul/2013, May/2016, Jul/2017, and Jul/2018) were chosen for the identification and quantification of mangrove areas. These images present a spatial resolution of 2.44 m (multispectral) and three bands (blue, green, red). All images were imported in GeoTIFF format into the Agisoft Metashape Professional version 1.6.2 software and orthorectified according to high-resolution orthoimages of drone, with a spatial accuracy of 10 cm. The drone images were orthorectified based on 102 ground control points (GCPs). All images were exported in GeoTIFF format into the Global Mapper version 18 software for analysis. Human interventions in the study area, such as houses and roads, were used to define reference points for spatial–temporal analysis.

3.1.2. Drone data

High-resolution images obtained by a Drone Phantom 4 Advanced DJI completed the spatial–temporal analysis. It is a battery-powered quadricopter, equipped with GPS and inertial measurement. It has a FC 6310 digital 4 K/20MP (RGB) camera with focal length and sensor width of 8.8 mm and 12.8 mm, respectively. It generated image width with 5472 pixels. This camera positioned on a motion-compensated

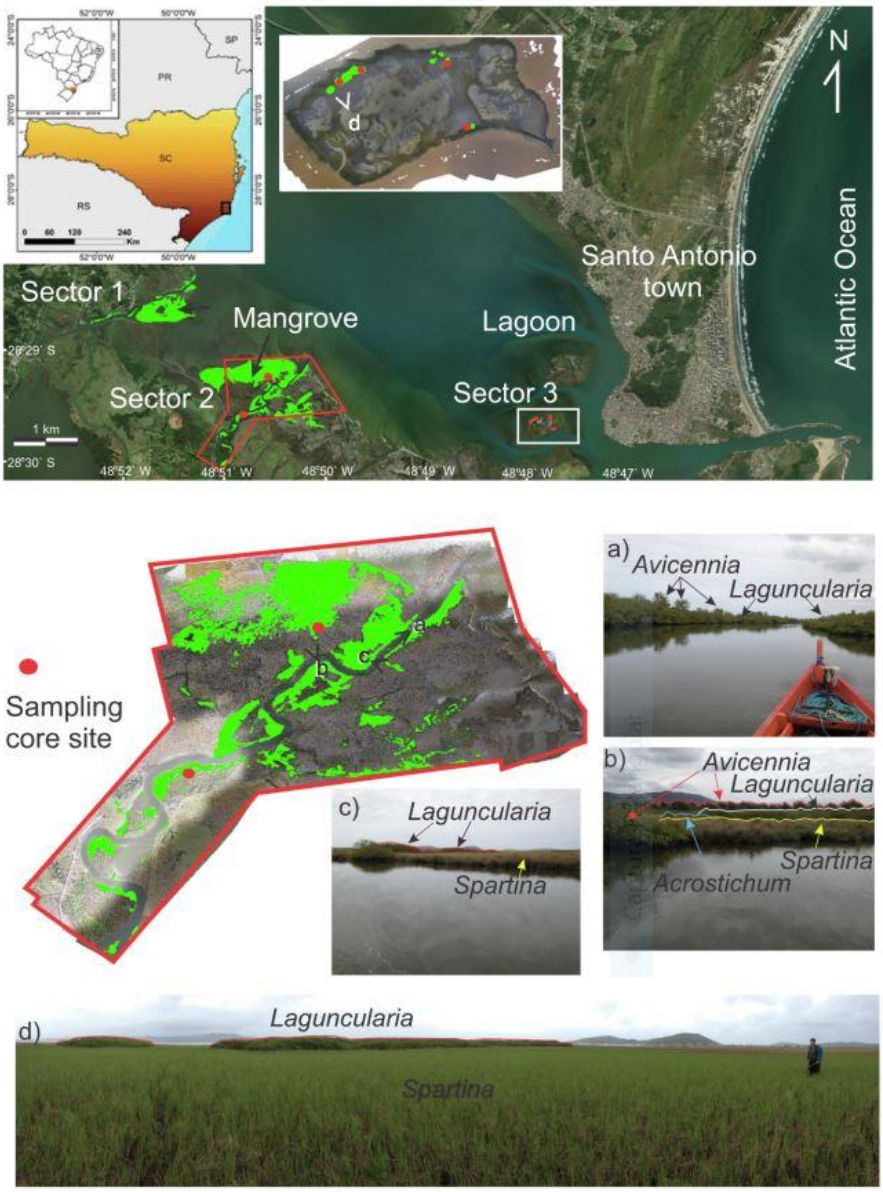

Fig. 1. Location of the study area, mangrove distribution in the sectors 1, 2 and 3, and sampling core sites; (a–c) Ground photos showing *Avicennia* and *Laguncularia* trees, as well as *Acrostichum* and *Spartina* along a channel in the sector 2; (d) Ground photo exhibiting clusters of *Laguncularia* shrubs surrounded by Spartina in the sector 3.

gimbal and calibrated by the DJI Assistant 2 Software obtained high spatial resolution images of 2.6 cm/pixel (flight height of 100 m) and 1.6 cm/pixel (60 m) for the study area. The drone mapped at 60 m altitude specific zones to identify the mangrove type. This spatial resolution was calculated using the following Eq. (1):

$$GSD = (Sw * H * 100/60) / (Fr * imH), \quad (1)$$

where GSD = Ground Sampling Distance (centimeters/pixel), Sw = sensor width of the camera (millimeters), H = the flight height (meters), Fr = the focal length of the camera (millimeters) and imH = the image width (pixels) (PIX4D, 2013).

The drone surveying was carried out using the DJI Ground Station Pro Software installed in an IPad Air tablet with predefined missions implemented autonomously to follow a route defined by several navigation way-points with 90° camera angle, 90% frontal and 75% lateral overlay. A total of ten missions (4632 images) were flown in Sep/2017, Oct/2019 (spring) at Santa Catarina, and covered 434 ha. A single mission was performed in each target mangrove area, with interruptions for drone battery replacements. Each battery allowed scanning ~48 ha (15–18 min).

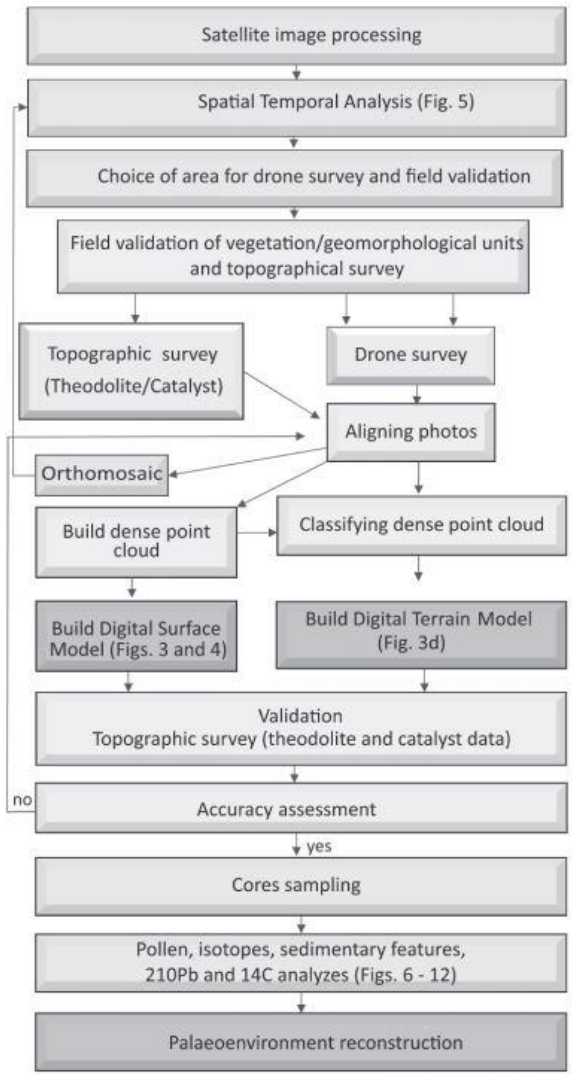

Fig. 2. Methodology flow chart modified from Cohen et al. (2018).

The major limitation of the drone survey is related to the incidence of sunlight during the flights. Data quality decreases significantly in low light, for instance, during sunrise, sunset, and when there are visibility constraints in the area, which can be caused by seasonal occurrences like fog, snowfall or rainfall. Then, it is recommended that such surveys occur during the summer and without clouds. Besides, the accuracy of the measurements depends on the flight height.

3.1.3. Ground control points

We carried out field trips in Oct/2015, Sep/2017, and Oct/2019. During these campaigns, planialtimetric data were obtained using an Antenna Trimble Catalyst with a differential Global Navigation Satellite System (GNSS). A sub-metric correction was applied to the GNSS data. After 30 min counting, the altimetric accuracy of the GCPs was in the order of ± 10 cm with the Real-Time Kinematic correction. This margin of error was calculated by comparing the data obtained by the Antenna Catalyst with the IBGE geodetic benchmarks. Physical obstacles such as buildings, tree canopy, and powerlines may affect the GNSS signals and reduce the accuracy of the planialtimetric data. Due to the long stabilization period of the Antenna Catalyst, the planialtimetric data, obtained with the Catalyst, were used as reference points for the topographic survey developed by an electronic theodolite (model CST Berger DGT10). Once a certain planialtimetric reference point based on the Catalyst was established, the theodolite was installed on that point to determine the relative topography of other Ground Control Points (GCPs). The planimetric (± 30 cm) and altimetric (± 10) data obtained for that GCPs were based on the Catalyst and theodolite, respectively. These data were used as GCPs (102 points) to calibrate the DEM obtained by photogrammetry.

Vegetation heights (VH) were calculated for mangrove and saltmarsh vegetation using a ruler of 4 m. These data were used to validate the vegetation height model obtained by photogrammetry. Visual observation and photographic documentation were used to confirm the key vegetation units.

3.1.4. Sediment cores

Cores LAG-3 (28°29′42.9″S/48°47′43.1″W), LAG-4 (28°29′34.0″S/48°47′49.6″W), LAG-5 (28°29′34.9″S/48°47′50.7″W), LAG-6 (28°29′37.5″S/48°0.47′57.2″W), RP-4 (28°29′14.6022″S/48°50′31.4710″W) and RP-3 (28°29′35.2333″S/48°50′52.9254″W) were collected during the spring season in October 2015, using Russian type sampling equipment. The sediment cores were taken from area colonized by mangroves mainly characterized by genus *Laguncularia,* and salt marsh characterized by *Spartina densiflora* and *Spartina alterninflora.* The cores were subsampled every 5 cm for grain-size, organic geochemistry, and pollen analysis. The geographical positions were determined by the Global Position System (GPS).

3.2. Methods used

3.2.1. Image classification

The categorization of vegetation cover was developed mainly under a visual classification by the Global Mapper Software, where a data set of locations with known land cover was used to determine the images features of each land cover type. The data collection for training and testing was based mainly on a range of image features (multispectral digital numbers) associated with the texture of a Quickbird image of 2018. The Create Area Features from the Equal Values tool allows for raster to vector or elevation grid to vector conversion of data based on the pixel values. The image was segmented based on spectral, physical, and geometric parameters. Regarding the multispectral digital numbers that best represented the mangroves, it was specified how close to an exact match a set of spectral values must be to match another set of spectral values, where the value of zero requires an exact match and 256 covers all valid spectral range. After the evaluation of the color fuzziness, the mangrove limits were adequately represented in the value 20. This set of information allowed us to individualize objects and compare them with a visual classification of drone orthoimages obtained in 2019 with spectral information between 380 and 710 nm. Drone images with a spatial resolution between 2.6 and 1.6 cm/pixel were able to individualize *Avicennia*and *Laguncularia* trees among the saltmarsh. These images were used as a reliable reference base to validate the classification developed on the Quickbird images. Ground photos were also used to facilitate the identification of vegetation units (Fig. 1a–d). The parameters that best represented the boundaries between the mangroves and saltmarshes were used to classify the Quickbird images of previous years. This procedure was followed by a visual check of each mangrove unit classified in the Quickbird images. This cross-validation data generated the highest accuracy for the identification of vegetation units. More details about the drone image processing may be obtained in Cohen et al. (2020, 2018).

3.2.2. 3D models generation and validation

Agisoft Metashape Professional version 1.6.2 software was used to process the drone images. This software develops photogrammetric processing based on digital images. It produced 3D spatial data and

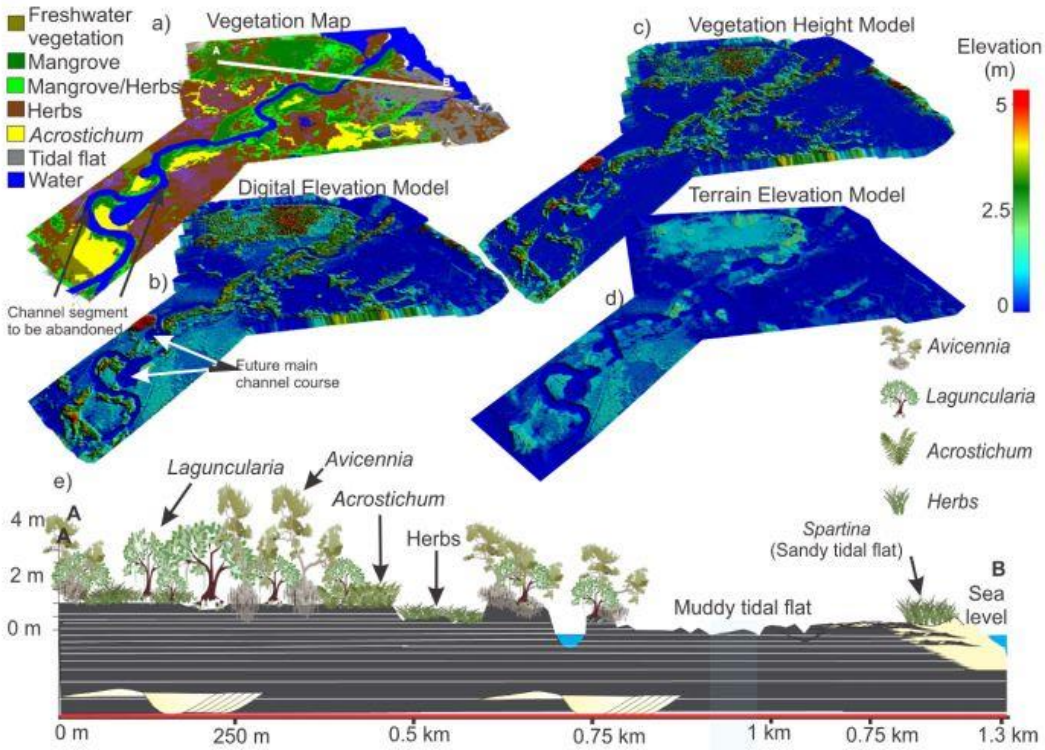

Fig. 3. (a) Vegetation map of the study area; (b) Digital elevation model, (c) Vegetation height model; (d) Terrain elevation model, (e) and a–b transect exhibiting the substrate topography and vegetation height.

orthomosaics with the support of ground control points (www.agisoft.com) (Figs. 3 and 4). The developed orthomosaic images of 2019 were used in the time series analysis.

A dense point cloud (spacing points from 3 to 5 cm) was executed in high resolution to obtain digital models of surface, terrain, and vegetation. Initially, this process generated a digital surface model (DSM) that represented the natural (trees, herbs, sediments, soils, and water) and built (power lines, buildings, and towers) features on the Earth's surface. A dense point cloud classification was developed to identify the terrain elevation. The digital terrain model (DTM) considers only the substrate surface without the vegetal covering and built features. The dense point clouds were split into cells, and the points in each cell were identified. Triangulation of these points allowed the first estimate of the DTM. Then, new points were added to the DTM, following these criteria: they occurred within a certain distance from the terrain model, and the angle between the terrain model and a line connecting the new points was less than a certain angle. For nearly flat terrain, it is recommended to use a default value of 15 deg. It is reasonable to set a higher value if the terrain contains steep slopes (Agisoft, 2018).

This procedure was applied in tidal flats without vegetation and in flats occupied by mangrove and marsh vegetation. The sharp differences in the elevations of point clouds enabled individualizing the points representing the vegetation cover and that reflecting the soil surface. Then a mesh of the soil surface was built based only on the points representing the topographic surface of the soil. This procedure extrapolated the topographic gradients of tidal flats without vegetation cover or with sparse vegetation to substrates with dense vegetation cover. This model was adjusted to the GCP obtained by the Antenna Catalyst and theodolite in areas under dense vegetation cover. Therefore, the digital terrain model below vegetation cover was a product of the combination of GCP interpolation from flats covered by vegetation with the topographic gradients of tidal flats without vegetation extrapolated to flats below vegetation cover. Tidal flats occupied by dense mangroves hinder an accurate topographic survey.

The vector data containing an elevation component were able to create an elevation grid based on the Triangulation. This setting uses a triangulated irregular network connecting the known elevation values. The vegetation height model was obtained by the Combine/Compare Terrain Layers tool. This command permits the generation of a new gridded elevation layer by combining and/or comparing the elevation values from two other loaded layers. For instance, this method was used to subtract the gridded elevation layer that represented the DSM from the DTM to obtain the digital vegetation height model (DVHM) of the sector 2 (Fig. 3c).

A quantitative analysis based on the vertical differences between check points and the DTM and DVHM of 2019 were obtained using the following Eq. (2), as suggested by Cohen et al. (2018):

$$Z_{dif} = Z_{DEM} - Z_{grd} \quad (2)$$

where Z_{dif} = the vertical differences, Z_{DEM} = the Z value of the 3D dense point cloud, and Z_{grd} = the Z value of the Antenna Catalyst/theodolite checkpoint. The Z_{dif} values were lower than 10 cm. Considering that Antenna Catalyst data have an error of ± 10 cm, a vertical margin of error of ± 10 cm was admitted for the 3D models. The final digital terrain model was adjusted using the Z_{dif} values.

3.2.3. Facies analysis

The cores were X-rayed to identify internal sedimentary structures. Grain size was determined by laser diffraction using a Laser Particle Size SHIMADZU SALD 2101 laser particle size analyzer in the Laboratory of Chemical Oceanography at UFPA. Around 0.5 g of each sample was rinsed with H_2O_2 to remove the organic matter, and the remaining sediments were disaggregated by ultrasound (França, 2010). The grain-size scale with sand (2–0.0625 mm), silt (62.5–3.9 μm), and clay fraction (3.9–0.12 μm) was considered for this work (Wentworth, 1922).

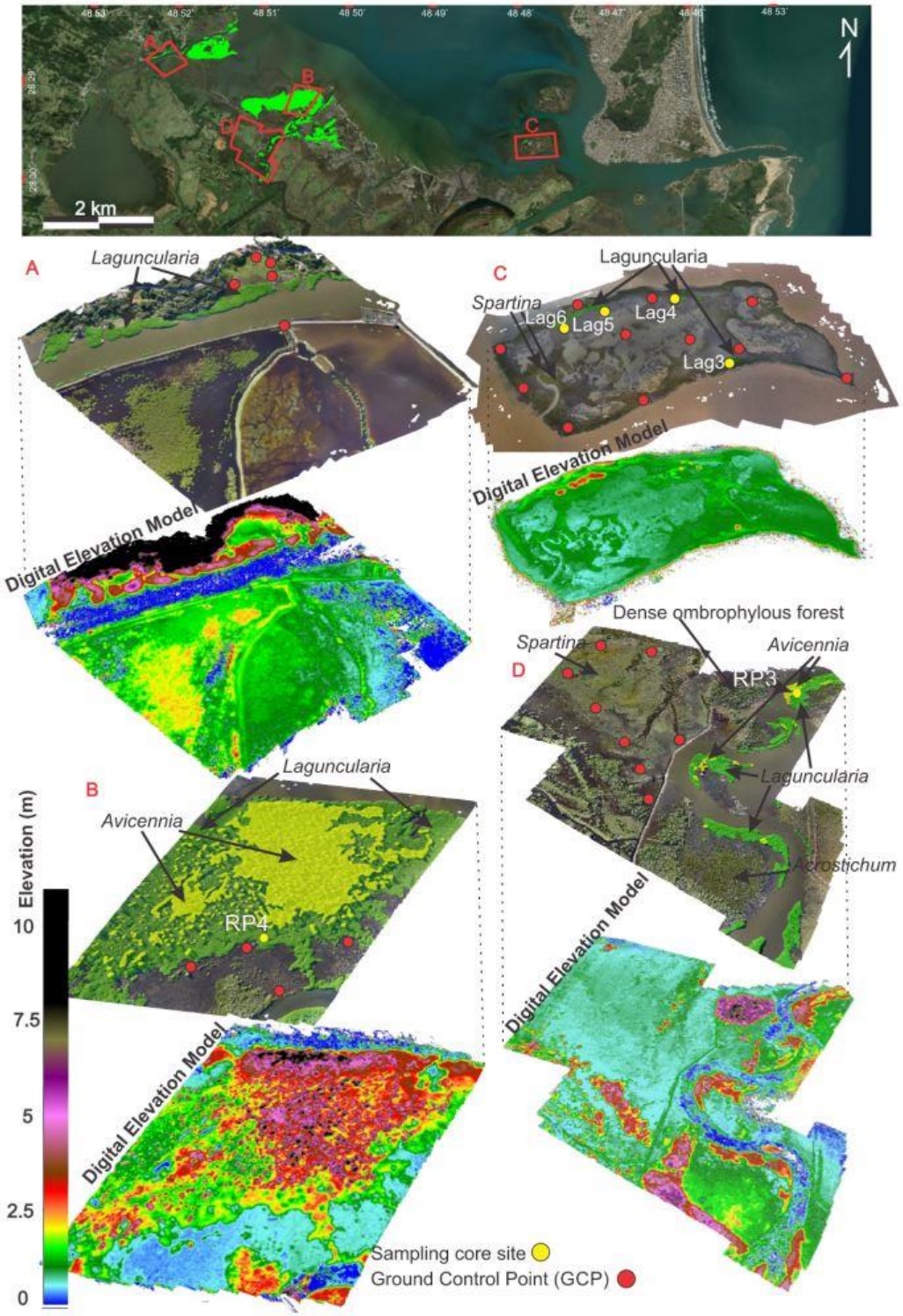

Fig. 4. Vegetation map highlighting the mangrove type location and the digital elevation model.

Following the methods of Harper (1984) and Walker (1992), facies analysis included a description of color (Color, 2009), lithology, texture, and structure. The sedimentary facies were codified following Miall (1978).

3.2.4. Pollen analysis

The sediment cores were sub-sampled (1 cm^3) at 5 cm intervals with 125 total samples. All samples were prepared using standard analytical techniques for pollen, including acetolysis (Faegri and Iversen, 1989). Reference morphological descriptions (Colinvaux et al., 1999; Herrera and Urrego, 1996; Roubik and Moreno, 1991) were consulted for the identification of pollen grains and spores. A minimum of 300 pollen grains was counted for the muddy samples. Sandy samples presented a lower amount of pollen grains, since the sandy sediments are not favorable to pollen preservation (Havinga, 1967), then a minimum of 100 pollen grains were counted for sandy samples. Considering the objective of this work was to identify the mangrove presence in the study area, such samples (< 300 pollen grains) were also presented in the pollen diagrams. Software packages TILIA and TILIAGRAPH were used to calculate and plot pollen diagrams (Grimm, 1990). CONISS was used for cluster analysis of pollen taxa, permitting the zonation of the pollen diagram (Grimm, 1987).

We consider important to mention that the spatial representativeness of pollen records obtained from lagoons or lakes depends on the winds blow and extension of its drainage system, in which the proportion of the pollen signal provided by each vegetation type is distance-weighted (e.g. Davis, 2000; Xu et al., 2012). However, preserved pollen in tidal flats and flood plain sediments present smaller spatial representativeness. Pollen traps from tidal flats occupied by herbaceous vegetation, which were located ~1.5 km distant from *Rhizophora* trees and 100 m distant from *Avicennia*, recorded an average of 410 *Rhizophora* grains/cm^2/yr and 8 *Avicennia* grains/cm^2/yr. This indicates that the dispersion of *Rhizophora* pollen grains, transported by wind, is wider than *Avicennia* pollen (Behling et al., 2001).

3.2.5. Organic geochemistry

A total of 100 samples (6–50 mg) were collected at 5 cm intervals from sediment cores to associate the vegetation changes and to understand the variations in organic matter source. Sediments were treated with 4% hydrochloric acid (HCl) to remove carbonate, washed with distilled water until the pH reached 6, dried at 50 °C, and finally homogenized. The samples were analyzed for total organic carbon (TOC) and total nitrogen (TN) at the Stable Isotope Laboratory of the CENA/USP. The results were expressed as a percentage of dry weight, with analytical precision of 0.09% (TOC) and 0.07% (TN), respectively. The $\delta^{13}C$ and $\delta^{15}N$ were expressed in per mille (‰) with respect to the VPDB and N_2 standards, respectively, with a precision of 0.2‰. Elemental results were used to calculate the C/N (weight/weight) for all samples. The determination of organic matter source will be environmental-dependent with $\delta^{13}C$, $\delta^{15}N$ and C/N composition (Lamb et al., 2006), as follows: the C_3 terrestrial plants show $\delta^{13}C$ values between −32‰ and −21‰ and C/N ratio > 12, while C_4 plants have $\delta^{13}C$ values ranging from −17‰ to −9‰ and C/N ratio > 20 (Deines, 1980; Meyers, 1994, 1997). Freshwater algae have $\delta^{13}C$ values between −25‰ and −30‰ (Meyers, 1997) and marine algae around −24‰ to −16‰ (Meyers, 1997, 2003). Meyers (1997) and Thornton and McManus(1994) used $\delta^{15}N$ values to differentiate organic matter from aquatic (> 10.0‰) and terrestrial plants (~0‰). The main limitation of the isotopic method is the eventual isotopic fractionation that can alter the original isotopic ratios, mainly of the $\delta^{15}N$ in anaerobic environments by denitrification. The fractionation can impair paleoenvironmental interpretations as the sedimentary organic matter becomes older (White, 2015).

3.2.6. Radiocarbon dating

The events chronology was based on 12 radiocarbon dates by accelerator mass spectrometer (AMS) (Table 2). The sedimentary samples were checked and physically cleaned under a stereomicroscope to avoid natural contamination. The organic matter was chemically treated to remove any more recent organic material such as fulvic and/or humic acids and carbonates. This process consisted of extracting residual material with 2% HCl at 60 °C for 4 h, washing with distilled water to neutralize the pH, and drying at 50 °C (Pessenda et al., 2012). Sedimentation rates were based on the relationship between depth and time intervals. Samples were analyzed at the ^{14}C Laboratory of Radiocarbon at UGAMS (University of Georgia-Center for Applied Isotope Studies). Radiocarbon ages were normalized to a $\delta^{13}C$ of −25‰ VPDB and reported as calibrated years (cal yr BP) (2σ) using CALIB 6.0 (Stuiver et al., 2017). The dates are presented along the text as the median of the range of calibrated ages (Table 2). This technique may be used to date anything that was alive during the last 60,000 years, such as charcoal from ancient fires, wood used in construction or tools, cloth, bones, seeds, and leather (Plastino et al., 2001).

Table 1
Mangrove area (ha) between 2003 and 2019 based on satellite/drone images.

Time (month/yr)	Sector 1 (ha)	Sector 2 (ha)	Sector 3 (ha)	Total (ha)
08/2003	23.27	72.6	0.2377	96.1077
06/2009	25.68	73.6	0.2474	99.5274
01/2012	25.8	74.3	0.2424	100.3424
07/2013	25.79	74.3	0.3188	100.4088
05/2016	25.82	75.9	0.3131	102.0331
07/2017	26.83	77.2	0.3112	104.3412
07/2018	28	77.2	0.3112	105.5112
06/2019	28.77	77	0.3131	106.0831
Expansion (ha)	5.5	4.4	0.0754	9.9754

3.2.7. Pb-210 dating

Pb-210 dating was conducted at UNESP-São Paulo State University, UNESPetro-Geosciences Center Applied to Petroleum, IGCE-Geosciences and Exacts Sciences Institute, Rio Claro, São Paulo State, Brazil. The sediment cores were analyzed by gamma spectrometry using a coaxial hyper-pure germanium gamma rays detector (HPGe). ^{210}Pb readings in the 46.54 keV photopeak provided data of the total ^{210}Pb (210PbT) activity in the sediment slices, whereas 226Ra readings in the 186.21 keV photopeak provided data of the in situ (supported) ^{210}Pb (210Pbs) activity. The excess (unsupported) ^{210}Pb (210Pbxs) activity aliquots were obtained by the difference $^{210}PbT - {}^{210}Pbs$. Plots of the ln $^{210}Pbxs$ against the cumulative dry weight/area allowed to construct straight lines required by the application of the Constant Flux: Constant Sedimentation (CF:CS) ^{210}Pb chronological model. The slopes of the straight lines permitted determine sedimentation rates of 5.3 mm/yr (Lag-6) and 16.1 mm/yr (Lag-3) for the cores analyzed. Then, deposition ages were estimated from these rates. This method is suitable for dating approximately 100 years back (Jia et al., 2018).

4. Results

4.1. Geomorphology and vegetation

The study site was carried out on tidal flats at the margin of the São Francisco Lagoon (Fig. 1). The tidal flats in the western sector are under the influence of a channel with a high sinuosity. Lateral migration may be recorded with erosion of the outer channel margins and sedimentation in its inner margins (Fig. 3a and b). Noteworthy is the presence of channel segments on the verge of being abandoned. (Fig. 4d). Such abandoned channels form stagnant zones favorable to the gradual accumulation of muddy sediments. Later, these muddy surfaces emerge to form tidal flats suitable for the establishment of mangroves and/or saltmarshes. The channel sediments are comprised of moderately sorted, medium- to very coarse-grained sands, which extend from

Table 2
Sediment samples selected for radiocarbon dating with laboratory number, code site/depth, ^{14}C yr BP and calibrated (cal) ages.

Laboratory (UGAMS)	Sample\Depth (cm)	^{14}C age yr, BP	pMC (± error)	Calibrated (Cal yr BP)	Mean (calyr BP)
27,333	LAG3\60–65 cm	361 ± 23		313–459	385
34,672	LAG3\90–95 cm	960 ± 26		766–916	840
34,673	LAG4\20–25 cm		103.819 (0.322)	1957 CE	
34,674	LAG4\60–65 cm	589 ± 23		519–560	540
34,675	LAG5\52–55 cm		104.329 (0.302)	1957 CE	
26,627	LAG5\90–95 cm	1019 ± 24		913–971	940
34,676	LAG6\35–40 cm	51 ± 23			50
34,680	RP4\30–32 cm		100.036 (0.298)	1956 CE	
34,681	RP4\60–65 cm	359 ± 23		312–455	380
34,682	RP4\170–175 cm	8130 ± 30		8974–9128	9050
34,677	RP3\32–35 cm		104.64 (0.302)	1957 CE	
34,679	RP3 100–105	685 ± 24		559–617	585

mountainous areas and tablelands. Muddy silt sediments characterize the tidal flats. The eastern area (sector 3) is characterized by islands formed from sandy bars with central depressions that favor the accumulation of muddy sediments (Figs. 1 and 4c).

Mangroves, represented by *Laguncularia* and *Avicennia* trees with a stature < 11 m, are distributed on ~1 km^2 of tidal flats (10–60 cm above mean sea level) and as fringe along the channel under brackish water influence (~15‰). *Avicennia* (< 11 m tall) represents the highest mangrove trees, surrounded by *Laguncularia* shrubs (< 2 m) in the northern area (sector 2, Fig. 4b). The tallest *Laguncularia* trees (~5 m) occur along the channels (Fig. 4a and d), while the lowest (< 4 m) are concentrated on small islands on sandy bars (Fig. 4c). Saltmarshes, mainly represented by *Spartina* and *Acrostichum,* occupy a significant part of the tidal flats. Sandy tidal flats (~10–50 cm amsl) and dunes may be colonized by *restinga* vegetation, mainly represented by *Ipomoea, Cereus, Sporobolus, Spartina ciliate* and *Alternanthera.* Dense ombrophylous forest, with trees between 5 and 11 m height, occurs upstream, mainly represented by Arecacea on floodplain under freshwater influence (Fig. 4d). Tidal flats, positioned on topographically lowest part (~0 cm amsl) and near the margin of the lagoon, are almost permanently flooded and without vegetation cover (Fig. 3).

4.2. Spatial-temporal analysis

Spatial-temporal analysis, based on satellite and drone images, indicated an expansion of mangrove forests in the study site between 2003 (96.1 ha of mangrove area) and 2019 (106 ha), mainly represented by *Laguncularia* trees (Fig. 5 and Table 1). Mangroves invaded tidal flats previously occupied by *Spartina* and *Acrostichum*. The migration of mangroves into marshes was progressive during that time. Satellite images obtained in 2009 recorded 99.52 ha of mangroves, a gain of 3.42 ha (3.5%) compared to 2003, followed by an expansion of 0.81 ha (2009–2012), 0.07 ha (2012–2013), 1.62 ha (2013–2016) and 2.3 ha (2016–2017), 1.17 ha (2017–2018), and 0.57 ha (2018–2019), representing a mangrove expansion of 0.62 ha/yr (Table 1). Proportionally, the sector 3 had the most extensive mangrove area gains between 2003 and 2019 (0.07 ha, 31.7%), followed by the sector 1 (5.5 ha, 23.6%) and 2 (4.4 ha, 6.1%) (Figs. 1 and 5).

4.3. ^{14}C, ^{210}Pb dates, and sedimentation rates

The ^{14}C and ^{210}Pb data are shown in Tables 2 and 3, respectively. Regarding the radiocarbon dates, the sedimentation rates estimated for the upper part of the core RP-4 was 5.1 mm/yr (30–0 cm) (Fig. 7). The Lag-4, Lag-5, Lag 6 and RP-3 presented 4.2 mm/yr (25–0 cm), 9.2 mm/yr (55–0 cm), 3.5 (40–0 cm) and 6.0 mm/yr (35–0 cm), respectively (Figs. 6–9 and 11). All the five samples dated by ^{14}C indicated that upper parts (< 100 cm) of the studied cores, interpreted as tidal flats, were formed over the past 120 years (Figs. 6–9, 11, and Table 2). The sedimentation rates (5.3 mm/yr and 16.1) obtained by ^{210}Pb for the cores Lag 3 (0–60 cm), and Lag 6 (0–50 cm) corroborate for that deposition ages (Tables 2 and 3, and Figs. 9 and 10). The use of multiple dating has allowed a corroboration between methods that would support one another in providing accurate chronologies (Piotrowska et al., 2010b). Age-depth models using the combined results of ^{210}Pb and ^{14}C dating may be obtained in De Vleeschouwer et al. (2009) and Piotrowska et al. (2010a). It should be highlighted the ^{14}C dating of the Lag 6 (40 cm) indicated an age 1922–1876 CE, while the ^{210}Pb revealed an age around 1943 CE, then 21 years younger than the margin of error of the ^{14}C dating. This chronological difference between the two methods can be considered acceptable because bioturbation caused by soil fauna can mix locally sedimentary organic matter of different stratigraphic levels (Boulet et al., 1995; Gouveia and Pessenda, 2000). Besides, considering the radiocarbon dating by AMS, small carbon content (< 0.5 g) in a small sample mass can contain a high concentration of young/old contaminants coming from the shallow/bottom soil horizons, even after the physical and chemical pretreatments. These procedures remove only the adsorbed contaminants, whereas, in some cases, the absorbed ones can keep preserved in the residual organic matter (humin fraction) (Pessenda et al., 1996).

4.4. Facies description

The studied cores are mainly characterized by olive-gray coarse sand (45–90%) and silt (10–55%) sediments with a small fraction of olive-brown clay (0–8%) sediments. The bottom of sedimentary deposits is predominantly formed by massive sands, while the top presents lenticular and wavy heterolithic bedding. Plant remains, roots, and roots marks evidenced bioturbation along the studied cores. The integration of sedimentary facies, pollen data, and geochemical records allowed to define three facies associations: (A) Herbaceous flood plain, (B) Sandy bar, and (C) Tidal flat (Table 4).

4.4.1. Facies association (A) herbaceous flood plain

This facies association was evidenced in the RP4 between 200 and 100 cm depth (Fig. 7). Sand, silt, and clay sediments oscillated between 2 and 50%, 15 and 80%, and 5–30%, respectively. Sedimentary successions with wavy (facies Hw)/lenticular (Hl)/flaser (Hf) heterolithic bedding characterize this facies association. These sediments began to accumulate at least 9050 cal yrs BP. Pollen analysis indicated four ecologic groups characterized by herbs (70–25%), trees, and shrubs (15–37%), palms (0–15%), and aquatic plants (0–8%). Herbs pollen are represented mainly by Poaceae (5–55%), Myrsinaceae (0–15%), Cyperaceae (0–10%) and Asteraceae (0–10%), while the arboreal group is represented by Euphorbiacea (0–18%), Myrtaceae (0–25%), Sapindaceae (0–10%) and Fabaceae (0–7%), followed by Cannabaceae (Trema), Araucariaceae, Cunoniaceae, Moraceae, *Podocarpus,* and *Mimosa* ranging from 0 to 10%. Anacardiaceae, Melastomataceae/Combretaceae, Salicaceae, Solanaceae, Annonaceae, Cletraceae, *Podocarpus*, and Piperaceae ranged from 0 to 5%. Aquatic plants were represented by

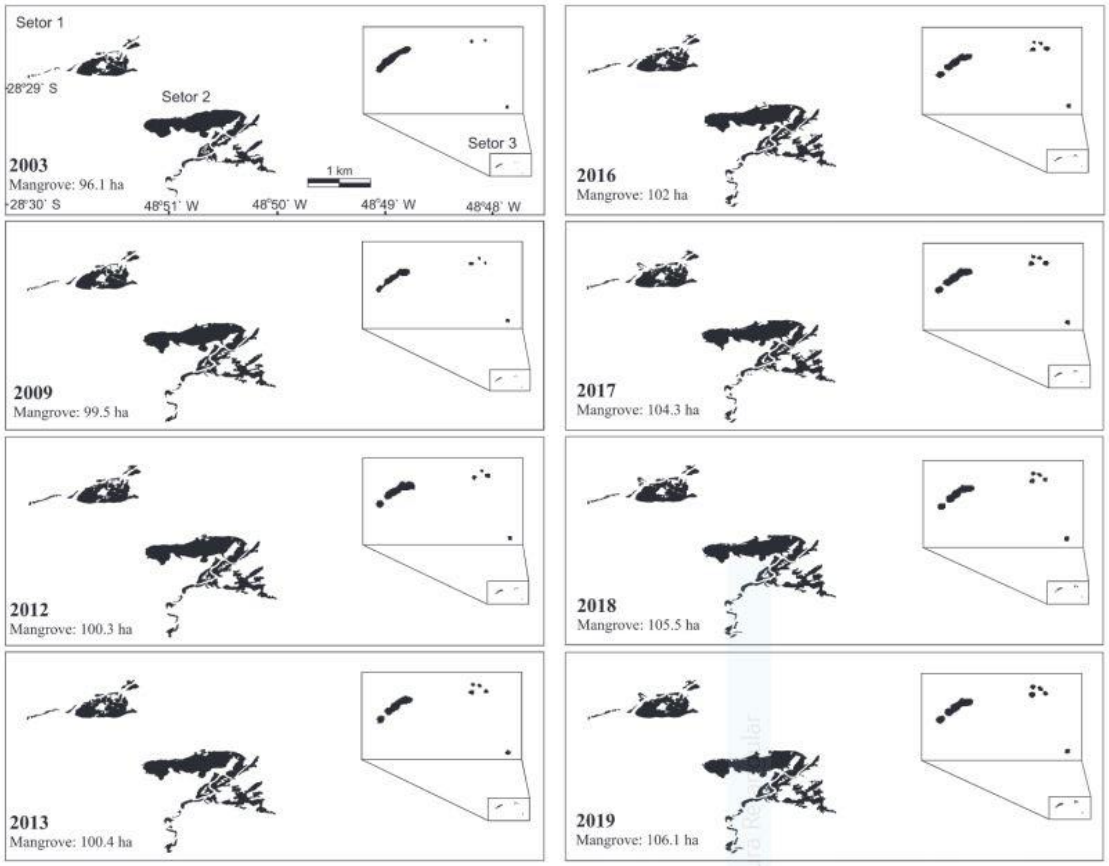

Fig. 5. Spatial-temporal analysis of the austral limit of mangroves in South America based on satellite and drone images between 2003 and 2019.

Table 3
Stratigraphic depth selected for identification of sedimentation rates based on ^{210}Pb dating.

Sample/Depth (cm)	^{210}Pb (AD) age
LAG3/0 cm	2015
LAG3/10 cm	2012
LAG3/20 cm	2008
LAG3/30 cm	2004
LAG3/40 cm	2000
LAG3/50 cm	1996
LAG3/58 cm	1993
LAG6/ 0 cm	2015
LAG 6/7 cm	2009
LAG 6/14 cm	1998
LAG 6/21 cm	1986
LAG 6/28 cm	1974
LAG 6/35 cm	1961
LAG6/42 cm	1943
LAG6/ 50 cm	1921

Alismataceae (0–8%), Typhaceae (0–2%) and Plantaginaceae (0–5%). The ferns are represented mainly by Polypodiaceae (Fig. 1, supplementary material). The δ^{13}C values presented an upward increase trend from −23 to −21‰, while the C/N of sedimentary organic matter presented an upward decrease trend from 28 to 8 (Fig. 7).

4.4.2. Facies association (B) sandy bar

This facies association is represented by the sedimentary units between 120 and 100 cm, 100 and 65 cm, 100 and 60 cm, 70 and 43 cm, and 100 and 55 cm depth in the cores RP-3, RP-4, Lag-3, Lag-4, and Lag-5, respectively, accumulated between ~940 and ~385 cal yr BP (Figs. 6–8, 10, and 11). It presents massive coarse-medium sand sediments (facies Sm) exhibiting a fining upward sandy deposit. The pollen data indicated four ecologic groups characterized by herbs, trees and shrubs, palms, and ferns. The herbs are represented by Poaceae (0–90%), Asteraceae (0–10%), Apiaceae (0–6%), Cyperaceae (0–10%), Myrsinaceae (5–10%), Amaranthaceae (0–10%), Araceae (0–10%), Apocynaceae (< 5%), and Loranthaceae (< 5%). The trees and shrubs are characterized by *Mimosa* (0–20%), Malpighiaceae (0–9%), Ericaceae (0–8%), Euphorbiaceae (0–5%), Cunoniaceae (0–5%), *Podocarpus* (0–2%), Fabaceae (0–5%), Moraceae (0–6%), Myrtaceae (0–8%), Rubiaceae (0–2%), Melastomataceae\Combretaceae (0–5%), Anacardiaceae (0–5%) e *Matayba* (0–10%). Arecaceae pollen occur with a small percentage (0–11%) (Figs. 1, 2, 4, and 5, Supplementary material).

The δ^{13}C values presented an increasing trend, especially the core Lag-3 that increased from −26 to −15‰ (mean −20‰, Fig. 10), while the δ^{15}N oscillated from 5 to 8‰ (mean 7.75‰) (Figs. 7, 8, and 10). The TOC results presented stable values around 1.5%, TN values show a slightly increasing trend from 0.01 to 0.15% (mean 0.08%), and C/N values presented also increased trends, mainly to the RP-4 and LAG-5 (Figs. 7, 8, and Table 4).

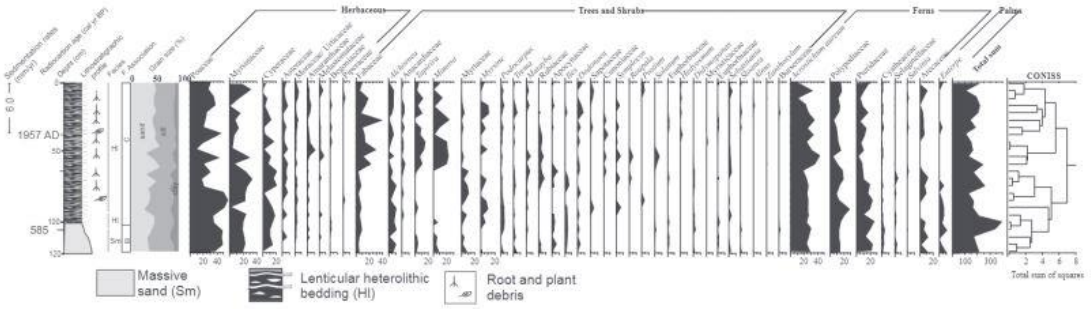

Fig. 6. Lithostratigraphic profile of the core RP-3 with sedimentary features and pollen diagram exhibiting percentages of the ecological groups and zones.

4.4.3. Facies association (C) tidal flat

Facies association C is present as the upper sedimentary unit of the cores Lag-3 (60–0 cm), Lag-4 (43–0 cm), Lag-5 (55–0 cm), Lag-6 (50–0 cm), RP-3 (100–0 cm) and RP-4 (65–0 cm) accumulated during the last decades (Figs. 6–11). It is characterized by lenticular (Hl) and wavy heterolithics (Hw) bedding and massive mud (Mm) with roots, root marks, and leaves. The radiocarbon dates indicated ages between ~50 cal yr BP and 1957 CE, while the ^{210}Pb suggest that sediments were accumulated during the last century under sedimentation rates between 5.3 mm/yr (Lag-6, Fig. 9) and 16.1 mm/yr (Lag-3, Fig. 10, Tables 2 and 3). The palynology shows five ecologic groups represented by herbs, trees, and shrubs, mangroves, palms, and ferns. Besides the pollen types found in the Facies Association A and B, it was possible to identify herbs pollen of Lentibulariaceae (0–20%) and Aizoaceae (0–2%) families, as well as trees and shrubs pollen of *Ílex* (0–5%), *Sebastiana* (0–5%), Boraginaceae (0–2%), Annonaceae (0–3%), Sapotaceae (0–2%), *Alnus* (0–5%), *Byrsonimia* (0–8%), Sapindaceae (0–5%), *Borreria* (0–10%), Myrcinaceae (0–5%) and Anacardiaceae (0–4%). Mangrove pollen are represented by *Laguncularia* (0–20%) and *Avicennia* (0–3%) (Figs. 1–5, Supplementary material). Mangrove pollen were not recorded in the RP-3 (Fig. 6).

Geochemical records indicate values of δ^{13}C, δ^{15}N e C/N oscillating from −24 to −17‰ (mean −20‰), 4 to 7‰ (mean 5.5‰) and 7 to 29 (mean 18) respectively. The C_{org} and N_{total} presented values varying between 1.2 and 4.5% (mean 2.85%) and 0.05 and 0.25% (mean 0.3%), respectively (Figs. 9–12, Table 4). The RP-4 exhibited an upward increase trend for the δ^{13}C values, while the C/N presented a decreased trend (Fig. 7).

5. Interpretation and discussion

5.1. Holocene

Along the south-northeastern Brazilian coast occurred a relative sea-level rise mainly during the early Holocene, and a mid Holocene highstand between 1 and 5 m above the modern sea-level at about 5500 cal yrs BP. During the mid and late Holocene occurred a gradual relative sea-level fall (Angulo et al., 2016, 2006; Caldas et al., 2006; Cohen et al., 2020). The stabilization or low rates of sea-level rise/fall around the mid Holocene allowed the establishment only of tropical mangroves at ~7000 cal yr BP along the coast of Espírito Santo (19°S), Bahia (17°S), Rio Grande do Norte (5°S), Pará (1°S), and Amapá (2°N) (Cohen et al., 2020, 2014, 2012; Fontes et al., 2017; França et al., 2015, 2013; Ribeiro et al., 2018). Although the trends of relative sea-level changes are the same for the tropical and subtropical Brazilian coast, the subtropical mangroves were established only at ~2200 cal yr BP (São Paulo, 25°S) and ~1630 cal yr BP (Santa Catarina-Brazil, 26°S) (França et al., 2019; Pessenda et al., 2012), suggesting that natural global warming during the Holocene (Kaufman et al., 2020) may have caused the mangrove expansion from tropical to subtropical areas during the late Holocene.

In the study area, the early-mid Holocene sea-level rise caused

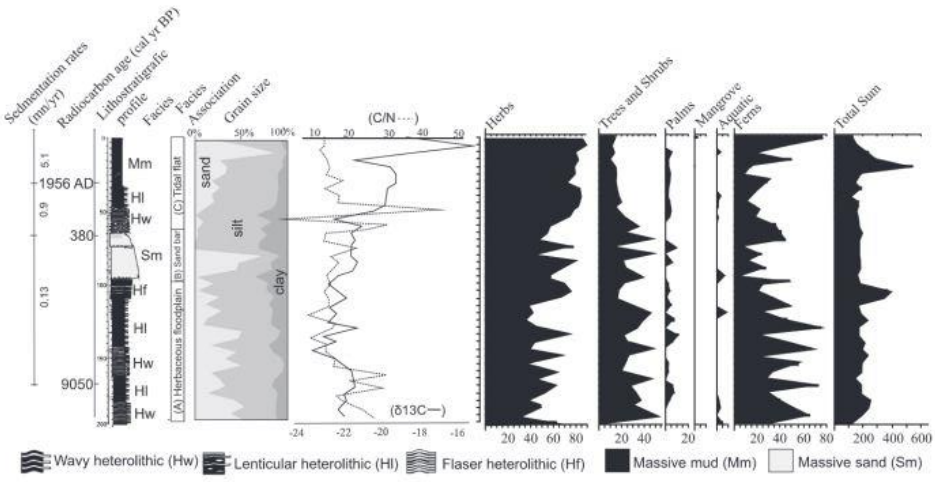

Fig. 7. Summary of the core RP-4, showing sedimentary features, pollen data, and geochemical results.

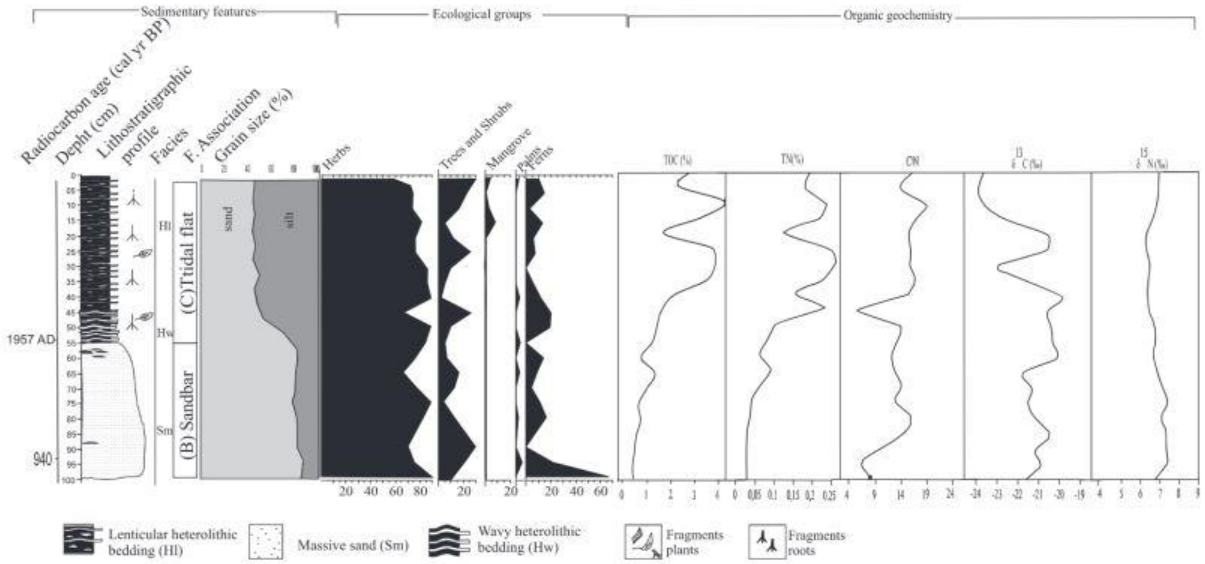

Fig. 8. Summary of the core LAG-5, showing sedimentary features, pollen data, and geochemical results.

erosion of the coastline, invasion of coastal depressions, and fluvial valleys along the southern Brazilian littoral (Cooper et al., 2018). During this time, lagoons and tidal channels were formed. The floodplains at the margin of fluvial valleys were filled by muddy and sandy sediments, as recorded at the base of the core RP-4 (~9000 cal yrs BP). It is characterized by lenticular, wavy, and flaser heterolithic bedding (Facies Association A) (Fig. 7). The marine transgression contributed to the expansion of tide-influenced environments, as indicated by massive mud and heterolithic beds. Also, the binary $\delta^{13}C$ and C/N showed an upward increase trend of marine influence along the Facies Association A (Fig. 12). The increased trend of herbs pollen percentage associated to the enrichment of $\delta^{13}C$ and decrease of C/N values from the base to the top of the core RP-4 suggests a transition of a fluvial floodplain dominated by a mixture of grasses, trees, shrubs and ferns (200–100 cm) to a tidal flat (65–0 cm, < ~380 cal yrs BP) dominated by herbs with a substantial contribution of sedimentary organic matter from estuarine origin (Figs. 7 and 12).

Considering the last 1000 years, the sandy bars deposits were accumulated between at least 940 and ~385 cal yrs BP (Figs. 6–8, 10, and 11). The $\delta^{13}C$ and C/N values revealed an increasing trend of estuarine influence during this time interval (Figs. 8, 10, 11, and 12). Probably, after the RSL stabilization, sandy bars deposits emerged isolated in the lagoon and allowed the establishment of muddy tidal flats. Such environmental conditions favor the establishment and expansion of mangroves. The temporal differences between the top of the Facies Association B (~380 cal yr BP, Figs. 7 and 10) and the base of the A (1921–1993 CE, Figs. 8–10) can be attributed to erosive events that preceded the deposition of that tidal flats.

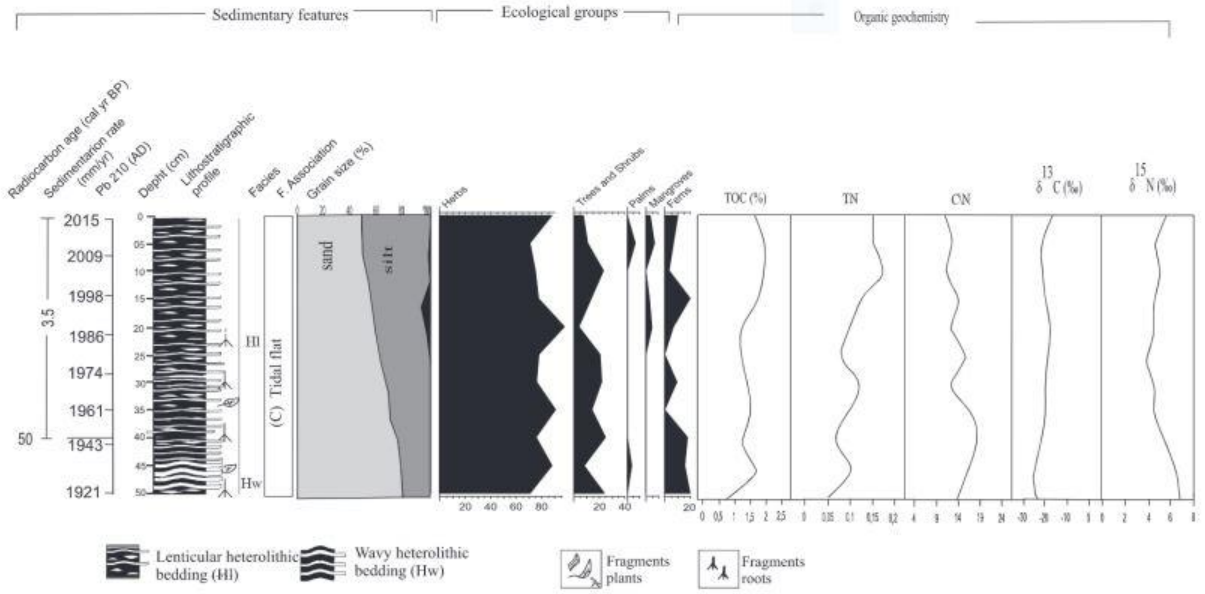

Fig. 9. Summary of the core LAG-6, showing sedimentary features, pollen data and geochemical results.

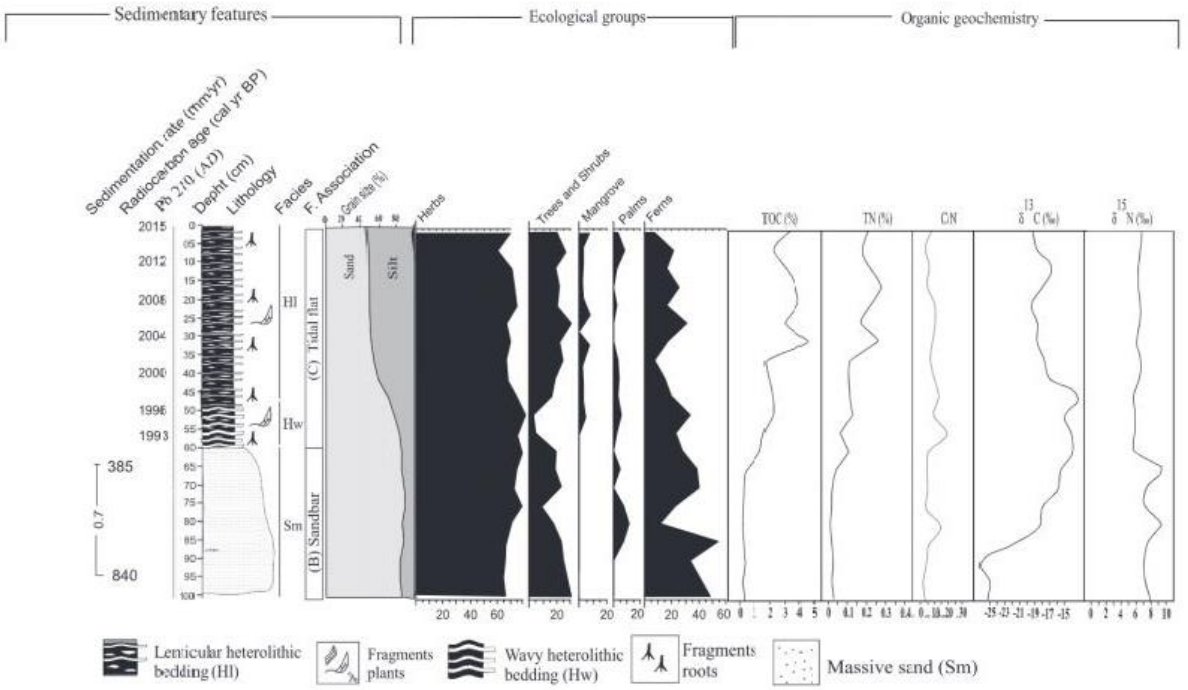

Fig. 10. Summary of the core LAG-3, showing sedimentary features, pollen data and geochemical results.

5.2. Anthropocene

The term Anthropocene, launched into public debate by Nobel Prize winner Paul Crutzen, has been used informally to describe the period during which human actions have had a drastic effect on the Earth and its ecosystems. The ratification process of the Anthropocene as a geological time unit is ongoing. Several start dates for the Anthropocene have been proposed, but the atomic bomb testing during the 1950s has been more favored than others (Zalasiewicz et al., 2018).

Our work revealed that mangrove pollen in the study area occurred only during the last decades. Regarding the Holocene, mangrove pollen were not recorded along the stratigraphic record of the RP-4

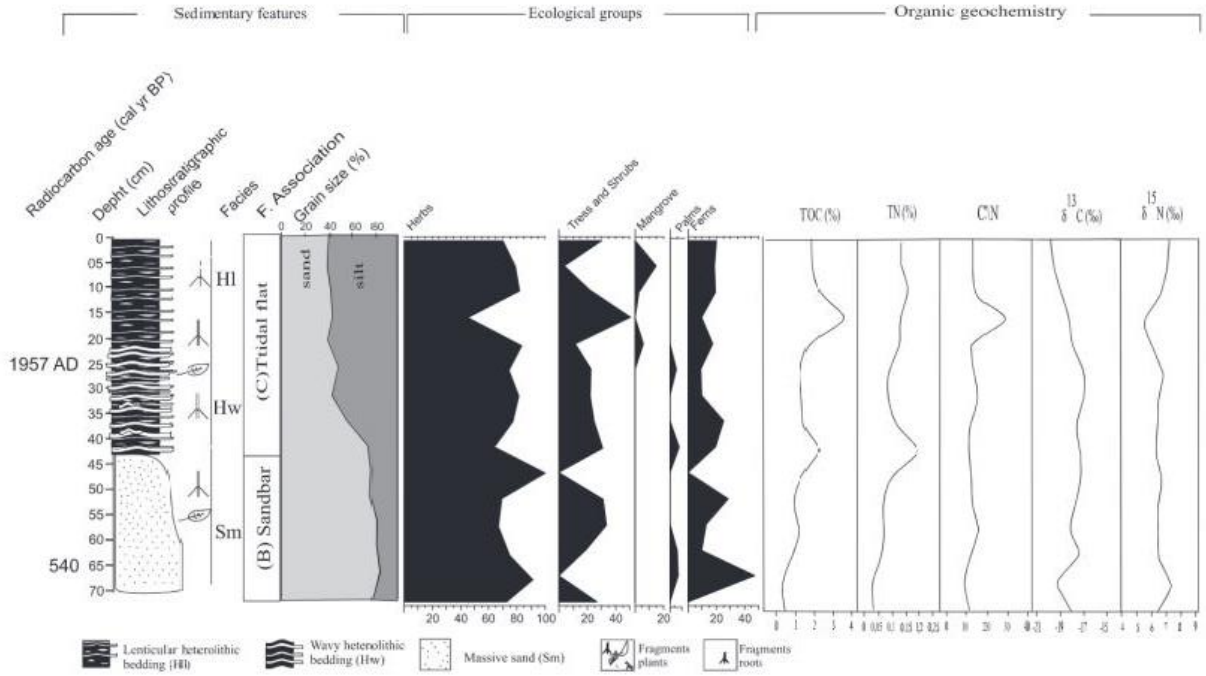

Fig. 11. Summary of the core LAG-4, showing sedimentary features, pollen data and geochemical results.

Table 4
Summary of facies association with sedimentary characteristics, predominance of pollen groups and geochemical data.

Facies association	Facies descripition	Polen predominance	Geochemical data	Interpretation
A	Wavy (Hw), flaser (Hf) and lenticular heterolitic bedding (facies Hl), with fine sand, silt and clay	Herbs, trees, shrubs and palmss	$\delta^{13}C$: −23 to −21‰ C_{total}:0.5–2‰ N_{total}:0.01–0.15‰ C/N: 10–30	Herbaceous floodplain
B	Massive sand (facies Sm) with medium–coarse sand	Trees, shrubs palms and herbs	$\delta^{13}C$: −24–−15‰ $\delta^{15}N$: 6–9.5‰ C_{total}:0.5–2‰ N_{total}:0.01–0.15‰ C/N: 6–30	Sandbar
C	Wavy (Hw) and Lenticular heterolitic bedding (facies Hl), with fine sand, silt and clay	Trees, shrubs, herbs, palms and mangroves	$\delta^{13}C$: −24 to −17‰ $\delta^{15}N$: 4–7‰ C_{total}: 1.2–4.5‰ N_{total}: 0.05–0.25‰ C/N: 7–22	Tidal flat

accumulated since 9000 cal yr BP (Fig. 7), although the sampling site, located in the modern southern limit of American mangroves (28°29′S), presents dense *Avicennia* and *Laguncularia* trees nowadays, with stature between 2 and 11 m (Fig. 4d). From the physicochemical and hydrodynamic point of view, environmental conditions were favorable for the establishment and expansion of mangroves since the mid Holocene, as it occurred along the Brazilian coast between latitudes of 25°S and 2°N (Cohen et al., 2020, 2014, 2012; França et al., 2015, 2013; Ribeiro et al., 2018; França et al., 2019; Pessenda et al., 2012). During this time occurred a significant contribution of organic matter sourced from estuary on tidal flats occupied by saltmarshes. As revealed by the spatial–temporal analysis (Fig. 5 and Table 1), the mangrove expansion in the study site has occurred at least between 2003 and 2019. Considering this period and a rate of continuous sedimentation of 6.0 mm/yr along the interval 35–0 cm in the RP-3, mangrove pollen should be preserved in the last 7 cm of this core (Fig. 6). Unfortunately, the samples from this interval did not record mangrove pollen, probably due to a loss of sediments from the upper part of this stratigraphic section at the time to remove the core from the substrate.

The cores Lag-3, Lag-5, Lag-6, Lag-4, and RP-4 indicated mangrove presence along 52 cm (sedimentation rate of 16.1 mm/yr), 17 cm (9.2 mm/yr), 20 cm (5.3 mm/yr), 22 cm (4.2 mm/yr), and 6 cm depth (5.1 mm/yr) (Figs. 7–11) respectively. Higher sedimentation rates for the core Lag-3 produced a longer stratigraphic section to preserve mangrove pollen for the last decades. In addition, these cores (Lag-3, Lag-4, Lag-5, Lag-6, and RP-4) were sampled during the low tide, which facilitated the removal of the upper section of the stratigraphic column. Based on these pollen profiles and ^{14}C and ^{210}Pb dates, mangrove vegetation mainly represented by *Laguncularia* trees was established on studied tidal flats under the estuarine influence between ~1957 and 1986 CE. Today, these areas are occupied by *Laguncularia* and *Avicennia* shrubs/trees (Figs. 1, 3, and 4).

The mangroves in the sector 2 show *Avicennia* and *Laguncularia* trees with stature up to 11 and 5 m, respectively (Figs. 1, 3, 4b, and d). In comparison, the sector 1 exhibits mainly *Laguncularia* trees with a maximum height of 5 m (Fig. 4a). The sector 3 presents small groups of *Laguncularia* shrubs with < 2 m tall (Fig. 4c). Probably, the difference in the mangrove structure can be attributed to the microclimate. Microclimate refers to climatic conditions in a reduced spatial scale (i.e., < 100 m horizontally and < 10 m vertically) (Geiger et al., 2012). It may be regulated by local factors, such as proximity to vegetation, soil, and water. Regarding the impacts of low winter temperatures on mangroves, Osland et al. (2019) proposed six microclimatic factors that may produce air temperature gradients and modulate mangrove responses to winter temperature extremes: (1) distance from the ocean; (2) distance from wind buffers; (3) mangrove canopy cover; (4) height

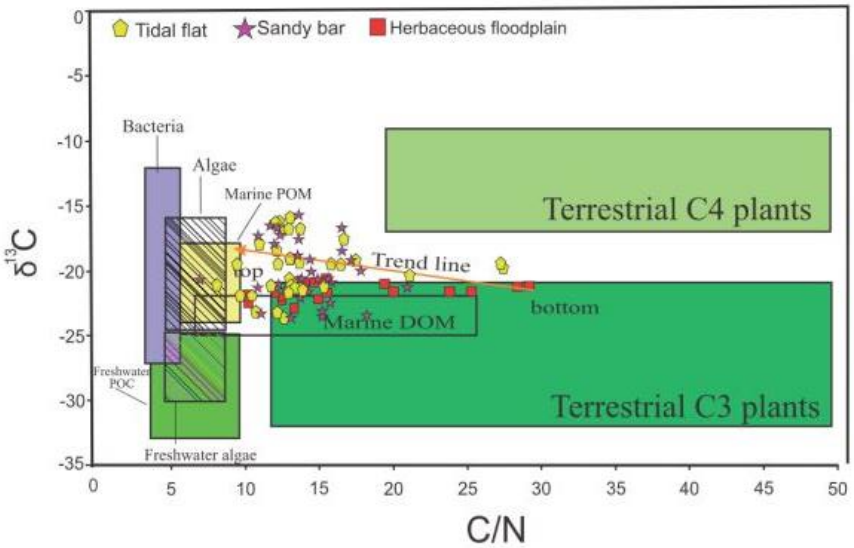

Fig. 12. Binary diagram illustrating the relationship between $\delta^{13}C$ and C/N for the different sedimentary facies association.

above the soil surface; (5) local slope concavity; and (6) tidal inundation. Regarding the study sites, the wind effects and mangrove canopy may have significant influences on mangrove structure. Sectors 2 and 3 are located in internal parts of the studied lagoon (Fig. 1), which offers some protection against the winter wind. In contrast, the sector 3 is isolated on an island, then more exposed to the winter winds than the sectors 1 and 2. Considering this hypothesis, some geomorphological characteristics of the studied lagoon could be more favorable for mangrove development. The gradual mangrove expansion could produce natural protection against the low winter temperatures, because mangrove canopy can reduce wind speeds and produce warmer winter temperatures into mangroves, causing temperature variations within the mangroves and impact gradients from the edge to the innermost sector of these forests (Devaney et al., 2017; Geiger et al., 2012; Guo et al., 2017).

Considering the macroclimate, *Spartina* dominates saltmarshes mainly along the south of the Santa Catarina littoral. This genus has a higher tolerance to low winter temperatures than mangrove trees, which occur predominantly in tropical regions (Idaszkin and Bortolus, 2011; Soares et al., 2012). The coast of Joinville, northern Santa Catarina littoral, mangroves exhibit *Rhizophora*, *Avicennia*, and *Laguncularia* trees, while the southern littoral presents a decreasing trend of *Rhizophora* trees density until its absence along the studied littoral (Soares et al., 2012). The study area presents mangroves represented only by *Lagungularia* with a few *Avicennia* shrubs/trees. This distribution of mangrove genus along the Santa Catarina coast should reveal its gradual intolerance to low winter temperatures, where *Lagungularia* and *Avicennia* are more tolerant to low temperatures than *Rhizophora* (Duke et al., 1998; Quisthoudt et al., 2012). A palynological study carried out in Babitonga Bay-northern littoral of Santa Catarina, 250 km distant from the study site, revealed the establishment of mangroves represented only by *Laguncularia* between ~1629 and ~853 cal. yr BP. After ~853 cal. yr BP occurred an increase of *Laguncularia* and the establishment of *Avicennia* (França et al., 2019). Probably, this mangrove succession was caused by a warming trend in South America during the late Holocene (Baker and Fritz, 2015). *Rhizophora* trees have arisen in Babitonga Bay only during the last decades (França et al., 2019), probably caused by warming during the Anthropocene (Bernardino et al., 2015).

Therefore, considering four relevant issues discussed in this work: (1) the stabilization or low rates of sea-level rise/fall around the mid Holocene that allowed the establishment of Brazilian tropical mangroves since ~7000 cal yr BP; (2) the mangroves expansion from tropical to subtropical zones along the Brazilian coast during the late Holocene; (3) the mangrove succession during the last 1600 years in Babitonga Bay (250 km north of the study area), and (4) the establishment of mangroves in Laguna de Santo Antônio only over the last decades, would be reasonable to propose that the gradual increase in winter temperatures (+0.4 °C per decade) at least between 1960 and 2002 (Marengo and Camargo, 2008) contributed significantly to the expansion of the austral limit of American mangroves into the temperate zone during the Anthropocene. Probably, the poleward mangrove migration since the late Holocene was caused by a natural Holocene global warming, but the industrial-era warming must have accentuated such mangrove expansion.

6. Conclusions

Sedimentary features, pollen, and isotopes data from six sediment cores, as well as geomorphological and vegetation analyses indicated a marine transgression during the Holocene, and it contributed to the expansion of tide-influenced environments and development of saltmarshes. From the physicochemical and hydrodynamic point of view, environmental conditions were favorable for the establishment and expansion of mangroves in the studied area during the mid and late Holocene, when mangroves were established along the tropical (2°N–19°S) and subtropical (25°–26°S) Brazilian coast, as a consequence of the stabilization or low rates of sea-level rise/fall around the mid Holocene, and the Holocene warming, respectively. However, the establishment of mangroves mainly represented by *Laguncularia* trees on the studied tidal flats (28°29′S) only began between ~1957 and ~1986 CE. Spatial-temporal analysis, based on satellite and drone images, revealed a mangrove expansion of ~10 ha in the study area between 2003 (96.1 ha) and 2019 (106.1 ha). Nowadays, in the study area, saltmarshes, mainly characterized by *Spartina* and *Acrostichum* are sharing tidal flats with mangroves, represented by *Laguncularia* (≤5 m tall) and *Avicennia* (≤11 m tall). Probably, the Anthropocene mangrove establishment and expansion are associated with a migration of the austral mangrove limit into the temperate zone, caused by the gradual increase in winter temperatures. This process may be related to a poleward mangrove migration since the late Holocene, caused by a natural Holocene global warming. However, the industrial-era warming must have accentuated the mangrove expansion into temperate zones.

Declaration of Competing Interest

The authors declare that they have no known competing financial interests or personal relationships that could have appeared to influence the work reported in this paper.

Acknowledgements

We want to thank the members of the Laboratory of Coastal Dynamic (LADIC-UFPA), Center for Nuclear Energy in Agriculture (CENA-USP), the students from the Laboratory of Chemical-Oceanography (UFPA), and Laboratory of C-14 (CENA-USP) for their support. This study was financed by FAPESP (2011/00995-7, 2017/03304-1), and the Brazilian Council for Technology and Science-CNPq (Project # 307497/2018-6).

Appendix A. Supplementary material

Supplementary data to this article can be found online at https://doi.org/10.1016/j.catena.2020.104775.

References

Agisoft, 2018. Agisoft PhotoScan User Manual Professional Edition, Version 1.4.

Allen, M.R., Dube, O.P., Solecki, W., Aragón-Durand, F., Cramer, W., Humphreys, S., Kainuma, M., Kala, J., Mahowald, N., Mulugetta, Y., Perez, R., Wairiu, M., Zickfeld, K., 2018. Framing and Context, in: Masson-Delmotte, V., Zhai, P., Pörtner, H.-O., Roberts, D., Skea, J., Shukla, P.R., Pirani, A., Moufouma-Okia, W., C. Péan, R.P., Connors, S., Matthews, J.B.R., Chen, Y., Zhou, X., Gomis, M.I., Lonnoy, E., Maycock, T., Tignor, M., Waterfield, T. (Eds.), Global Warming of 1.5°C. An IPCC Special Report on the Impacts of Global Warming of 1.5°C above Pre-Industrial Levels and Related Global Greenhouse Gas Emission Pathways, in the Context of Strengthening the Global Response to the Threat of Climate Change.

Alongi, D.M., 2008. Mangrove forests: Resilience, protection from tsunamis, and responses to global climate change. Estuar. Coast. Shelf Sci. 76, 1–13. https://doi.org/10.1016/j.ecss.2007.08.024.

Angulo, R.J., Giannini, P.C.F., Souza, M.C. De, Lessa, G.C., Angulo, R.J., Giannini, P.C.F., Souza, M.C. De, Lessa, G.C., 2016. Holocene paleo-sea level changes along the coast of Rio de Janeiro, southern Brazil: Comment on Castro et al. (2014). An. Acad. Bras. Cienc. 88, 2105–2111. https://doi.org/10.1590/0001-3765201620140641.

Angulo, R.J., Giannini, P.C.F., Suguio, K., Pessenda, L.C.R., 1999. Relative sea-level changes in the last 5500 years in southern Brazil (Laguna-Imbituba region, Santa Catarina State) based on vermetid 14C ages. Mar. Geol. 159, 323–339. https://doi.org/10.1016/S0025-3227(98)00204-7.

Angulo, R.J., Lessa, G.C., Souza, M.C. De, 2006. A critical review of mid- to late-Holocene sea-level fluctuations on the eastern Brazilian coastline. Quat. Sci. Rev. 25, 486–506. https://doi.org/10.1016/j.quascirev.2005.03.008.

Baker, P.A., Fritz, S.C., 2015. Nature and causes of Quaternary climate variation of tropical South America. Sci. Rev. Quat. https://doi.org/10.1016/j.quascirev.2015.06.011.

Behling, H., 1995. Investigations into the late Pleistocene and Holocene history of vegetation and climate in Santa Catarina (S Brazil). Veg. Hist. Archaeobot. 4, 127–152. https://doi.org/10.1007/BF00203932.

Behling, H., Cohen, M.C.L., Lara, R.J., 2001. Studies on Holocene mangrove ecosystem dynamics of the Bragança Peninsula in north-eastern Pará, Brazil. Bosque 167,

225–242.
Bernardino, A.F., Netto, S.A., Pagliosa, P.R., Barros, F., Christofoletti, R.A., Rosa Filho, J.S., Colling, A., Lana, P.C., 2015. Predicting ecological changes on benthic estuarine assemblages through decadal climate trends along Brazilian Marine Ecoregions. Estuar. Coast. Shelf Sci. 166, 74–82. https://doi.org/10.1016/j.ecss.2015.05.021.
Blasco, F., Saenger, P., Janodet, E., 1996. Mangroves as indicators of coastal change. CATENA 27, 167–178. https://doi.org/10.1016/0341-8162(96)00013-6.
Boulet, R., Pessenda, L.C.R., Telles, E.C.C., Melfi, A.J., 1995. Une évaluation de la vitesse de l'accumulation superficielle de matière par la faune du sol à partir de la datation des charbons et de l'humine du sol. Exemple des latosols des versants du lac Campestre, Salitre, Minas Gerais, Brésil. Comptes Rendus L'academie Des Sci. Paris 320, 287–294.
Burrows, M.T., Schoeman, D.S., Buckley, L.B., Moore, P., Poloczanska, E.S., Brander, K.M., Brown, C., Bruno, J.F., Duarte, C.M., Halpern, B.S., Holding, J., Kappel, C.V., Kiessling, W., O'Connor, M.I., Pandolfi, J.M., Parmesan, C., Schwing, F.B., Sydeman, W.J., Richardson, A.J., 2011. The pace of shifting climate in marine and terrestrial ecosystems. Science 334, 652–655. https://doi.org/10.1126/science.1210288.
Caldas, L.H. de O., de Oliveira, J.G., de Medeiros, W.E., Stattegger, K., Vital, H., 2006. Geometry and evolution of Holocene transgressive and regressive barriers on the semi-arid coast of NE Brazil. Geo-Mar. Lett. 26, 249–263. https://doi.org/10.1007/s00367-006-0034-2.
Carvalho do Amaral, P.G., Fonseca Giannini, P.C., Sylvestre, F., Ruiz Pessenda, L.C., 2013. Paleoenvironmental reconstruction of a Late Quaternary lagoon system in southern Brazil (Jaguaruna region, Santa Catarina state) based on multi-proxy analysis. J. Quat. Sci. 27, 181–191. https://doi.org/10.1002/jqs.1531.
Cavanaugh, K.C., Kellner, J.R., Forde, A.J., Gruner, D.S., Parker, J.D., Rodriguez, W., Feller, I.C., 2014. Poleward expansion of mangroves is a threshold response to decreased frequency of extreme cold events. Proc. Natl. Acad. Sci. 111, 723–727. https://doi.org/10.1073/pnas.1315800111.
Chapman, V.J., 1976. Mangrove vegetation. Forest.: Int. J. For. Res. https://doi.org/10.1016/0006-3207(78)90025-3.
Cohen, M.C.L., de Souza, A.V., Rossetti, D.F., Pessenda, L.C.R., França, M.C., 2018. Decadal-scale dynamics of an Amazonian mangrove caused by climate and sea level changes: inferences from spatial-temporal analysis and Digital Elevation Models. Earth Surf. Process. Landforms 43, 2876–2888. https://doi.org/10.1002/esp.4440.
Cohen, M.C.L., Figueiredo, B.L., Oliveira, N.N., Fontes, N.A., França, M.C., Pessenda, L.C.R., de Souza, A.V., Macario, K., Giannini, P.C.F., Bendassolli, J.A., Lima, P., 2020. Impacts of Holocene and modern sea-level changes on estuarine mangroves from northeastern Brazil. Earth Surf. Process. Landforms 45, 375–392. https://doi.org/10.1002/esp.4737.
Cohen, M.C.L., França, M.C., Rossetti, D.F., Pessenda, L.C.R., Giannini, P.C.F., Lorente, F.L., Buso Junior, A., Castro, D., Macario, K., 2014. Landscape evolution during the late Quaternary at the Doce River mouth, Espírito Santo State, Southeastern Brazil. Palaeogeogr. Palaeoclimatol. Palaeoecol. 415, 48–58.
Cohen, M.C.L., Pessenda, L.C.R., Behling, H., de Fátima Rossetti, D., França, M.C., Guimarães, J.T.F., Friaes, Y., Smith, C.B., 2012. Holocene palaeoenvironmental history of the Amazonian mangrove belt. Quat. Sci. Rev. 55, 50–58.
Colinvaux, P., De Oliveira, P.E., Patiño, J.E.M., 1999. Amazon Pollen Manual and Atlas. Harwood Academic Publishers, Dordrecht.
Color, M., 2009. Munsell Soil Color Charts, New Revised Edition. Macbeth Division of Kollmorgen Instruments, New Windsor, NY.
Cooper, J.A.G., Meireles, R.P., Green, A.N., Klein, A.H.F., Toldo, E.E., 2018. Late Quaternary stratigraphic evolution of the inner continental shelf in response to sea-level change, Santa Catarina. Brazil. Mar. Geol. 397, 1–14. https://doi.org/10.1016/j.margeo.2017.11.011.
Cordazzo, C.V., Seeliger, U., 1995. Guia Ilustrado da vegetação costeira no extremo sul do Brasil. Rio Grande.
Davis, M.B., 2000. Palynology after Y2K—Understanding the source area of pollen in sediments. Annu. Rev. Earth Planet. Sci 28, 1–18.
De Vleeschouwer, F., Piotrowska, N., Sikorski, J., Pawlyta, J., Cheburkin, A., Le Roux, G., Lamentowicz, M., Fagel, N., Mauquoy, D., 2009. Multiproxy evidence of 'Little Ice Age' palaeoenvironmental changes in a peat bog from northern Poland. The Holocene 19, 625–637. https://doi.org/10.1177/0959683609104027.
Deines, P., 1980. The isotopic composition of reduced organic carbon. Terr. Environ. A. https://doi.org/10.1016/B978-0-444-41780-0.50015-8.
Devaney, J.L., Lehmann, M., Feller, I.C., Parker, J.D., 2017. Mangrove microclimates alter seedling dynamics at the range edge. Ecology 98, 2513–2520. https://doi.org/10.1002/ecy.1979.
Duke, N.C., Ball, M.C., Ellison, J.C., 1998. Factors influencing biodiversity and distributional gradients in mangroves. Glob. Ecol. Biogeogr. Lett. 7, 27–47. https://doi.org/10.2307/2997695.
Easterling, D.R., Karl, T.R., Gallo, K.P., Robinson, D.A., Trenberth, K.E., Dai, A., 2000. Observed climate variability and change of relevance to the biosphere. J. Geophys. Res. Atmos. 105, 20101–20114. https://doi.org/10.1029/2000JD900166.
Eichler, P., Castelão, G., Pimenta, F., Eichler, B.B., 2006. Avaliação da saúde ecológica do Sistema Estuarino de Laguna (SC) baseado nas espécies de foraminíferos e tecamebas. Pesqui. em Geociências 33, 101–115.
Faegri, K., Iversen, J., 1989. Textbook of Pollen Analysis, fourth ed. Wiley.
Field, C.D., 1995. Impact of expected climate change on mangroves. Hydrobiologia 295, 75–81. https://doi.org/10.1007/BF00029113.
Fontes, N.A., Moraes, C.A., Cohen, M.C.L., Alves, I.C.C., França, M.C., Pessenda, L.C.R., Francisquini, M.I., Bendassolli, J.A., Macario, K., Mayle, F., 2017. The impacts of the middle holocene high sea-level stand and climatic changes on mangroves of the Jucuruçu River, Southern Bahia – Northeastern Brazil. Radiocarbon 59, 215–230. https://doi.org/10.1017/RDC.2017.6.
França, 2010. Mudanças na vegetação do litoral leste da Ilha de Marajó durante o Holoceno.
França, M.C., Alves, I.C.C., Castro, D.F., Cohen, M.C.L., Rossetti, D.F., Pessenda, L.C.R., Lorente, F.L., Fontes, N.A., Junior, A.A.B., Giannini, P.C.F., Francisquini, M.I., 2015. A multi-proxy evidence for the transition from estuarine mangroves to deltaic freshwater marshes, Southeastern Brazil, due to climatic and sea-level changes during the late Holocene. Catena 128. https://doi.org/10.1016/j.catena.2015.02.005.
França, M.C., Cohen, M.C.L., Pessenda, L.C.R., Rossetti, D.F., Lorente, F.L., Buso Junior, A.Á., Guimarães, J.T.F., Friaes, Y., Macario, K., 2013. Mangrove vegetation changes on Holocene terraces of the Doce River, southeastern Brazil. Catena 110, 59–69.
França, M.C., Pessenda, L.C., Cohen, M.C., de Azevedo, A.Q., Fontes, N.A., Silva, F.B., de Melo, J.C., Piccolo, M. de C., Bendassolli, J.A., Macario, K., 2019. Late-Holocene subtropical mangrove dynamics in response to climate change during the last millennium. The Holocene 29, 445–456. https://doi.org/10.1177/0959683618816438.
Fromard, F., Vega, C., Proisy, C., 2004. Half a century of dynamic coastal change affecting mangrove shorelines of French Guiana. A case study based on remote sensing data analyses and field surveys. Mar. Geol. 208, 265–280. https://doi.org/10.1016/j.margeo.2004.04.018.
Gee, C.T., 2001. The mangrove palm Nypa in the geologic past of the New World. Wetl. Ecol. Manag. 9, 181–203. https://doi.org/10.1023/A:1011148522181.
Geiger, R., Aron, R.H., Todhunter, P., 2012. The Climate Near the Ground. Harvard University Press, Cambridge.
Gilman, E.L., Ellison, J., Duke, N.C., Field, C., 2008. Threats to mangroves from climate change and adaptation options: A review. Aquat. Bot. 89, 237–250. https://doi.org/10.1016/J.AQUABOT.2007.12.009.
Giri, C., Ochieng, E., Tieszen, L.L., Zhu, Z., Singh, A., Loveland, T., Masek, J., Duke, N., 2011. Status and distribution of mangrove forests of the world using earth observation satellite data. Glob. Ecol. Biogeogr. 20, 154–159. https://doi.org/10.1111/j.1466-8238.2010.00584.x.
Gouveia, S., Pessenda, L.C.R., 2000. Datation par le C-14 de charbons inclus dans le sol pour l'étude du rôle de la remontée biologique de matière et du colluvionnement dans la formation de latosols de l'état de São Paulo. Brésil 330, 133–138.
Grimm, E., 1990. TILIA and TILIAGRAPH: PC spreadsheet and graphic software for pollen data. INQUA Subcommission on Data-Handling Methods. Newsletter.
Grimm, E.C., 1987. CONISS: a FORTRAN 77 program for stratigraphically constrained cluster analysis by the method of incremental sum of squares. Comput. Geosci. 13, 13–35.
Guo, H., Weaver, C., Charles, S.P., Whitt, A., Dastidar, S., D'Odorico, P., Fuentes, J.D., Kominoski, J.S., Armitage, A.R., Pennings, S.C., 2017. Coastal regime shifts: Rapid responses of coastal wetlands to changes in mangrove cover. Ecology 98, 762–772. https://doi.org/10.1002/ecy.1698.
Harper, C.W., 1984. Improved methods of facies sequence analysis. In: Walker, R.G. (Ed.), Facies Models Geoscience Canada, (Reprint Series 1). Geological Association of Canada, Toronto, pp. 11–13.
Havinga, A.J., 1967. Palynology and pollen preservation. Rev. Paleobot. Palynol. 2, 81–98.
Herrera, L.F., Urrego, L.E., 1996. Atlas de polen de plantas útiles y cultivadas de La Amazonia colombiana (Pollen atlas of useful and cultivated plants in the Colombian Amazon region). Estud. en la Amaz. Colomb. 9, 462.
Ibáñez, C., Morris, J.T., Mendelssohn, I.A., Day, J.W., 2012. Coastal Marshes. In: Estuarine Ecology. John Wiley & Sons, Inc., Hoboken, NJ, USA, pp. 129–163. https://doi.org/10.1002/9781118412787.ch6.
Idaszkin, Y.L., Bortolus, A., 2011. Does low temperature prevent Spartina alterniflora from expanding toward the austral-most salt marshes? Plant Ecol. 212, 553–561. https://doi.org/10.1007/s11258-010-9844-4.
INMET, 2017. Estação Meteorológica de Observação [WWW Document].
Jia, J., Yang, Y., Cai, T., Gao, J., Xia, X., Li, Y., Gao, S., 2018. On the sediment age estimated by 210Pb dating: probably misleading "prolonging" and multiple-factor-caused "loss". Acta Oceanol. Sin. 37, 30–39. https://doi.org/10.1007/s13131-018-1214-4.
Kangas, P.C., Lugo, A.E., Lugo, A.E., 1961. The distribution of mangroves and saltmarsh in Florida. Trop. Ecol. 31, 32–39.
Kaufman, D., McKay, N., Routson, C., Erb, M., Davis, B., Heiri, O., Jaccard, S., Tierney, J., Dätwyler, C., Axford, Y., Brussel, T., Cartapanis, O., Chase, B., Dawson, A., de Vernal, A., Engels, S., Jonkers, L., Marsicek, J., Moffa-Sánchez, P., Morrill, C., Orsi, A., Rehfeld, K., Saunders, K., Sommer, P.S., Thomas, E., Tonello, M., Tóth, M., Vachula, R., Andreev, A., Bertrand, S., Biskaborn, B., Bringué, M., Brooks, S., Caniupán, M., Chevalier, M., Cwynar, L., Emile-Geay, J., Fegyveresi, J., Feurdean, A., Finsinger, W., Fortin, M.C., Foster, L., Fox, M., Gajewski, K., Grosjean, M., Hausmann, S., Heinrichs, M., Holmes, N., Ilyashuk, B., Ilyashuk, E., Juggins, S., Khider, D., Koinig, K., Langdon, P., Larocque-Tobler, I., Li, J., Lotter, A., Luoto, T., Mackay, A., Magyari, E., Malevich, S., Mark, B., Massaferro, J., Montade, V., Nazarova, L., Novenko, E., Park, P., Pearson, E., Peros, M., Pienitz, R., Płóciennik, M., Porinchu, D., Potito, A., Rees, A., Reinemann, S., Roberts, S., Rolland, N., Salonen, S., Self, A., Seppä, H., Shala, S., St-Jacques, J.M., Stenni, B., Syrykh, L., Tarrats, P., Taylor, K., van den Bos, V., Velle, G., Wahl, E., Walker, I., Wilmshurst, J., Zhang, E., Zhilich, S., 2020. A global database of Holocene paleotemperature records. Sci. Data 7, 1–34. https://doi.org/10.1038/s41597-020-0445-3.
Keller, C.F., 2003. Global warming: the balance of evidence and its policy implications. A review of the current state-of-the-controversy. Sci. World J. [electronic Resour. https://doi.org/10.1100/tsw.2003.26].
Kennedy, J.P., Pil, M.W., Proffitt, C.E., Boeger, W.A., Stanford, A.M., Devlin, D.J., 2016. Postglacial expansion pathways of red mangrove, Rhizophora mangle, in the Caribbean Basin and Florida. Am. J. Bot. 103, 260–276. https://doi.org/10.3732/ajb.1500183.
Lamb, A.L., Wilson, G.P., Leng, M.J., 2006. A review of coastal palaeoclimate and relative sea-level reconstructions using δ13C and C/N ratios in organic material. Earth-Sci.

Rev. 75, 29–57. https://doi.org/10.1016/j.earscirev.2005.10.003.
Marengo, J.A., 2006. Mudanças climáticas globais e seus efeitos sobre a biodiversidade: caracterização do clima atual e definição das alterações climáticas para o território brasileiro ao longo do século XXI. Ministério do Meio Ambiente, Brasilia.
Marengo, J.A., Camargo, C.C., 2008. Surface air temperature trends in Southern Brazil for 1960–2002. Int. J. Climatol. 28, 893–904. https://doi.org/10.1002/joc.1584.
Medhaug, I., Stolpe, M.B., Fischer, E.M., Knutti, R., 2017. Reconciling controversies about the "global warming hiatus". Nature. https://doi.org/10.1038/nature22315.
Meyers, P.A., 1997. Organic geochemical proxies of paleoceanographic, paleolimnologic, and paleoclimatic processes. Org. Geochem. 27, 213–250. https://doi.org/10.1016/S0146-6380(97)00049-1.
Meyers, P.A., 2003. Applications of organic geochemistry to paleolimnological reconstructions: A summary of examples from the Laurentian Great Lakes. Org. Geochem. https://doi.org/10.1016/S0146-6380(02)00168-7.
Meyers, P.A., 1994. Preservation of elemental and isotopic source identification of sedimentary organic matter. Chem. Geol. 114, 289–302. https://doi.org/10.1016/0009-2541(94)90059-0.
Miall, 1978. Facies types and vertical profilemodels in braided river deposits: a summary. In: Miall, A.D. (Ed.), Fluvial Sedimentology. Canadian Society of Petroleum Geologists, Calgary, pp. 597–604.
Osland, M.J., Day, R.H., Hall, C.T., Brumfield, M.D., Dugas, J.L., Jones, W.R., 2017. Mangrove expansion and contraction at a poleward range limit: climate extremes and land-ocean temperature gradients. Ecology 98, 125–137. https://doi.org/10.1002/ecy.1625.
Osland, M.J., Feher, L.C., López-Portillo, J., Day, R.H., Suman, D.O., Guzmán Menéndez, J.M., Rivera-Monroy, V.H., 2018. Mangrove forests in a rapidly changing world: Global change impacts and conservation opportunities along the Gulf of Mexico coast. Estuar. Coast. Shelf Sci. 214, 120–140. https://doi.org/10.1016/j.ecss.2018.09.006.
Osland, M.J., Hartmann, A.M., Day, R.H., Ross, M.S., Hall, C.T., Feher, L.C., Vervaeke, W.C., 2019. Microclimate influences mangrove freeze damage: implications for range expansion in response to changing macroclimate. Estuar. Coasts 42, 1084–1096. https://doi.org/10.1007/s12237-019-00533-1.
Parmesan, C., Ryrholm, N., Stefanescu, C., Hill, J.K., Thomas, C.D., Descimon, H., Huntley, B., Kaila, L., Kullberg, J., Tammaru, T., Tennent, W.J., Thomas, J.A., Warren, M., 1999. Poleward shifts in geographical ranges of butterfly species associated with regional warming. Nature 399, 579–583. https://doi.org/10.1038/21181.
Parmesan, C., Yohe, G., 2003. A globally coherent fingerprint of climate change impacts across natural systems. Nature 421, 37–42. https://doi.org/10.1038/nature01286.
Perry, C.L., Mendelssohn, I.A., 2009. Ecosystem effects of expanding populations of Avicennia germinans in a Louisiana salt marsh. Wetlands 29, 396–406. https://doi.org/10.1672/08-100.1.
Pessenda, L.C.R., Valencia, E.P.E., Martinelli, L.A., Cerri, C.C., 1996. 14C measurements in tropical soil developed on basic rocks. Radiocarbon 38 (2), 203–208.
Pessenda, L.C.R., Vidotto, E., De Oliveira, P.E., Buso, A.A., Cohen, M.C.L., Rossetti, D. de F., Ricardi-Branco, F., Bendassolli, J.A., 2012. Late Quaternary vegetation and coastal environmental changes at Ilha do Cardoso mangrove, southeastern Brazil. Palaeogeogr. Palaeoclimatol. Palaeoecol. 363, 57–68.
Piotrowska, N., Blaauw, M., Mauquoy, D., Chambers, F.M., 2010a. Constructing deposition chronologies for peat deposits using radiocarbon dating. Mires Peat 7, 1–14.
Piotrowska, Natalia, Vleeschouwer, F. De, Sikorski, J., Pawlyta, J., Fagel, N., Roux, G. Le, Pazdur, A., 2010b. Intercomparison of radiocarbon bomb pulse and 210Pb age models. A study in a peat bog core from North Poland. Nucl. Instrum. Methods Phys. Res. Sect B Beam Interact. Mater. Atoms 268, 1163–1166. https://doi.org/10.1016/j.nimb.2009.10.124.
PIX4D, 2013. Pix4dmapper Software Manual Pix4D Support [WWW Document]. Lausanne, Suiça. Pix4D SA.
Plastino, W., Kaihola, L., Bartolomei, P., Bella, F., 2001. Cosmic background reduction in the radiocarbon measurements by liquid scintillation spectrometry at the underground laboratory of Gran Sasso. Radiocarbon 43, 157–161. https://doi.org/10.1017/s0033822200037954.
Poloczanska, E.S., Brown, C.J., Sydeman, W.J., Kiessling, W., Schoeman, D.S., Moore, P.J., Brander, K., Bruno, J.F., Buckley, L.B., Burrows, M.T., Duarte, C.M., Halpern, B.S., Holding, J., Kappel, C.V., O'Connor, M.I., Pandolfi, J.M., Parmesan, C., Schwing, F., Thompson, S.A., Richardson, A.J., 2013. Global imprint of climate change on marine life. Nat. Clim. Chang. 3, 919–925. https://doi.org/10.1038/Nclimate1958.
Porter, T.J., Schoenemann, S.W., Davies, L.J., Steig, E.J., Bandara, S., Froese, D.G., 2019. Recent summer warming in northwestern Canada exceeds the Holocene thermal maximum. Nat. Commun. 10, 1631. https://doi.org/10.1038/s41467-019-09622-y.
Quisthoudt, K., Schmitz, N., Randin, C.F., Dahdouh-Guebas, F., Robert, E.M.R., Koedam, N., 2012. Temperature variation among mangrove latitudinal range limits worldwide. Trees – Struct. Funct. 26, 1919–1931. https://doi.org/10.1007/s00468-012-0760-1.
Ribeiro, S.R., Batista, E.J.L., Cohen, M.C., França, M.C., Pessenda, L.C., Fontes, N.A., Alves, I.C., Bendassolli, J.A., 2018. Allogenic and autogenic effects on mangrove dynamics from the Ceará Mirim River, north-eastern Brazil, during the middle and late Holocene. Earth Surf. Process. Landforms. https://doi.org/10.1002/esp.4342.
Roubik, D.W., Moreno, J.E., 1991. Pollen and Spores of Barro Colorado Island. Missouri Botanical Garden.
Saintilan, N., Wilson, N.C., Rogers, K., Rajkaran, A., Krauss, K.W., 2014. Mangrove expansion and salt marsh decline at mangrove poleward limits. Glob. Chang. Biol. 20, 147–157. https://doi.org/10.1111/gcb.12341.
Sandoval-Castro, E., Muñiz-Salazar, R., Enríquez-Paredes, L.M., Riosmena-Rodríguez, R., Dodd, R.S., Tovilla-Hernández, C., Arredondo-García, M.C., 2012. Genetic population structure of red mangrove (Rhizophora mangle L.) along the northwestern coast of Mexico. Aquat. Bot. 99, 20–26. https://doi.org/10.1016/J.AQUABOT.2012.01.002.
Sherrod, C.L., McMillan, C., 1985. The distributional history and ecology of mangrove vegetation along the northern Gulf of Mexico coastal region. Contrib. Mar. Sci. 129–140.
Soares, M.L.G., Estrada, G.C.D., Fernandez, V., Tognella, M.M.P., 2012. Southern limit of the Western South Atlantic mangroves: Assessment of the potential effects of global warming from a biogeographical perspective. Estuar. Coast. Shelf Sci. 101, 44–53. https://doi.org/10.1016/j.ecss.2012.02.018.
Stuiver, M., Reimer, P.J., Reimer, R.W., 2017. CALIB 7.1.
Sturm, M., Racine, C., Tape, K., 2001. Increasing shrub abundance in the Arctic. Nature 411, 546–547. https://doi.org/10.1038/35079180.
Thomas, C.D., Lennon, J.J., 1999. Birds extend their ranges northwards. Nature 399https://doi.org/10.1038/20335. 213–213.
Thornton, S.F., McManus, J., 1994. Application of organic carbon and nitrogen stable isotope and C/N ratios as source indicators of organic matter provenance in estuarine systems: evidence from the Tay Estuary, Scotland. Estuar. Coast. Shelf Sci. 38, 219–233.
Van Grunsven, R.H.A., Van Der Putten, W.H., Martijn Bezemer, T., Berendse, F., Veenendaal, E.M., 2010. Plant-soil interactions in the expansion and native range of a poleward shifting plant species. Glob. Chang. Biol. 16, 380–385. https://doi.org/10.1111/j.1365-2486.2009.01996.x.
Walker, R.G., 1992. facies models and modern stratigrahic concepts. In: Walker, R.G., James, N.P. (Eds.), Facies Models Response to Sea Level Change. Geological Association of Canada, Ontario, pp. 1–14.
Walsh, G.E., 1974. Mangroves: a review. Ecol. Halophytes. 51–174. https://doi.org/10.1016/B978-0-12-586450-3.50008-1.
Walther, G.-R., Post, E., Convey, P., Menzel, A., Parmesan, C., Beebee, T.J.C., Fromentin, J.-M., Hoegh-Guldberg, O., Bairlein, F., 2002. Ecological responses to recent climate change. Nature 416, 389–395. https://doi.org/10.1038/416389a.
Wentworth, C.K., 1922. A scale of grade and class terms for clastic sediments. J. Geol. 30, 377–392.
Westgate, J.W., Gee, C.T., 1990. Paleoecology of a middle Eocene mangrove biota (vertebrates, plants, and invertebrates) from southwest Texas. Palaeogeogr. Palaeoclimatol. Palaeoecol. 78, 163–177. https://doi.org/10.1016/0031-0182(90)90210-X.
White, W.M., 2015. Isotope Geochemistry. Wiley-Blackwell, Oxford.
Woodroffe, C.D., Grindrod, J., 1991. Mangrove biogeography: the role of quaternary environmental and sea-level change. J. Biogeogr. 18, 479–492. https://doi.org/10.2307/2845685.
Xu, Q., Tian, F., Bunting, M.J., Li, Y., Ding, W., Cao, X., He, Z., 2012. Pollen source areas of lakes with inflowing rivers: modern pollen influx data from Lake Baiyangdian, China. Quat. Sci. Rev. 37, 81–91. https://doi.org/10.1016/j.quascirev.2012.01.019.
Yamano, H., Sugihara, K., Nomura, K., 2011. Rapid poleward range expansion of tropical reef corals in response to rising sea surface temperatures. Geophys. Res. Lett. 38. https://doi.org/10.1029/2010GL046474.
Zalasiewicz, J., Waters, C.N., Williams, M., Summerhayes, C., 2018. The Anthropocene as a Geological Time Unit: A Guide to the Scientific Evidence and Current Debate. Cambridge University Press.

CAPÍTULO IV: IMPACTS OF SEA-LEVEL CHANGES ON MANGROVES FROM SOUTHEASTERN BRAZIL DURING THE HOLOCENE AND ANTHROPOCENE USING A MULTI-PROXY APPROACH

Bettina S. Bozi[a], Beatriz Figueiredo[ab], Erika Rodrigues[a], Marcelo C. L. Cohen[a*], Luiz C.R. Pessenda[b]; Elton E. N. Alves[b], José Bendassolli[c]

[a] Graduate Program of Geology and Geochemistry, Federal University of Pará. Av. Perimetral 2651, Terra Firme, 66077-530, Belém (PA), Brazil.

[b]University of São Paulo,CENA/^{14}C Laboratory, Av. Centenário 303, 13400-000, Piracicaba, São Paulo,

[c]University of São Paulo, CENA/Stable Isotopes Laboratory, São Paulo, Brazil

*Corresponding author: Marcelo Cancela Lisboa Cohen

Federal University of Pará - Brazil

Rua Augusto Corrêa, 01 - Guamá. CEP 66075-110, Belém (PA), Brazil.

Tel.: +55 91 3201-7988. e-mail address: mcohen80@hotmail.com

Submitted to Geomorphology journal

Geomorphology 390 (2021) 107860

Contents lists available at ScienceDirect

Geomorphology

journal homepage: www.elsevier.com/locate/geomorph

Impacts of sea-level changes on mangroves from southeastern Brazil during the Holocene and Anthropocene using a multi-proxy approach

Bettina S. Bozi [a], Beatriz L. Figueiredo [a,b], Erika Rodrigues [a], Marcelo C.L. Cohen [a,*], Luiz C.R. Pessenda [b], Elton E.N. Alves [b], Adriana V. de Souza [a], José A. Bendassolli [c], Kita Macario [d], Pablo Azevedo [e], Nicholas Culligan [f]

[a] Graduate Program of Geology and Geochemistry, Federal University of Pará, Av. Perimetral 2651, Terra Firme, 66077-530, Belém, PA, Brazil
[b] University of São Paulo, CENA/^{14}C Laboratory, Av. Centenário 303, 13400-000 Piracicaba, São Paulo, Brazil
[c] University of São Paulo, CENA/Stable Isotopes Laboratory, São Paulo, Brazil
[d] Physics Department, LAC-UFF AMS Laboratory-Fluminense Federal University, Niterói, RJ 24220-900, Brazil
[e] Physical Geography Laboratory - UFES, Vitória, Espírito Santo, Brazil
[f] Department of Oceanography and Coastal Sciences, College of the Coast and Environment, Louisiana State University, Baton Rouge, LA 70803, United States

ARTICLE INFO

Article history:
Received 30 January 2021
Received in revised form 8 July 2021
Accepted 9 July 2021
Available online 18 July 2021

Keywords:
Climate change
Guarapari
Mangrove
Photogrammetry
Pollen
Sea-level
Stable isotopes

ABSTRACT

Globally, mangroves are expected to move inland as sea-level rises. However, local characteristics mainly related to mangrove structure, geomorphology and coastal hydrodynamics may change the mangrove response to sea-level rise. The most useful evidence to support projections for the future likely comes from mangrove history reconstruction corresponding to past sea-level changes. This study characterized modern (1985–2018 CE) and past (<6300 cal yr BP) mangrove dynamics according to sea-level changes along two estuarine valleys on the southeastern Brazilian coast to predict the mangrove response to sea-level rise by 2100. Relative Sea-Level (RSL) rise triggered changes from a tidal flat occupied by herbs, palms, tree/shrubs to a lagoon surrounded by mangroves between ~6300 and ~4230 cal yr BP. More recently, the RSL fall converted that lagoon into flats occupied by herbs, trees/shrubs, and palms on higher surfaces, and mangroves on lower flats during the mid-late Holocene. The last thousand years were characterized by a mangrove contraction between 390 and 77 cal yr BP, caused by a RSL fall. By contrast, mangrove expansion began at 77 cal yr BP (1873 CE) and continued after 1950 CE, migrating onto higher tidal flats previously occupied by herbs, palms, and trees/shrubs. Spatial-temporal analysis also indicated a mangrove invasion onto higher flats since 1985 CE. These trends are likely related to RSL rise since the end of the Little Ice Age and they intensified during recent decades, when the lower mangrove boundaries remained stable, and mangroves expanded to higher surfaces. Mangroves, confined between steep surfaces, will expand ~22ha under the influence of a sea-level rise of 98 cm by 2100. However, an upstream mangrove migration by 2100 on low and extensive fluvial plains (~4030 ha) will depend mainly on the interaction between fluvial discharge/sea-level rise.

1. Introduction

Mangroves have considerable social, economic, and ecological value, including supporting fisheries, aiding in coastal protection, and sequestering carbon (Nagelkerken et al., 2008; Barbier et al., 2011; Tue et al., 2018; Matos et al., 2020). However, sea-level rise can threaten the long-term stability of mangroves (Lovelock et al., 2015a; Cohen et al., 2018, Cohen et al., 2020a) since these forests are unlikely to persist if the rate of sea-level rise is >5 mm year^{-1} (McKee et al., 2007). Although several factors can influence the patterns of mangrove advance or retreat, studies have shown that sea-level rise controls tropical mangrove distribution mainly at their seaward margin (Woodroffe, 1995; Kirwan and Megonigal, 2013), determining an equilibrium morphology (Cahoon et al., 2006; Kirwan and Murray, 2007; D'Alpaos et al., 2008; Cohen et al., 2012; Cohen et al., 2020a, 2020b). Considering high rates of sea-level rise (52–98 cm by 2100, IPCC, 2013), mangroves may be drowned along the lowest zone of tidal flats and move inland to higher tidal flats, previously occupied by herbaceous vegetation adapted to a hypersaline environment (Lara and Cohen, 2006; Cohen et al., 2018, 2020a). Flood patterns of mangrove substrates are differentiated, affecting their structure (Pascoalini et al., 2014). Supposing the topography favors landward mangrove migration (Cohen and Lara, 2003; Di Nitto et al., 2013b; Peterson and Bell, 2015; Cohen et al., 2018) with no anthropogenic obstacles related to infrastructure, mangroves can withstand submergence by 'back-stepping' into adjacent habitats (Saintilan et al., 2014). Sediment supply is essential to maintain vertical sediment accretion and thus prevent mangrove area loss in the future (Lovelock et al., 2015b). In addition, along the topographic gradient of tidal flats,

* Corresponding author at: Federal University of Pará, Rua Augusto Corrêa, 01 – Guamá, CEP 66075-110 Belém, PA, Brazil.
E-mail address: mcohen@ufpa.br (M.C.L. Cohen).

https://doi.org/10.1016/j.geomorph.2021.107860
0169-555X/

tidal flooding frequency controls porewater salinity in the flats (Lara and Cohen, 2006). The Relative Sea-Level (RSL) rise increases the tidal inundation frequency across the tidal flats, causing salt leaching from sediments. This process contributes to landward mangrove migration (Cohen and Lara, 2003; Cohen et al., 2018).

Mangrove dynamics according to sea-level changes in recent decades also need to be analyzed from both a broad spatial (sedimentary environment) and temporal (secular- millennial) perspective (Cohen et al., 2012, 2014, 2020a; França et al., 2013; Yao et al., 2015; Yao and Liu, 2017). During the Holocene, the sea-level was highest (2–5 m above the modern sea-level) between the south and northeastern Brazilian coast from 5.8 to 5.0 Kyr BP (Martin et al., 2003; Angulo et al., 2006; de O Caldas et al., 2006; Suguio et al., 2013; de F Toniolo et al., 2020), which enabled the infilling of estuaries and landward mangrove migration (Castro et al., 2013; Lorente et al., 2014; Cohen et al., 2014, 2020b; França et al., 2015; Rossetti et al., 2015). The RSL in the Rio Grande do Norte coast (northeast/northern Brazilian coast), reached the modern level at ~7000 cal yr BP (Ribeiro et al., 2018), with the highstand (~1.3 m) at ~5900 cal yr BP (de O Caldas et al., 2006). A palaeoecological study 380 km north of the study area indicated a highstand (~3.25 m) around 5350 cal yr BP (Cohen et al., 2020a). The RSL fell along the south and northeast coast of Brazil in the late Holocene (Angulo et al., 2006; de F Toniolo et al., 2020). However, the amplitudes and trends of Brazilian Holocene RSL is a topic still open to discussion because the middle Holocene high sea-level stand tends to be higher in the southeast (~5 m) than the northeast (~1 m) and north (~0.6m) coast of Brazil (Boski et al., 2015; Ribeiro et al., 2018; Cohen et al., 2020a, 2021; de F Toniolo et al., 2020), and some studies suggest RSL oscillations, rather than a continuous RSL fall during the mid-late Holocene (Martin et al., 2003; Suguio et al., 2013).

During the last millennium, the sea-level reached its highest (12–21 cm) stand at ~1150 CE, while the lowest (−19 and −26 cm) level occurred at ~1730 CE (Grinsted et al., 2009). This millennial RSL trend affected the mangroves from northern Brazil (Cohen et al., 2005). Rates of global sea-level rise have intensified during the Anthropocene (since the mid-twentieth century (Zalasiewicz et al., 2018), from ~2.5 mm/yr in the 1990s to ~3.4 mm/yr presently (Nerem et al., 2018). Some models estimate that global sea level rise will reach 53–77 cm (Nerem et al., 2018), 38–73 cm (RCP6.0), or 52–98 cm (RCP8.5) by the end of the 21st century (Nerem et al., 2018).

Mangroves on the northern Brazilian coast, in one of the largest continuous mangrove areas on Earth, have migrated onto higher tidal flats occupied by herbaceous vegetation over recent years (1984–2017 CE) due mainly to RSL rise (Cohen et al., 2009, 2018). A time-series analysis (1996–2008 CE) along the northern Brazilian coast indicated increased mangrove coverage area (Nascimento et al., 2013). It seems this process is occurring globally. Di Nitto et al. (2013a) address whether mangroves can be resilient to an increase in sea-level according to their potential to migrate landward in East Africa. Combining data from remote sensors, digital terrain models and topographic data under different projections of sea-level rise until the end of the century (IPCC, 2013) reveals how mangroves can change under these different predictions (9–88 cm by the year 2100 CE). Under the scenario of up to 48 cm of sea level rise by the year 2100, mangrove area in Sri Lanka will increase landward, while a sea-level rise scenario of +88 cm suggests a decrease in the landward mangrove migration (Di Nitto et al., 2013b). The mangrove response to different rates of sea-level rise also depends on annual average temperatures, mangrove structure/productivity, coastal topography, sediment supply to the coastal depositional system, tidal range and action of currents and waves along the coast (Cohen and Lara, 2003; McKee et al., 2007; Cohen et al., 2012, 2020a, 2020b; Lovelock et al., 2015a; Spencer et al., 2016; Rodrigues et al., 2021). In this context, it is imperative to identify the mangrove dynamics according to Holocene RSL changes along coasts with climatic, vegetational, geomorphological, and oceanographic particularities to understand the possible responses of these forests to RSL rise in the Anthropocene.

Mangrove response to sea-level changes is poorly documented and understood for the southeastern sector of the Brazilian coast, mainly across steep-relief coasts characterized by estuaries confined between crystalline rocks. Therefore, this work aims to answer two questions: 1) How did tropical mangroves confined to two estuarine valleys between crystalline rocky promontories respond to depositional environment changes caused by RSL fluctuations during the Holocene and Anthropocene? 2) What are the impacts of a sea-level rise of 98 cm by 2100 on mangroves under the influence of both small and large fluvial discharges? These questions can be answered by integrating digital elevation models, analysis of modern mangrove structure and mangrove dynamics during recent decades, and multi-proxy data obtained down sediment cores sampled from a coastal plain at the State of Espírito Santo, southeastern Brazilian coast.

2. Modern settings

2.1. Study area and geological setting

Mangrove areas (70 km^2) in the State of Espírito Santo, on the southeastern Brazilian coast, extend from the Riacho Doce, in the extreme north of this state, to the Itabapoana river, on the southern border with the State of Rio de Janeiro. The study areas are under the influence of the Jabuti, Aldeia Velha and Benevente River estuaries (Fig. 1b), near the towns of Guarapari and Anchieta. This is one of the most extensive and conserved mangrove forests in the State of Espírito Santo, covering an area of ~4.6 km^2 (Vale and Ferreira, 1998). This coast is affected by a maximal tidal range of 1.8 m (DHN, 2014). The Jabuti and Aldeia Velha Rivers are <20 km long and influence regions 1 and 2, while the ~80 km long Benevente River affects region 3 (Fig. 1b) and has a hydrographic basin which drains 1207 km^2 with a fluvial discharge ranging from 22 to 78 $m^3\ s^{-1}$ (Aparecida and Uliana, 2011).

The State of Espírito Santo fits into the Mantiqueira Province (Almeida, 1977; Almeida et al., 1977) of Neoproterozoic-Cambrian age. Orthogneisses mainly constitute the basement (Vieira and de Menezes, 2015). The Barreiras Formation sediments were deposited during the early/middle Miocene (Rossetti and Góes, 2009). The studied coastal zone includes paleolagoons, mainly characterized by pelitic sediments, rich in organic matter with wood fragments and mollusk shells (Vieira and de Menezes, 2015).

Three geomorphological regions characterize the study area: (1) Mountain range with Precambrian rocks (<~2900 m) and very rugged reliefs, (2) Coastal terraces whose elevation is predominantly ~27 m above mean sea-level, developed over the Barreiras Formation (Bricalli and de Souza, 2017), and (3) Coastal plain with Quaternary deposits accumulated on lower surfaces (0 to ~3 m), consisting of beaches, sandbanks, and continental alluvium (Fig. 1b). This division reflects the regional tectonic evolution and lithology associated with the climate (EMBRAPA, 1978).

2.2. Climate and vegetation

The study area presents a hot and humid tropical climate characterized by a mean annual rainfall of ~1400 mm, with a rainy season between November and January, and a dry season between May and September. The average temperature varies between 20° and 26 °C (Peixoto and Gentry, 1990; Carvalho et al., 2004; Franca et al., 2016).

The modern coastal vegetation in the study area consists of dense ombrophilous forests, herbaceous plains, and mangroves. Mangroves cover a significant part of the study area, with trees ranging from 3 to 15 m tall. *Rhizophora mangle* occurs mainly along the channel margins, while *Avicennia germinans* grows at higher topographic elevations. The herbaceous vegetation occurs on sandy flats topographically higher than tidal flats occupied by mangroves. Herbs and some small shrubs

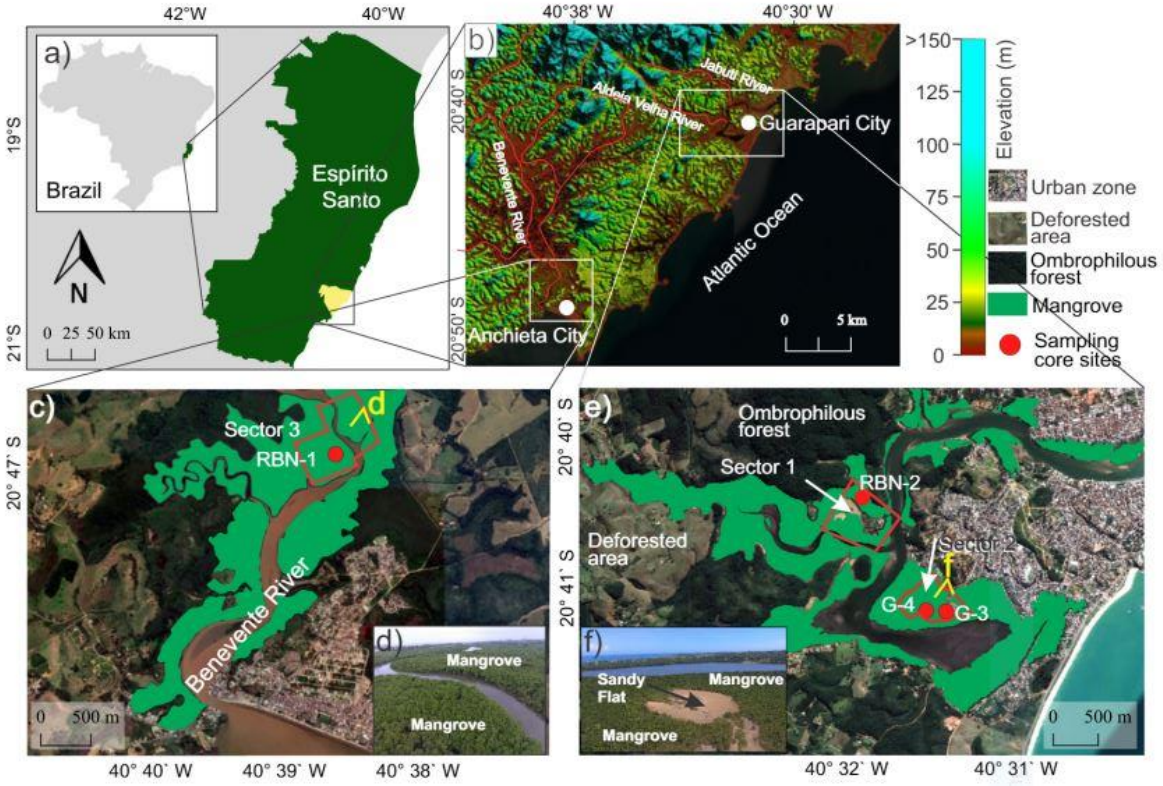

Fig. 1. a) Location of the study area, b) topographic map based on SRTM data, c) distribution of mangroves along the Benevente river, d) panoramic drone photo from mangroves of the sector 3 along the rivers, e) Aldeia and Jabuti River, and the sampling core sites; and f) a panoramic drone photo from the transition mangrove/sandy flat in the highest tidal flats of the sector 2.

characterize this vegetation unit, mainly represented by the following families: Poaceae, Asteraceae, Cyperaceae, and Fabaceae. The dense ombrophilous forest is made up of mainly Arecaceae, Myrtaceae, Euphorbiaceae, Fabaceae, and Rubiaceae. These vegetation units occur under specific rainfall regimes, tidal inundation frequency, sediment size, and porewater salinities (Cohen et al., 2014, 2018, 2020a; Franca et al., 2016).

3. Material and methods

Coastal deposits are highly heterogeneous and challenging to investigate based only on sediment cores due to lateral and vertical variability. Integration of remote sensing with stratigraphy has contributed to three-dimensional analysis of the depositional environments and vegetation (Sahoo and Gani, 2015; Nieminski and Graham, 2017; Cohen et al., 2020b; Cohen et al., 2020a). This study combined planialtimetric and stratigraphic data, following a pre-designed methodology flow chart divided into four phases (Fig. 1, supplementary material): 1) Spatial-temporal analysis based on satellite images; 2) Choice of tidal flats for a topographic survey and vegetation structure studies (stature, density and genera of mangrove trees) based on photogrammetry of drone images as well as field validation of mangrove structure and topography of tidal flats determined by the drone images; 3) Choice of the core sampling sites that can better record the Holocene mangrove dynamics; 4) Integration and interpretation of surface and subsurface data to reconstruct the paleoenvironment and paleoflora, and predict mangrove dynamics by 2100.

3.1. Data sources

3.1.1. Aerial and satellite data

This study used Landsat (ground resolution of 30 m) recorded in April/1985, and Quickbird images (resolution of 2.44 m) recorded in December/2003, July/2007, September/2012, and July/2018 (Fig. 2). The Landsat and Quickbird images were downloaded from the collection of the USGS (United States Geological Survey) and from Google Earth. The regional altimetric data were derived from Shuttle Radar Topography Mission (SRTM), downloaded from the USGS website. These data were imported in GeoTIFF format into the Agisoft Metashape version 1.6.3 software. The satellite and drone images were accurately orthorectified based on 30 Ground Control Points (GCPs) (Table 1, Figs. 3b and 4f). For the geomorphological/vegetation characterization and spatial-temporal analysis, all images were processed using the PCI 16, Qgis 3, and Global Mapper version 18 software. The spatial-temporal analysis was carried out in the mangrove area under the influence of the Jabuti and Aldeia Velha River, where it was possible to validate the data by fieldwork. Difficulties in accessing the sandy and muddy flats occupied by herbs and mangroves and under influence by the Benevente River prevented an adequate field validation of the planialtimetric data obtained by remote sensing (Fig. 1).

3.1.2. Drone data

Spatial analysis was also based on high-resolution images obtained by a Drone Phantom 4 DJI, with a FC 330 digital 4 K/12MP

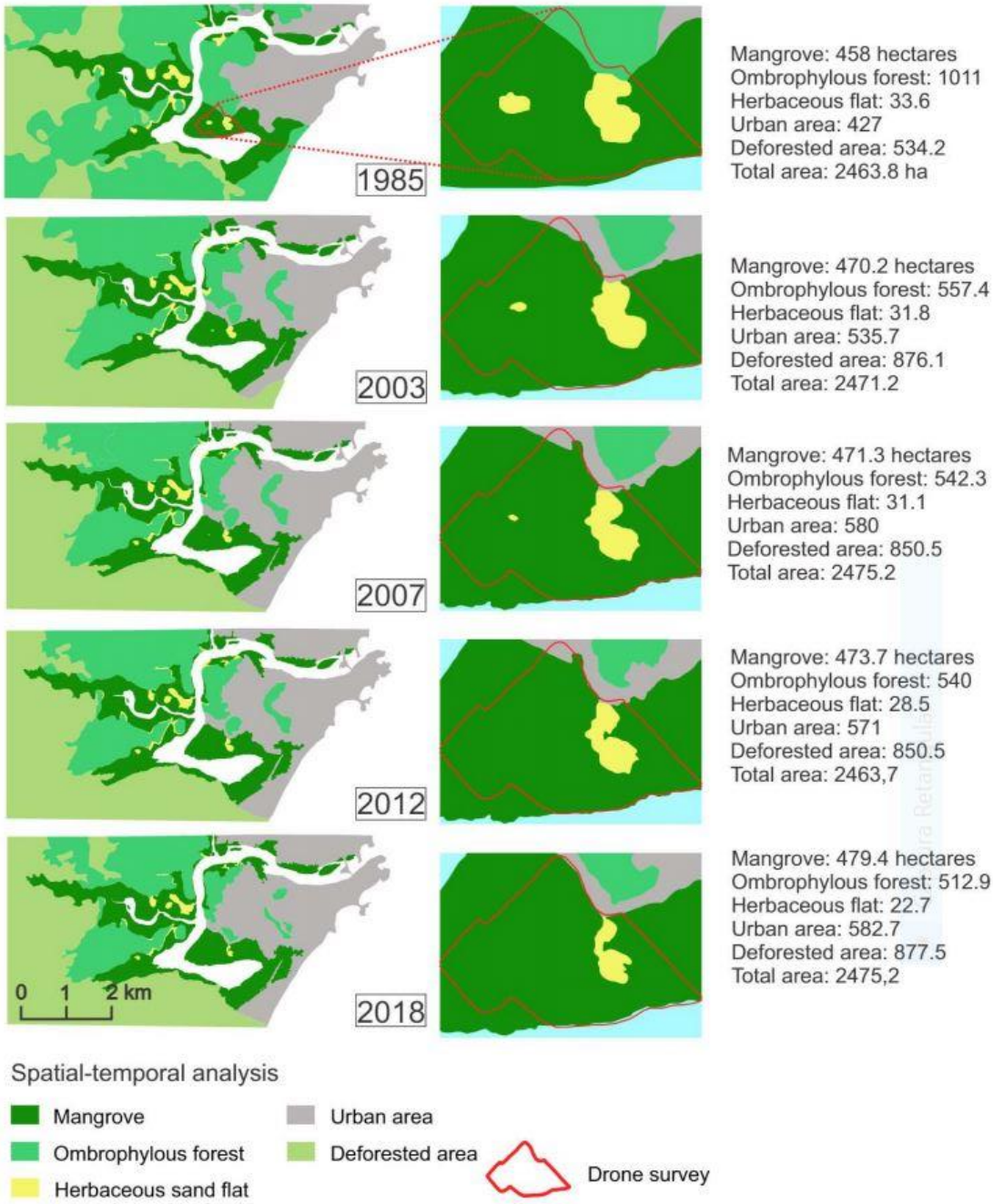

Fig. 2. Spatial-temporal analysis of the vegetation under influence from the Jabuti and Aldeia Velha river estuaries based on satellite and drone images between 1985 and 2018, highlighting sector 2 of the study area.

(RGB) camera. The drone surveying was developed using the DJI Ground Station Pro Software installed in an Ipad Air tablet. Predefined missions were carried out autonomously with 90° camera angle, 90% frontal and 75% lateral overlay, and 100 m (resolution of 4.17 cm) altitude. Missions were also acquired at 60 m (resolution of 2.5 cm) to accurately analyze the mangrove/herbaceous flat or sandy flat areas. A total of 28 missions and 4994 images were recorded to scan 12.75 sq.km in April/2019.

3.1.3. Ground control points

A smartphone linked to an Antenna Trimble Catalyst supported by differential Global Navigation Satellite System (GNSS) was used to acquire planialtimetric data during field trips in April/2019 (fall). A decimetric correction, obtained by a subscription to the Trimble website, increased the GNSS data accuracy. The planialtimetric accuracy of the GCPs was ±10 cm with Real-Time Kinematic correction. This value was validated comparing planialtimetric data indicated by the

Table 1
Ground Control Points (GCPs) of the study area with longitude, latitude, porewater salinity, mangrove height, mangrove trees density, soil orthometric height, and planialtimetric differences between the models and GCPs data.

Fieldwork						Photogra. analysis	Planialtimetric differences = Model – GCPs data			
GCP	Longitude	Latitude	Pore water salin. (‰)	Mang. height (m)	Substrate orthometric height (m)	Density (trees/ha)	Long. error (m)	Lat. error (m)	Elev. error (m)	Mang. height error (m)
1	−40.522339	−20.684059			0.880		0.14	−0.26	−0.04	
2	−40.522628	−20.682133			2.680		−0.14	−0.00	−0.08	
3	−40.522679	−20.682202	65	3.2	1.745	1200	0.04	0.08	0.02	0.2
4	−40.522743	−20.684257	65	1.9	0.738	1300	−0.06	−0.03	0.05	0.4
5	−40.521918	−20.683612	60	2	0.840	1200	0.064	−0.06	−0.01	−0.2
6	−40.521806	−20.684419	65	3	0.813	1300	−0.02	0.16	−0.00	−0.3
7	−40.522641	−20.682858		2	0.930	1300	−0.16	−0.18	0.09	0.1
8	−40.522632	−20.682533		2.5	1.320	1300	0.14	−0.00	0.11	0.2
9	−40.522802	−20.683133			1.29		0.19	−0.03	−0.06	
10	−40.522765	−20.683331		1	0.843	1300	0.07	0.13	0.10	0.0
11	−40.523909	−20.685403	20	13	0.200	190	0.00	−0.00	0.00	0.6
12	−40.524792	−20.685229	20	13	0.200	200	0.00	−0.00	0.00	0.2
13	−40.522788	−20.684325	55	5	0.70	1100	0.3	0.2	−0.12	−0.3
14	−40.522881	−20.684372	55	5	0.630	1500[a]	0.1	0.1	0.05	0.1
15	−40.526350	−20.683364	45	3.5	0.720	400[a]	0.13	0.14	0.14	0.1
16	−40.526353	−20.683367	45	5	0.700	400[a]	−0.02	0.2	0.13	0.1
17	−40.523192	−20.684677	50	5	0.560	2600[a]	0.4	0.23	0.16	0.1
18	−40.523292	−20.684833	47	7.5	0.500	2000[a]	0.5	0.26	0.12	−0.3
19	−40.526350	−20.683364	37	15	0.420	650[a]	−0.2	−0.1	0.14	0.4
20	−40.523521	−20.685287	30	15	0.350	400[a]	0.2	0.13	0.06	0.5
21	−40.523681	20.685438	30	15	0.200	200[a]	0.1	0.16	−0.08	−0.4
22	−40.522647	−20.683709	65	3	0.79		−0.28	0.21	−0.00	−0.1
23	−40.534324	−20.674385			1.36		0.27	−0.05	−0.03	
24	−40.533524	−20.673680	55	4	1.23		0.34	−0.18	−0.01	−0.1
25	−40.533127	−20.673484	55	2	1.38		0.13	0.55	−0.02	−0.1
26	−40.534254	−20.674608			1.73		0.41	−0.83	0.06	
27	−40.534059	−20.672539	55	4	1.22		0.54	0.11	0.01	0.1
28	−40.532216	−20.673715	55	4.5	1.27		−0.10	−0.24	0.02	0.1
29	−40.532619	−20.673095	55	3	1.21		−0.63	0.12	−0.00	0.0
30	−40.532876	−20.674100	55	4.4	1.20		−0.01	−0.50	−0.03	−0.2

[a] Validated data in field.

Antenna Catalyst with the geodetic benchmark (IBGE 8130991) from Guarapari (20° 37′ 41″ S/40° 31′ 49″ W) at the end of the topographic survey. The planialtimetric data obtained by the Antenna Trimble Catalyst were used as an absolute elevation point for the installation of an electronic theodolite (model CST Berger DGT10). The theodolite and a gauge of 4 m enabled identification of the relative surface elevation of mangrove substrates, mangrove/herbaceous flat, and sandy flat. The combination of the Antenna Catalyst with theodolite allowed us to record planialtimetric data on 30 ground control points (GCP) in the study area. These GCPs were used to determine the margin of error of the digital elevation model (DEM) obtained by photogrammetry (Table 1).

3.1.4. Mangrove density, height, and porewater salinity

50 × 50 m areas were used during fieldwork to identify mangrove tree genus and tree counting. These results were compared with those obtained by the Global Mapper based on drone images. Vegetation heights (VH) were calculated in photos using a 4 m ruler as reference. A rangefinder (Halo, model XL450), which uses a laser beam and a clinometer to determine distances and angles, respectively, was also used to measure tree height inside the mangrove forest. These field data allowed us to validate the vegetation height model based on photogrammetry. Ground and drone records validated the vegetation unit classification. Porewater salinity was obtained at 10 cm depth by a refractometer in the GCPs (Table 1).

3.2. Methods

3.2.1. Image classification

The geomorphology and vegetation were manually classified by photointerpretation in the Global Mapper Software. Locations with known land cover were used as a reference for each land cover type. This information enabled classification of vegetation and geomorphologic units and comparison with a visual interpretation based on drone orthophotos and field trips. Drone panoramic aerial photos were also used to identify the vegetation and geomorphologic units. Identification of the two genera of mangroves was based on the texture, color contrast, shape, and diameter of the treetops. This analysis was developed for areas with orthoimages obtained by drone surveys at 60 m altitudes.

3.2.2. 3D models

Drone images were processed using the Agisoft Metashape version 1.6.3. to generate 3D spatial data and orthomosaics with the support of planialtimetric GCPs (AgisoftPhotoScan, 2018). Dense point clouds were generated in high resolution with spacing points between 3 and 5 cm to develop digital models of surface (DSM), terrain (DTM), and vegetation (DVM). The DSM represents the natural (water, trees, and other types of vegetation) and built features (houses, streets, sidewalks, and power poles) on the surface. The sharp differences in the colors and elevations of points enabled us to classify the points representing the ground, built features, and vegetation. This process allowed development of the DTM and DVM that considers only the substrate and vegetation surface, respectively.

These models were validated by the GCPs obtained by the Antenna Catalyst/theodolite. The software implemented interpolation of the GCPs in areas of dense vegetation cover to identify the ground elevation. Therefore, the DTM below the dense vegetation cover was a product of the combination of GCP interpolation from flats covered by dense vegetation with the ground point gradients of non-vegetated tidal flats, extrapolated to flats below the dense vegetation cover. The DVM was developed by the Combine/Compare Terrain Layers tool, which subtracts the DSM from the DTM.

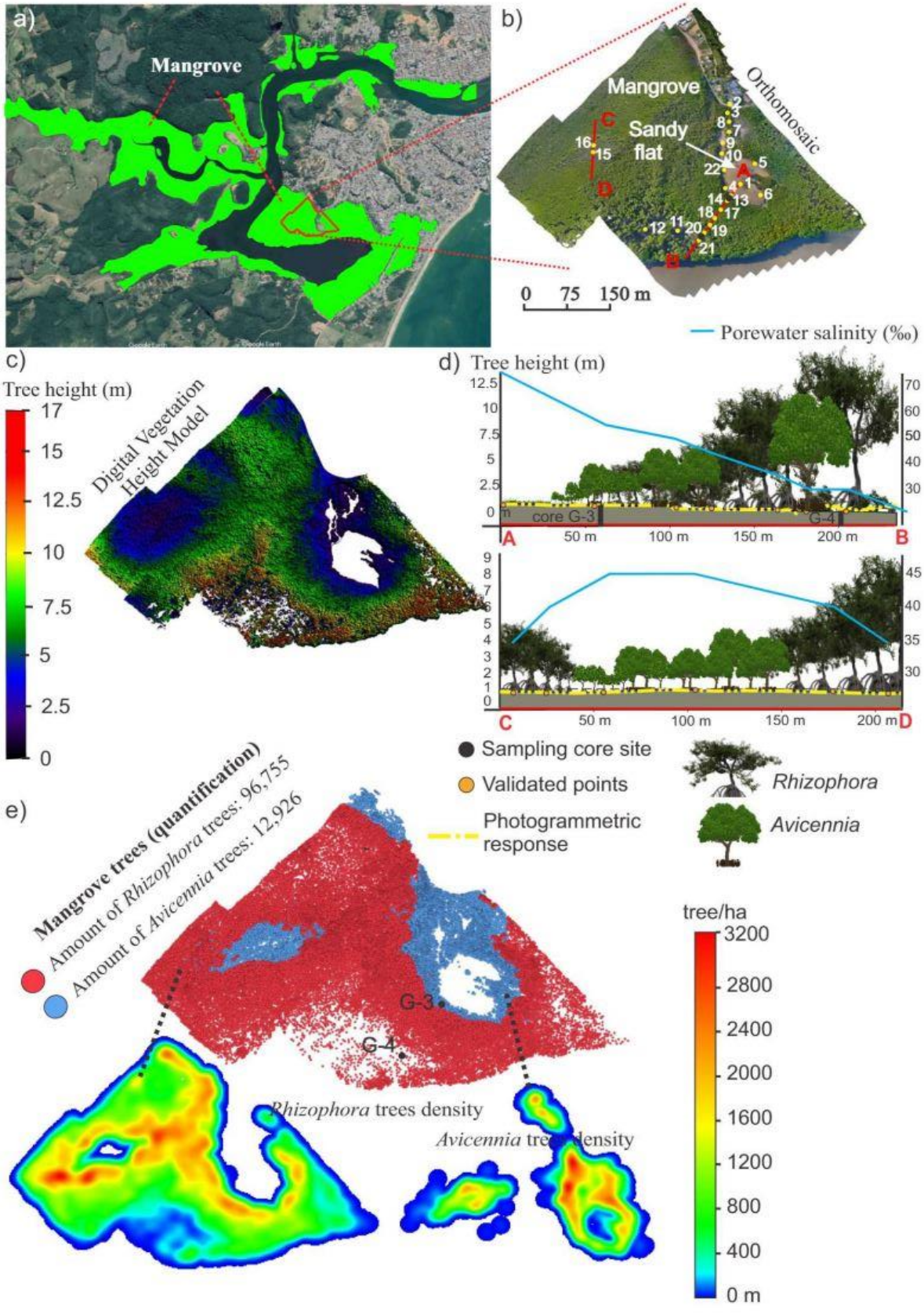
a)
Mangrove
b)
Mangrove
Sandy flat
Orthomosaic
0 75 150 m
Porewater salinity (‰)
c)
Tree height (m)
17
15
12.5
10
7.5
5
2.5
0
Digital Vegetation Height Model
d) Tree height (m)
core G-3
G-4
A
B
C
D
50 m
100 m
150 m
200 m
Sampling core site
Validated points
Photogrammetric response
Rhizophora
Avicennia
e)
Mangrove trees (quantification)
Amount of Rhizophora trees: 96,755
Amount of Avicennia trees: 12,926
G-3
G-4
Rhizophora trees density
Avicennia trees density
tree/ha
3200
2800
2400
2000
1600
1200
800
400
0 m

A quantitative assessment was carried out using the altimetric differences between GCPs and the DTM and DVM, following Eq. (2), as suggested by Cohen et al. (2018)):

$$Z_{dif} = Z_{DEM} - Z_{grd} \quad (2)$$

where Z_{dif} = the vertical differences, Z_{DEM} = the Z value of the models, and Z_{grd} = the Z value of the GCPs. The Z_{dif} values were between +14 and −11 cm (Table 1). The differences between the latitude/longitude of the 3D model and the planimetric data obtained by the Antenna Catalyst were between +55 and − 83 cm (Table 1). The GCPs have an error of ±10 cm, then a vertical and horizontal margin of error of ±24 cm and ± 93 cm was admitted for the 3D models, respectively.

3.2.3. Mangrove density

Avicennia and *Rhizophora* tree positions were manually extracted in the Global Mapper Software using the orthomosaics obtained by drone images at 60 m. After the manual tree point extraction, the tool "Create Density Grid" produced a new layer by calculating density values from the tree points. In addition, the tree density data from the eight areas (50 × 50 m) obtained during the fieldwork were compared with the tree density data obtained by the drone orthomosaic images. This analysis indicated a maximum difference of 10% between the two methods.

3.2.4. Sampling cores

Cores were collected with a Russian sampler. Three cores here called G-3 (20°41′4.60″S/40°31′21.48″W, G-4 (20°41′7.66″S/40°31′24.11″W) and RBN-2 (20°40′21.24″S/ 40°31′57.61″W) were sampled from tidal flats topographically positioned in 0.7, 0.2 and 1.0 m amsl occupied by mangroves under the influence of Jabuti and Aldeia Velha Rivers. The core RBN-1 (20°47′1.42″S/40°38′34.06″O) was sampled from a tidal flat 0.1 m amsl occupied by mangroves and influenced by the Benevente River (Figs. 1c,e, 3, and 4).

3.2.5. Facies description

The cores were radiographed (X-ray) to distinguish sedimentary features. Sediment samples (0.5 g) were obtained at 5 cm intervals to determine sediment particle size in a laser diffraction particle size analyzer (SHIMADZU SALD 2101) at the Laboratory of Coastal Dynamics - Federal University of Pará (UFPA). Hydrogen peroxide was used to remove organic matter and an ultrasonic bath disaggregated sediment particles. Grain sizes were classified according to Wentworth (1922): sand (2 mm–62.5 mm), silt (62.5–3.9 μm) and clay (3.9–0.12 μm). Sedimentary features, such as color, texture, lithology, and structure, characterized the facies (Harper, 1984; Walker, 1992). The codes of sedimentary facies were based on Miall (1978). The sedimentary facies, pollen, isotopes, and elemental analyses were grouped into facies associations to determine sedimentary environments (Reading, 1996).

3.2.6. Palynological analysis

1 cm^3 of sediments were sampled at 2.5-cm intervals in cores G-3, G-4, and RBN-2. The samples were processed according to pollen analytical techniques (Faegri and Iversen, 1989). Pollen and spore identification was based on reference collections of about 4000 Brazilian forest taxa as well as various pollen keys (Markgraf and D'Antoni, 1978; Roubik and Moreno, 1991; Salgado-Labouriau, 1997; Colinvaux et al., 1999), and the reference collection of the Laboratory of Coastal Dynamics – UFPA and 14C Laboratory of the Center for Nuclear Energy in Agriculture (CENA/USP). At least 300 pollen grains were identified for each sample. Pollen and spore profiles are exhibited as percentages of the total pollen sum. The pollen taxa groups were based on the pollen source: mangroves, trees and shrubs, palms, and herbs (Figs. 2, 3, 4 and 5, supplementary material). The software TILIA was used for calculation and plotting of pollen diagrams (Grimm, 1990). Cluster analysis was based on CONISS that supported the identification of vegetation succession over time.

3.2.7. Isotopic and chemical analysis

A total of 66 samples (5–60 mg), obtained at 10 cm intervals along the cores, were processed with 4% HCl to remove carbonate, washed with distilled water (pH 6), and dried at 50 °C. These sediments were analyzed for total organic carbon and nitrogen at the Stable Isotope Laboratory of the Center for Nuclear Energy in Agriculture (CENA/USP). The concentration results are expressed in percent of dry weight after removing carbonate, with an analytical precision of 0.09% (TOC) and 0.07% (TN). The C/N data indicated the molar ratio between carbon and nitrogen. The organic matter $\delta^{13}C$ results are expressed as $\delta^{13}Corg$ with respect to VPDB standard. Analytical precision is ±0.2‰ (Pessenda et al., 2004).

The $\delta^{13}C$, $\delta^{15}N$ and C/N of sedimentary organic matter depend on the assemblage of autotrophs in the surrounding environment (e.g. Lamb et al., 2006): C3 terrestrial plants ($\delta^{13}C$: −32‰ to −21‰ and $C/N > 12$), C4 plants ($\delta^{13}C$: −17‰ to −9‰ and $C/N > 20$) (Deines, 1980; Tyson, 1995; Meyers, 1997), freshwater algae ($\delta^{13}C$: −25‰ to −30‰) (Schidlowski et al., 1983; Meyers, 1997) and marine algae (−24‰ to −16‰) (Meyers, 1997). Bacteria and algae have C/N ratios of 4–6 and <10, respectively (Tyson, 1995; Meyers, 1997). Organic matter from terrestrial and aquatic plants exhibits $\delta^{15}N$ values between ~0‰ and ~10‰, respectively (Schidlowski et al., 1983). Mangrove trees present the following values: *Rhizophora* ($\delta^{13}C$: −31.8‰ to −30.2‰ and $C/N = 35.6 \pm 0.8$), *Avicennia* ($\delta^{13}C$: −30.4‰ to −29.1‰ and $C/N = 35 \pm 4.3$), and *Laguncularia* ($\delta^{13}C$: −30.4‰ to −29.2‰ and $C/N = 31.4 \pm 2.3$) (Matos et al., 2020).

3.2.8. XRF data

XRF analysis was performed by scanning the core at 2 cm intervals using a portable energy-dispersive X-ray fluorescence spectrometer (pED-XRF – model Tracer III-SD, Bruker AXS, Madison, USA). The major chemical elements in coastal sediments representative of marine (e.g. Br, Ca, Cl, K, and Sr) origins were selected for this analysis (Yao et al., 2015).

3.2.9. Radiocarbon dating

Nine bulk samples (10 g each), chosen for radiocarbon analysis (Table 2), were physically cleaned under the stereomicroscope. The samples were chemically processed to eliminate adsorbed carbonates and fulvic and/or humic acids, considered younger organic fractions (Pessenda et al., 2010; Pessenda et al., 2012). Radiocarbon dates were obtained by accelerator mass spectrometry (AMS) at the Radiocarbon Laboratory of the Universidade Federal Fluminense (LAC-UFF). Radiocarbon ages were normalized to a $\delta^{13}C$ of −25‰ VPDB and reported as calibrated years (calibrated years before the present; 2σ) using CALIB 6.0 (Reimer et al., 2013). The dates are presented in the text as the median of the range of calibrated ages (Table 2).

4. Results

4.1. Coastal vegetation and topography

The sandy flats occupy the highest surface (~1.1–2.5 m above mean sea level, amsl) of the study area, covering ~22 ha. Herbaceous vegetation occupies part of these surfaces (Figs. 3b and 4f), mainly composed

Fig. 3. a) Mangrove distribution in the Aldeia and Jabuti River; a) Orthomosaic of the sector 2 exhibiting mangroves, sandy flat and location of the ground control points (see Table 1); c) vegetation height model; d) topographic profile showing the vegetation height, porewater salinities and the cores location; and e) distribution of *Rhizophora* and *Avicennia* trees and their densities.

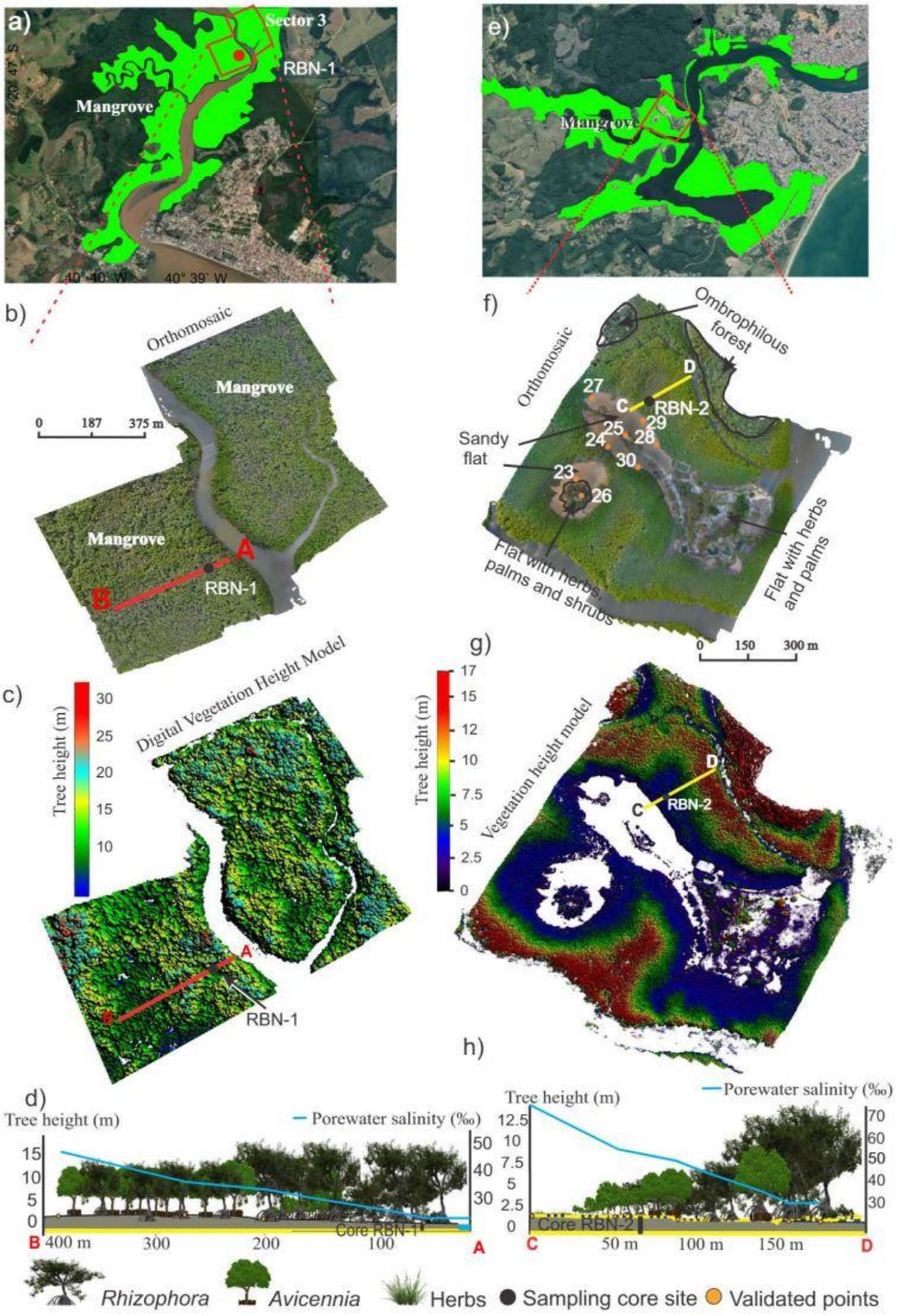
a)
Sector 3
RBN-1
Mangrove
26° 47' S
40° 40' W
40° 39' W
e)
Mangrove
b)
Orthomosaic
Mangrove
0 187 375 m
Mangrove
A
B
RBN-1
f)
Ombrophilous forest
Orthomosaic
D
27
C
RBN-2
29
25
24
28
Sandy flat
30
23
26
Flat with herbs, palms and shrubs
Flat with herbs and palms
0 150 300 m
c)
Digital Vegetation Height Model
Tree height (m)
30
25
20
15
10
A
B
RBN-1
g)
Tree height (m)
17
15
12
10
7.5
5
2.5
0
Vegetation height model
D
C
RBN-2
h)
d)
Tree height (m)
Porewater salinity (‰)
15
10
5
0
50
40
30
Core RBN-1
B 400 m 300 200 100 A
Tree height (m)
Porewater salinity (‰)
12.5
10
7.5
5
2.5
0
70
60
50
40
30
Core RBN-2
C 50 m 100 m 150 m D
Rhizophora
Avicennia
Herbs
Sampling core site
Validated points

of Cyperaceae and Poaceae. The porewater salinity in this vegetation was between 60 and 95‰, presenting crystals of sodium chloride. *Avicennia* trees with a stature gradient between 30 cm and 5 m surrounded this zone in sectors 1 and 2 (Figs. 3 and 4). The muddy tidal flats that occur on lower surfaces (0 to ~1.1 m amsl) are occupied by mangroves, mainly represented by *Rhizophora*, *Avicennia*, and some *Laguncularia* trees. *Rhizophora* trees occur predominantly on lower tidal flats (0–0.5 m amsl), exhibiting the tallest trees (~15 m tall and diameter 25–30 cm) on the lowest flats with porewater salinity between 30 and 35‰, while the smallest trees (~4 m tall and diameter < 10 cm) occupy intermediate elevations (0.5–0.6 m amsl) with porewater salinity between 40 and 45‰ (Figs. 3d and 4h). The densest groups (1200–2600 trees/ha) of *Rhizophora* occurred among the shortest trees, while the lowest densities (200–600 trees/ha) were identified on the lowest tidal flats, where the tallest trees were dominant (Fig. 3). *Avicennia* trees are spread mainly on the highest muddy tidal flats (~0.6 to ~1.3 m amsl) with porewater salinity between 45 and 65‰, also presenting the highest statures (~5 m tall, and diameter ~ 20 cm) on lower surfaces, resulting in a transition with the lowest *Rhizophora* trees. The tallest *Avicennia* trees (~10 m) occur isolated among the tallest *Rhizophora* on the lowest tidal flats, while some *Laguncularia* trees (~5 m tall and diameter ~ 20 cm) occur in a smaller quantity spread mainly among *Avicennia* trees on the highest tidal flats (Figs. 3 and 4). Tidal flats occupied by mangroves and under the influence of the Benevente River also revealed the same trends along the lowest flats. The highest tidal flats were occupied by herbs were identified in satellite images, but it was not possible to access them for an in-situ study (Fig. 4a-d).

4.2. Spatial-temporal analysis

The total vegetation area (mangrove, ombrophilous forest, herbaceous flat and pasture) and urban zone considered in the spatial-temporal analysis oscillated between 2463 and 2475 ha (Fig. 2). This difference (0.4%) in the total area analyzed between 1985 and 2018 can be attributed to the margin of error related to the pixel ground resolution of the images (Landsat: 30 m, Quickbird: 2.44 m) and an eventual error to delimit the vertices of each analyzed area in the respective years. This analysis revealed a significant mangrove expansion in the study area under the Jabuti and Aldeia Velha Rivers influence between 1985 (458 ha) and 2018 (479 ha). During this period, mangroves on lower tidal flats remained stable. The mangrove forests expanded onto the highest tidal flats that had a predominance of sandy sediments and were occupied by Cyperaceae, Poaceae, and Arecaceae (palms). Mangroves occupied 458 ha in 1985 and increased to 470 ha and 479 in 2003 and 2017, respectively, a gain of 12 ha (2.6%) and 9 ha (1.9%) (Fig. 2). The sandy tidal flats, mainly occupied by herbaceous vegetation, have decreased during that time interval from 33 to 22 ha. During the field trip *Avicennia* shrubs (20–50 cm tall) were recorded growing on the sandy flats (~1.3–1.4 m amsl) and herbaceous flat.

4.3. Radiocarbon ages and sedimentation rates

Radiocarbon dates and sedimentation rates are given in Table 2, and no age inversions were observed. The results revealed ages ranging from ~6300 cal yr BP to 2007 CE. The studied cores presented high sedimentation rates between ~6300 and ~4200 cal yr BP (1.4–4 mm/yr) and particularly during recent decades (4–15 mm/yr), while low rates were estimated for the interval ~ 4200 to ~1400 cal yr BP (~0.35 mm/yr). Core RBN-2 exhibited the following rates: 2.16 mm/yr (170–143 cm), 1.16 mm/yr (143–97 cm), and 14.8 mm/yr (97–0 cm). Core G3 presented the following values: 0.12 mm/yr (75–40 cm), 0.03 mm/yr (40–28 cm), and 4.66 mm/yr (28–0 cm). The estimated sedimentation rates for core G4 were 0.18 mm/yr (82–35 cm) and 2.41 mm/yr (35–0 cm), while core RBN-1 revealed 2.41 mm/yr (400–350 cm), 4 mm/yr (350–300 cm), 1.44 mm/yr (300–250 cm), 0.36 mm/yr (250–200 cm), 0.35 mm/yr (200–150 cm), 4.43 mm/yr (150–100 cm), 0.37 mm/yr (100–50 cm), and 7.57 mm/yr (50–0 cm) (Figs. 5, 6, 7, and 8).

Table 2
Samples of sedimentary organic matter selected for radiocarbon dating with code site (depth), laboratory number, percent modern carbon (pMC), 14C age, calibrated (cal) ages and median of cal ages.

LACUFF	ID	pMC	±	Age (14C yr BP)	±	Age (cal yr BP, 2σ)	Median of age range (cal yr BP)
190419	G3–28cm	104.5	0.43	Modern			~1958 CE
190690	G3–40 cm			3274	49	3390–3609	~3500
190691	G3–75 cm			5497	57	6194–6404	~6300
190692	G4–35 cm			117	73	0–155	~77
190693	G4–82 cm			2585	57	2486–2795	~2704
190420	RBN2 53–55	106.441	0.689	Modern			~2007 CE
190421	RBN2 95–97	100.802	0.617	Modern			~1955 CE
190422	RBN2 141–143			314	54	286–498	~390
190423	RBN2 168–170			505	57	463–570	~515
190410	RBN1-50–52	103.669	0.555	Modern			~1957 CE
190412	RBN1-104–106			1434	65	1261–1423	~1342
190413	RBN1-155–157			1575	58	1343–1570	~1457
190414	RBN1-203–205			2710	60	2745–2930	~2838
190415	RBN1-253–255			3818	41	4137–4317	~4227
190416	RBN1-303–305			4077	36	4498–4651	~4575
190417	RBN1-353–355			4156	41	4569–4831	~4700
190418	RBN1-394–396			4334	36	4840–4974	~4907

4.4. Facies association

RSL fluctuations affect the action of currents and waves along the littoral, contributing to development of coastal depositional environments (Davis, 2013), and physicochemical characteristics of estuarine waters (Lara and Cohen, 2006). Coastal vegetation establishment on tidal flats depends mainly on estuarine salinity gradients and sediment grain size (Bird, 1980; Augustinus, 1995; Woodroffe et al., 2016). Local vegetation and fluvial and marine algae determine the isotopic and elemental characteristics of the sedimentary organic matter accumulated in the studied tidal flats (Dittmar et al., 2001, 2006). Therefore, physical (sedimentary features), isotopic/elemental geochemical ($\delta^{13}C$, $\delta^{15}N$, C/N) and biological (pollen) indicators down the studied cores were grouped into facies associations to determine sedimentary environments (Reading, 1996). The cluster analysis of pollen percentages defined pollen assemblages, reflecting the coastal vegetation zones in the study area (Figs. 1, 3, 4, and Table 3). Altogether, these multi-proxy data allowed us to define four facies associations: (A) Sandy flat, (B) Herbaceous sand flat, (C) Lagoon with mangrove, and (D) Mangrove tidal flat.

4.4.1. Facies association A (sandy flat)

This facies association was characterized in cores G3 (100–75 cm) and G4 (100–85 cm), and accumulated before 6300 and 2700 cal yr BP, respectively. It was represented by medium sand (Sm, 60–90% sand, 40–10% silt) showing a clear fining upward sand deposit. No pollen or fern spores were identified along this facies association. XRF analysis indicated the lowest concentration of Sr (25–90 mg/kg), Cl (3–9 g/kg), Br (22–28 mg/kg), K (0–0.8 g/kg), and Ca (15–25 g/kg). $\delta^{13}C$, $\delta^{15}N$ and C/N values oscillated between −27‰ and − 24‰ ($\bar{x}$ =

Fig. 4. a) Mangrove distribution along the Benevente River; b) orthomosaic of the sector 3 showing mangroves; c) digital vegetation height model; d) topographic profile showing the vegetation height, porewater salinities and location of the core RBN-1; e) mangrove distribution along the Aldeia and Jabuti Rivers; f) orthomosaic of the sector 1 showing the mangroves, sandy flats, herbaceous plain, location of ground control points (see Table 1), and location of the core RBN-2; g) vegetation height model; and h) topographic profile showing the vegetation height, porewater salinities and location of the core RBN-2.

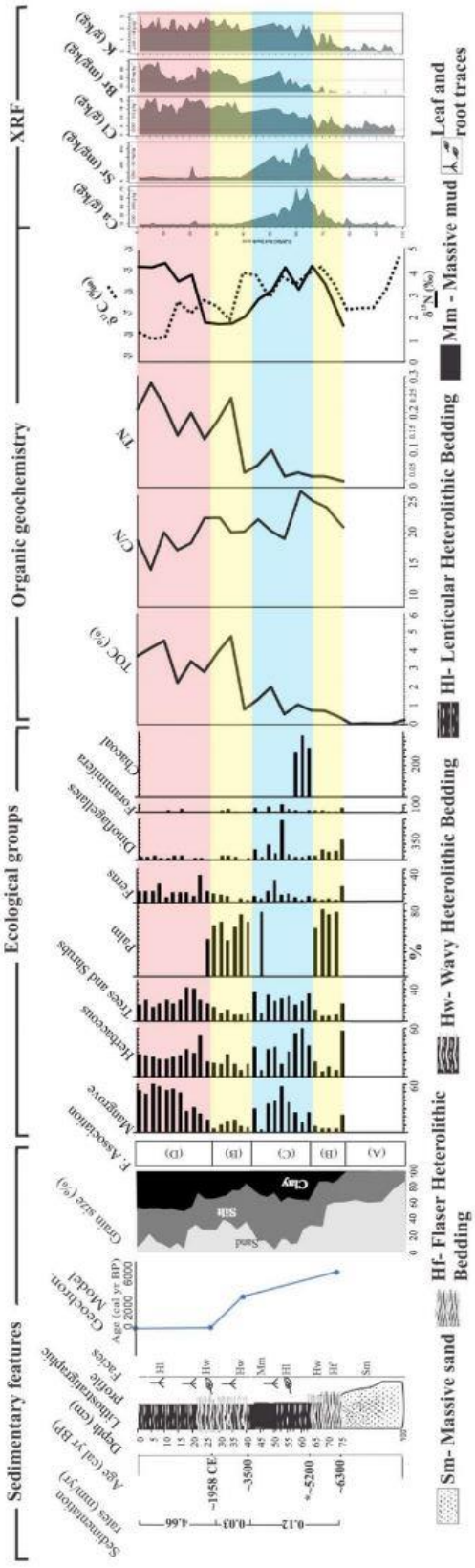

70,0,0,0,0.1,0.0,0.0,0.5;0b7]Fig. 5. Lithostratigraphy of the core G-3 with facies association, pollen diagram exhibiting percentages of the ecological groups, geochemical and XRF dada.

− 26‰), 0.21‰ and 2.3‰ ($\bar{x}$ = − 1‰), and 15 and 21 ($\bar{x}$ = 19), respectively (Figs. 5 and 6).

4.4.2. Facies association B (herbaceous sand flat)

This facies association was evident in cores G3 (75–62 cm and 40–26 cm) and RBN-2 (143–97 cm) (Figs. 5 and 7. These sediments were accumulated between ~6300 cal yr BP and ~5200 cal yr BP (extrapolated age), and 3500 cal yr BP and 1958 CE in core G3 (Fig. 5), and between ~390 cal yr BP and 1955 CE in RBN-2 (Fig. 7). They consisted of dark gray (4/1 10Y) wavy (Hw) and flaser (Hf) heterolithic bedding deposits (30–60% sand, 30–50% silt, 10–30% clay) with some layers more enriched in organic matter (0–4% of TOC). Herbs (10–85%), palms (0–80%), and trees/shrubs (10–40%) pollen characterize this facies association. Mangrove pollen (0–20%), represented only by *Rhizophora*, presented the lowest percentages in this facies association. *Solanum* (20–70%), Poaceae (5–20%), Asteraceae (1–20%), and Cyperaceae (1–10%) represented the herb pollen. Tree/shrubs were mainly characterized by Fabaceae (2–10%), *Trema* (3–20%), Malpiguiaceae (1–8%), and *Myrsine* (0–10%) (Figs. 2 and 3, supplementary material). XRF analysis indicated higher concentrations of Sr (25–300 mg/kg), Cl (5–22 g/kg), Br (0–80 mg/kg), K (0.5–2.8 g/kg), and Ca (15–39 g/kg) than facies association A. $\delta^{13}C$, $\delta^{15}N$ and C/N values oscillated between −28‰ and −24‰ ($\bar{x}$ = − 26‰), 2‰ and 3.6‰ ($\bar{x}$ = 2.9‰), and 20 and 28 ($\bar{x}$ = 24), respectively (Figs. 5 and 7).

4.4.3. Facies association C (lagoon with mangrove)

These deposits were identified in cores RBN-1, between 400 cm (~4900 cal yr BP) and 250 cm (~4230 cal yr BP), and G-3, between 62 cm (~5200 cal yr BP) and 40 cm (~3500 cal yr BP) (Figs. 5 and 8). This facies association consisted of dark gray (4/1 10Y), lenticular heterolithic bedding (Hl), and massive mud (Mm) deposits (2–10% sand, 50–60% silt, 20–50% clay), with organic matter (1–2% of TOC), and fragments of roots and leaves. Pollen analysis revealed the predominance of mangrove pollen (5–60%), followed by herbs (10–55%) and tree/shrubs (10–60%). An increased occurrence of ferns, dinoflagellates, and foraminifera also characterized this facies association (Figs. 2 and 5, supplementary material). This core also presented elevated concentration of Sr (125–1500 mg/kg), Cl (10–18 g/kg), Br (40–70 mg/kg), K (1–5 g/kg), and Ca (20–140 g/kg). The $\delta^{13}C$ values oscillated between −26.5‰ and − 25‰ ($\bar{x}$ = − 26‰), while C/N ratios presented values ranging from 18 to 26 ($\bar{x}$ = 21). These sediments also presented an enrichment of $\delta^{15}N$, oscillating between 2.5 and 7.2‰ ($\bar{x}$ = 5.8‰) (Figs. 5, and 8, Table 3).

4.4.4. Facies association D (mangrove tidal flat)

These deposits were identified in core G3 between the 26 cm (1958 CE) and 0 cm depth intervals (Fig. 5), while in core G4, it was recorded between 85 cm (~2700 cal yr BP) and 0 cm depth (Fig. 6). This facies association was also characterized in RBN-1 between 250 cm (~4230 cal yr BP) and 0 cm, and in core RBN-2 between 170 cm (515 cal yr BP) and 143 cm (390 cal yr BP), and 97 cm (1958 CE) and 0 cm depth (Figs. 7 and 8). The cores consisted of dark gray (4/1 10Y) wavy (Hw) and lenticular (Hl) heterolithic bedded deposits (2–20% sand, 40–60% silt, 20–50% clay), with organic matter (1–9% of TOC), and many fragments of roots and leaves. Pollen analysis revealed the predominance of mangrove pollen (5–85%), followed by herbs (5–60%), tree/shrubs (1–50%), and palms (1–15%). An increased occurrence of ferns, dinoflagellates, and foraminifera also characterized this facies association (Figs. 2, 3, 4 and 5, supplementary material). It also presented high concentrations of Sr (50–1300 mg/kg), Cl (10–32 g/kg), Br (40–130 mg/kg), K (0.8–6 g/kg), and Ca (15–140 g/kg). The $\delta^{13}C$ values oscillated between −28‰ and −26‰ ($\bar{x}$ = −27‰), while C/N ratios presented the lowest values ranging from 25 to 11 ($\bar{x}$ = 18). $\delta^{15}N$ oscillated between 2 and 6‰ ($\bar{x}$ = 3.5‰), with an increased trend during the last decades evidenced along the four cores (Figs. 5, 6, 7, and 8, Table 3.

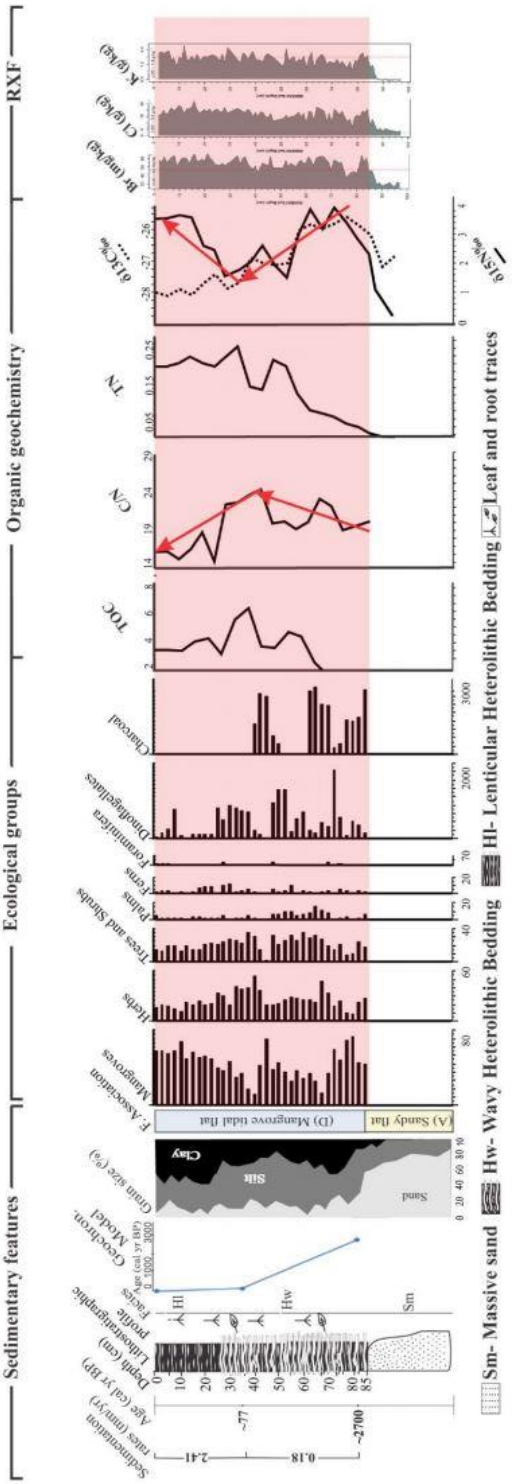

Fig. 6. Lithostratigraphy of core G-4 with facies association, pollen diagram exhibiting percentages of the ecological groups, geochemical and XRF dada.

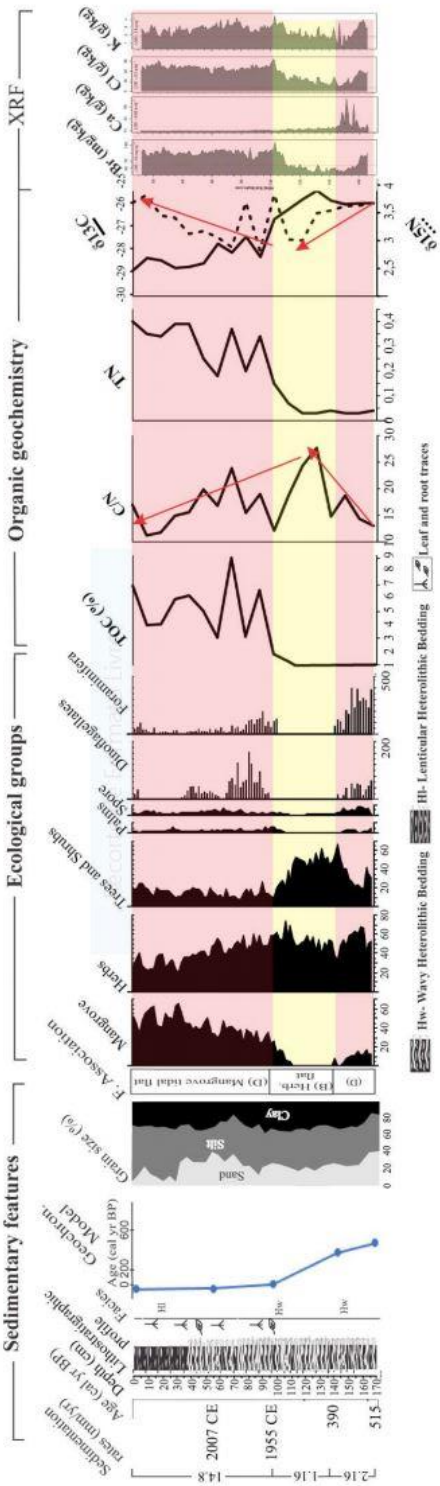

Fig. 7. Lithostratigraphy of core RBN-2 with facies association, pollen diagram exhibiting percentages of the ecological groups, geochemical and XRF dada.

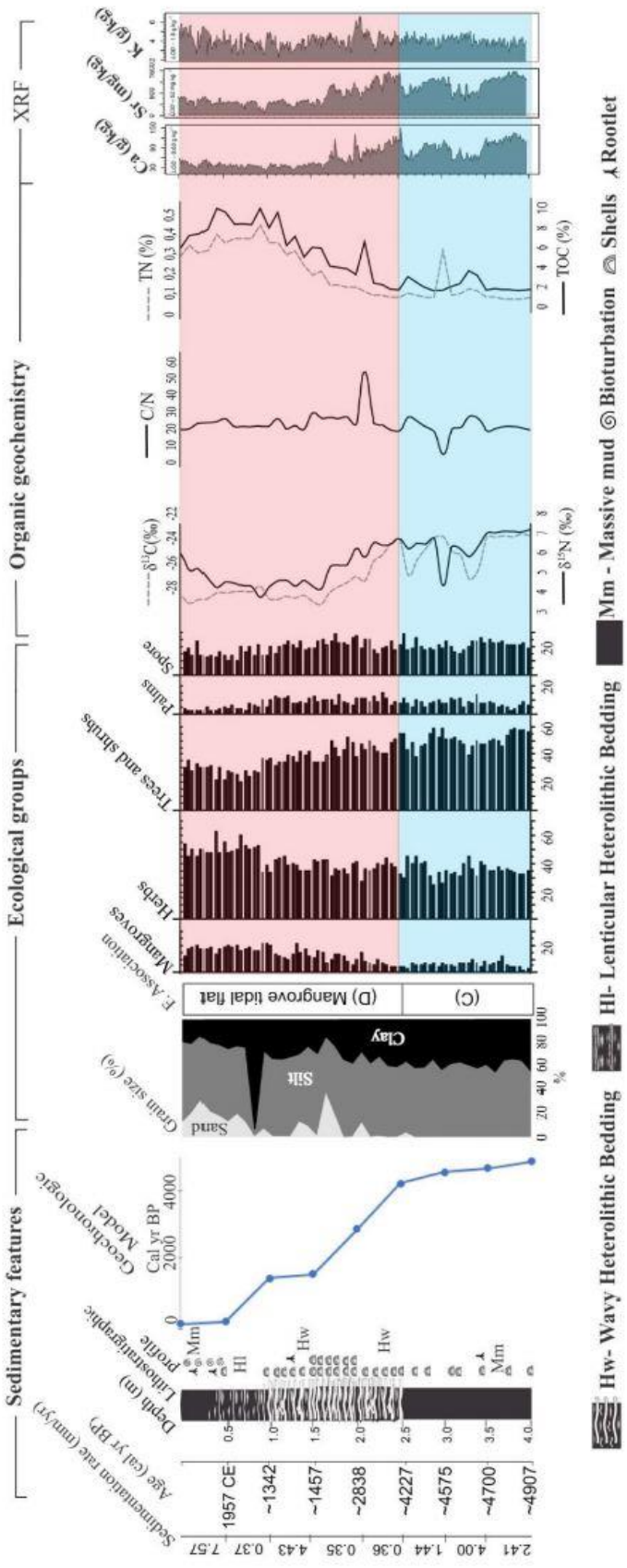

Fig. 8. Lithostratigraphy of core RBN-1 with facies association, pollen diagram exhibiting percentages of the ecological groups, geochemical and XRF dada.

Table 3
Summary of facies association of the studied cores with sedimentary characteristics, pollen groups, geochemical data, and elements predominance.

Facies association	Facies description	Ecological group	Geochemical data	Elements predominance (mg/kg)	Interpretation
A	Massive sand (Sm)	No pollen/ferns	$\delta^{13}C = -27$ to $-24‰$ $\delta^{15}N = 0.21$ to $2.3‰$ $C/N = 20–30$	Sr: 25–90 mg/kg Cl: 3–9 g/kg Br: 22–28 mg/kg K: 0–0.8 g/kg Ca: 15–25 g/kg	Sandy flat
B	Flaser (Hf) and wavy (Hw) heterolithic bedding	Herbs, palms, trees/shrubs and mangrove	$\delta^{13}C = -28$ to $-24‰$ $\delta^{15}N = 2–3.6‰$ $C/N = 20–28$	Sr: 25–300 mg/kg Cl: 5–22 g/kg Br: 0–80 mg/kg K: 0.5–2.8 g/kg Ca: 15–39 mg/kg	Herbaceous sand flat
C	Lenticular heterolithic bedding (Hl) and massive mud (Mm)	Mangrove, herbs, trees/shrubs, palms, ferns, dinoflagellates, and foraminifera.	$\delta^{13}C = -27$ to $-23‰$ $\delta^{15}N = 2.5–7.2‰$ $C/N = 18–26$	Sr: 125–1500 mg/kg Cl: 10–18 g/kg Br: 40–70 mg/kg K: 1–5 g/kg Ca: 20–140 mg/kg	Lagoon with mangrove
D	Lenticular (Hl) and wavy (Hw) heterolithic bedding	Mangrove, herbs, trees/shrubs, palms, ferns, dinoflagellates, and foraminifera.	$\delta^{13}C = -28$ to $-26‰$ $\delta^{15}N = 2–6‰$ $C/N = 11–30$	Sr: 50–1300 mg/kg Cl: 10–32 g/kg Br: 40–130 mg/kg K: 0.8–6 g/kg Ca: 15–140 mg/kg	Mangrove tidal flat

5. Interpretation and discussion

5.1. Holocene

The coastal morphology of southeastern and northeastern Brazil was affected by a RSL rise in the early-middle Holocene with a highstand (2–5 m amsl) around 5.8 to 5.0 Kyr BP (Martin et al., 2003; Angulo et al., 2006; de O Caldas et al., 2006; Suguio et al., 2013; de F Toniolo et al., 2020). This event caused a marine transgression that triggered erosion of the shoreline, inundation of coastal depressions and fluvial valleys (Cooper et al., 2018), as well as landward migration of mangroves into embayments, estuaries, and lagoons (Castro et al., 2013; Lorente et al., 2014; Cohen et al., 2014, 2015, Cohen et al., 2020a, 2020b; Rossetti et al., 2015). However, during the middle-late Holocene a gradual RSL fall occurred (Angulo et al., 2006; de O Caldas et al., 2006; Cohen et al., 2020b; de F Toniolo et al., 2020), which facilitated the infilling of estuaries and the building of deltas. Mangrove forests migrated seaward during this time (Cohen et al., 2014; França et al., 2015; Cohen et al., 2020a, 2020b).

The effects of the middle Holocene high sea-level stand were recorded in core G-3, positioned in the highest tidal flats (0.7 m above mean sea-level-amsl, Figs. 3d and 5) and in a transition zone between mangroves, mainly represented by *Avicennia*, and palms/herbaceous vegetation. It revealed a conversion from flats occupied by palms and herbs to a lagoon surrounded by mangroves, characterized by an increased trend of mangrove pollen from 5% to 60% between ~6300 cal yr BP and ~4650 cal yr BP (extrapolated age). During this period, a decrease in the pollen percentage of palms from 60% to 0% and an increase in dinoflagellates occurred. C/N values decreased from 27 to 18, while the $\delta^{15}N$ increased from 1.9 to 4.2, suggesting an increase in aquatic influence in the sedimentary organic matter. XRF analysis also indicated an increased trend in concentrations of Ca (from 15 to 75 g/kg), Sr (50 to 430 mg/kg), Cl (3 to 18 g/kg), Br (0 to 75 mg/kg), and K (0.25 to 2.5 g/kg) (Fig. 5).

The middle Holocene high sea-level stand also was recorded in core RBN-1, 17 km away from core G-3. The multi-proxy data indicated a lagoon with sedimentary organic matter sourced from C3 terrestrial plants and marine dissolved organic carbon (Fig. 9), and mangroves (5–15% of mangrove pollen) present along its margin between ~4900 and ~4230 cal yr BP (Fig. 10). XRF analysis also indicated the highest Ca (from 60 to 150 g/kg) and Sr concentrations (500 to 1600 mg/kg). High sedimentation rates (1.4–4 mm/yr) were recorded between ~4900 and ~4230 cal yr BP suggesting a coastal depression, such as a lagoon, with space available for sediment accumulation during that middle Holocene high sea-level stand (Fig. 8).

By contrast, the RSL fall in the middle-late Holocene allowed flats to emerge on the previous coastal depression filled by sediments. This process favored herb and palm expansion on the highest flats, and mangroves on the lowest tidal flats (Fig. 10), as evidenced in cores G-3 (Fig. 5) and RBN-1 (Fig. 8) by the trend of decreased mangrove pollen percentage from 50% to 6%, and an increase in palm pollen from 0 to 70% between ~4650 and ~3500 cal yr BP in core G-3. Dinoflagellate cyst occurrences also decreased during this time. C/N ratios increased from 18 to 22, and the $\delta^{15}N$ values decreased from 4.2 to 1.7, indicating a decreased trend of sedimentary organic matter sourced from algae. Concentrations of Ca (75 to 15 g/kg), Sr (430 to 50 mg/kg), and Br (75 to 40 mg/kg) decreased during this time (Fig. 5).

Core RBN-1 (0.1 m amsl), sampled from a tidal flat lower than core G-3 (0.7 m amsl) and whose pollen assemblage was dominated by *Rhizophora*, presented an increase of mangrove pollen from 10 to 20%. This topographically lower zone favored mangrove expansion during the RSL fall. The relatively high percentages of pollen grains sourced from terrestrial trees and shrubs may be attributed to hills occupied by the Atlantic Forest, which surrounds the study area, and favors a high influx of pollen grains from higher to lower surfaces by winds (Weng et al., 2004; Hicks and Hyvärinen, 2010; Pan et al., 2013). Between ~4230 and ~1450 cal yr BP a decreased trend of $\delta^{13}C$ and $\delta^{15}N$ occurred, from −24 to −29‰ and from 7 to 4‰, respectively, likely reflecting an increase of C3 terrestrial plants and terrestrial influence (Fig. 8). This phase presented the lowest sedimentation rates (~0.35 mm/yr), indicating a decrease of space available for sediment accumulation caused by the RSL fall (Fig. 8).

The effects of the RSL fall during the late Holocene were partially recorded along core G-4 (0.2 m amsl), positioned in a tidal flat lower than core G-3 (0.7 m amsl) and which was dominated by *Rhizophora* (Figs. 3 and 6). The C/N and $\delta^{15}N$ values increased from 13 to 25 and decreased

from 3.67 to 1.67‰ between ~2700 and ~77 cal yr BP, respectively, suggesting an increased trend of terrestrial contribution to the sedimentary organic matter during that time interval. The pollen profile indicated oscillations of mangrove (20–80%), tree/shrub (15–35%), and herb (15–45%) pollen percentages. These oscillations in the pollen percentages likely reflect alternations in the mangrove limits according to RSL fluctuations between ~2700 and ~77 cal yr BP, within a general trend of RSL fall between ~4230 and ~1460 cal yr BP.

Considering the last 1000 years and according to Grinsted et al. (2009), a maximum sea-level between 12 and 21 cm, and minimum sea-level between −19 and −26 cm, occurred globally at ~1150 CE and ~1730 CE, respectively. This low sea-level stand may be attributed to the Little Ice Age (LIA) that occurred during the last six or seven centuries (Lean and Rind, 1999), having ended between 1850 and 1890 CE (Bradley and Jones, 1992). Cores sampled from Bragança mangroves, northern Brazil (Cohen et al., 2005), and core RBN-2 (1 m amsl), sampled from the ecotone between the *Avicennia* mangrove forest and herbaceous vegetation each recorded impacts of the LIA event. Core RBN-2 exhibited an ecotone with mangrove (pollen 5–20%), herbs (35–70%), and trees and shrubs (20–40%) with foraminifera and dinoflagellate cysts between 515 and 390 cal yr BP (Fig. 5). Between 390 cal yr BP (1560 CE) and 1955 CE mangrove pollen was almost entirely absent (0–15%), and there was an increase of herbs and trees/shrubs pollen compared to the previous phase (515–390 cal yr BP), oscillating between 35 and 75%, and 15 and 70%, respectively. Foraminifera and dinoflagellate cysts were not identified between 390 cal yr BP (1560 CE) and 1955 CE. This period was also characterized by a trend of increasing C/N ratios from 13 to 27, suggesting a decrease in aquatic influence in the sedimentary organic matter. The concentrations of Br (100 to 25 mg/kg), Ca (115 to 27 g/kg), Cl (22 to 6 g/kg), and K (4 to 2 g/kg) decreased during that time interval, likely as a consequence of a RSL fall.

5.2. Anthropocene

The ice melting in Greenland and Antarctica and thermal expansion of warmed ocean waters have caused a global sea-level rise, with increases in the rates from 1.1 to 2.5 mm/yr between 1902 and 1990 to current rates of 3.1–3.4 mm/yr (IPCC, 2014; Dangendorf et al., 2017; Nerem et al., 2018). The multi-proxy data in cores RBN-2, G-3, and G4 suggest a RSL rise during recent decades, revealing a mangrove incursion onto the highest tidal flats, occupying sandy flats previously dominated by herbaceous vegetation. Core RBN-2 presented a trend of increasing mangrove pollen from 0 to 60% and a trend of decreasing herb pollen (from 70 to 40%) since ~1955 CE. C/N ratios decreased from 27 to 15, while the $\delta^{15}N$ values increased from 2.6 to 3.7‰, revealing an increased influence of aquatic organic matter during the Anthropocene. The Br, Cl, and K concentrations also increased, suggesting a marine influence during this period (Fig. 7).

Similar trends were identified in core G-3 that presented increased mangrove pollen (from 5 to 60%), and palm pollen being absent since 1958 CE. C/N ratios presented a decrease from 22.5 to 15, while $\delta^{15}N$ values increased from 1.7 to 4.4‰ (Fig. 5). Core G-4 also presented

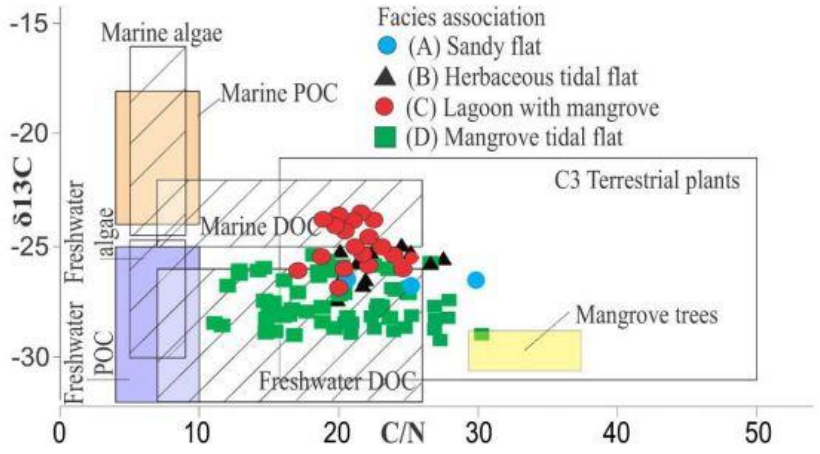

Fig. 9. Binary diagram of $\delta^{13}C$ and C/N for the facies association in the study area based on ranges recorded in coastal environments (Deines, 1980; Lamb et al., 2006; Matos et al., 2020; Meyers, 1994; Schidlowski et al., 1983; Tyson, 1995).

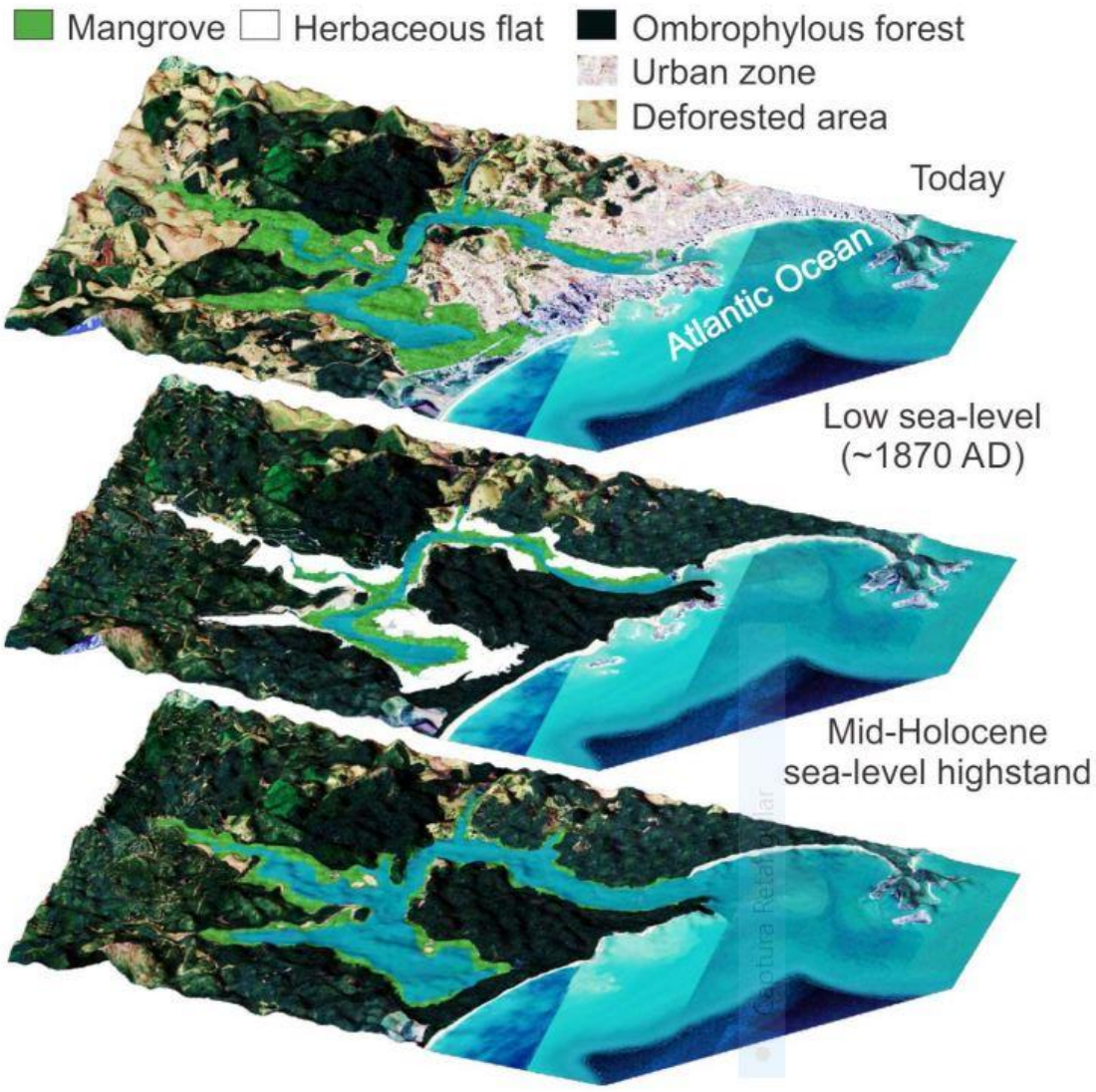

Fig. 10. Model of geomorphology and vegetation development under Holocene relative sea-level changes.

increasing levels of mangrove pollen (from 15 to 65%) since ~77 cal yr BP (~1870 CE) (Fig. 6). The C/N and $\delta^{15}N$ values presented a decreased and increased levels from 24 to 16 and from 1.6 to 3.6, respectively, suggesting an increase in the aquatic influence during the last ~77 cal yr BP. According to the binary $\delta^{13}C$ and C/N ratio (Fig. 9), the sedimentary organic matter of the facies associations sandy flat (A) and herbaceous flat (B) is mainly sourced from C3 terrestrial plants, while the lagoon with mangrove (C), and mangrove tidal flat (D) presented an organic matter contribution from fresh/marine waters and C3 terrestrial plants. These data indicated that the mangrove phase was more influenced by estuarine waters than herbaceous sand flats and sandy flats, suggesting a RSL that was higher during the mangrove development. Core G-4, sampled from the lowest zone of the tidal flats and presently occupied primarily by *Rhizophora*, indicated a trend of increasing *Rhizophora* pollen percentage since 77 cal yr BP (1873 CE). However, cores G-3 and RBN-2, sampled from the highest tidal flats occupied by mangroves in the ecotone between mangrove/herbaceous vegetation, revealed a trend of increasing *Rhizophora*, *Avicennia*, and *Laguncularia* pollen percentages since 1958 and 1955 CE. These trends must be related to the increase in estuarine influence by a RSL rise since the end of the Little Ice Age and intensified during recent decades.

The spatial-temporal analysis, based on satellite and drone images, corroborates this interpretation. According to this study, mangroves had invaded the highest flats occupied by palms and herbaceous vegetation since at least 1985, causing an increase in mangrove area, from 458 ha in 1985 to 470 ha in 2003 and to 479 in 2018, a gain of 4.6% between 1985 and 2018 (Fig. 2). The spatial-temporal analysis did not reveal loss of mangrove areas in the lower tidal flats since 1985.

A tidal flat in the eastern part of sector 2 should be noted. It had an elevation of 0.7 m amsl, porewater salinity of ~60‰, and was occupied by *Avicennia* trees (with a maximum height of 5 m) and herbs (Figs. 1, 3d, transects C–D). Between 1985 and 2007, this area was occupied by herbs, and was gradually invaded by mangroves. Since 2012, *Avicennia* trees occupy this area completely (Fig. 2). Currently, the highest tidal flats occupied by mangroves (~0.7–1.3 m amsl) are mainly characterized by highly salt tolerant *Avicennia* trees with a density between ~1200 and ~3000 trees ha^{-1} (Figs. 3 and 4). The relationship between the density of *Rhizophora* and *Avicennia* trees and topography revealed

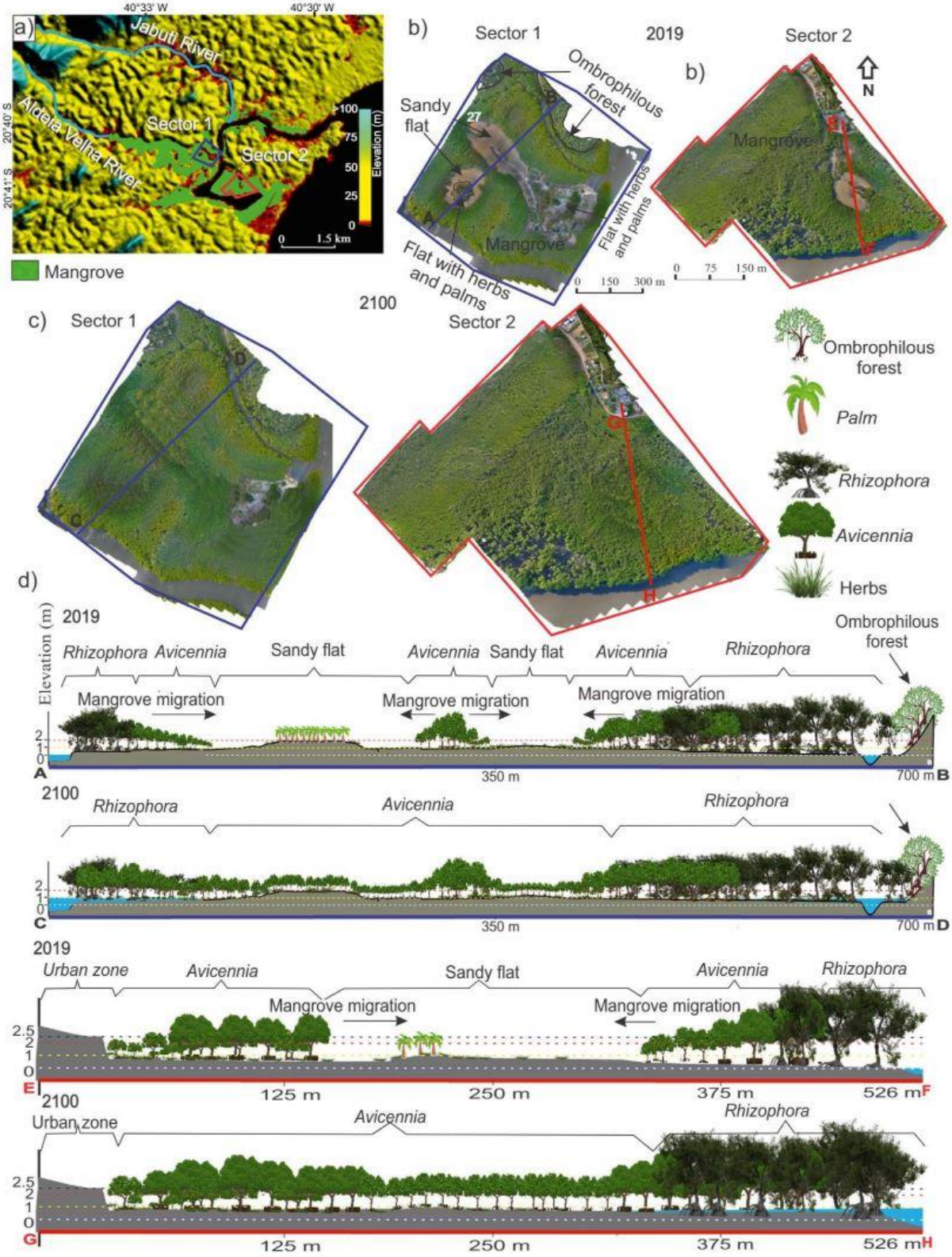
a)
40°33' W
40°30' W
20°40' S
20°41' S
Jabuti River
Aldeia Velha River
Sector 1
Sector 2
Elevation (m)
100
75
50
25
0
0 1.5 km
Mangrove
b)
Sector 1
2019
Ombrophilous forest
Sandy flat
27
Mangrove
Flat with herbs and palms
0 150 300 m
Sector 2
N
Mangrove
0 75 150 m
2100
c)
Sector 1
Sector 2
Ombrophilous forest
Palm
Rhizophora
Avicennia
Herbs
d)
2019
Elevation (m)
Rhizophora
Avicennia
Sandy flat
Avicennia
Sandy flat
Avicennia
Rhizophora
Ombrophilous forest
Mangrove migration
Mangrove migration
Mangrove migration
A
350 m
700 m B
2100
Rhizophora
Avicennia
Rhizophora
C
350 m
700 m D
2019
Urban zone
Avicennia
Sandy flat
Avicennia
Rhizophora
Mangrove migration
Mangrove migration
E
125 m
250 m
375 m
526 m F
2100
Urban zone
Avicennia
Rhizophora
G
125 m
250 m
375 m
526 m H

that the highest densities were identified in the highest tidal flats (Fig. 3). This may be attributed to an inverse relationship between tree height and density, because the taller the trees, the more space is occupied by its canopy, and the tallest trees tend to occur on the lower tidal flats ($r = 0.82$, $n = 109{,}681$, $p < 0.0001$) (Fig. 3). This interaction between mangrove structure and topography is essential for interpreting pollen profiles.

Modern pollen accumulation rates from northern Brazil indicate that *Rhizophora* produces more pollen than *Avicennia* and *Laguncularia*. Pollen traps located on an herbaceous flat, located ~1 km distant from the closest *Rhizophora* trees and 100 m from *Avicennia* shrubs, indicated an average of 410 *Rhizophora* grains/cm^2/yr and an average of 8 *Avicennia* grains/cm^2/yr (Behling et al., 2001). Because of the higher pollen production by *Rhizophora*, even cores sampled from mangrove tidal flats with a predominance of *Avicennia* and *Laguncularia* trees contain higher *Rhizophora* pollen percentages than *Avicennia* and *Laguncularia* (Figs. 3, 4) (Figs. 2 and 3, supplementary material). An integrated analysis of pollen concentration and mangrove pollen percentage reinforces these interpretations based on a pollen profile. In this context, the pollen concentration increased in recent decades in cores G-3 (100,000 to 250,000 pollen/cm^3), G-4 (50,000 to 300,000 pollen/cm^3), and RBN-2 (100,000 to 300,000 pollen/cm^3) along with an increase in *Rhizophora* pollen percentage in cores G-3 (from 15 to 60%), G-4 (20 to 60%), and RBN-2 (10 to 55%). The increase in pollen concentration and *Rhizophora* pollen percentage suggest an incursion of the lower mangrove zone, dominated by *Rhizophora*, into higher tidal flats in recent decades (Figs. 3, 4, and 5, Supplementary material).

The *Avicennia* trees current stature gradient from 30 cm height in the highest flats (with porewater salinity of ~70‰) to 5 m height at a lower surface (with porewater salinity of ~50‰) in sectors 1 and 2, suggest a relationship between sediment physicochemistry and mangrove structure (Figs. 3 and 4). In this context, a RSL rise has caused an increase in the tidal inundation frequency, resulting in a decrease in the time exposure allowing for the evaporation of tidal waters. This process causes a decrease in porewater salinity; consequently, it decreases the saline stress in the *Avicennia* trees, allowing such trees to become taller and invade the higher tidal flats in the next years. The landward mangrove migration onto higher tidal flats may be considered a global phenomenon, suggesting a common driving force, likely related to sea-level rise driven by global warming (Adam, 2002; Cohen and Lara, 2003; Gaiser et al., 2006; Gilman et al., 2007; Krauss et al., 2011; Peterson and Bell, 2015; Cohen et al., 2018).

5.3. Sea-level rise of 98 cm by 2100

Some studies indicated that mangroves are stressed during a sea-level rise between 0.9 and 1.2 mm/yr, and higher rates could further threaten mangroves (Ellison and Stoddart, 1991). This interpretation was contested by Snedaker et al. (1994), who indicated historical records showing mangrove expansion under relative sea-level rise nearly twice that of the critical maximum threshold. Soil elevation analysis revealed that Caribbean mangrove substrates would not keep pace with a sea-level rise >5 mm year^{-1} (McKee et al., 2007), and the rate of surface accretion can only keep pace with sea-level rise scenario RCP 8.5 (52–98 cm by 2100) to 2070 in basin mangrove settings and 2055 in fringe mangrove settings (IPCC, 2013; Sasmito et al., 2015). According to Spencer et al. (2016), a loss of coastal wetlands worldwide between 392 and 578 × 10^3 km^2 would occur with a sea-level rise of 110 cm by 2100.

Mangrove resilience in the face of sea-level rise depends not only on the rates of sea-level rise but also local characteristics, such as annual average temperatures, structure and productivity of mangroves, dynamics of the sedimentary environment, coastal geomorphology, lateral accommodation space across an elevation gradient, tidal range, sediment type/supply, estuarine salinity gradients, and hydrodynamics related to tides, waves and littoral currents (Cohen and Lara, 2003; Lara and Cohen, 2006; McKee et al., 2007; Cohen et al., 2009, 2012, 2014, 2018, 2020a, 2020b; Lovelock et al., 2015b; Spencer et al., 2016; Woodroffe et al., 2016; Rodrigues et al., 2021). Among these factors, the biological and physical processes that trap mineral sediments, refractory mangrove roots, and other organic inputs in mangrove substrates to adjust their vertical position according to sea-level rise should be highlighted (Parkinson et al., 1994; Furukawa and Wolanski, 1996; Mckee and Faulkner, 2000; Cahoon et al., 2006; McKee et al., 2007; Krauss et al., 2014; Lovelock et al., 2015a). Flats under the influence of low sediment supply and small tidal ranges are more vulnerable to loss of mangrove areas than flats exposed to high sediment supply and large tidal ranges (Lovelock et al., 2015b; Spencer et al., 2016). In addition, tidal ranges, which are amplified along the estuaries, may be magnified by sea-level rise according to shelf slope, size and shape of the estuarine basin (e.g. Bhattacharya, 2011). The interaction of each of these drivers will determine the local mangrove fate in the face of sea-level rise (Bruun, 1962; Schwartz, 1965; Cohen et al., 2012; Woodroffe and Murray-Wallace, 2012; Cohen et al., 2014; Ellison, 2016).

In this context, estimated sedimentation rates in the studied cores between ~6300 cal yr BP and 1950 CE (0.03 to 4.4 mm year^{-1}) were lower than the Anthropocene (4.4 to 14 mm year^{-1}) (Figs. 5, 6, 7 and 8). These relatively low sedimentation rates may be attributed to the RSL fall during the mid-late Holocene. By contrast, higher sedimentation rates during the Anthropocene are likely related to the response of the depositional environment and mangroves to the high rates of sea-level rise in recent decades (3.1–3.4 mm/yr, IPCC, 2014; Dangendorf et al., 2017; Nerem et al., 2018). Surface accretion rates from 5 to 14 mm year^{-1} have been recorded on modern mangrove substrates, for instance, in Australia, Honduras, and Micronesia (Cahoon et al., 2006; Rogers et al., 2006; Krauss et al., 2010; Lovelock et al., 2011; Sasmito et al., 2015). Stratigraphic successions are controlled by the interplay of sedimentation rate and accommodation space (Schlager, 1993), which depends mainly on sediment supply and RSL changes, respectively (Schlager, 1993; Soreghan and Dickinson, 1994). The structure (zonation and mangrove density/stature) and mangroves productivity also contribute to sediment accumulation (Furukawa and Wolanski, 1996; Kathiresan Kandasamy, 2003; Ellis et al., 2004; McKee et al., 2007; Phillips et al., 2017; Matos et al., 2020). Mangrove species composition affects the mangrove resistance and resilience to sea-level rise as specific genera have different tolerances to porewater salinity, tidal inundation frequency and depth of inundation, causing different sedimentation rates (Krauss et al., 2003; Rogers et al., 2005; McKee et al., 2007; Di Nitto et al., 2013b). Species with prop roots, such as *Rhizophora* spp., favor vertical accretion more than species with pneumatophores, such as *Avicennia* spp. (Furukawa and Wolanski, 1996; Krauss et al., 2003), and sites with an *Avicennia-Rhizophora* interphase are more efficient than more homogenous *Avicennia* or *Rhizophora* zones in trapping sediment (Kathiresan Kandasamy, 2003). Therefore, it is reasonable to propose the high mangrove tree density (200–3000 trees/ha, Fig. 3 and Table 1), stature (<15 m, Figs. 3, 4 and Table 1) and zonation each contributed to retain fluvial sediments on the studied estuarine basin and increase the sedimentation rates during the Anthropocene (Figs. 5, 6, 7 and 8).

The most vulnerable mangrove forests are in the lower tidal flats (0–0.3 m amsl), have the lowest *Rhizophora* densities (200–600 trees/ha,

Fig. 11. a) Digital elevation model of the studied area under the influence of the Aldeia Velha and Jabuti rivers based on SRTM data; b) orthomosaics recorded in 2019 of sectors 1 and 2 evidencing mangrove boundaries; c) projections for the mangrove boundaries according to a sea-level rise of 98 cm by 2100; d) topographic profiles showing the lowest and highest tidal flats occupied by mangrove in 2019 and projections for 2100 under a sea-level rise of 98 cm.

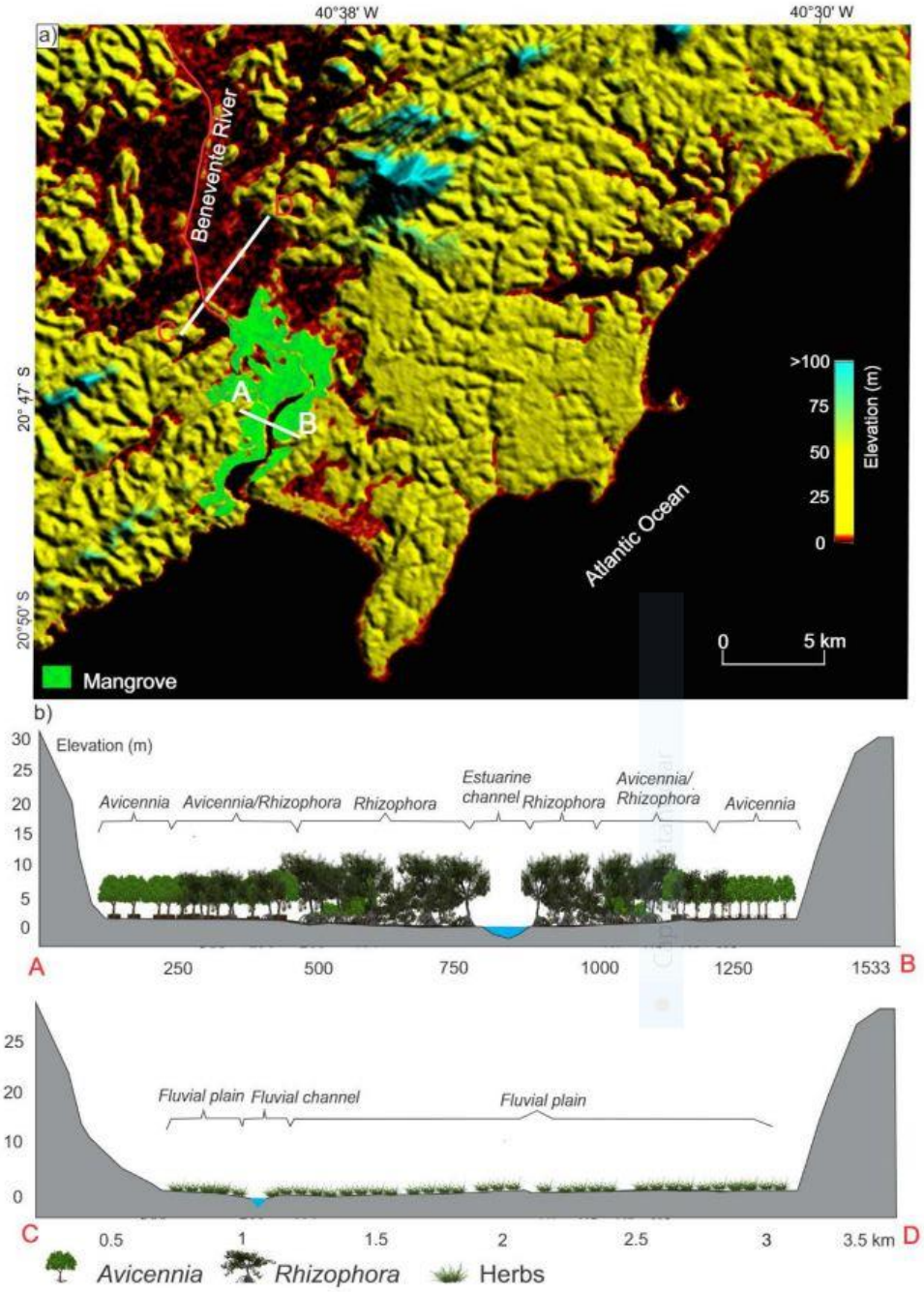

Fig. 12. a) Digital elevation model of the studied area under the influence of the Benevente River (sector 3) based on SRTM data; b) topographic profiles showing mangroves and herbaceous vegetation, influenced by brackish and freshwater, respectively, confined between coastal terraces.

Fig. 3 and Table 1), and are more exposed to the action of waves and currents. As recorded along the northern Brazilian coast, these hydrodynamic forces may cause erosion and/or sand accumulation on mangrove mud layers, degrading mangrove forests (Cohen and Lara, 2003; Cohen et al., 2009). However, in this study, the spatial-temporal analysis between 1985 and 2018 indicated stability for mangrove areas on the lowest tidal flats, suggesting that mangroves were not degraded (Fig. 2). Considering the highest muddy tidal flats (0.8–1.1 m amsl) have the highest mangrove tree densities (1000–3000 trees/ha), *Avicennia* mangroves may migrate upwards to the higher sandy tidal flats (1.1–2.5 m amsl) that currently makes up ~22 ha of the coastal plain, and partially replace palms and herbaceous vegetation through the end of the century (Figs. 2 and 11). The ombrophilous forest and deforested areas that occupy the crystalline terrain and coastal terraces (>3 m amsl) with steep surfaces (Fig. 11) will not be affected by flooding. Urban areas, occurring >2.5 m amsl, will also not be exposed

to landward mangrove migration this century. Mangrove expansion will be restricted to sandy flats between crystalline terrains and coastal terraces. Artificial or natural landward obstructions to mangrove migration may move landward in response to erosive forces, but the crystalline terrain and coastal terraces will withstand the effects of sea-level rise on a secular scale.

These predictions are supported by the spatial-temporal and pollen analyses that revealed a mangrove invasion onto higher flats since 1985 and 1955 CE, respectively (Figs. 2, 5 and 7). Therefore, the recorded sedimentation rates, mangrove dynamics during the Anthropocene, modern mangrove structure (stature, density, and zonation), coastal geomorphology and lateral accommodation space suggest that mangrove area will increase in the study sites under the influence of a 98 cm sea level rise by 2100. However, after mangrove establishment on the highest flats with low elevation gradients, further mangrove migration will be limited by the steeper relief surrounding the coastal plain (Fig. 11a and b).

This prediction is also valid for flats under the Benevente River influence (sector 3), which has a drainage basin larger than the Jabuti and Aldeia Velha Rivers (sectors 1 and 2, Fig. 1). Benevente River and its drainage produces extensive flood plains (~4030 ha) occupied by freshwater herbaceous vegetation and is topographically (0–2 m amsl, elevation based on SRTM data) suitable for future mangrove establishment (Fig. 12). However, upstream mangrove migration in this area will depend on the interaction between fluvial discharge and RSL rise rates that control the landward incursion of saltwater along the fluvial valley. Similarly, predictions about the impact of sea-level rise on mangroves along estuarine valleys have previously been presented for a coastal region in northeastern Brazil (Cohen et al., 2020a, 2020b).

6. Conclusions

Multi-proxy analysis from four sediment cores recorded the effects of the middle Holocene high sea-level stand on Brazil's southeast coast during the Holocene. The RSL rise converted a flat occupied by herbs and palms into a lagoon surrounded by mangroves, followed by an increase in sedimentary organic matter sourced from estuarine waters during the early-middle Holocene. These coastal depressions were filled with sediments during the high sea-level stand, which contributed to the conversion of lagoons into tidal flats occupied by mangroves during a RSL fall between 4230 and 1340 cal yr BP. Mangroves migrated from the highest to lowest tidal flats, causing an expansion of herbs and palms on elevated flats. The last thousand years were characterized by a significant decrease in mangrove pollen occurrence between 390 cal yr BP (1560 CE) and 77 cal yr BP (1873 CE), which must be related to a RSL fall. Core G-4, sampled from the *Rhizophora* dominant lowest zone of the tidal flats, revealed a trend of increasing *Rhizophora* pollen percentages since 77 cal yr BP (1873 CE). Cores sampled from the highest tidal flats, currently presenting a mangrove/herbaceous vegetation ecotone, indicated an increase of pollen percentages of *Rhizophora*, *Avicennia*, and *Laguncularia*, suggesting mangrove migration onto higher tidal flats previously occupied by herbs, palms, and trees/shrubs since 1958 (core G-3) and 1955 CE (core RBN-2). Satellite and drone images indicated that lower mangrove boundaries remained stable along the studied estuary and the upper boundary expanded, with mangroves invading higher flats between 1985 and 2018. These trends must be related to the increase in estuarine influence by a RSL rise since the end of the Little Ice Age and have intensified during recent decades. Under a sea-level rise scenario, the potential of mangrove expansion onto higher surfaces is limited to ~22 ha of sandy flats currently occupied by ombrophilous forests, confined between crystalline terrains and coastal terraces (>3 m amsl) with steep surfaces. However, mangrove colonization by 2100 of the extensive flood plains (~4030 ha) under the Benevente River influence with elevation suitable for upstream mangrove migration will depend mainly on the interaction between fluvial discharge and sea-level rise. This study illustrates the efficiency of integrating planialtimetric data with multiproxy stratigraphic analysis for a thorough palaeoenvironment and paleoflora reconstruction on millennial and decadal scales and to predict the mangrove distributions in a near-future scenario.

Supplementary data to this article can be found online at https://doi.org/10.1016/j.geomorph.2021.107860.

Declaration of competing interest

The authors declare that they have no known competing financial interests or personal relationships that could have appeared to influence the work reported in this paper.

Acknowledgements

We want to thank the members of the Laboratory of Coastal Dynamic (LADIC-UFPA), Center for Nuclear Energy in Agriculture (CENA-USP), Laboratory of Nuclear Instrumentation (USP-CENA), the students from the Laboratory of Chemical-Oceanography (UFPA), and C-14 Laboratory (CENA-USP) for their support. This study was financed by CNPQ (307497/2018-6) and FAPESP (2011/00995-7, 2017/03304-1, 2015-19121-8).

References

Adam, P., 2002. Saltmarshes in a time of change. Environ. Conserv. 29, 39–61. https://doi.org/10.1017/S0376892902000048.

AgisoftPhotoScan, 2018. AgiSoft PhotoScan Professional. Version 1.4.5. Agisoft LLC, St. Petersburg, Russia Retrieved from. http://www.agisoft.com/downloads/installer/.

Almeida, F.F.M., 1977. O Cráton do São Francisco. Rev. Bras. Geociências 7, 349–364.

Almeida, F.F.M., Hasui, Y., Neves, B.B.B., 1977. Províncias estruturais brasileiras. Simpósio de Geologia do Centro-Oeste. Simpósio de Geologia Do Centro-Oeste. Atas, Campina Grande, pp. 363–391 SBG/GO - BS.

Angulo, R., Lessa, G., Souza, M., 2006. A critical review of mid- to late-Holocene sea-level fluctuations on the eastern Brazilian coastline. Quat. Sci. Rev. 25, 486–506. https://doi.org/10.1016/j.quascirev.2005.03.008.

Aparecida, C., Uliana, E., 2011. Estimativa da vazão e da precipitação máxima utilizando modelos probabilísticos na Bacia Hidrográfica do Rio Benevente. ENCICLOPÉDIA Biosf. 7, 1–11.

Augustinus, P.G.E.F., 1995. Geomorphology and sedimentology of mangroves. Dev. Sedimentol. 53, 333–357. https://doi.org/10.1016/S0070-4571(05)80032-9.

Barbier, E.B., Hacker, S.D., Kennedy, C., Koch, E.W., Stier, A.C., Silliman, B.R., 2011. The value of estuarine and coastal ecosystem services. Ecol. Monogr. 81, 169–193. https://doi.org/10.1890/10-1510.1.

Behling, H., Cohen, M.C.L., Lara, R.J., 2001. Studies on Holocene mangrove ecosystem dynamics of the Bragança Peninsula in north-eastern Pará, Brazil. Bosque 167, 225–242.

Bhattacharya, J.P., 2011. Deltas. Facies Models Revisited. SEPM (Society for Sedimentary Geology), pp. 237–292 https://doi.org/10.2110/pec.06.84.0237.

Bird, E.C.F., 1980. Mangroves and coastal morphology. Vic. Nat. 97, 48–58.

Boski, T., Bezerra, F.H.R., de Fátima Pereira, L., Souza, A.M., Maia, R.P., Lima-Filho, F.P., 2015. Sea-level rise since 8.2ka recorded in the sediments of the Potengi–Jundiai Estuary, NE Brasil. Mar. Geol. 365, 1–13. https://doi.org/10.1016/j.margeo.2015.04.003.

Bradley, R.S., Jones, P.D., 1992. When was the "Little Ice Age"? In: Mikami, T. (Ed.), Proceedings of the International Symposium on the "Little Ice Age" Climate. Department of Geography, Tokyo Metropolitan University, pp. 1–4

Bricalli, L.L., de Souza, B.S., 2017. Caracterização geológica-geomorfológica da bacia do rio Juara (Espírito Santo, sudeste do Brasil). Os Desafios Da Geografia Física Na Fronteira Do Conhecimento. INSTITUTO DE GEOCIÊNCIAS - UNICAMP, pp. 6219–6232 https://doi.org/10.20396/sbgfa.v1i2017.2517.

Bruun, P., 1962. Sea level rise as a cause of shore erosion. J. Waterw. Harb. Div. Am. Soc. Civ. Eng. 88, 117–130.

Cahoon, D.R., Hensel, P.F., Spencer, T., Reed, D.J., McKee, K.L., Saintilan, N., 2006. Coastal wetland vulnerability to relative sea-level rise: Wetland elevation trends and process controls. In: Verhoeven, J.T.A., Beltman, B., Bobbing, R., Whigham, D.F. (Eds.), Wetlands and Natural Resource Management. Springer-Verlag, Berlin, pp. 271–292.

Carvalho, L.M.V., Jones, C., Liebmann, B., Carvalho, L.M.V., Jones, C., Liebmann, B., 2004. The South Atlantic Convergence Zone: Intensity, Form, Persistence, and Relationships with Intraseasonal to Interannual Activity and Extreme Rainfall. https://doi.org/10.1175/1520-0442(2004)017<0088:TSACZI>2.0.CO;2.

Castro, D.F., Rossetti, D.F., Cohen, M.C.L., Pessenda, L.C.R., Lorente, F.L., 2013. The growth of the Doce River Delta in northeastern Brazil indicated by sedimentary facies and diatoms. Diatom Res. 28, 455–466. https://doi.org/10.1080/0269249X.2013.841100.

Cohen, M.C.L., Lara, R.J., 2003. Temporal changes of mangrove vegetation boundaries in Amazonia: Application of GIS and remote sensing techniques. Wetl. Ecol. Manag. 11, 223–231. https://doi.org/10.1023/A:1025007331075.

Cohen, M.C.L., Behling, H., Lara, R.J., 2005. Amazonian mangrove dynamics during the last millennium: the relative sea-level and the Little Ice Age. Rev. Palaeobot. Palynol. 136, 93–108. https://doi.org/10.1016/j.revpalbo.2005.05.002.

Cohen, M.C.L., Behling, H., Lara, R.J., Smith, C.B., Matos, H.R.S., Vedel, V., 2009. Impact of sea-level and climatic changes on the Amazon coastal wetlands during the late Holocene. Veg. Hist. Archaeobot. 18, 425–439. https://doi.org/10.1007/s00334-008-0208-0.

Cohen, M.C.L., Pessenda, L.C.R., Behling, H., de Fátima Rossetti, D., França, M.C., Guimarães, J.T.F., Friaes, Y., Smith, C.B., 2012. Holocene palaeoenvironmental history of the Amazonian mangrove belt. Quat. Sci. Rev. 55, 50–58.

Cohen, M.C.L., França, M.C., Rossetti, D., Pessenda, L.C.R., Giannini, P.C.F., Lorente, F.L., Junior, A.Á.B., Castro, D., Macario, K., 2014. Landscape evolution during the late Quaternary at the Doce River mouth, Espírito Santo State, Southeastern Brazil. Palaeogeogr. Palaeoclimatol. Palaeoecol. 415, 48–58. https://doi.org/10.1016/j.palaeo.2013.12.001.

Cohen, M.C.L., Alves, I.C.C., França, M.C., Pessenda, L.C.R., de F Rossetti, D., 2015. Relative sea-level and climatic changes in the Amazon littoral during the last 500 years. CATENA 133, 441–451. https://doi.org/10.1016/j.catena.2015.06.012.

Cohen, M.C.L., de Souza, A.V., Rossetti, D.F., Pessenda, L.C.R., França, M.C., 2018. Decadal-scale dynamics of an Amazonian mangrove caused by climate and sea level changes: inferences from spatial-temporal analysis and Digital Elevation Models. Earth Surf. Process. Landforms 43, 2876–2888. https://doi.org/10.1002/esp.4440.

Cohen, M.C.L., Figueiredo, B.L., Oliveira, N.N., Fontes, N.A., França, M.C., Pessenda, L.C.R., de Souza, A.V., Macario, K., Giannini, P.C.F., Bendassolli, J.A., Lima, P., 2020a. Impacts of Holocene and modern sea-level changes on estuarine mangroves from northeastern Brazil. Earth Surf. Process. Landforms 45, 375–392. https://doi.org/10.1002/esp.4737.

Cohen, M.C.L., Rodrigues, E., Rocha, D.O.S., Freitas, J., Fontes, N.A., Pessenda, L.C.R., de Souza, A.V., Gomes, V.L.P., França, M.C., Bonotto, D.M., Bendassolli, J.A., 2020b. Southward migration of the austral limit of mangroves in South America. CATENA 195, 104775. https://doi.org/10.1016/j.catena.2020.104775.

Cohen, M.C.L., Camargo, P.M.P., Pessenda, L.C.R., Lorente, F.L., Souza, A.V.De, Corrêa, J.A.M., Bendassolli, J., Dietz, M., 2021. Effects of the middle Holocene high sea-level stand and climate on Amazonian mangroves. J. Quat. Sci., jqs.3343 https://doi.org/10.1002/JQS.3343.

Colinvaux, P., De Oliveira, P.E., Patiño, J.E.M., 1999. Amazon Pollen Manual and Atlas. Harwood Academic Publishers, Dordrecht.

Cooper, J.A.G., Meireles, R.P., Green, A.N., Klein, A.H.F., Toldo, E.E., 2018. Late Quaternary stratigraphic evolution of the inner continental shelf in response to sea-level change, Santa Catarina, Brazil. Mar. Geol. 397, 1–14. https://doi.org/10.1016/j.margeo.2017.11.011.

D'Alpaos, A., Lanzoni, S., Marani, M., Rinaldo, A., 2008. Landscape evolution in tidal embayments: Modeling the interplay of erosion, sedimentation, and vegetation dynamics. J. Geophys. Res. 112, 1–17.

Dangendorf, S., Marcos, M., Wöppelmann, G., Conrad, C.P., Frederikse, T., Riva, R., 2017. Reassessment of 20th century global mean sea level rise. Proc. Natl. Acad. Sci. U. S. A. 114, 5946–5951. https://doi.org/10.1073/pnas.1616007114.

Davis, R.A., 2013. Evolution of coastal landforms. Treatise on Geomorphology. Elsevier Inc., pp. 417–448 https://doi.org/10.1016/B978-0-12-374739-6.00293-1.

Deines, P., 1980. The isotopic composition of reduced organic carbon. In: Fritz, P., Fontes, J.C. (Eds.), Handbook of Environmental Isotope Geochemistry. The Terrestrial Environments. Elsevier, Amsterdam, pp. 329–406.

DHN, 2014. Directorate of hydrography and navigationon. Tide Table Porto De Ilhéus – Malhado - BA.

Di Nitto, D., Erftemeijer, P.L.A., van Beek, J.K.L., Dahdouh-Guebas, F., Higazi, L., Quisthoudt, K., Jayatissa, L.P., Koedam, N., 2013a. Modelling drivers of mangrove propagule dispersal and restoration of abandoned shrimp farms. Biogeosciences 10, 5095–5113. https://doi.org/10.5194/bg-10-5095-2013.

Di Nitto, D., Neukermans, G., Koedam, N., Defever, H., Pattyn, F., Kairo, J.G., Dahdouh-Guebas, F., 2013b. Mangroves facing climate change: landward migration potential in response to projected scenarios of sea level rise. Biogeosci. Discuss. 10, 3523–3558. https://doi.org/10.5194/bgd-10-3523-2013.

Dittmar, T., Lara, R.J., Kattner, G., 2001. River or mangrove? Tracing major organic matter sources in tropical Brazilian coastal waters. Mar. Chem. 73, 253–271. https://doi.org/10.1016/S0304-4203(00)00110-9.

Dittmar, T., Hertkorn, N., Kattner, G., Lara, R.J., 2006. Mangroves, a major source of dissolved organic carbon to the oceans. Global Biogeochem. Cycles, 1–7 https://doi.org/10.1029/2005GB002570.

Ellis, J., Nicholls, P., Craggs, R., Hofstra, D., Hewitt, J., 2004. Effects of terrigenous sedimentation on mangrove physiology and associated macrobenthic communities. Mar. Ecol. Prog. Ser. 270, 71–82. https://doi.org/10.3354/meps270071.

Ellison, J.C., Stoddart, D.R., 1991. Mangrove ecosystem collapse during predicted sea-level rise: Holocene analogues and implications. J. Coast. Res. 7, 151–165.

Ellison, J.C., 2016. Mangrove vulnerability assessment methodology and adaptation prioritisation. Malaysian For. 79, 95–108.

EMBRAPA, 1978. Empresa Brasileira de Pesquisa Agropecuária. Levantamento de Reconhecimento dos Solos do Estado do Espírito Santo. BoletimTécnico, Rio de Janeiro.

de F Toniolo, T., Giannini, P.C.F., Angulo, R.J., de Souza, M.C., Pessenda, L.C.R., Spotorno-Oliveira, P., 2020. Sea-level fall and coastal water cooling during the Late Holocene in Southeastern Brazil based on vermetid bioconstructions. Mar. Geol. 428. https://doi.org/10.1016/j.margeo.2020.106281.

Faegri, K., Iversen, J., 1989. Textbook of Pollen Analysis. 4th ed. Wiley.

França, M.C., Cohen, M.C.L., Pessenda, L.C.R., Rossetti, D.F., Lorente, F.L., Buso Junior, A.Á., Guimarães, J.T.F., Friaes, Y., Macario, K., 2013. Mangrove vegetation changes on Holocene terraces of the Doce River, southeastern Brazil. CATENA 110, 59–69. https://doi.org/10.1016/j.catena.2013.06.011.

França, M.C., Alves, I.C.C., Castro, D.F., Cohen, M.C.L., Rossetti, D.F., Pessenda, L.C.R., Lorente, F.L., Fontes, N.A., Junior, A.Á.B., Giannini, P.C.F., Francisquini, M.I., 2015. A multi-proxy evidence for the transition from estuarine mangroves to deltaic freshwater marshes, Southeastern Brazil, due to climatic and sea-level changes during the late Holocene. CATENA 128, 155–166. https://doi.org/10.1016/j.catena.2015.02.005.

Franca, M.C., Alves, I.C.C., Cohen, M.C., Rossetti, D.F., Pessenda, L.C., Giannini, P.C., Lorente, F.L., Buso Junior, A.A., Bendassolli, J.A., Macario, K., 2016. Millennial to secular time-scale impacts of climate and sea-level changes on mangroves from the Doce River delta, Southeastern Brazil. The Holocene 26, 1733–1749. https://doi.org/10.1177/0959683616645938.

Furukawa, K., Wolanski, E., 1996. Sedimentation in mangrove forests. Mangroves Salt Marshes 1, 3–10. https://doi.org/10.1023/A:1025973425404.

Gaiser, E.E., Zafiris, A., Ruiz, P.L., Tobias, F.A.C., Ross, M.S., 2006. Tracking rates of ecotone migration due to salt-water encroachment using fossil mollusks in coastal South Florida. Hydrobiologia 569, 237–257. https://doi.org/10.1007/s10750-006-0135-y.

Gilman, E., Ellison, J., Coleman, R., 2007. Assessment of mangrove response to projected relative sea-level rise and recent historical reconstruction of shoreline position. Environ. Monit. Assess. 124, 105–130. https://doi.org/10.1007/s10661-006-9212-y.

Grimm, E., 1990. TILIA and TILIAGRAPH: PC spreadsheet and graphic software for pollen data. INQUA Sub-commission on Data-Handling Methods Newsletter.

Grinsted, A., Moore, J.C., Jevrejeva, S., 2009. Reconstructing sea level from paleo and projected temperatures 200 to 2100 ad. Clim. Dyn. 34, 461–472. https://doi.org/10.1007/s00382-008-0507-2.

Harper, C.W., 1984. Improved methods of facies sequence analysis. In: Walker, R.G. (Ed.), Facies Models Geoscience Canada. Reprint Series 1. Geological Association of Canada. Geological Association of Canada, Toronto, pp. 11–13.

Hicks, S., Hyvärinen, H., 2010. Pollen Influx Values Measured in Different Sedimentary Environments and their Palaeoecological Implications. https://doi.org/10.1080/00173130070044618.

IPCC, 2013. Intergovernmental Panel on Climate Change (IPCC) Climate Change 2013: The Physical Science Basis Cambridge University Press. UK, Summary for Policymakers.

IPCC, 2014. Contribution of working groups I, II and III to the Fifth Assessment Report of the Intergovernmental Panel on Climate Change. In: Pachauri, R.K., Meyer, L.A. (Eds.), Climate Change 2014: Synthesis Report. Geneva, p. 151.

Kandasamy, Kathiresan, 2003. How do mangrove forests induce sedimentation? Rev. Biol. Trop. 51, 355–359.

Kirwan, M.L., Megonigal, J.P., 2013. Tidal wetland stability in the face of human impacts and sea-level rise. Nature. https://doi.org/10.1038/nature12856.

Kirwan, M.L., Murray, A.B., 2007. A coupled geomorphic and ecological model of tidal marsh evolution. Proc. Natl. Acad. Sci. U. S. A. 104, 6118–6122. https://doi.org/10.1073/pnas.0700958104.

Krauss, K.W., Allen, J.A., Cahoon, D.R., 2003. Differential rates of vertical accretion and elevation change among aerial root types in Micronesian mangrove forests. Estuar. Coast. Shelf Sci. 56, 251–259. https://doi.org/10.1016/S0272-7714(02)00184-1.

Krauss, K.W., Cahoon, D.R., Allen, J.A., Ewel, K.C., Lynch, J.C., Cormier, N., 2010. Surface elevation change and susceptibility of different mangrove zones to sea-level rise on Pacific High Islands of Micronesia. Ecosystems 13, 129–143. https://doi.org/10.1007/s10021-009-9307-8.

Krauss, K.W., From, A.S., Doyle, T.W., Doyle, T.J., Barry, M.J., 2011. Sea-level rise and landscape change influence mangrove encroachment onto marsh in the Ten Thousand Islands region of Florida, USA. J. Coast. Conserv. 15, 629–638. https://doi.org/10.1007/s11852-011-0153-4.

Krauss, K.W., McKee, K.L., Lovelock, C.E., Cahoon, D.R., Saintilan, N., Reef, R., Chen, L., 2014. How mangrove forests adjust to rising sea level. New Phytol. 202, 19–34. https://doi.org/10.1111/nph.12605.

Lamb, A.L., Wilson, G.P., Leng, M.J., 2006. A review of coastal palaeoclimate and relative sea-level reconstructions using $\delta^{13}C$ and C/N ratios in organic material. Earth-Science Rev. 75, 29–57. https://doi.org/10.1016/j.earscirev.2005.10.003.

Lara, R.J., Cohen, M.C.L., 2006. Sediment porewater salinity, inundation frequency and mangrove vegetation height in Bragança, North Brazil: an ecohydrology-based empirical model. Wetl. Ecol. Manag. 14, 349–358. https://doi.org/10.1007/s11273-005-4991-4.

Lean, J., Rind, D., 1999. Evaluating sun-climate relationships since the Little Ice Age. Jounal Amospheric Solar-Terrestrial Phys. 61, 25–36.

Lorente, F.L., Pessenda, L.C.R., Oboh-Ikuenobe, F., Buso, A.A. Cohen, M.C.L., Meyer, K.E.B., Giannini, P.C.F., de Oliveira, P.E., de F Rossetti, D., Borotti Filho, M.A., de Castro França, M.C., Bendassolli, J.A., Macario, K., 2014. Palynofacies and stable C and N isotopes of Holocene sediments from Lake Macuco (Linhares, Espírito Santo, southeastern Brazil): Depositional settings and palaeoenvironmental evolution. Palaeogeogr. Palaeoclimatol. Palaeoecol. 415, 69–82. https://doi.org/10.1016/j.palaeo.2013.12.004.

Lovelock, C.E., Bennion, V., Grinham, A., Cahoon, D.R., 2011. The role of surface and subsurface processes in keeping pace with sea level rise in intertidal wetlands of Moreton Bay, Queensland, Australia. Ecosystems 14, 745–757. https://doi.org/10.1007/s10021-011-9443-9.

Lovelock, C.E., Adame, M.F., Bennion, V., Hayes, M., Reef, R., Santini, N., Cahoon, D.R., 2015a. Sea level and turbidity controls on mangrove soil surface elevation change. Estuar. Coast. Shelf Sci. 153, 1–9. https://doi.org/10.1016/j.ecss.2014.11.026.

Lovelock, C.E., Cahoon, D.R., Friess, D.A., Guntenspergen, G.R., Krauss, K.W., Reef, R., Rogers, K., Saunders, M.L., Sidik, F., Swales, A., Saintilan, N., Thuyen, L.X., Triet, T., 2015b. The vulnerability of Indo-Pacific mangrove forests to sea-level rise. Nature 526, 559–563. https://doi.org/10.1038/nature15538.

Markgraf, V., D'Antoni, H.L., 1978. Pollen Flora of Argentina. AZ Univ. Arizona Press, Tucson.

Martin, L., Dominguez, J.M.L., Bittencourt, A.C.S.P., 2003. Fluctuating holocene sea levels in Eastern and Southeastern Brazil: evidence from multiple fossil and geometric indicators. J. Coast. Res. 19, 101–124.

Matos, C.R.L., Berrêdo, J.F., Machado, W., Sanders, C.J., Metzger, E., Cohen, M.C.L., 2020. Carbon and nutrients accumulation in tropical mangrove creeks, Amazon region. Mar. Geol. 429, 106317. https://doi.org/10.1016/j.margeo.2020.106317.

Mckee, K.L., Faulkner, P.L., 2000. Mangrove peat analysis and reconstruction of vegetation history at the Pelican Cays, Belize. Atoll Res. Bull. 47–58.

McKee, K.L., Cahoon, D.R., Feller, I.C., 2007. Caribbean mangroves adjust to rising sea level through biotic controls on change in soil elevation. Glob. Ecol. Biogeogr. 16, 545–556. https://doi.org/10.1111/j.1466-8238.2007.00317.x.

Meyers, P.A., 1994. Preservation of elemental and isotopic source identification of sedimentary organic matter. Chem. Geol. 114, 289–302. https://doi.org/10.1016/0009-2541(94)90059-0.

Meyers, P.a., 1997. Organic geochemical proxies of paleoceanographic, paleolimnologic, and paleoclimatic processes. Org. Geochem. 27, 213–250. https://doi.org/10.1016/S0146-6380(97)00049-1.

Miall, A.D., 1978. Facies types and vertical profile models in braided river deposits: A summary. In: Miall, A.D. (Ed.), Fluvial Sedimentology. Canadian Society of Petroleum Geologists, Calgary, pp. 597–604.

Nagelkerken, I., Blaber, S.J.M., Bouillon, S., Green, P., Haywood, M., Kirton, L.G., Meynecke, J.-O., Pawlik, J., Penrose, H.M., Sasekumar, A., Somerfield, P.J., 2008. The habitat function of mangroves for terrestrial and marine fauna: A review. Aquat. Bot. 89, 155–185. https://doi.org/10.1016/j.aquabot.2007.12.007.

Nascimento, W.R., Souza-Filho, P.W.M., Proisy, C., Lucas, R.M., Rosenqvist, A., 2013. Mapping changes in the largest continuous Amazonian mangrove belt using object-based classification of multisensor satellite imagery. Estuar. Coast. Shelf Sci. 117, 83–93. https://doi.org/10.1016/j.ecss.2012.10.005.

Nerem, R.S., Beckley, B.D., Fasullo, J.T., Hamlington, B.D., Masters, D., Mitchum, G.T., 2018. Climate-change-driven accelerated sea-level rise detected in the altimeter era. Proc. Natl. Acad. Sci. U. S. A. 115, 2022–2025. https://doi.org/10.1073/pnas.1717312115.

Nieminski, N.M., Graham, S.A., 2017. Modeling stratigraphic architecture using small unmanned aerial vehicles and photogrammetry: examples from the Miocene East Coast Basin, New Zealand. J. Sediment. Res. 87, 126–132. https://doi.org/10.2110/jsr.2017.5.

de O Caldas, L.H., de M Oliveira, J.G., de Stattegger, W.E., Stattegger, K., Vital, H., 2006. Geometry and evolution of Holocene transgressive and regressive barriers on the semi-arid coast of NE Brazil. Geo-Marine Lett. 26, 249–263. https://doi.org/10.1007/s00367-006-0034-2.

Pan, Y., Yan, S., Behling, H., Mu, G., 2013. Transport of airborne Picea schrenkiana pollen on the northern slope of Tianshan Mountains (Xinjiang, China) and its implication for paleoenvironmental reconstruction. Aerobiologia (Bologna). 29, 161–173. https://doi.org/10.1007/s10453-012-9270-2.

Parkinson, R.W., DeLaune, R.D., White, J.R., 1994. Holocene sea-level rise and the fate of mangrove forests within the wider Caribbean region. J. Coast. Res. 10, 1077–1086.

Pascoalini, S.S., Lopes, D.M.S., Falqueto, A.R., Tognella, M.M.P., 2014. Abordagem Ecofisiológica dos Manguezais: uma revisão. Biotemas 27, 1–11.

Peixoto, A.L., Gentry, A., 1990. Diversidade e composição florística da mata de tabuleiros na Reserva Florestal de Linhares (Espírito Santo, Brasil). Rev. Bras. Botânica 13, 19–25.

Pessenda, L.C.R., Ribeiro, A.D.S., Gouveia, S.E.M., Aravena, R., Boulet, R., Bendassolli, J.A., 2004. Vegetation dynamics during the late Pleistocene in the Barreirinhas region, Maranhão State, northeastern Brazil, based on carbon isotopes in soil organic matter. Quat. Res. 62, 183–193. https://doi.org/10.1016/j.yqres.2004.06.003.

Pessenda, L.C.R., Gouveia, S.E.M., de Sribeiro, A., de Oliveira, P.E., Aravena, R., 2010. Late Pleistocene and Holocene vegetation changes in northeastern Brazil determined from carbon isotopes and charcoal records in soils. Palaeogeogr. Palaeoclimatol. Palaeoecol. 297, 597–608. https://doi.org/10.1016/j.palaeo.2010.09.008.

Pessenda, L.C.R., Vidotto, E., De Oliveira, P.E., Buso, A.A., Cohen, M.C.L., de Rossetti, D., Ricardi-Branco, F., Bendassolli, J.A., 2012. Late Quaternary vegetation and coastal environmental changes at Ilha do Cardoso mangrove, southeastern Brazil. Palaeogeogr. Palaeoclimatol. Palaeoecol. 363, 57–68.

Peterson, J.M., Bell, S.S., 2015. Saltmarsh boundary modulates dispersal of mangrove propagules: Implications for mangrove migration with sea-level rise. PLoS One 10, e0119128. https://doi.org/10.1371/journal.pone.0119128.

Phillips, D.H., Kumara, M.P., Jayatissa, L.P., Krauss, K.W., Huxham, M., 2017. Impacts of Mangrove Density on Surface Sediment Accretion, Belowground Biomass and Biogeochemistry in Puttalam Lagoon, Sri Lanka. Wetlands 37, 471–483. https://doi.org/10.1007/s13157-017-0883-7.

Reading, H.G., 1996. Sedimentary Environments: Processes, Facies and Stratigraphy. 3a ed. Blackwell Science.

Reimer, P.J., Bard, E., Bayliss, A., Beck, J.W., Blackwell, P.G., Ramsey, C.B., Buck, C.E., Cheng, H., Edwards, R.L., Friedrich, M., Grootes, P.M., Guilderson, T.P., Haflidason, H., Hajdas, I., Hatté, C., Heaton, T.J., Hoffmann, D.L., Hogg, A.G., Hughen, K.A., Kaiser, K.F., Kromer, B., Manning, S.W., Niu, M., Reimer, R.W., Richards, D.A., Scott, E.M., Southon, J.R., Staff, R.A., Turney, C.S.M., van der Plicht, J., 2013. IntCal13 and Marine13 radiocarbon age calibration curves 0–50,000 years cal BP. Radiocarbon 55, 1869–1887. https://doi.org/10.2458/azu_js_rc.55.16947.

Ribeiro, S.R., Batista, E.J.L., Cohen, M.C., França, M.C., Pessenda, L.C., Fontes, N.A., Alves, I.C., Bendassolli, J.A., 2018. Allogenic and autogenic effects on mangrove dynamics from the Ceará Mirim River, north-eastern Brazil, during the Middle and Late Holocene. Earth Surf. Process. Landforms. https://doi.org/10.1002/esp.4342.

Rodrigues, E., Cohen, M.C.L., Liu, K., Pessenda, L.C.R., Yao, Q., Ryu, J., Rossetti, D., de Souza, A., Dietz, M., 2021. The effect of global warming on the establishment of mangroves in coastal Louisiana during the Holocene. Geomorphology 107648. https://doi.org/10.1016/j.geomorph.2021.107648.

Rogers, K., Saintilan, N., Cahoon, D., 2005. Surface elevation dynamics in a regenerating mangrove forest at Homebush Bay, Australia. Wetl. Ecol. Manag. 13, 587–598. https://doi.org/10.1007/s11273-004-0003-3.

Rogers, K., Wilton, K.M., Saintilan, N., 2006. Vegetation change and surface elevation dynamics in estuarine wetlands of southeast Australia. Estuar. Coast. Shelf Sci. 66, 559–569. https://doi.org/10.1016/j.ecss.2005.11.004.

Rossetti, D.F., Góes, A.M., 2009. Marine influence in the Barreiras Formation, State of Alagoas, northeastern Brazil. An. Acad. Bras. Cienc. 81, 741–755. https://doi.org/10.1590/s0001-37652009000400012.

Rossetti, D.F., Polizel, S.P., Cohen, M.C.L., Pessenda, L.C.R., 2015. Late Pleistocene-Holocene evolution of the Doce River delta, southeastern Brazil: Implications for the understanding of wave-influenced deltas. Mar. Geol. 367, 171–190. https://doi.org/10.1016/j.margeo.2015.05.012.

Roubik, D.W., Moreno, J.E., 1991. Pollen and Spores of Barro Colorado Island. Missouri Botanical Garden.

Sahoo, H., Gani, N.D., 2015. Creating three-dimensional channel bodies in LiDAR-integrated outcrop characterization: A new approach for improved stratigraphic analysis. Geosphere 11, 777–785. https://doi.org/10.1130/GES01075.1.

Saintilan, N., Wilson, N.C., Rogers, K., Rajkaran, A., Krauss, K.W., 2014. Mangrove expansion and salt marsh decline at mangrove poleward limits. Glob. Chang. Biol. 20, 147–157. https://doi.org/10.1111/gcb.12341.

Salgado-Labouriau, M.L., 1997. Late quaternary palaeoclimate in the savannas of South America. J. Quat. Sci. 12, 371–379. https://doi.org/10.1002/(SICI)1099-1417(199709/10)12:5<371::AID-JQS320>3.0.CO;2-3.

Sasmito, S.D., Murdiyarso, D., Friess, D.A., Kurnianto, S., 2015. Can mangroves keep pace with contemporary sea level rise? A global data review. Wetl. Ecol. Manag. https://doi.org/10.1007/s11273-015-9466-7.

Schidlowski, M., Hayes, J.M., Kaplan, I.R., 1983. Isotopic inferences of ancient biochemistries - carbon, sulfur, hydrogen, and nitrogen. NASA, United States (32 p.).

Schlager, W., 1993. Accommodation and supply-a dual control on stratigraphic sequences. Sediment. Geol. 86, 111–136. https://doi.org/10.1016/0037-0738(93)90136-S.

Schwartz, M.L., 1965. Laboratory study of sea-level rise as a cause of shore erosion. J. Geol. 73, 528–534.

Snedaker, S.C., Meeder, J.F., Ross, M.S., Ford, R.G., 1994. Discussion of Ellison, Joanna C. and Stoddart, David R., 1991. Mangrove ecosystem collapse during predicted sea-level rise: Holocene analogues and implications. J. Coast. Res. 10, 497–498.

Soreghan, G.S., Dickinson, W.R., 1994. Generic types of stratigraphic cycles controlled by eustasy. Geology 22, 759–761. https://doi.org/10.1130/0091-7613(1994)022<0759:GTOSCC>2.3.CO;2.

Spencer, T., Schuerch, M., Nicholls, R.J., Hinkel, J., Lincke, D., Vafeidis, A.T., Reef, R., McFadden, L., Brown, S., 2016. Global coastal wetland change under sea-level rise and related stresses: the DIVA Wetland Change Model. Glob. Planet. Change 139, 15–30. https://doi.org/10.1016/j.gloplacha.2015.12.018.

Suguio, K., Barreto, A.M.F., Oliveira, P.E., Bezerra, F.H.R., Vilela, M.C.S.H., 2013. Indicators of Holocene sea level changes along the coast of the states of Pernambuco and Paraíba, Brazil. Geol. - Série Científica USP 13, 141–152. https://doi.org/10.5327/Z1519-874X201300040008.

Tue, N.T., Nguyen, P.T., Quan, D.M., Dung, L.V., Quy, T.D., Nhuan, M.T., Thai, N.D., 2018. Sedimentary composition and organic carbon sources in mangrove forests along the coast of northeast Vietnam. Reg. Stud. Mar. Sci. 17, 87–94. https://doi.org/10.1016/j.rsma.2017.12.001.

Tyson, R.V., 1995. Sedimentary Organic Matter: Organic Facies and Palynofacies. Chapman and Hall, London.

Vale, C.C., Ferreira, R.D., 1998. Os manguezais do litoral do Estado do Espírito Santo. Anais Do Simpósio de Ecossistemas Da Costa Brasileira. ACIESP, São Paulo, pp. 88–94.

Vieira, V.S., de Menezes, R.G., 2015. Geologia e Recursos Minerais do Estado do Espírito Santo: texto explicativo do mapa geológico e de recursos minerais Belo Horizonte.

Walker, R.G., 1992. Facies, facies models and modern stratigrahic concepts. In: Walker, R.G., James, N.P. (Eds.), Facies Models - Response to Sea Level Change. Geological Association of Canada, Ontario, pp. 1–14.

Weng, C., Bush, M.B., Silman, M.R., 2004. An analysis of modern pollen rain on an elevational gradient in southern Peru. J. Trop. Ecol. 20, 113–124. https://doi.org/10.1017/S0266467403001068.

Wentworth, C.K., 1922. A scale of grade and class terms for clastic sediments. J. Geol. 377–392.

Woodroffe, C.D., 1995. Response of tide-dominated mangrove shorelines in Northern Australia to anticipated sea-level rise. Earth Surf. Process. Landforms 20, 65–85. https://doi.org/10.1002/esp.3290200107.

Woodroffe, C.D., Murray-Wallace, C.V., 2012. Sea-level rise and coastal change: the past as a guide to the future. Quat. Sci. Rev. https://doi.org/10.1016/j.quascirev.2012.05.009.

Woodroffe, C.D., Rogers, K., McKee, K.L., Lovelock, C.E., Mendelssohn, I.A., Saintilan, N., 2016. Mangrove sedimentation and response to relative sea-level rise. Annu. Rev. Mar. Sci. 8, 243–266. https://doi.org/10.1146/annurev-marine-122414-034025.

Yao, Q., Liu, K., 2017. Dynamics of marsh-mangrove ecotone since the mid-Holocene: a palynological study of mangrove encroachment and sea level rise in the Shark River Estuary, Florida. PLoS One 12, e0173670. https://doi.org/10.1371/journal.pone.0173670.

Yao, Q., Liu, K., Platt, W.J., Rivera-Monroy, V.H., 2015. Palynological reconstruction of environmental changes in coastal wetlands of the Florida Everglades since the mid-Holocene. Quat. Res. 83, 449–458. https://doi.org/10.1016/j.yqres.2015.03.005.

Zalasiewicz, J., Waters, C.N., Williams, M., Summerhayes, C., 2018. The Anthropocene as a Geological Time Unit: a Guide to the Scientific Evidence and Current Debate. Cambridge University Press.

CAPÍTULO V: SOUTHWARD MANGROVE EXPANSION IN SOUTH AMERICA DURING THE LATE HOLOCENE AND ANTHROPOCENE

Erika Rodrigues[a]; Marcelo Cancela Lisboa Cohen[a], Ph.D.; Dr; Luiz Carlos R Pessenda[b]; Evandro Magalhães[b]; Qiang Yao[c]; Adriana Souza[a]

[a] Laboratory of Coastal Dynamics, Graduate Program of Geology and Geochemistry, Federal University of Pará, Brazil Federal University of Pará. Rua Augusto Corrêa, 01-Guamá. CEP 66075-110, Belém (PA), Brazil.

[b] University of São Paulo, CENA/1413 C Laboratory, Av. Centenário 303, 13400-000, Piracicaba, São Paulo, Brazil.

[c] Department of Oceanography and Coastal Sciences, Louisiana State University, Baton Rouge, Louisiana 70803, U.S.A

*Corresponding author: Érika Ferreira Rodrigues

Federal University of Pará - Brazil

Rua Augusto Corrêa, 01 - Guamá. CEP 66075-110, Belém (PA), Brazil.

Tel.: +55 91 3201-7988. e-mail address: mcohen80@hotmail.com

Submitted to Geomorphology journal

ABSTRACT

Temperature influences the global biogeography of mangroves, and global warming may be driving a poleward mangrove expansion. This work aims to study the impacts of climate change in the subtropical mangroves during the late-Holocene and Anthropocene on a southern Brazilian coastal plain and discuss the environmental conditions to the mangrove establishment near the austral limit of South America mangroves. The main result of this research was a vegetation succession: saltmarshes (>1460 cal yr BP), *Laguncularia* (~1000 cal yr BP), *Avicennia* ~500 cal yr BP), and *Rhizophora* (~1950 AD). Probably, this vertical mangrove succession is associated with the low-temperature tolerance of mangroves, where the sequence *Rhizophora, Avicennia, and Laguncularia* occurs from the northern to the southern limits of Santa Catarina coast, respectively, reflecting the temperature gradient. The absence of mangroves between ~1460 and ~1000 cal yr BP, followed by their *Laguncularia*, *Avicennia* establishment in the late Holocene and *Rhizophora* in the Anthropocene in the subtropical zone, is associated with a migration of the austral mangrove limit into the temperate zone, caused by the gradual increase in winter temperatures. This process may be related to a poleward mangrove migration since the late Holocene, which is caused by natural Holocene global warming. However, the Anthropocene warming must have intensified the mangrove expansion into temperate zones.

Keywords: global warming, palyno-diatoms, sedimentary features, subtropical mangrove

1 INTRODUCTION

The global annual temperature is increasing at an alarming rate of 0.18°C per decade since the early 1980s (Dunn *et al.* 2020), shifting the geographic distribution of biomes worldwide (Pecl *et al.* 2017). As a result, many wildlife (birds, mammals, butterflies, bees, and polar bears) and coastal vegetation (saltmarshes and mangroves) have migrated into higher latitudes (Walker *et al.* 2019, Gilman *et al.* 2008, Walther *et al.* 2002, Kullman 2001).

Biogeographic studies indicated that the modern global distribution of mangroves is mainly controlled by temperature (Sherrod & McMillan 1985a, Ellison 2002, Stevens *et al.* 2006b, Stuart *et al.* 2007, Quisthoudt *et al.* 2012, Alongi 2015, Osland *et al.* 2017). Mangrove forests occur along tropical and subtropical coasts where the annual average temperature is above 20°C (Duke *et al.* 1998) and the minimum temperature is above −7°C (Osland *et al.* 2020). The Atlantic and Caribbean coasts comprise more than half of the total mangrove area of the American continent, and a nearly continuous mangrove belt is found from the southern United States to southern Brazil along the Atlantic coast (Lacerda *et al.* 2002).

As a response to the Anthropocene global warming, mangroves have migrated into temperate zones (Cavanaugh *et al.* 2018), replacing saltmarshes and increasing their poleward limits on five continents over the past half-century (Osland *et al.* 2018a). In North America, such mangrove expansion and contraction have also been recorded in the paleoecological record. For instance, the boreal limit of mangroves in Texas, Louisiana, Mississippi, Alabama, Georgia, and Tennessee was further north than their current distribution before the Quaternary (Gee 2001, Sherrod & McMillan 1985b, Westgate & Gee 1990). During the Pleistocene, due to colder temperature (Clark *et al.* 2009), the range of North American mangroves was limited to equatorial zones in the Caribbean (Lacerda *et al.* 2002, Sherrod & McMillan 1985b), followed by a poleward expansion post- LGM (Kennedy *et al.* 2016, Sandoval-Castro *et al.* 2012b). In the southern hemisphere, similar mangrove dynamics have been revealed by some paleoecological reconstructions (Ellison & Stoddart 1991, Gilman *et al.* 2008, Cohen *et al.* 2020, França *et al.* 2019). Mangroves were established in the tropical Brazilian littoral (2º N - 19º S) at ~7000 cal yr BP (Cohen *et al.* 2012, 2014, 2020a, Pessenda *et al.* 2012, França *et al.* 2013, 2015, Fontes *et al.* 2017, Ribeiro *et al.* 2018). However, in subtropical Brazilian coast (26°S), mangroves occur since ~1630 cal yr BP, with *Rhizophora* trees arising only during the last few decades (França *et al.* 2019). In addition, pollen studies from the austral

limit of American mangroves at Laguna Santa Catarina, southern Brazilian coast (28º 29´ S), indicate that mangroves were absent during the Holocene and were established during the Anthropocene epoch (Cohen *et al.* 2020b).

The time lag between mangroves establishment in tropical and subtropical Brazil is generally attributed to different mangrove physiology and more frequent winter freeze events in the higher latitudes (Stuart *et al.* 2007, Osland *et al.* 2015). For example, *Avicennia schaueriana, Laguncularia racemosa,* and *Rhizophora mangle* are found in Praia dos Sonhos (27°53'S), while only *Avicennia schaueriana* and *Laguncularia racemosa* are found in Laguna (28°30'S). *Avicennia schaueriana* and *Laguncularia racemosa* were reported to be more tolerant to low temperatures, and they are currently absent at Aranhanguá (28°55'S), the southernmost of Santa Catarina, where the winter climate is intense and occur more frequently than in the other two sites that have a mangrove cover (Ximenes *et al.* 2019). In this context, did mangroves ever appear in Sao Francisco do Sul Bay (North of Santa Catarina State) during the Holocene? Are there any local factors inhibiting mangroves from migrating to Brazilian southernmost? Very few studies have documented the history of mangrove biogeography from the austral limit of American mangroves. Hence, large data gaps exist in the literature.

To fill the aforementioned data gaps, this paper aims to reconstruct the late-Holocene history of mangrove establishment from São Francisco Bay (SF. Bay), 300 km away from the austral limit of mangroves, based on sedimentological, pollen, diatoms, elemental and stable isotope analyses ($\delta^{13}C$, $\delta^{15}N$, TOC, NT, C\N and C/S) of a 1 m sediment core.

2 MODERN SETTINGS

2.1 STUDY AREA, GEOLOGICAL AND GEOMORPHOLOGICAL SETTING

The study area is comprised of approximately 160 km² of estuarine complex, where occur mangrove tidal flats near São Francisco do Sul Bay (SF. Bay) in the north coast of Santa Catarina (S 26° 6'48.10"/ W 48°47'17.00"), south of Brazil (Figure 1) (Barros *et al.* 2010, Mazzer & Gonçalves 2011). The SF. Bay has an average depth and salinity of 6 m and 5‰ and was formed during the highstand of the last glacial cycle when the rising sea-level flooded river valleys (Mazzer & Gonçalves 2011). Pleistocene and Holocene sediments constitute the coastal plain of the study area (Angulo *et al.* 2009). Pleistocene sediments are characterized by intertidal marine and lagoon deposits, presenting elevations between 17 and 10 m (Horn Filho & Simó 2008). Holocene sediments are represented by aeolian, fluvial, and anthropogenic conchiferous deposits (shell-middens named "sambaqui") in addition to the marine and lagoon deposits (Horn Filho *et al.* 2014). The bay sector presents silt, clay, and fine to medium sandy sediments constituted by quartz and heavy minerals (Horn Filho & Simó 2008). The dune fields, coastal plains and fluvial plains constitute the coastal geomorphology (Hesp *et al.* 2009)

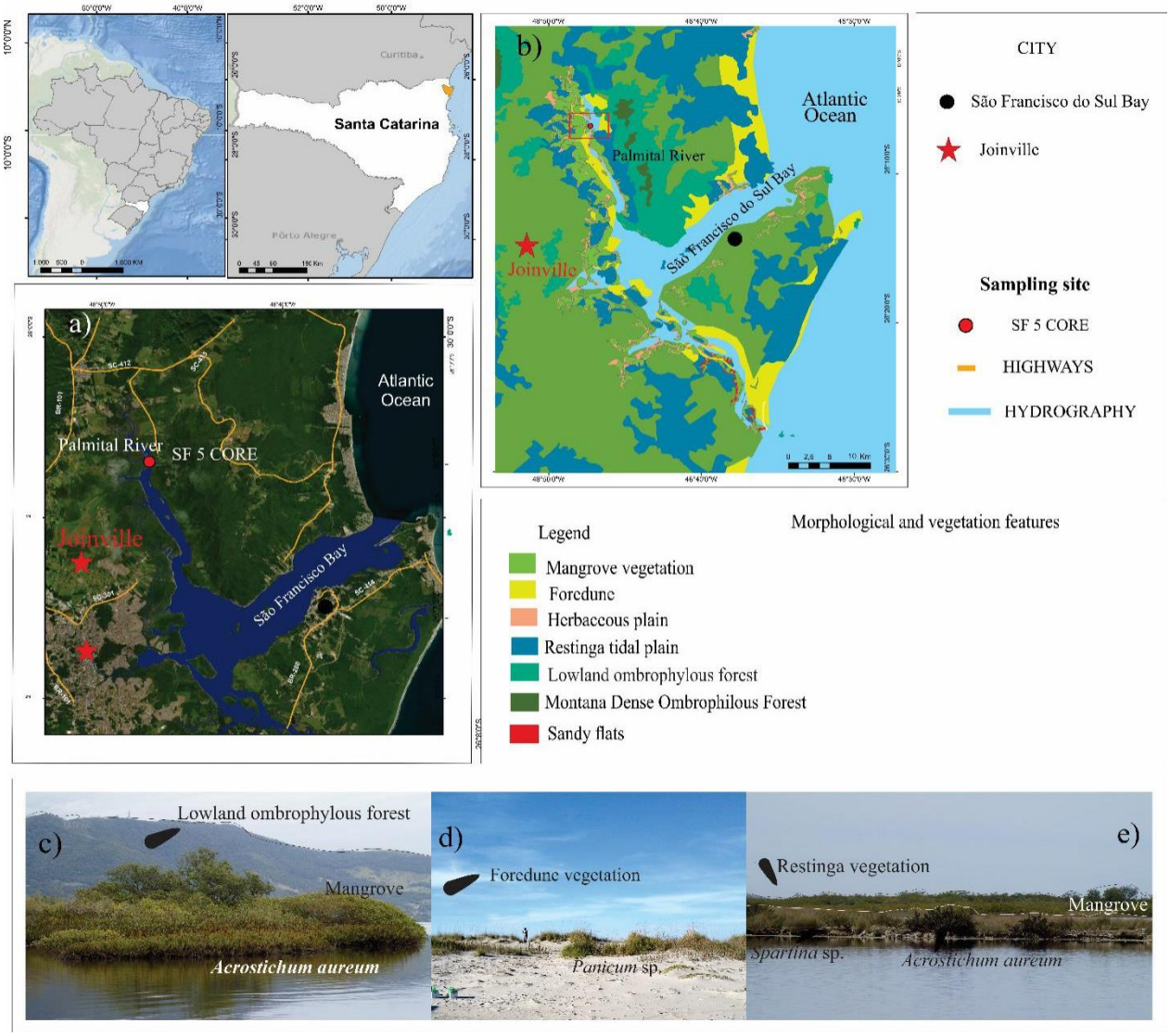

Fig 1- Location of the study area: (a) State of Santa Catarina (Brazil); (b) morphological and vegetation fetures (c) sampling site highlighting the Lowland ombrophilous forest, mangrove and *Acrostichum* vegetation; (d) Foredune vegetation with grass *Panicum* sp. and (e) the contact with restinga vegetation *(coastal woodland)*, mangrove and *Spartina*.

2.2 CLIMATIC AND OCEANOGRAPHIC SETTING

The study region is characterized by the wet subtropical climate "Cfa" (according to the Koppen's classification) with an average annual precipitation and temperature of ~2265 mm and ~20°C, respectively (Vieira 2008). The study area receives a great influence from the Serra do Mar slope, which acts as a natural barrier that traps moisture from the ocean resulting in high precipitation. Two distinct seasonality are identified, summer season from November to April and winter season from May to October. During summer, the weather is characterized by a high temperature and humidity, with intense precipitation. During winter, polar air

masses bring a cooler and drier climate to the region. (Grace *et al.* 2008). Cold fronts associated with the northward migration of Polar anticyclones occur throughout the year at a 1–2-week intervals but they are more intense and frequent during the winter (Garreaud 1999, Zular *et al.* 2013). In contrast, the warm-season precipitation (South Atlantic anticyclone) from late September to April is associated with the South American Summer Monsoon (SASM, Cruz *et al.* 2006). The SASM accounts for ~ 50% of the total summer precipitation at south Brazil (Cruz *et al.* 2006). In addition, the study area is characterized by semidiurnal microtides, with a mean and maximum tidal range of ~0.8 and 1.2 m (Trucollo 1998). The estuarine in SF. Bay circulates ~7. 8 x 10^8 m^3 of water, with a residence time of approximately 140 days (IME / DNIT, 2004, Mazzer & Gonçalves 2011).

2.3 VEGETATION

The vegetation in the study region can be categorized into 4 classifications: Atlantic rainforest, restinga (coastal woodland), beach dune, and mangrove (Gasper *et al.* 2012). The Atlantic rainforest is characterized by evergreen species with broad leaves, such as *Psychotria* (Rubiaceae), *Jacobinia carnea* (Acanthaceae), *Aphelandra liboniana* (Acanthaceae), *Salpinga margaritacea* (Melastomataceae), and *Macrocarpaea rubra* (Gentianaceae) (Ziffer-Berger 2008). The beach dune environments contain succulent plants with creeping roots, such as *Hydrocotyle* (Apiaceae) and *Ipomoea* (Covolvulaceae) (Alquini *et al.* 2018). The restinga communities can be divided into subgroups, well-drained sandbank consists of *Smilax* campestre (Smilacaceae), *Rumobbra antecediformis* (Dryopteridaceae), *Cordia curassavica* (Boraginaceae), *Dalbergia ecastaphyllum* (Fabaceae) and *Epidendrum fulgens* (Orchidaceae); and humid shrub restinga consists of *Dalbergia ecastaphyllum* (Fabaceae), *Schinus terebinthifolius* (Anacardiaceae), *Baccharis conyzoides* and *Baccharis singularis* (Asteraceae) (Silva & Britez 2005). In addition, mangrove forests grow on muddy and organic soil and form low and dense woody communities in the mid- to high tidal zones at the inner banks of the bay. In the mangrove forest, *Rhizophora mangle* (Rhizophoraceae), *Laguncularia racemosa* (Combretaceae), and *Avicennia schaueriana* (Acanthaceae) form the tree layer, and *Spartina* spp. and *Fimbristylis spadicea* (Cyperaceae) grow under the canopy. Epiphytic bromeliads and parasitic Loranthaceae and Viscaceae also prevail (Ziffer-Berger 2008).

3 MATERIALS AND METHODS

3.1 FIELDWORK AND REMOTELY-SENSED DATA

The sedimentary core SF05 (1.00 m depth; 26°6'48.10"S, 48°47'17.00"W) was retrieved in September 2015 via a Russian Peat Borer (USEPA 1999) from mangrove forest near the margins of the Palmital channel (Figure 1). The core was measured, photographed, and wrapped in the field and stored in a cold room (4°C) at CENA-USP Laboratory. A LANDSAT 7 image was obtained from INPE (National Institute of Space Research, Brazil) on spring, 2002. A three-color band composition (RGB 543) image was created and processed using the SPRING 3.6.03 image processing system to discriminate geological features. High spatial resolution images (2.6cm) of the study area was obtained by a Phantom 4 Advanced DJI drone. The drone images were processed using Agisoft Metashape Professional version 1.6.2 software, which provides photogrammetric processing of the digital images and generates 3D spatial data and orthomatics with a high level of precision (www.gisoft.com). Topographic data derived from SRTM-90 were also downloaded from the USGS Seamless Data Distribution System (https://dds.cr.usgs.gov/srtm/version2_1/SRTM3/). Image interpretation of elevation data was carried out using the Global Mapper software.

3.2 FACIES DESCRIPTION

The core was scanned with X-ray to identify sedimentary structures. Surface samples taken from the top 5 cm at each station were selected for grain-size analysis at the Laboratory of Chemical Oceanography/UFPA. For each sample, approximately 0.5 g of sediment was used, and Hydrogen peroxide was added to remove organic matters. Residual sediments were disaggregated by ultrasound. The distribution of sand (2–0.0625 mm), silt (62.5–3.9 µm), and clay fraction (3.9–0.12 µm) was determined following the methods developed by Wentworth (1922). Facies analysis involved a description of color (Color 2009), lithology, texture, and structure (Miall 1978).

3.3 DIATOMS ANALYSIS

The diatom processing followed the methods developed by Smol, 1986. Five samples consisted of ~1 cm^3 of sediments each were collected at a 25 cm interval consisting of five different depth levels. Each sample was pre-treated with 30% hot H_2O_2 and 10% hot HCL (Vermeulen & Gobert 2012). Diatoms identification was based on microstructural analysis of the silicified cell wall such as external layer, pore size, shapes and volume of diatoms (Bigunas

2005). For quantitative analysis, at least 500 valves was counted for each sample, and the percentage diatoms diagrams were plotted using Tilia and CONISS (Grimm & Troostheide 1994)

3.4 PALYNOMORPHS ANALYSIS

The sediment core was sub-sampled at intervals of 2 cm, which in $1cm^3$ of sediment was taken for palynological analysis. The samples were processed using conventional methods (Liu *et al.* 2008) and a minimum of 300 pollen grains were counted for each sample (except when pollen concentration was too low) to ensure the results are statistically significant. It was consulted pollen and spores reference collections (Lorente *et al.* 2017, Behling 1993), jointly with the reference collection of the Laboratory of Coastal Dynamics – Federal University of Pará and 14C Laboratory of the Center for Nuclear Energy in Agriculture (CENA/USP) to identify pollen grains and spores. The software TILIA and TILIAGRAF were used for calculation and to plot the pollen diagram (Grimm 1990). CONISS was used for cluster analysis of pollen taxa, permitting the zonation of the pollen diagram (Grimm 1987)

3.5 ISOTOPIC AND CHEMICAL ANALYSIS

A total of 20 samples (6–50 mg) were collected at 1–5 cm intervals from the sediment core. Sediments were treated with hydrochloric acid (HCl-2%) to avoid presence of carbonate and washed with distilled water until the pH reached 6, dried at 50ºC, and finally homogenized. These samples were analyzed for total organic carbon (TOC), total nitrogen (TN), stable isotopes of carbon and nitrogen, and total sulfur (TS) carried out at the 'Laboratório de Isótopos Estáveis' and 'Laboratório de Ciclagem de Nutrientes' of the Center for Nuclear Energy in Agriculture (CENA/USP), analyzed in an ANCA SL2020 mass spectrometer and Sulfur Analyzer SC 144DRLECO, respectively. The standard for sulfur analysis was 0.031% (dry soil), from 0.028% to 0.034%. The results are expressed as a percentage of dry weight, with analytical precision of 0.09% (TOC), 0.07% (TN), and 0.02% (TS) respectively. The $\delta^{13}C$ and $\delta^{15}N$ results are expressed VPDB standard and atmospheric air (Pessenda *et al.* 2004). Surface sediment samples (1 cm) were collected to verify the isotopic composition of modern organic matter. The application of carbon isotopes is based on the ^{13}C composition. Photosynthetic C3 cycle plants show values of $\delta^{13}C$ between −32 ‰ and −22 ‰ ($\bar{x}$ = -27. 0) and C4 plants present greater enrichment ranging from -17 ‰ to -9

‰ ($\bar{x}$ = -13.0 ‰). Phytoplankton and macrophytes has C:N ratio values from 4 to 10 while for terrestrial plants they have higher values (<12). For C3 plants derived from lacustre environments, isotopic values of $\delta^{13}C$ reaches of -28‰ and marine environments of -20‰ (Meyers 2003). Isotopic values of $\delta^{15}N$ closer to 0‰ and 10‰ are related of terrestrial and aquatic plants respectively (Ogrinc 2005).

3.6 RADIOCARBON DATING

A total of four bulk samples of ~2g each were taken for radiocarbon dating. These sediments were chemically treated and analyzed by Accelerator Mass Spectrometry (AMS) at 14C Laboratory of CENA/USP, LACUFF (Fluminense Federal University, Brazil) and Center for Applied Isotope Studies of Georgia University (UGAMS). The radiocarbon ages are reported in years before 1950 AD (yr. BP) and normalized to δ13C of −25‰ VPDB with a precision of 2σ (Reimer *et al.* 2020). (Table 1).

Table 1- Sediment samples selected for radiocarbon dating and results from SF-5 core (São Francisco Bay) with material, depth, $\delta^{13}C$, ^{14}C conventional and calibrated ages (using CALIB 6.0; Reimer *et al.* 2020).

Sediment core	Code site and laboratory number	Depth (m)	Ages (^{14}C yr BP, 1σ)	Ages (cal. yr BP, 2σ deviation)	Sedimentation rate (mm/yr)	Median of calibrated ages (cal. yr BP)
SF05	LACUFF180247	15-20	100.88 ± 0.340*	-	3.3 mm/yr	1958-1957
SF05	UGAMS34683	40-45	360 ±23	424-496	0.50 mm/yr	429
SF05	LACUFF180246	60-65	1540 ± 20	1452-1522	0.17 mm/yr	1462

4 RESULTS

4.1 VEGETATION

The study area is occupied by tropical ombrophilous forest represented mainly by Anacardiaceae, Arecaceae, Asteraceae, Bignoniaceae, Calophyllaceae, Chloranthaceae, Euphorbiaceae, Fabaceae, Lauraceae, Melastomataceae, Meliaceae, Myrtaceae, Piperaceae, Rubiaceae, and Urticaceae. The coastal dunes present restinga vegetation, mainly characterized by Asteraceae, Bromeliaceae, Dryopteridaceae, Fabaceae, Mytaceae, Rubiaceae and Poaceae. Tidal flats are occupied by mangroves (*Rhizophora mangle*, *Laguncularia racemosa* and *Avicennia germinans*) and Malvaceae (e.g. *Talipariti tiliaceum*), Polypodiaceae (e.g. *Acrostichum aureum*), and Ruppiaceae (e.g. *Ruppia maritima*). Forty-four genus and species of the most representative vegetation were identified at the study site and the $\delta^{13}C$ values ranged between -27. 3‰ to -25. 9‰ and indicate a predominance of C3 plants (Figs 2 and 6).

4.2 RADIOCARBON AGES AND SEDIMENTATION RATES

Radiocarbon dates ranged from 1462 cal yr BP to 1958 AD (Fig 2 - Table 1) and indicated the following sedimentation rates: 0.17 mm/yr (65 to 42 cm depth), 0.50 mm/yr (42 to 20 cm depth), and 3.3 mm/yr (20 – 0 cm depth) supporting the range recorded in other cores (0.1 to 3 mm/year) sampled along the Brazilian coast (França *et al.* 2018).

5 FACIES DESCRIPTION

Three facies associations were recognized in the studied core (Fig 3). Facies association "A" consists of massive sand (facies - Sm) and lenticular heterolithic bedding deposits (facies - Hl), and it is related to tidal channel dynamics. The facies association "B" consists of massive mud deposits (facies - Mm), related to a tidal flat environment. The top of SF05 core is represented by facies association "C", formed by massive mud (Mm) and wavy heterolithic bedding deposits (Hw), and these sediments were also accumulated under a tidal flat influence. These environments were interpreted based on the integration of sedimentary features, palyno-diatoms description and elemental and isotopic values (δ13C, δ15N, TOC, TN, C/N and C/S).

5.1 FACIES ASSOCIATION A (TIDAL CHANNEL)

Facies association "A" corresponds to depth interval from the 100 to 75 cm accumulated before 1462 cal yr BP, and it consists of int dark brown sediment (2.5/110Y) with massive sand (Sm) and lenticular heterolithic bedding deposits (Sm - Hl; 10 - 95 % sand, 5 - 70% silt, 0-19% clay). Root traces and physical structures produced by the benthic community are visible. The pollen assembly revealed four ecological groups (Figs 2 and 3): trees and shrubs pollen (0-70%), herbs (0-41%), palms (0-67%) and aquatic plants (0-28%). The trees and shrubs taxa are predominantly composed by *Braccharis* (0-34%), *Marlierea* (0-30%), *Forsteronia* (0-27%), *Dalbergia* (0-20%), *Eugenia* (0-20%), *Cordia* (0-18%), *Ilex* (0-18%), Myrtaceae (0-15%), *Opundia* (0- 20%), *Mikania* (0-7%) and *Handroanthus* (0-10%). Herbs taxa are mainly represented by Cyperaceae (0-30%), *Alternanthera* (0-30%), *Ipomea* (0-20%), *Sisyrinchium* (0-9%), Poaceae (0-8%), Asteraceae (0-6%). Aquatic plants were represented by *Cyperus* (0-28%) as well as restinga palm (restinga vegetation occurs mean coastal sandy soils) composed by *Butia* (0-40%) (Fig. 2). Marine indicators were defined by microforaminifera as well as *Acritarchs* cysts and others dinoflagellates (Figs 2 and 3). This facies association consists in 91% of marine diatoms taxa, 8% estuarine taxa and 1% freshwater diatoms taxa (Fig 4). Marine diatoms are represented by *Skeletonema costatum* (10%), *Actinoptychus senarius* (8%), *Coscinodiscus rothii* (7%), *Thalassionema synedriforme* (6%), *Triceratium* sp.(6%), *Nitzschia fasciculate* (5%), *Thalassionema nitzschioides* (5%), *Corethron criophilum* (4%), *Navicula rhaphoneis* (4%), *Minidiscus* sp. (4%), Cymatodiscus *planetophorus* (4%), *Psammodictyon panduriforme* (4%), *Thalassionema synedriforme* (4%)

and *Coscinodiscus* sp. (3%). Estuatine taxa is composed by *Navicula binodulosa*(3%), *Pleurosigma* spp.(1%), *Cylindrotheca closterium*(1%), *Thalassiosira* sp.(1%) and *Thalassionema nitzschioides*(1%.) Freshwater diatoms are represented by *Nitzschia* sp.(1%). The $\delta^{13}C$, $\delta^{15}N$, TOC, TN, C/N and C/S values range between -26.8‰ – -25.9‰ ($\overline{x}$ = - 26.3‰), 3.9 to 1.3 ($\overline{x}$ = 2.1‰), 8.7 to 1.8($\overline{x}$ = 5.2%), 0.62 to 0.06 ($\overline{x}$ = 0.3%), 18 to 14 ($\overline{x}$ = 16) and 1.8 to 0.2 ($\overline{x}$ = 1.0), respectively (Fig. 3).

5.2 FACIES ASSOCIATION B (TIDAL FLAT WITH SALTMARSHES)

Facies association "B" corresponds to the depth interval 75 - 52 cm and consists of light olive gray deposits with massive mud (Mm; 11-14% sand, 69-71% silt, 15-16% clay), (5Y5/2). The pollen assemblages are composed by four ecological groups (Fig 3): Trees and shrubs (53-68%), herbs (22-37%), aquatics plants (4-7%) and restinga (1-5%). Arboreal pollen are represented by *Braccharis* (5-6%), *Mikania* (3-6%), *Myrsine* (3-6%), Myrtaceae (2-6%), *Ilex* (2-6%), *Erythrina*(1-6%), *Myrcia*(2-5%), *Annona*(0-4%), *Schinus*(2-4%), *Forsteronia*(1-3%), *Maytenus*(0-3%), *Handroanthus(*1-2%), *Miconia*(0-2%), *Pera*(0-2%), *Pouteria*(0-2%), *Struthanthus* (0-2%), *Dalbergia* (0-2%), *Cordia* (0-2%), *Guatteria* (1-2%), *Psychotria* sp. (0-2%), *Marlierea* (0-2%), *Symplocos* (0-2%) and *Ricinus* (0-1%). Herbs are characterized by Poaceae (5-9%), Asteraceae (5-6%), *Solanum* (1-4%), *Scoparia* (1-4%), Euphorbiaceae (0-4%), Cyperaceae (1-4%) and *Sisyrinchium* (0-1%). Palms genus (*Euterpe* and *Butia*) and aquatic pollen (*Typha* and *Cyperus*) are below 3%. Ferns are composed mostly by *Asplenium* (0-1%). Marine indicators are absent along this facies association (Fig 2 and 3). It consists in 82% marine, 13% estuarine and 5% freshwater diatoms taxa (Fig 4). The marine diatoms taxa is represented by *Skeletonema costatum*(8%), *Thalassionema synedriforme* (4%), *Triceratium* sp.(6%), *Corethron criophilum*(5%), *Navicula rhaphoneis*(6%), *Actinoptychus senarius* (6%), *Coscinodiscus rothii*(7%), Nitzschia fasciculate(4%), Thalassionema nitzschioides (4%), Minidiscus sp.(5%), Cymatodiscus planetophorus(4%), *Coscinodiscus* sp.(4%), *Thalassionema synedriforme* (4%) and *Psammodictyon panduriforme* (3%). Estuarine diatoms taxa is composed by *Navicula binodulosa*(4%), *Pleurosigma* spp. (2%), *Cylindrotheca Closterium*(2%), *Thalassiosira* sp.(2%) and *Thalassionema nitzschioides*(1%). Freshwater diatoms are represented by *Nitzschia* sp.(3%) and *Fragilaria capucina*(1%). The $\delta^{13}C$ shows stable values of -26.6 to -26.7 ‰ ($\overline{x}$ = - 26.6‰). The $\delta^{15}N$ record indicate values range 0.9 to 1.3‰ ($\overline{x}$ = 1.1‰). TOC and NT results were also relatively

stable between 8.7 to 9.7% ($\bar{x}$ = 9.3%) and 0.5 to 0.6% ($\bar{x}$ = 0.6%) respectively. The C/N and C/S ratio alternated between 13.9 to 17.0 ($\bar{x}$ =15.4) and 1.9 to 2.7($\bar{x}$ =2.3) respectively (Fig. 3).

5.3 FACIES ASSOCIATION C (TIDAL FLAT WITH MANGROVES)

Facies association "C" were inferred for the 52 – 0 cm interval, accumulated during the last 1462 cal yr BP. Mangrove tidal flat deposits consist of greenish gray 4/1 10Y to dark brown (2.5/110Y) sediments with massive mud and wavy heterolithic bedding (Mm-Hw; 9-80 % sand, 13-73% silt, 3-16% clay). Pollen record revealed five ecological groups: 1) Mangrove, represented by *Laguncularia* (0-9%), *Avicennia* (0-1%) and *Rhizophora* (0-1%); 2). Trees and shrubs, composed by *Braccharis*(2-7%), Myrtaceae(0-7%), *Ilex*(0-7%), *Shinus* (4-6%), *Myrcia* (2-6%), *Senna* (0-6%), *Myrsine*(0-6%), *Hibiscus tiliaceus*(2-6%), *Annona* (2-5%), *Handroanthus*(0-4%), *Maytenus*(0-3%), *Dalbergia*(0-4%), *Pinus*(0-3%); 3) Herbs, characterized by Poaceae(7-27%), Asteraceae(5-10%), *Spartina*(0-7%), *Solanum*(0-2%), *Scoparia*(0-6%), Euphorbiaceae(0-6%), Amaranthaceae(0-4%); 4) Aquatic plants, represented by *Eichhornia*(0-5%), *Typha*(0-4%), and *Cyperus*(0-3%); and 5) Palms, exemplified by *Euterpe*(0-7%) and *Butia*(0-2%). Ferns were composed by Polypodiaceae and *Acrostichum sp*., associated with mangrove vegetation (Fig 2). It consists of marine (56%), estuarine (27%) and freshwater (17%) diatoms taxa. Marine diatoms taxa are represented by *Skeletonema costatum*(6%), *Thalassionema synedriforme*(6%), *Triceratium sp*.(5%), *Corethron criophilu*(4%), *Navicula rhaphoneis*(4%), *Actinoptychus senarius*(4%), *Coscinodiscus rothii*(2%), *Nitzschia fasciculate*(3%), *Thalassionema nitzschioides*(2%), *Minidiscus sp*.(2%), *Cymatodiscus planetophorus*(2%), *Psammodictyon panduriforme*(2%), *Coscinodiscus sp*.(2%). Estuatine taxa is composed by *Navicula binodulosa*(2%), *Pleurosigma sp*.(6%), *Cylindrotheca Closterium*(5%), *Thalassiosira sp.*(4%), *Thalassionema nitzschioides*(4%), *Cyclotella sp.*(3%) and *Diploneis smithii*(1%). The freswarer diatoms are represented by *Nitzschia sp.(*5%), *Fragilaria sp.*(2%), *Fragilaria capucina*(2%), *Nitzschia angustata*(2%), *Cyclotella meneghiniana*(2%), *Aulacoseira granulata*(1%) and *Rhopalodia gibberula*(1%) (Fig 4). The $\delta^{13}C$ (‰) and $\delta^{15}N$ (‰) results were between -27. 2 to -26. 4 ‰ ($\bar{x}$ = -26.8‰) and 3.0 to 1.1 ‰ ($\bar{x}$ =2.0‰), respectively. TOC, NT values and C/N and C/S ratio ranged 3 to 10% ($\bar{x}$ = 7.3%), 0.2 to 0.6% ($\bar{x}$= 0.5%), 12.7 to 18.2 ($\bar{x}$ = 14.2) and 1.7 to 6.1 ($\bar{x}$ = 3.9), respectively (Fig 3)

6 DISCUSSION

Therefore, multi-proxy data recorded along the core SF05 suggests three environmental phases during the Late Holocene: 1) Tidal channel, 2) tidal flat with saltmarshes, 3) and tidal flat with mangroves.

6.1 PHASE I - FACIES ASSOCIATION "A"-TIDAL CHANNEL

This phase is characterized by a tidal channel with trees and shrubs, herbs, restinga palms, and aquatic plants along its margin. No mangrove pollen was recorded during this phase, despite the estuarine influence at the study site. Southern Brazilian restinga is associated with edaphic factors (e.g. substrate under brackishwater influence) and occurring near the coastline (Korte *et al.* 2013). Biological indicators of marine environments (e.g microforaminifera, marine diatoms, *acritarchs* cysts and others dinoflagellates) also suggest a coastal sedimentary environment under marine influence. *Acritarchs* cysts are characteristic of shallow coastal water (Félix & Souza 2012). The binary diagram $\delta^{13}C$ ($\overline{x}$ = - 26.3‰) and C/N values ($\overline{x}$ = ~16) indicated contributions of C3 terrestrial plants, marine and freshwater algae to the sedimentary organic matter (Fig 6)

6.2 PHASE II - FACIES ASSOCIATION "B"- TIDAL FLAT WITH SALTMARSHES

Facies Association "B" (75 - 55 cm depth) is marked by the formation and expansion of tidal mudflat under estuarine influence. The increase of ferns (Figs 2 and 3) – a typical freshwater indicator (Rodrigues *et al.* 2021), estuarine diatom species (Fig 4), as well as the binary diagram of S vs. TOC (Fig 5) also support this interpretation. The relation of S and TOC (Fig 5) can provide information about the marine or freshwater origin of the sediments (Berner & Raiswell 1984, Lorente *et al*. 2020). In addition, no mangrove pollen grains were found in this phase, suggesting that the physical conditions, probably temperature, in our study area did not permit the establishment of mangroves (Toniolo *et al.* 2020). The relationship between $\delta^{13}C$ vs C/N values indicates the predominance of C3 plants in freshwater/estuarine environment (Fig 6) (Meyers 2003) represented by mostly arboreal trees and herbs that occurred along tidal flat around ~1462 cal yr BP (Fig 3)

6.3 PHASE III - FACIES ASSOCIATION "C"- TIDAL FLAT WITH MANGROVE

Phase III (50 - 0 cm) is marked by the expansion of *Laguncularia* trees on the tidal flats since ~1000 cal yr BP, followed by the establishment of *Avicennia* at ~500 cal BP

and *Rhizophora* since the early 20th century (Fig 2). According to the binary diagram ($\delta^{13}C$ vs. C/N) (Fig. 6), the organic matter in Phase III is mainly sourced from C3 plants growing in freshwater-estuarine conditions. This interpretation is supported by microfossil analyses and abundant ferns and freshwater-estuarine diatoms (Fig. 4), and isotope data, suggesting an increased contribution of estuarine organic matter (Meyers 1994, δ15N ~5.0‰, Sukigara & Saino 2005). These data indicate that *Laguncularia* established and prevailed in a low-salinity environment predominantly influenced by freshwater. Nearby the study area, rivers and several streams (Barros *et al.* 2010) converge, resulting in low salinity (~5‰) in the SF. bay (França *et al.* 2018*). Laguncularia* likely was established in the upper estuary, where freshwater output from the rivers exerts more influence than seawater from the Atlantic Ocean.

7 MANGROVE ESTABLISMENT AND CLIMA

Pollen result of core SF-5 shows that our study site was dominated by saltmarshes represented by *Spartina* sp. (Fig 2 - 55cm depth) until *Laguncularia* establishment at ~1000 cal yr BP, followed by *Avicennia* and *Rhizophora* at ~500 cal yr BP and 1950 AD (Figs 2 and 3). Previous studies across South and North America revealed that the mangrove habitats were previously colonized by saltmarsh species (e.g., *Spartina* sp) under a stable environmental condition (Cunha-Lignon *et al*. 2009, Yao *et al.* 2015, Yao & Liu 2017). Saltmarshes act as a sediment fixator that reduces erosion and facilitates the establishment of *Laguncularia* and *Avicennia*. Thus, our pollen record indicates that the environmental conditions at the study site were gradually becoming more suitable to sustain a mangrove population at ~1000 cal yr BP.

The main factors controlling the mangrove establishment are temperature, sea-level changes, precipitation, and human activities (Blasco *et al.* 1996, Osland *et al.* 2016, Ward *et al.* 2016, Saintilan *et al.* 2020). Along the southern and northeastern Brazilian coast, the relative sea-level gradually fell during the late-Holocene (Angulo *et al.* 2006), causing a coastal progradation with mangroves along the tropical latitudes. These forests were first established at northern and northeastern Brazilian littoral (1º - 19º S) at ~7000 cal yr BP (Cohen *et al.* 2012, 2014, 2020a, Pessenda *et al.* 2012, França *et al.* 2013, 2015, Fontes *et al.* 2017, Ribeiro *et al.* 2018), and migrated further south (São Paulo, 25º S at ~2200 cal yr BP, Santa Catarina, 28º S, in recent decades) due to warming temperature during the late-Holocene (Cohen *et al.* 2020). *Laguncularia* and *Avicennia* has been documented to be more tolerant to cold temperature (Melo *et al.* 2011, Quisthoudt *et al.* 2012, Duke *et al.* 1998). Therefore, the establishment succession of mangrove genera: *Laguncularia*, *Avicennia* and *Rhizophora* during the last 1400 cal yr BP in the study area, which situates at ~300 km to the southern limit of American mangrove (28º 29`S) (Cohen *et al.* 2020b), may be attributed to an increasing trend of temperature during the late-Holocene.

During the mid-late-Holocene, strengthened solar insolation has been documented to be the prominent cause of mangrove expansion in their latitudinal limits (Prado *et al.* 2013, Quisthoudt *et al.* 2012). In particular, the establishment of *Laguncularia* at our study area coincided with the medieval climatic anomaly (MCA, ~1000–700 cal years BP). It is reasonable to believe that the warmer climate during MCA further accelerated the

establishment and expansion of mangroves at their austral limit and facilitated the colonization *of Laguncularia* in SF Bay. However, why did *Rhizophora* show up at a much later time? It has been well documented that *Laguncularia* and *Avicennia* are more tolerant to cold temperatures than *Rhizophora* (Duke *et al.* 1998). Thus, it is easy to understand the recent establishment of *Rhizophora* during the Current Warm Period (CWP, since the early 20th century). As for *Avicennia,* a simpler explanation will be the particular strand of *Laguncularia* in South American is more cold-tolerant than *Avicennia*, and the Sea Surface Temperature (SST) and physiological differences among different mangrove species may also played an important part in the subsequent colonization of mangroves along southeastern Brazilian coast (Duke *et al.* 1998). Previous studies have documented that the propagules of *Rhizophora* cannot tolerate low SST (≤17˚C), and no *Avicennia* seedling germination would have occurred if the SST is < 15 ˚C. On the other hand, *Laguncularia* propagules can survive in an environment where SST is lower than ≤15 ˚C (Oliveira 2005). This may explain the pioneering population formation of *Laguncularia* at SF. Bay (Ximenes *et al.* 2018). Alternatively, this phenomenon might be related to the coincidence of *Avicennia* establishment (~500 cal yr BP) during the Little Ice Age (LIA, ~700-100 cal yr BP). It is possible that the colder than usual climate during the LIA destabilized the dominance of *Laguncularia* at SF Bay and facilitated the expansion of *Avicennia*. In particular, the 3 climate intervals - the MCA, LIA, and CWP are characterized by significant temperature fluctuations in South America (Ledru *et al.* 2013), and are clearly visible throughout the pollen record (Fig. 2). Thus, it is reasonable to believe that they likely have influenced the mangroves establishment and succession at SF. Bay.

In addition, the IPCC report indicates that the current global temperature is ~1.0°C warmer than the pre-industrial era, and the warming trend will continue by the mid of the 21st century (Allen *et al*. 2018). Moreover, decades warmer than usual years have become more frequent in south Brazilian coastal region and the temperature is ~1.5°C above the mean temperature in Brazil (Bernardino *et al.* 2015). Furthermore, the temperature is expected to increase ~3 to 5°C by the end of the 21st century due to greenhouse gases increase (Marengo *et al.* 2009). Therefore, while our data suggest that the poleward mangrove migration along the Brazilian coast is related to the fluctuation of solar insolation during the late Holocene, the mangrove expansion was also accelerated by the industrial-era warming marked by the arising of *Rhizophora* at SF. Bay (Fig. 2). Overall, the findings of this study are in line with

the previous record that the SF. Bay experienced an increase in air and sea surface temperature during the late-Holocene that enabled the colonization and expansion of mangroves (França *et al.* 2019).

8 CONCLUSION

Sedimentary features, pollen - diatoms, and isotopes data along core, as well as geomorphological and vegetation analyses indicated the estableishment of tidal flats since > 1462 cal yr BP in the study area. From the physicochemical and hydrodynamic point of view, environmental conditions were favorable for the establishment and expansion of mangroves in the studied area during the late Holocene. Mangroves were established along the tropical (2º N – 19º S) and subtropical (25º - 26º S) Brazilian coast, as a consequence of the stabilization or low rates of sea-level rise/fall around the mid Holocene, and the late Holocene warming, respectively. The establishment of mangroves mainly represented by *Laguncularia*, *Avicennia* and *Rhizophora* trees on the studied tidal flats (26º 20´S) only began at ~1000, ~500 cal yr BP and ~1950 AD, respectively. Nowadays, in the study area, saltmarshes, mainly characterized by *Spartina* and *Acrostichum* are sharing tidal flats with mangroves, represented by *Laguncularia*, *Avicennia* and *Rhizophora*. Probably, the Anthropocene *Rhizophora* establishment and expansion are associated with a migration of the austral mangrove limit into the temperate zone, caused by the gradual increase in winter temperatures. This process may be related to a poleward mangrove migration since the late Holocene, caused by a natural Holocene global warming. However, the industrial-era warming must have accentuated the mangrove expansion into temperate zones.

Acknowledgements

We would like to thank the members of the Laboratory of Costal Dynamic (LADIC-UFPA), Center for Nuclear Energy in Agriculture (CENA-USP), the students from Laboratory of Chemical-Oceanography (UFPA), and Laboratory of C-14 (CENA-USP) for their support. This study was financed by FAPESP (2020/13715-1) and the Brazilian Council for Technology and Science-CNPq (Project # 307497/2018-6).

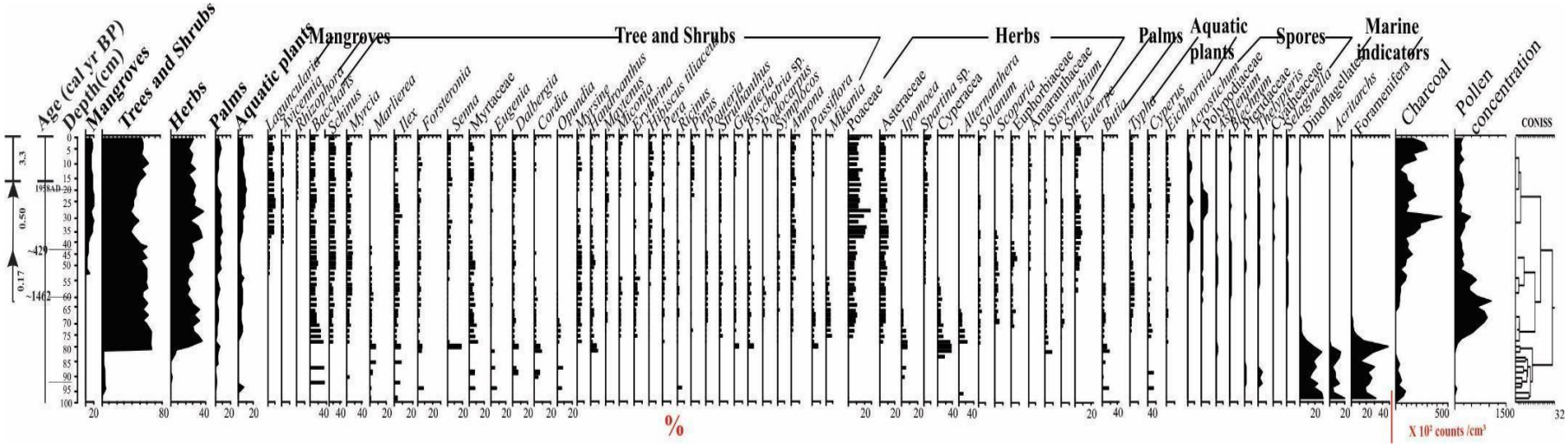

Fig. 2- Chronological profile with sedimentary facies and pollen diagram with zones based on cluster analysis for SF05 core

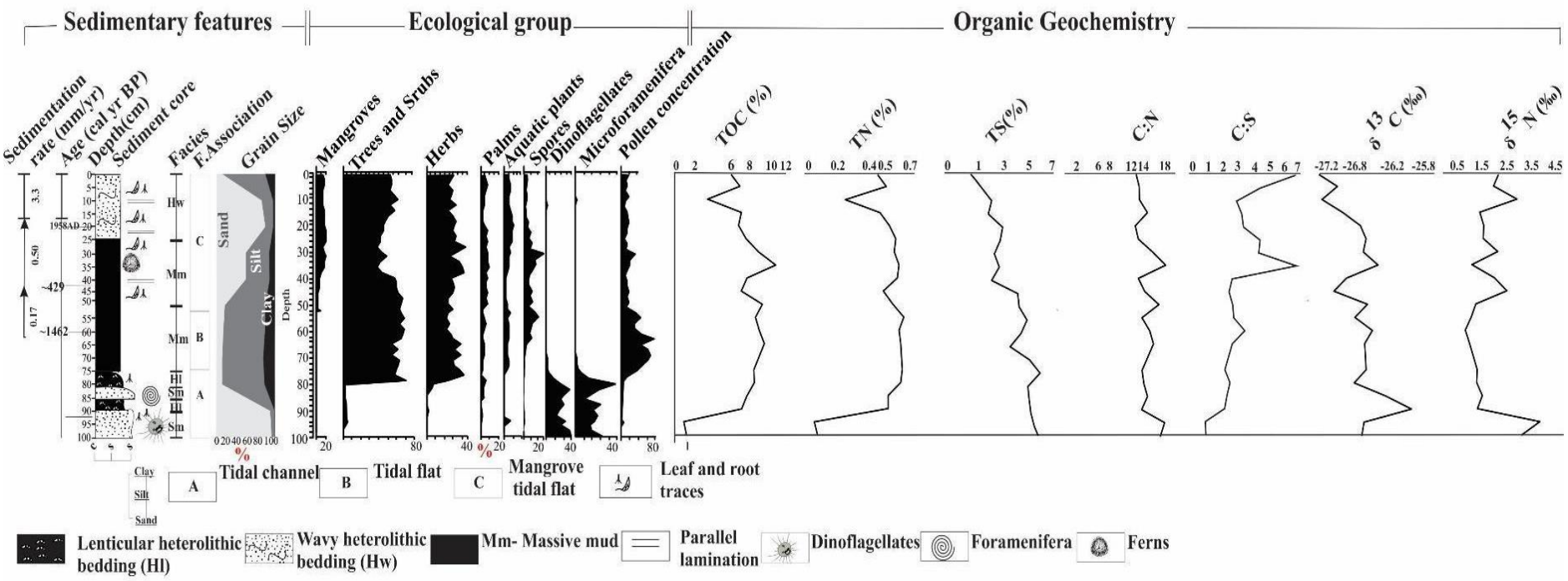

Fig. 3- ^{14}C dates, sedimentary, ecological group organic and geochemistry variables diagram for SF05 core

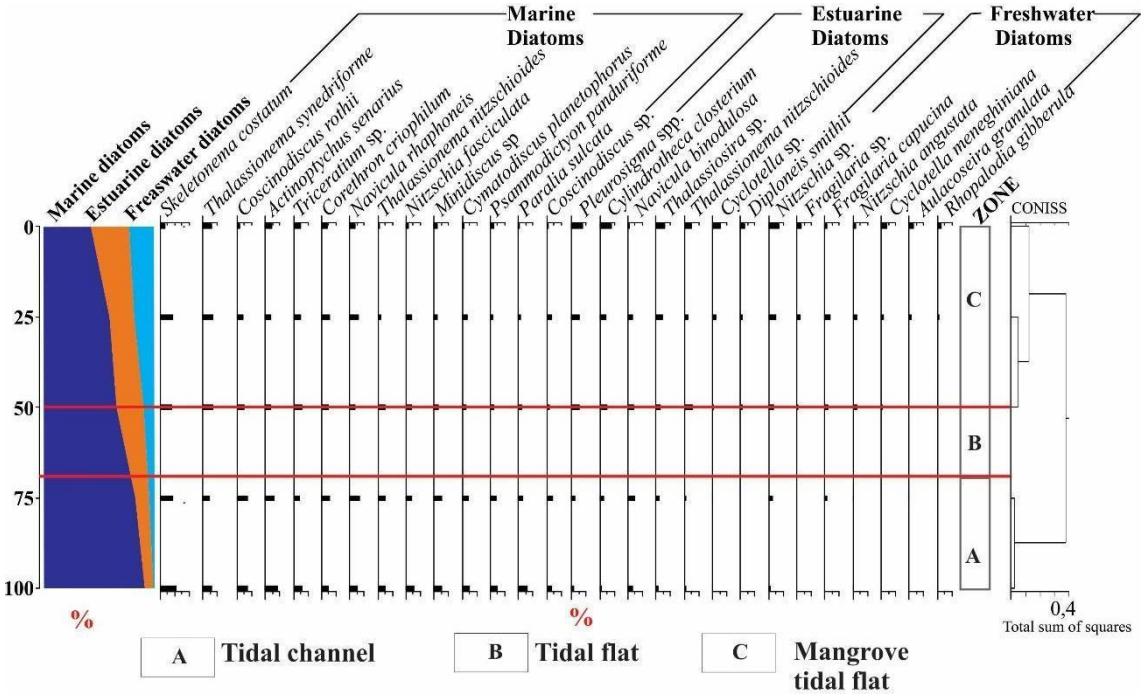

Fig. 4- Relative frequencies (%) of diatoms

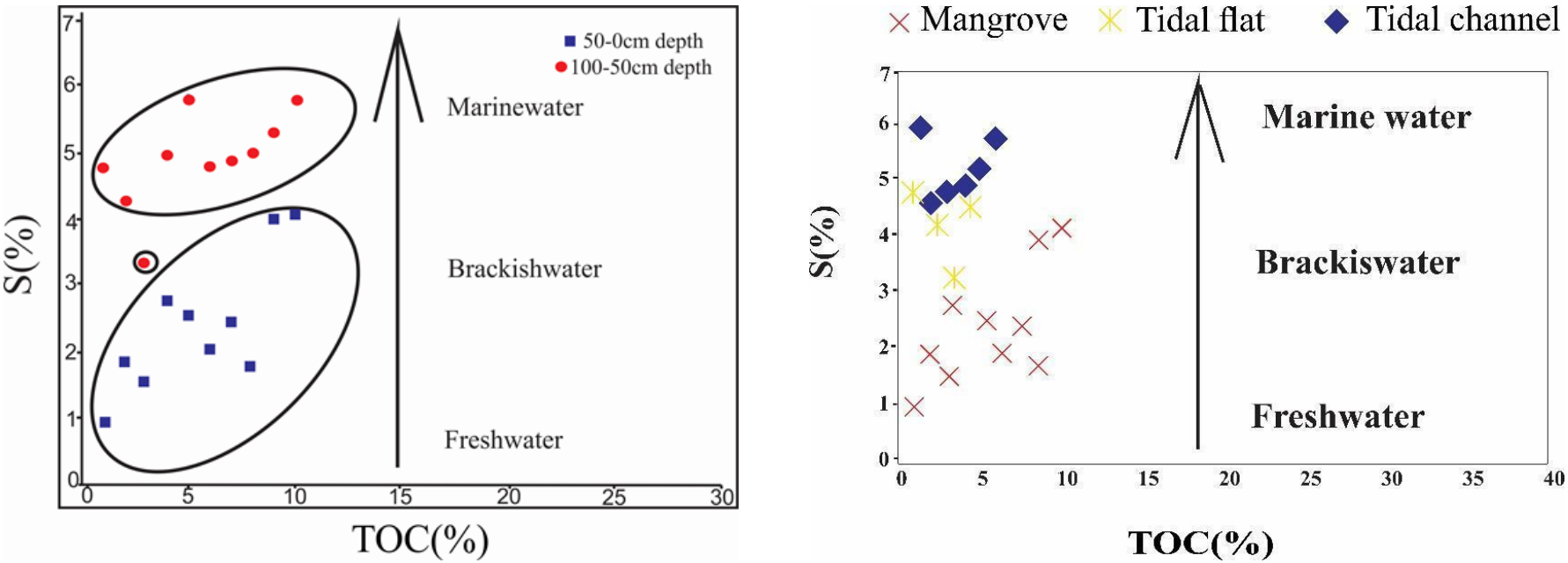

Fig. 5- S vs. TOC of SF05 organic matter. The interpretation was based on data by Lorente *et al*. (2020).

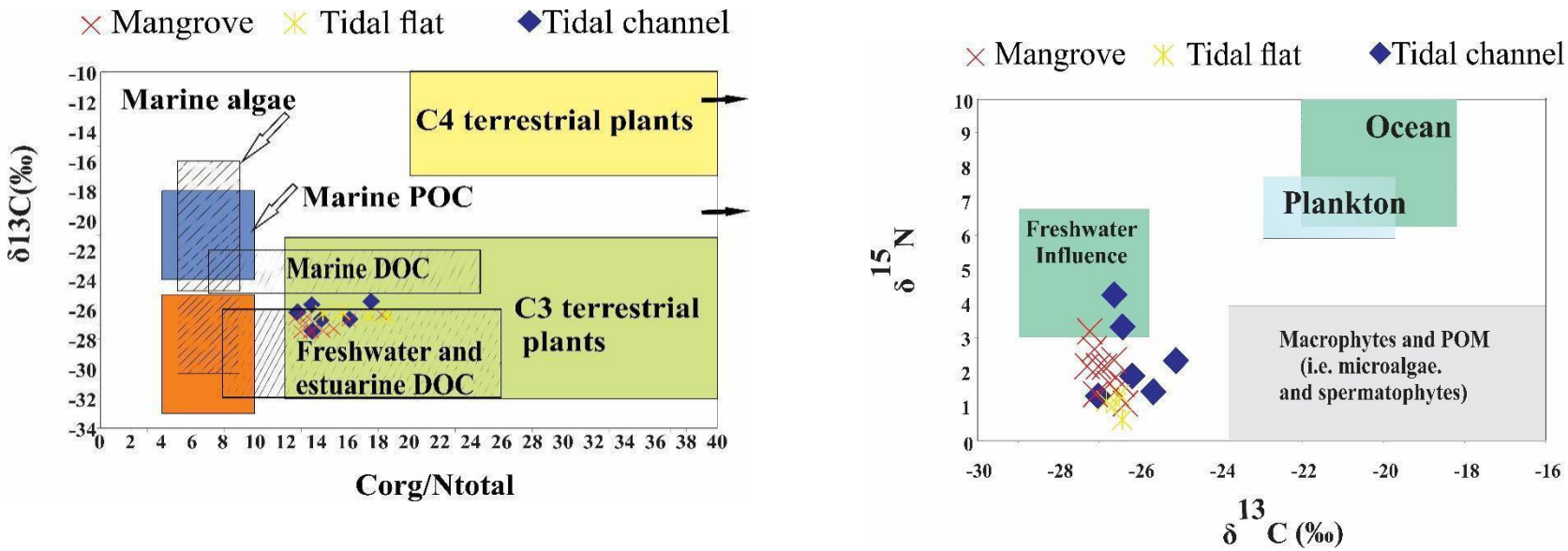

Fig. 6- Binary diagram illustrating **δ13** vs. Corg/Norg and $\delta^{15}N$ vs. δ^{13} of SF5 core for the different sedimentary facies association.

REFERENCE

Angulo R. J., Lessa G. C., Souza M. C.de. 2006. A critical review of mid-to late-Holocene sea-level fluctuations on the eastern Brazilian coastline. *Quaternary science reviews*, **25**(5-6): 486-506. https://doi.org/:10.1016/j.quascirev.2005.03.008.

Angulo R. J., Souza M. C.de, Lessa G. C. 2009. The Holocene barrier systems of Paranaguá and northern Santa Catarina coasts, southern Brazil. *In:* Dillenburg Sérgio R. & Hesp Patrick A. *Geology and geomorphology of Holocene Coastal Barriers of Brazil*. Berlin, Heidelberg, Springer, p. 135-176. https://doi.org/10.1007/978-3-540-44771-9_5.

Alongi D. M. 2015. The impact of climate change on mangrove forests. *Current Climate Change Reports*, **1**(1): 30-39. https://doi.org/10.1007/s40641-015-0002-x.

Alquini F., Bertoni D., Sarti G., Vieira C. V., Melo Júnior J. C. F. 2018. Morpho-sedimentological and vegetational characterization of Grande beach at São Francisco do Sul island (Santa Catarina, Brazil). *Journal of Maps*, **14**(2): 105-113. https://doi.org/10.1080/17445647.2018.1438317.

Barros G. V., Martinelli L. A., Novais T. M. O., Ometto J. P. H., Zuppi G. M. 2010. Stable isotopes of bulk organic matter to trace carbon and nitrogen dynamics in an estuarine ecosystem in Babitonga Bay (Santa Catarina, Brazil). *Science of the Total Environment*, **408**(10): 2226-2232. https://doi.org/10.1016/j.scitotenv.2010.01.060.

Behling H. 1993. *Untersuchungen zur spätpleistozänen und holozänen Vegetations- und Klimageschichte der tropischen Küstenwälder und der Araukarienwälder in Santa Catarina* (Südbrasilien). Dissertationes Botanicae 206; Cramer, Berlin, Stuttgart: J. Cramer https://doi.org/10.1016/S0034-6667(97)00044-4.

Berner R. A. & Raiswell R. 1984. C/S method for distinguishing freshwater from marine sedimentary rocks. *Geology*, **12**(6): 365-368. https://doi.org/10.1130/0091-7613(1984)12<365:CMFDFF>2.0.CO;2.

Bernardino A.F., Antonio Netto S., Pagliosa P.R., Barros F., Christofoletti R.A., Rosa Filho J.S., Colling A., Lana P.C. 2015. Predicting ecological changes on benthic estuarine assemblages through decadal climate trends along Brazilian Marine Ecoregions. *Estuarine, Coastal and Shelf Science*, **166**(Part A): 74–82. https://doi.org/10.1016/j.ecss.2015.05.021.

Bigunas P.I.T. 2005. *Diatomáceas (Ochrophyta) do rio Guaraguaçu, litoral do Paraná, Brasil*. Dissertation, Universidade Federal do Paraná, Curitiba,482p.

Blasco F., Saenger P., Janodet E. 1996. Mangroves as indicators of coastal change. **Catena**, **27**(3-4): 167-178. https://doi.org/10.1016/0341-8162(96)00013-6.

Cavanaugh K. C., Osland M. J., Bardou R., Hinojosa-Arango G., López-Vivas J. M., Parker J. D., Rovai A. S. 2018. Sensitivity of mangrove range limits to climate variability. *Global Ecology and Biogeography*, **27**(8): 925-935. https://doi.org/10.1111/geb.12751.

Clark P. U., Dyke A. S., Shakun J. D., Carlson A. E., Clark J., Wohlfarth B., McCabe A. M. 2009. The last glacial *Maximum science*, **325**(5941): 710-714. https://doi.org/10.1126/science.1172873.

Cohen M. C. L., Pessenda L. C. R., Behling H., Rossetti, D. de Fátima, França M. C., Guimarães J. T. F., Smith C. B. 2012. Holocene palaeoenvironmental history of the Amazonian mangrove belt. *Quaternary Science Reviews*, **55**: 50-58. https://doi.org/ 10.1016/j.quascirev.2012.08.019.

Cohen M. C. L., França M. C., Rossetti D. de Fátima, Pessenda L. C. R., Giannini P. C. F., Lorente F. L., Macario K. 2014. Landscape evolution during the late Quaternary at the Doce River mouth, Espírito Santo State, southeastern Brazil. *Palaeogeography, Palaeoclimatology, Palaeoecology***, 415**: 48-58. https://doi.org/10.1016/j.palaeo.2013.12.001.

Cohen M. C., Rodrigues E., Rocha D. O., Freitas J., Fontes N. A., Pessenda L. C., Bendassolli J. A. 2020. Southward migration of the austral limit of mangroves in South America. *Catena*, **195**: 104775.https://doi.org/10.1002/esp.4737.

Cruz Jr F. W., Burns S. J., Karmann I., Sharp W. D., Vuille M. 2006. Reconstruction of regional atmospheric circulation features during the late Pleistocene in subtropical Brazil from oxygen isotope composition of speleothems. *Earth and Planetary Science Letters*, **248**(1-2): 495-507.https://doi.org/ 10.1016/j.epsl.2006.06.019.

Cunha-Lignon M., Menghini R. P., Santos L. C. M., Niemeyer-Dinóla C., Schaeffer-Novelli Y. 2009. Estudos de Caso nos Manguezais do Estado de São Paulo (Brasil): Aplicação de Ferramentas com Diferentes Escalas Espaço-Temporais. Revista de Gestão Costeira Integrada-*Journal of Integrated Coastal Zone Management*, **9**(1): 79-91. http://dx.doi.org/10.5894/rgci125.

Departamento Nacional de Infra-Estrutura de Transportes (DNIT). Instituto Militar de Engenharia (IME). 2004. *Diagnóstico dos estudos de circulação de água no Canal do Linguado e na Baía da Babitonga*. Disponível em http://www.centran.eb.br/br_280_03.htm. March 20 2021.

Duke N., Ball M., Ellison J. 1998. Factors influencing biodiversity and distributional gradients in mangroves. *Global Ecology & Biogeography Letters*, **7**(1): 27-47.

Dunn R. J., Stanitski D. M., Gobron N., Willett K. M., Ades M., Adler R., Arosio C., 2020. *Global climate. Bulletin of the American Meteorological Society*, **101**(8): S9-S127. https://doi.org/10.1175/BAMS-D-20-0104.1.

Ellison A. M. 2002. Macroecology of mangroves: large-scale patterns and processes in tropical coastal forests. *Trees*, **16**(2-3): 181-194. https://doi.org/10.1007/s00468-001-0133-7.

Ellison J. C. & Stoddart D. R. 1991. Mangrove ecosystem collapse during predicted sea-level rise: Holocene analogues and implications. *Journal of Coastal research*, **7**(1):151-165.

Fan D., Shang S., Cai G., Tu J. 2015. Distinction and grain-size characteristics of intertidal heterolithic deposits in the middle Qiantang Estuary (East China Sea). *Geo-Marine Letters*, **35**(3): 161-174. https://doi.org/ 10.1007/s00367-015-0398-2.

Félix C. M. & Souza, P. A.de. 2012. Acritarcos (Grupo Acritarcha Evitt 1963): conceitos gerais, aplicações e importância na análise estratigráfica do intervalo Pennsilvaniano e Permiano da Bacia do Paraná. *Revista do Instituto Geológico*, **33**(1): 71-88. http://dx.doi.org/10.5935/0100-929X.20120005.

França M.C., Alves I.C.C., Castro D.F., Cohen M.C.L., Rossetti D.F., Pessenda L.C.R., Lorente F.L., Fontes N.A., Buso Junior, A.Á., Giannini P.C.F., Francisquini M.I. 2015. A multi-proxy evidence for the transition from estuarine mangroves to deltaic freshwater marshes, Southeastern Brazil, due to climatic and sea-level changes during the late Holocene. *Catena*, **128**: 155–166. https://doi.org/10.1016/j.catena.2015.02.005.

França M. C., Cohen M. C., Pessenda L. C., Rossetti D. F., Lorente F. L., Buso Junior, A. Á., Macario K., 2013. Mangrove vegetation changes on Holocene terraces of the Doce River, southeastern Brazil. *Catena*, **110**: 59-69 https://doi.org/10.1016/j.catena.2013.06.011.

França M. C., Pessenda L. C., Cohen M. C., Azevedo A. Q.de, Fontes N. A., Silva F. B., Macario K. 2019. Late-Holocene subtropical mangrove dynamics in response to climate change during the last millennium. *The Holocene*: **29**(3): 445-456. https://doi.org/10.1177/0959683618816438.

Freitas T. T.de, Giannini P. C. F., Angulo R. J., Souza M. C.de, Pessenda L. C. R., Spotorno-Oliveira P. 2020. Sea-level fall and coastal water cooling during the Late Holocene in Southeastern Brazil based on vermetid bioconstructions. *Marine Geology*, **428**: 106281. https://doi.org/10.1016/j.margeo.2020.106281.

Fontes N. A., Moraes C. A., Cohen M. C., Alves I. C. C., França M. C., Pessenda L. C., Mayle F. 2017. The impacts of the middle Holocene high sea-level stand and climatic changes on mangroves of the Jucuruçu River, southern Bahia–northeastern Brazil. *Radiocarbon*, **59**(1): 215-230. https://doi.org/10.1017/RDC.2017.6.

Garreaud R.D. & Battisti D.S. 1999. Interannual (ENSO) and interdecadal (ENSO-like) variability in the Southern Hemisphere tropospheric circulation. J. *Climate*, **2**: 2113–2123 https://doi.org/10.1175/1520-0442(1999)012<2113:IEAIEL>2.0.CO;2.

Gee C. T. 2001. The mangrove palm Nypa in the geologic past of the New World. *Wetlands Ecology and Management*, **9**(3): 181-203. https://doi.org/10.1023/A:1011148522181.

Gilman E.L., Ellison J., Duke N.C., Field C. 2008. Threats to mangroves from climate change and adaptation options: a review. *Aquat Bot* **89**:237–250. https://doi.org/10.1016/j.aquabot.2007.12.009.

González C., Urrego L.E., Martínez J.I. 2006 Late Quaternary vegetation and climate change in the Panama Basin: Palynological evidence from marine cores ODP 677B and TR 163-38. *Palaeogeography, Palaeoclimatology, Palaeoecology* **234**: 62–80. https://doi.org/10.1016/j.palaeo.2005.10.019.

Grace V. B., Mas-Pla J., Novais T. O., Sacchi E., Zuppi G. M. 2008. Hydrological mixing and geochemical processes characterization in an estuarine/mangrove system using environmental tracers in Babitonga Bay (Santa Catarina, Brazil). *Continental Shelf Research*, **28**(4-5): 682-695. https://doi.org/10.1016/j.csr.2007.12.006.

Graham R. W. & Grimm E. C. 1990. Effects of global climate change on the patterns of terrestrial biological communities. Trends in *Ecology & Evolution*, **5**(9): 289-292. https://doi.org/10.1016/0169-5347 (90)90083-P.

Grimm E. C. & Troostheide C. D. 1994. *Tilia 2.00, program for plotting palynological diagrams*. Springfield, Illinois State Museum.

Grimm E. C. 1987. CONISS: a FORTRAN 77 program for stratigraphically constrained cluster analysis by the method of incremental sum of squares. *Computers & geosciences*, **13**(1): 13-35. https://doi.org/10.1016/0098-3004(87)90022-7.

Haug G. H., Hughen K. A., Sigman D. M., Peterson L. C., Röhl U. 2001. Southward migration of the intertropical convergence zone through the Holocene. *Science*, **293**(5533): 1304-1308. https://: 10.1126/science.1059725.

Kennedy J. P., Pil M. W., Proffitt C. E., Boeger W. A., Stanford A. M., Devlin D. J. 2016 Postglacial expansion pathways of red mangrove, Rhizophora mangle, in the Caribbean Basin and Florida. American *Journal of Botany*, **103**(2): 260-276. https://doi:10.3732/ajb.1500183.

Korte A., Gasper A. L., Kruger A., Sevegnani L. 2013. Composição florística e estrutura das restingas de Santa Catarina. *Inventário florístico florestal de Santa Catarina*, **4**: 285-309.

Kullman L. 2001. 20th century climate warming and tree-limit rise in the southern Scandes of Sweden. Ambio: *A journal of the Human Environment*, **30**(2): 72-80. https://doi.org/10.1579/0044-7447-30.2.72.

Joo-Chang J. C., Islebe G. A., Torrescano-Valle N. 2015. Mangrove history during middle-and late-Holocene in Pacific south-eastern Mexico. *The Holocene*, **25**(4): 651-662. https://doi.org/10.1177/0959683614566217.

Lacerda L. D., Conde J. E., Kjerfve B., Alvarez-León R., Alarcón C., Polanía J. 2002. American mangroves. *In*: Lacerda L. D. *et al.* (ed.). *Mangrove ecosystems*. Berlin, Heidelberg, Springer, p. 1-62. https://10.1007/978-3-662-04713-2.

Ledru M.-P., Jomelli V., Bremond L., Cruz P., Ortuño T., Bentaleb I., Sylvestre F., Kuentz A., Beck S., Martin C., Paillès C., Subitani S. 2013. Evidence for moisture niches in the Bolivian Andes during the mid-Holocene arid period. *The Holocene* **23** (11): 1545–1557. https://doi.org/10.1177/0959683613496288.

Liu K. B., Lu H., Shen C. 2008. A 1200-year proxy record of hurricanes and fires from the Gulf of Mexico coast: Testing the hypothesis of hurricane–fire interactions. *Quaternary Research*, **69**(1): 29-41. https://doi.org/10.1016/j.yqres.2007.10.011.

Lorente F. L., Castro D. F., Francisquini M. I., Pessenda L. C. R., Fontes N. A., Cohen M. C. L., Macario K. 2020. An integrated analysis of palynofacies and diatoms in the Jucuruçu River valley, northeastern Brazil: Holocene paleoenvironmental changes. *Journal of South American Earth Sciences*, **103**:102731. https://doi.org/10.1016/j.jsames.2020.102731.

Lorente F. L., Bus Junior A. A., Oliveira P. E. de, Pessenda L. C. R. 2017. *Atlas palinológico*: Laboratório 14C. FEALQ.

Marengo J. A. & Camargo C. C. 2008. Surface air temperature trends in Southern Brazil for 1960–2002. *International Journal of Climatology*: *A Journal of the Royal Meteorological Society*, **28**(7): 893-904. https://10.1002/joc.1584.

Mazzer A. M. & Gonçalves M. L. 2012. Aspectos geomorfológicos da baía da Babitonga, Santa Catarina, Brasil: caracterização morfométrica. *Revista Brasileira de Geomorfologia*, **12**. https://10.20502/rbg.v12i0.264.

Metcalfe S. E., O'Hara S. L., Caballero M., Davies S. J. 2000. Records of Late Pleistocene–Holocene climatic change in Mexico - a review. *Quaternary Science Reviews*, **19**(7): 699-721. https://10.1016/S0277-3791(99)00022-0.

Meyers P. A. 1994. Preservation of elemental and isotopic source identification of sedimentary organic matter. *Chemical geology*, **114**(3-4): 289-302. https://doi.org/10.1016/0009-2541(94)90059-0.

Meyers P. A. 2003. Applications of organic geochemistry to paleolimnological reconstructions: a summary of examples from the Laurentian Great Lakes. *Organic geochemistry*, **34**(2): 261-289. https://doi.org/10.1016/S0146-6380(02)00168-7.

Miall A.D. 1978. Facies types and vertical profilemodels in braided river deposits: a summary. *In*: Miall A.D. (ed.). *Fluvial sedimentology*. Canadian Society of Petroleum Geologists, Calgary, p. 597–604.

Mueller A. D., Islebe G. A., Hillesheim M. B., Grzesik D. A., Anselmetti F. S., Ariztegui D., Venz K. A. 2009. Climate drying and associated forest decline in the lowlands of northern Guatemala during the late Holocene. *Quaternary Research*, **71**(2): 133-141. https://doi.org/10.1016/j.yqres.2008.10.002.

Munsell C. 2009. *Munsell soil color charts.* New revised edition. Macbeth Division of Kollmorgen Instruments, New Windsor.

Novello V. F., Cruz F. W., Karmann I., Burns S. J., Stríkis N. M., Vuille M., Barreto E. A. 2012. Multidecadal climate variability in Brazil's Nordeste during the last 3000 years based on speleothem isotope records. *Geophysical Research Letters*, **39**(23) https://doi.org/:10.1029/2012GL053936.

Oliveira V.F. 2005. *Influência do estresse hídrico e salino na germinação de propágulos de Avicennia schaueriana Stapf e Leechman ex Moldenke e Laguncularia racemosa (L.)* Gaertn. f. MS Dissertation, Programa de Pós-Graduação em Botânica, Instituto de Pesquisas Jardim Botânico do Rio de Janeiro (JBRJ), Rio de Janeiro, 92 p.

Osland M. J., Feher L. C., Griffith K. T., Cavanaugh K. C., Enwright N. M., Day R. H., Rogers K. 2017. Climatic controls on the global distribution, abundance, and species richness of mangrove forests. *Ecological Monographs*, **87**(2): 341-359. : https://doi.org/10.5066/F78C9TDM.

Osland M. J., Feher L. C., López-Portillo J., Day R. H., Suman D. O., Menéndez J. M. G., Rivera-Monroy V. H. 2018. Mangrove forests in a rapidly changing world: Global change impacts and conservation opportunities along the Gulf of Mexico coast. *Estuarine, Coastal and Shelf Science*, **214**: 120-140.https://doi.org/10.1016/j.ecss.2018.09.006.

Osland M. J., Day R. H., Hall C. T., Feher L. C., Armitage A. R., Cebrian J., Snyder C. M. 2020. Temperature thresholds for black mangrove (Avicennia germinans) freeze damage, mortality and recovery in North America: Refining tipping points for range expansion in a warming climate. *Journal of Ecology*, **108**(2): 654-665. https://doi.org/10.1111/1365-2745.13285.

Ogrinc N., Fontolan G., Faganeli J., Covelli S. 2005. Carbon and nitrogen isotope compositions of organic matter in coastal marine sediments (the Gulf of Trieste, N Adriatic Sea): indicators of sources and preservation. *Marine chemistry*, **95**(3-4): 163-181. https://doi.org/10.1016/j.marchem.2004.09.003.

Pecl G. T., Araújo M. B., Bell J. D., Blanchard J., Bonebrake T. C., Chen I.-C., Williams S. E. 2017. Biodiversity redistribution under climate change: Impacts on ecosystems and human well- being. *Science*, **355**, eaai9214. https://doi.org/10.1126/science.aai9214.

Pessenda L. C. R., Ribeiro, A.de Souza, Gouveia S. E. M., Aravena R., Boulet R., Bendassolli J. A. 2004. Vegetation dynamics during the late Pleistocene in the Barreirinhas region, Maranhão State, northeastern Brazil, based on carbon isotopes in soil organic matter. *Quaternary Research*, **62**(2): 183-193. https://doi.org/10.1016/j.yqres.2004.06.003.

Pessenda L. C. R., Vidotto E., Oliveira P. E.de, Buso Junior A. A., Cohen M. C. L., Rossetti D. de Fátima, Bendassolli J. A. 2012. Late Quaternary vegetation and coastal environmental changes at Ilha do Cardoso mangrove, southeastern Brazil. *Palaeogeography, Palaeoclimatology, Palaeoecology*, **363:** 57-68. http://dx.doi.org/10.1016/j.palaeo.2013.12.001.

Prado L. F., Wainer I., Chiessi C. M., Ledru M. P., Turcq B. 2013a. A mid-Holocene climate reconstruction for eastern South America. *Climate of the Past*, **9**(5): 2117-2133. https://doi.org/:10.5194/cp-9-2117-2013.

Quisthoudt K., Schmitz N., Randin C. F., Dahdouh-Guebas F., Robert E. M., Koedam N. 2012. Temperature variation among mangrove latitudinal range limits worldwide. *Trees*, **26**(6): 1919-1931. https://doi.org/10.1007/s00468-012-0760-1.

Reimer P. J. 2020. Composition and consequences of the IntCal20 radiocarbon calibration curve. *Quaternary Research*, **96**: 22-27. https://doi.org/10.1017/qua.2020.42.

Ribeiro S. R., Batista E. J. L., Cohen M. C., França M. C., Pessenda L. C., Fontes N. A., Bendassolli J. A. 2018. Allogenic and autogenic effects on mangrove dynamics from the Ceará Mirim River, north- eastern Brazil, during the middle and late Holocene.*Earth Surface Processes and Landforms*,**43**(8): 1622-1635. https://doi.org/10.1002/esp.4342.

Rodrigues E., Cohen M. C., Liu K. B., Pessenda L. C., Yao Q., Ryu J., Dietz M. 2021. The effect of global warming on the establishment of mangroves in coastal Louisiana during the Holocene. *Geomorphology*, **381**: 107648. https://doi.org/ 10.1016/j.geomorph.2021.107648.

Saintilan N., Khan N. S., Ashe E., Kelleway J. J., Rogers K., Woodroffe C. D., Horton B. P. 2020. Thresholds of mangrove survival under rapid sea level rise. *Science*, **368**(6495): 1118-1121. https://doi.org/10.1126/science.aba2656.

Sandoval-Castro E., Muñiz-Salazar R., Enríquez-Paredes L. M., Riosmena-Rodríguez R., Dodd R. S., Tovilla-Hernández C., Arredondo-García M. C. 2012. Genetic population structure of red mangrove (Rhizophora mangle L.) along the northwestern coast of Mexico.*Aquatic botany*, **99**: 20-26. https://doi.org/10.1016/j.aquabot.2012.01.002.

Sherrod C. L. & McMillan C. 1985. The distributional history and ecology of mangrove vegetation along the northern Gulf of Mexico coastal region. *Contrib. Mar. Sci*. : 129–140.

Silva S. M. & Britez R. M. 2005. A vegetação da planície costeira. *In:* Marques M. C. M., Britez R. M. de, Salino A. *História Natural e Conservação da Ilha do Mel*. Curitiba: Ed. UFPR, 49-84.

Smol J. P., Battarbee R. W., Davis R. B., Merilainen J. 1986. *Diatoms and lake acidity*. Holanda, [ETDEWeb].

Soares M. L. G., Estrada G. C. D., Fernandez V., Tognella M. M. P. 2012. Southern limit of the Western South Atlantic mangroves: Assessment of the potential effects of global warming from a biogeographical perspective. *Estuarine, Coastal and Shelf Science*, **101**: 44-53. https://doi.org/10.1016/j.ecss.2012.02.018.

Stevens P. W., Fox S. L., Montague C. L. 2006. The interplay between mangroves and saltmarshes at the transition between temperate and subtropical climate in Florida.*Wetlands Ecology and Management*, **14**(5): 435-444. https://doi.org/10.1007/s11273-006-0006-3.

Stuart S. A., Choat B., Martin K. C., Holbrook N. M., Ball M. C. 2007. The role of freezing in setting the latitudinal limits of mangrove forests. *New Phytologist*, **173**(3): 576-583. https://doi.org/10.1111/j.1469-8137.2006.01938.x.

Sukigara C. & Saino T. 2005. Temporal variations of δ13C and δ15N in organic particles collected by a sediment trap at a time-series station off the Tokyo Bay. *Continental Shelf Research*, **25**(14): 1749-1767. https://doi.org/10.1016/j.csr.2005.06.002.

Truccolo E. C. 1998. *Maré meteorológica e forçantes atmosféricas locais em São Francisco do Sul-SC*. MS Dissertation, Centro tecnológico, Universidade Federal de Santa Catarina, Florianópolis, xvi, 100 p.

USEPA. 1999. *Innovative technology verification report*: sediment sampling technology, aquatic research instruments russian peat borer. EPA/600/R-01/010. Washington, DC: Office of Research and Development.

Vermeulen S., Lepoint G., Gobert S. 2012. Processing samples of benthic marine diatoms from Mediterranean oligotrophic areas. *Journal of Applied Phycology*, **24**(5): 1253-1260. https://doi.org/10.1007/s10811-011-9770-4.

Vieira C. V., Horn Filho N. O., Bonetti C. V. D. H. C., Bonetti J. 2008. Caracterização morfosedimentar e setorização do complexo estuarino da Baía da Babitonga/SC. *Boletim Paranaense de Geociências*, **62**. http://dx.doi.org/10.5380/geo.v62i0.12783.

Vuille M., Burns S. J., Taylor B. L., Cruz F. W., Bird B. W., Abbott M. B., Novello V. F. 2012. A review of the South American monsoon history as recorded in stable isotopic proxies over the past two millennia. *Climate of the Past*, **8**(4): 1309-1321 https://doi.org/10.5194/cp-8-1309-2012.

Walther G. R., Post E., Convey P., Menzel A., Parmesan C., Beebee T. J., Bairlein F. 2002. Ecological responses to recent climate change. *Nature*, **416**(6879): 389-395. https://doi.org/10.1038/416389a.

Walker W. H., Meléndez- Fernández O. H., Nelson R. J., Reiter R. J. 2019. Global climate change and invariable photoperiods: A mismatch that jeopardizes animal fitness. *Ecology and Evolution*, **9**(17): 10044-10054. https://doi.org/10.1002/ece3.5537.

Wentworth C. K. 1922. A scale of grade and class terms for clastic sediments. *The journal of geology*, **30**(5): 377-392.

Westgate J. W., Gee C. T. 1990. Paleoecology of a middle Eocene mangrove biota (vertebrates, plants, and invertebrates) from southwest Texas. Palaeogeography, *Palaeoclimatology, Palaeoecology*, **78**(1-2): 163-177. https://doi.org/10.1016/0031-0182(90)90210-X.

Ximenes A. C., Ponsoni L., Lira C. F., Koedam N., Dahdouh-Guebas F. 2018. Does sea surface temperature contribute to determining range limits and expansion of mangroves in eastern South America (Brazil)? *Remote Sensing*, **10** (11): 1787. 7; https://doi.org/10.3390/rs1.

Yao Q., Liu K. B., Platt W. J., Rivera-Monroy V. H. 2015. Palynological reconstruction of environmental changes in coastal wetlands of the Florida Everglades since the mid-Holocene. *Quaternary Research*, **83**(3): 449-458. https://doi.org/10.1016/j.yqres.2015.03.005.

Yao Q. & Liu K. B. 2017. Dynamics of marsh-mangrove ecotone since the mid-Holocene: A palynological study of mangrove encroachment and sea level rise in the Shark River Estuary, Florida., *PloS one*, **12**(3): e0173670. https://doi.org/10.1371/journal.pone.0173670.

Ziffer-Berger J. 2008. *Vascular flora of the babitonga bay region (Santa Catarina, Brazil)*: diversity and origins. PhD Theses, Friedrich-Alexander-Universität Erlangen-Nürnberg (FAU), 215p.

Zular A. 2011. *Sedimentologia e cronologia por luminescência da Ilha de São Francisco do Sul (SC)*: considerações sobre a evolução holocênica de barreiras arenosas da costa sul e sudeste do Brasil. Dissertation, IGc, Universidade de São Paulo, São Paulo, 95p.

REFERÊNCIAS

Angulo RJ, Lessa GC, Souza MC de. 2006b. A critical review of mid- to late-Holocene Sea sevel fluctuations on the eastern Brazilian coastline. *Quaternary Science Reviews* **25**: 486–506. https://doi.org/10.1016/j.quascirev.2005.03.008.

Angulo R. J., Souza M. C.de, Lessa G. C. 2009. The Holocene barrier systems of Paranaguá and northern Santa Catarina coasts, southern Brazil. *In:* Dillenburg Sérgio R. & Hesp Patrick A. *Geology and geomorphology of Holocene Coastal Barriers of Brazil*. Berlin, Heidelberg. Springer, p. 135-176. https://doi.org/10.1007/978-3-540-44771-9_5.

Alvares C.A., Stape J.L., Sentelhas P.C., Gonçalves J.L.M., Sparovek G. 2013. Köppen's climate classification map for Brazil. *Meteorologische Zeitschrift*; **22**(6): 711-728. https://doi.org/10.1127/0941-2948/2013/0507.

Allen M. *et al*. 2018. Global warming of 1.5° C. An IPCC Special report on the impacts of global warming of 1.5° C above pre-industrial levels and related global greenhouse gas emission pathways, in the context of strengthening the global response to the threat of climate change, sustainable development, and efforts to eradicate poverty. *Sustainable Development, and Efforts to Eradicate Poverty*.

Alongi D. M. 2015. The impact of climate change on mangrove forests. *Current Climate Change Reports*, **1**(1): 30-39. https://doi.org/10.1007/s40641-015-0002-x.

Barker P. A., Pates J. M., Payne R. J., Healey R. M. 2005. Changing nutrient levels in Grasmere, English Lake District, during recent centuries. *Freshwater Biology*, **50**(12): 1971-1981. https://doi.org/10.1111/j.1365-2427.2005.01439.x.

Baker P.A. & Fritz S.C. 2015. Nature and causes of Quaternary climate variation of tropical South America. *Sci. Rev. Quat.* https://doi.org/10.1016/j.quascirev.2015.06.011.

Battarbee R. W. 1988. The use of diatom analysis in archaeology: a review. *Journal of Archaeological Science*, **15**(6): 621-644. https://doi.org/10.1016/0305-4403(88)90057-X.

Behling H., Pillar V. D., Orlóci L., Bauermann S. G. 2004. Late Quaternary Araucaria Forest, grassland (Campos), fire and climate dynamics, studied by high-resolution pollen, charcoal and multivariate analysis of the Cambará do Sul core in southern Brazil. *Palaeogeography, Palaeoclimatology, Palaeoecology*, **203**(3-4): 277-297.

Berner R. A. & Raiswell R. 1984. C/S method for distinguishing freshwater from marine sedimentary rocks. *Geology*, **12**(6): 365-368. https://doi.org/10.1130/0091-7613(1984)12<365:CMFDFF>2.0.CO;2.

Berger J. Z. 2008. Vascular Flora of the Babitonga Bay Region (Santa catarina, Brazil): Diversity and Origins. Universitat Erlangen- Nurnberg. 219p.

Boulet R., Pessenda L.C.R., Telles E.C.C., Melfi A.J. 1995. Une évaluation de la vitesse de l'accumulation superficielle de matière par la faune du sol à partir de la datation des charbons et de l'humine du sol. Exemple des latosols des versants du lac Campestre, Salitre, Minas Gerais, Brésil. *Comptes Rendus L'academie Des Sci*. Paris **320**: 287–294.

Blasco F., Saenger P., Janodet E. 1996. Mangroves as indicators of coastal change. *Catena*, **27**(3-4): 167-178. https://doi.org/10.1016/0341-8162(96)00013-6.

Blum M.D., Carter A.E., Zayac T., Goble R. 2002. Middle Holocene Sea-Level and Evolution of The Gulf of Mexico Coast (USA). J. *Coast. Res*. **36**: 65–80. https://doi.org/10.2112/1551-5036-36.sp1.65.

Bradley R.S. & Jones P.D. 1992. When was the "Little Ice Age"? *In:* Mikami T (ed). *Proceedings of the International Symposium on the "Little Ice Age" Climate*. Department of Geography, Tokyo Metropolitan University. p 1–4.

Camargo M. G. 1999. *SYSGRAN para Windows*: sistema de análises granulométricas. Pontal do Sul, 2.

Cohen M.C.L. & Lara J. 2003. Temporal changes of mangrove vegetation boundaries in Amazonia: application of GIS and remote sensing techniques. *Wetlands Ecologia and Management*, **11**(4): 223–231. https://doi.org/10.1023/A:1025007331075.

Cohen MCL, Behling H, Lara RJ 2005a. Amazonian mangrove dynamics during the last millennium: The relative sea-level and the Little Ice Age. *Rev Palaeobot Palynol* **136**: 93–108. https://doi.org/10.1016/j.revpalbo.2005.05.002.

Cohen M. C. L., Pessenda L. C. R., Behling H., Rossetti D.de Fátima, França M. C., Guimarães J. T. F., Smith C. B. 2012. Holocene palaeoenvironmental history of the Amazonian mangrove belt. *Quaternary Science Reviews*, **55**: 50-58. https://doi.org/ 10.1016/j.quascirev.2012.08.019.

Cohen M.C.L., França M.C., Rossetti D. de F., Pessenda L.C.R., Giannini P.C.F., Lorente F.L., Buso Junior A.Á., Castro D., Macario K. 2014. Landscape evolution during the late Quaternary at the Doce River mouth, Espírito Santo State, Southeastern Brazil. Palaeogeogr. *Palaeoclimatol. Palaeoecol*. **415**: 48–58. https://doi.org/10.1016/j.palaeo.2013.12.001.

Cohen M.C.L., Souza A. V. de, Rossetti D. de F., Pessenda L.C.R., França M.C. 2018. Decadal-scale dynamics of an Amazonian mangrove caused by climate and sea level changes: inferences from spatial-temporal analysis and Digital Elevation Models. *Earth Surf. Process. Landforms* **43**: 2876–2888.

Cohen M.C.L., Figueiredo B.L., Oliveira N.N. 2019. Impacts of Holocene and modern sea-level changes on estuarine mangroves from Northeastern Brazil. *Earth Surf Process Landforms* esp.4737. https://doi.org/10.1002/esp.4737.

Cohen M. C., Rodrigues E., Rocha D. O., Freitas J., Fontes N. A., Pessenda L. C., Bendassolli J. A. 2020. Southward migration of the austral limit of mangroves in South America. *Catena*, **195**: 104775.https://doi.org/10.1002/esp.4440.

Cohen M. C. L., Souza A. V.de, Liu K. B., Rodrigues E., Yao Q., Pessenda L. C. R., Dietz M. 2021. Effects of Beach Nourishment Project on Coastal Geomorphology and Mangrove Dynamics in Southern Louisiana, USA. *Remote Sensing*, **13**(14): 2688.

Colinvaux P., Oliveria P.E. de, Moreno P.J.E. 1999. *Amazon pollen manual and atlas*. Dordrecht, Harwood Academic Publishers, 332 p.

CPRM 2015. *Geologia e recursos minerais do Estado do Espírito Santo*: texto explicativo do mapa geológico e de recursos minerais. (orgs. Valter Salino Vieira, Ricardo Gallart de Menezes). Belo Horizonte. 294p.

Cunha S.R., Tognella-de-Rosa M.M.P., Costa C.S.B. 2006. Structure and litter production of mangrove forests under different tidal influences in Babitonga Bay, Santa Catarina, southern Brazil. *Journal of Coastal Research*, **39**: 1169–1174. https://www.researchgate.net/publication/264898049.

Debrot A. O., Veldhuizen A., Van Den Burg S. W., Klapwijk C. J., Islam M., Alam M., Poelman M. 2020. Non-Timber Forest Product Livelihood-Focused Interventions in Support of Mangrove Restoration: *A Call to Action. Forests*, **11**(11): 1224. https://doi.org/10.3390/f11111224.

Dietz M., Liu K., Bianchette T., Dietz M.E., Liu K., Bianchette T.A. 2018. Hurricanes as a Major Driver of Coastal Erosion in the Mississippi River Delta: A Multi-Decadal Analysis of Shoreline Retreat Rates at Bay Champagne, Louisiana (USA). *Water* **10**: 1480. https://doi.org/10.3390/w10101480.

Donoghue J.F. 2011. Sea level history of the northern Gulf of Mexico coast and sea level rise scenarios for the near future. *Climate Change* **107**: 17–33. https://doi.org/10.1007/s10584-011-0077-x.

Duke N., Ball M., Ellison J. 1998. Factors influencing biodiversity and distributional gradients in mangroves. *Global Ecology & Biogeography Letters*, **7**(1): 27-47.

Ellison J. C. 2008. Long-term retrospection on mangrove development using sediment cores and pollen analysis: a review. *Aquatic Botany*, **89**(2): https://doi.org/doi:10.1016/j.aquabot.2008.02.007.

Faegri K. & Iversen J. 1989. *Textbook of pollen analysis.* 4th ed. Chichester, John Wiley and Sons.

Félix C. M. & Souza P. A.de. 2012. Acritarcos (Grupo Acritarcha Evitt 1963): conceitos gerais, aplicações e importância na análise estratigráfica do intervalo Pennsilvaniano e Permiano da Bacia do Paraná. *Revista do Instituto Geológico*, **33**(1): 71-88. http://dx.doi.org/10.5935/0100-929X.20120005.

Fisk H. N.1944. *Geological investigation of the alluvial Valley of the Lower Mississippi River*. Vicksburg, Mississippi River Commission.

Fisk Harold N. 1952. *Geological investigation of the Atchafalaya basin and the problem of Mississippi River Diversion*. Vicksburg: Mississippi River Commission.

Field D. W. 1991. *Coastal wetlands of the United States*: an accounting of a valuable national resource. National Oceanic and Atmospheric Administration.

Fontes N. A., Moraes C. A., Cohen M. C., Alves I. C. C., França M. C., Pessenda L. C., Mayle F. 2017. The impacts of the middle Holocene high sea-level stand and climatic changes on mangroves of the Jucuruçu River, southern Bahia–northeastern Brazil.*Radiocarbon*, **59**(1): 215-230. https://doi.org/10.1017/RDC.2017.6.

França M. C., Cohen M. C., Pessenda L. C., Rossetti D. F., Lorente F. L., Buso Junior, A. Á., Macario K. 2013. Mangrove vegetation changes on Holocene terraces of the Doce River, southeastern Brazil. *Catena*, **110**: 59-69 https://doi.org/10.1016/j.catena.2013.06.011.

França M.C., Alves I.C.C., Castro D.F., Cohen M.C.L., Rossetti D.F., Pessenda L.C.R., Lorente F.L., Fontes N.A., Buso Junior A.A., Giannini P.C.F., Francisquini M.I. 2015. A multi-proxy evidence for the transition from estuarine mangroves to deltaic freshwater marshes, Southeastern Brazil, due to climatic and sea-level changes during the late Holocene. *Catena* **128**. https://doi.org/10.1016/j.catena.2015.02.005.

França M. C., Pessenda L. C., Cohen M. C., Azevedo A. Q.de, Fontes N. A., Silva F. B., Macario K. 2019. Late-Holocene subtropical mangrove dynamics in response to climate change during the last millennium. *The Holocene*: **29**(3): 445-456. https://doi.org/10.1177/0959683618816438.

Giannini P.C.F. 1993. *Sistemas deposicionais no Quaternário costeiro entre jaguaruna e Imbituba*. PhD Theses, Instituto de Geociências, Universidade de São Paulo, São Paulo. 278 p.

Gilman E., Ellison J., Coleman R. 2007. Assessment of Mangrove Response to Projected Relative Sea-Level Rise and Recent Historical Reconstruction of Shoreline Position. *Environ. Monit. Assess*. **124**: 105–130. https://doi.org/10.1007/s10661-006-9212-y.

Giri C., Ochieng E., Tieszen L.L., Zhu Z., Singh A., Loveland T., Masek J., Duke N. 2011. Status and distribution of mangrove forests of the world using earth observation satellite data. Glob. *Ecol. Biogeogr*., **20**: 154–159. https://doi.org/10.1111/j.1466-8238.2010.00584.x.

Gouveia S. & Pessenda L.C.R. 2000. Datation par le C-14 de charbons inclus dans le sol pour l'étude du rôle de la remontée biologique de matière et du colluvionnement dans la formation de latosols de l'état de São Paulo. Brésil, *Comptes Rendus de l'Académie des Sciences-Series IIA-Earth and Planetary Science*, **330** (2): 133–138.

Grinsted A., Moore J.C., Jevrejeva S. 2009. Reconstructing Sea level from paleo and projected temperatures 200 to 2100 AD. *Clim Dyn* **34**:461–472. https://doi.org/10.1007/s00382-008-0507-2.

Grimm E. C. & Troostheide C. D. 1994. *Tilia 2.00, program for plotting palynological diagrams*. Springfield, Illinois State Museum.

Grimm E. 1990. *Tilia and Tiliagraph*: PC spreadsheet and graphic software for pollen data, INQUA. Sub-Commission on Data-Handling Methods Newsletter.

Harding W. R., Archibald C. G. M., Taylor J. C. 2005. The relevance of diatoms for water quality assessment in South Africa: A position paper. *Water Sa*, **31**(1): 41-46.

Instituto Nacional de Metereologia (INMET). 2017. *Estação meteorológica de observação*. Disponível em: http://www.inmet.gov.br. Acesso em: 30.01.2020.

Johnson C.L., Chen Q., Ozdemir C.E. 2020. Lidar time-series analysis of a rapidly transgressing low-lying mainland barrier (Caminada Headlands, Louisiana, USA). *Geomorphology* **352**: 106979. https://doi.org/10.1016/j.geomorph.2019.106979.

Kilca R.V., Costa M.P., Zanini R.R., Carvalho F.A., Costa A. F. 2010. Estrutura de manguezais em diferentes estágios sucessionais no estuário do rio Piauí, Sergipe-Brasil. *Pesquisas, Sér.Botânica*, **61**:171-189.

Krauss K.W., From A.S., Doyle T.W., Doyle T.J., Barry M.J. 2011. Sea-level rise and landscape change influence mangrove encroachment onto marsh in the Ten Thousand Islands region of Florida, USA. *J. Coast. Conserv*. **15**: 629–638. https://doi.org/10.1007/s11852-011-0153-4

Korte A., Gasper A. L., Kruger A., Sevegnani L. 2013. Composição florística e estrutura das restingas de Santa Catarina. *Inventário florístico florestal de Santa Catarina*, **4**: 285-309.

Lacerda L. D. 1999. Os manguezais do Brasil. *In*: Vannucci M. (ed.). *Os manguezais e nós*: uma síntese de percepções. São Paulo, Ed USP, p.185-196.

Lean J. & Rind D. 1999. Evaluating sun-climate relationships since the Little Ice Ag. *Jounal Amospheric Solar-Terrestrial Phys* **61**:25–36.

Liu K-b. & Fearn M. L. 2000. Reconstruction of Prehistoric Landfall Frequencies of Catastrophic Hurricanes in Northwestern Florida from Lake Sediment Records. *Quat. Res*. 2000, **54**: 238−245.

Liu Z., Zhu J., Rosenthal Y., Zhang X., Otto-Bliesner B.L., Timmermann A., Smith R.S., Lohmann G., Zheng W., Timm O.E. 2014. The Holocene temperature conundrum. *Proc. Natl. Acad. Sci. U.S.A.*, **111**: E3501–E3505. https://doi.org/10.1073/pnas.1407229111.

Lorente F.L., Buso Junior A.A., Oliveira P.E., Pessenda L.C.R. 2017. *Atlas palinológico*: laboratório 14C - Cena-USP. Piracicaba-SP, FEALQ 2017. 333p.

Lorente F. L., Castro D. F., Francisquini M. I., Pessenda L. C. R., Fontes N. A., Cohen M. C. L., Macario K. 2020. An integrated analysis of palynofacies and diatoms in the Jucuruçu River valley, northeastern Brazil: Holocene paleoenvironmental changes. *Journal of South American Earth Sciences*, **103**: 102731. https://doi.org/10.1016/j.jsames.2020.102731.

Lloyd F.E. & Tracy S.M. 1901. The insular flora of Mississippi and Louisiana. Bull. Torrey Bot. Club 28, 61. https://doi.org/10.2307/2477884

Marengo J. A. 2006. *Mudanças climáticas globais e seus efeitos sobre a biodiversidade*; caracterização do clima atual e definição das alterações climáticas pata o território brasileiro ao longo do século 21.

Meyer R. R. & Turcan A. N. 1955. *Geology and ground water resources of the Baton Rouge area*, Louisiana. Washington, DC: US Government Printing Office, 138p.. https://doi.org/10.3133/wsp1296.

Meyers P. A. 1997. Organic geochemical proxies of paleoceanographic, paleolimnologic, and paleoclimatic processes. *Org. Geochem*. **27**: 213–250. https://doi.org/10.1016/S0146-6380 (97)00049-1

Miall A.D. 1978. Facies types and vertical profilemodels in braided river deposits: a summary. In: Miall A.D. (ed.). *Fluvial sedimentology*. Canadian Society of Petroleum Geologists, Calgary, p. 597–604.

Miranda L.B, Castro B.M. Kjerfve B. 2002. *Princípios de oceanografia física de estuários*. São Paulo, EDUSP, 424 p. (v. 42).

Munsell C. 2009. *Munsell soil color charts.* New revised edition. Macbeth Division of Kollmorgen Instruments, New Windsor.

McCarthy M. C., Gottlieb C. A., Thaddeus P., Horn M., Botschwina P. 1995. Structure of the CCCN and CCCCH radicals: Isotopic substitution and ab initio theory. *The Journal of chemical physics*, **103** (18): 7820-7827.

McKee K. L., Cahoon D. R., Feller I. C. 2007. Caribbean mangroves adjust to rising sea level through biotic controls on change in soil elevation. *Global Ecology and Biogeography*, **16(**5): 545-556. https://doi.org/10.1111/j.1466-8238.2007. 00317.x.

McKee K. L. & Vervaeke W. C. 2018. Will fluctuations in salt marsh–mangrove dominance alters vulnerability of a subtropical wetland to sea- level rise? *Global Change Biology*, **24**(3): 1224-1238. https://doi.org/10.1111/gcb.13945.

Nordt L. C., Boutton T. W., Jacob J. S., Mandel R. D. 2002. C4 plant productivity and climate-CO2 variations in south-central Texas during the late Quaternary. *Quaternary Research*, **58**(2): 182-188. https://doi.org/10.1006/qres.2002.2344.

Oppenheimer M., Glavovic B., Hinkel J., van de Wal R., Magnan A.K., AbdElgawad A., Cai R., Cifuentes-Jara M., DeConto R.M., Ghosh T., Hay J., Isla F., Marzeion B., Meyssignac B., Sebesvari Z. 2019. Sea level rise and implications for low-lying islands, coasts and communities. *In*: Pörtner H.O., Roberts D.C., Masson-Delmotte V., Zhai P., Tignor M., Poloczanska E., Mintenbeck K., Alegría A., Nicolai M., Okem A., Petzold J., Rama B., Weyer N.M. (eds). *IPCC Special report on the ocean and cryosphere in a changing climate*. https://www.ipcc.ch/site/assets/uploads/sites/3/2019/11/08_SROCC_Ch04_FINAL.pdf.

Osland M. J., Day R. H., Hal, C. T., Brumfield M. D., Dugas J. L., Jones W. R. 2017. Mangrove expansion and contraction at a poleward range limit: climate extremes and land-ocean temperature gradients. *Ecology*, **98**(1): 125-137. https://doi.org/10.1002/ecy.1625.

Peixoto A.L. & Gentry A. 1990. Diversidade e composição florística da mata de tabuleiros na Reserva Florestal de Linhares (Espírito Santo, Brasil). *Revista Brasileira de Botânica*, **13**: 19 25.

Perry C. L. & Mendelssohn I. A. 2009. Ecosystem effects of expanding populations of Avicennia germinans in a Louisiana salt marsh. *Wetlands*, **29**(1): 396-406.

Pessenda L.C.R., Gouveia S.E.M., Ribeiro A.de S. 2010. Late Pleistocene and Holocene vegetation changes in northeastern Brazil determined from carbon isotopes and charcoal records in soils. *Palaeogeogr Palaeoclimatol Palaeoecol* **297**:597–608. https://doi.org/10.1016/j.palaeo.2010.09.008

Pessenda L.C.R., Vidotto E., Oliveira P.E.de, Buso Junior A.A., Cohen M.C.L., Rossetti D. de F., Ricardi-Branco F., Bendassolli J.A., 2012. Late Quaternary vegetation and coastal environmental changes at Ilha do Cardoso mangrove, southeastern Brazil. Palaeogeogr. *Palaeoclimatol. Palaeoecol*., **363**:57–68.

Piotrowska N., Blaauw M., Mauquoy D., Chambers F.M. 2010a. Constructing deposition chronologies for peat deposits using radiocarbon dating. *Mires Peat* **7**: 1–14.

Quisthoudt K., Schmitz N., Randin C.F., Dahdouh-Guebas F., Robert E.M.R., Koedam N. 2012. Temperature variation among mangrove latitudinal range limits worldwide. *Trees Struct. Funct*. **26**: 1919–1931. https://doi.org/10.1007/s00468-012-0760-1.

Ribeiro S. R., Batista E. J. L., Cohen M. C., França M. C., Pessenda L. C., Fontes N. A., Bendassolli J. A. 2018. Allogenic and autogenic effects on mangrove dynamics from the Ceará Mirim River, north-eastern Brazil, during the middle and late Holocene.*Earth Surface Processes and Landforms*, **43** (8): 1622-1635. https://doi.org/10.1002/esp.4342.

Ritchie W. & Penland S. 1988a. Cyclical changes in the coastal dunes of southern Louisiana. *Journal of Coastal Research*, (3): 111-114.

Rodrigues E., Cohen M. C., Liu K. B., Pessenda L. C., Yao Q., Ryu J., Dietz M. 2021. The effect of global warming on the establishment of mangroves in coastal Louisiana during the Holocene. *Geomorphology*, **381** (80):107648. https://doi.org/10.1016/j.geomorph.2021.107648.

Roubik D.W. & Moreno J.E. 1991. *Pollen and Spores of Barro Colorado Island*. Missouri Botanical Garden.

Sandoval-Castro E., Muñiz-Salazar R., Enríquez-Paredes L. M., Riosmena-Rodríguez R., Dodd R. S., Tovilla-Hernández C., Arredondo-García M. C. 2012. Genetic population structure of red mangrove (Rhizophora mangle L.) along the northwestern coast of Mexico. *Aquatic botany*, **99**: 20-26. https://doi.org/10.1016/j.aquabot.2012.01.002.

Santa Catarina 1986. *Atlas de Santa Catarina*. Santa Catarina, 173 p.

Soares M.L.G., Estrada G.C.D., Fernandez V., Tognella M.M.P. 2012. Southern limit of the Western South Atlantic mangroves: assessment of the potential effects of global warming from a biogeographical perspective. *Estuarine Coastal and Shelf Science*, **101** (10):44–53. doi.org/10.1016/j.ecss.2012.02.018

Shepherd A., Ivins E., Rignot E., Smith B., Van Den Broeke M., Velicogna I. 2019. Mass balance of the Greenland ice sheet from 1992 to 2018. *Nature*, **558**: 219–222. https://doi.org/10.1038/s41586-019-1855-2.

Sherrod C.L. & McMillan C. 1985. The distributional history and ecology of mangrove vegetation along the northern Gulf of Mexico coastal region. *Contrib. Mar. Sci*.: 129–140.

Snyder C. M., Feher L. C., Osland M. J., Miller C. J., Hughes A. R., Cummins K. L. 2021. The Distribution and Structure of Mangroves (Avicennia germinans and Rhizophora mangle) Near a Rapidly Changing Range Limit in the Northeastern Gulf of Mexico. *Estuaries and Coasts*, : 1-15.

Suguio K., Barreto A.M.F., Oliveira P.E., Bezerra F.H.R., Vilela M.C.S.H. 2013. Indicators of Holocene Sea level changes along the coast of the states of Pernambuco and Paraíba, Brazil. *Geol.* Série Científica USP, **13**: 141–152. https://doi.org/10.5327/Z1519-874X201300040008.

Taillardat P., Willemsen P., Marchand C., Friess D.A., David FW., Baudron P., Truong V.V., Nguyen T-N, Ziegler A.D. 2018. Assessing the contribution of porewater discharge in carbon export and CO2 evasion in a mangrove tidal creek (Can Gio, Vietnam). *J. Hydrol*., **563**:303– 318. https://doi.org/10.1038/20335.

Tomlinson P.B. (ed.). 1986. The botany of mangroves. Cambridge University Press, Cambridge, United Kingdom, 413 p.

Toomey III R. S., Blum M. D., Valastro Junior S. 1993. Late Quaternary climates and environments of the Edwards Plateau, Texas. *Global and planetary change*, **7** (4): 299-320. https://doi.org/10.1016/0921-8181(93)90003-7.

Toniolo, T. de F., Giannini, P.C.F., Angulo, R.J., de Souza, M.C., Pessenda, L.C.R., Spotorno-Oliveira, P., 2020. Sea-level fall and coastal water-cooling during the Late Holocene in Southeastern Brazil based on vermetid bioconstructions. *Mar. Geol*. **428**. https://doi.org/10.1016/j.margeo.2020.106281.

Tomaziello A.C.N., Carvalho L.M.V., Gandu A.W. 2016. Intraseasonal variability of the Atlantic Intertropical Convergence Zone during austral summer and winter. *Clim Dyn* **47**:1717–1733. https://doi.org/10.1007/s00382-015-2929-y

Tremarin P. I., Ludwig T. A. V., Moreira Filho H. 2008. Thalassiosirales (Diatomeae) do rio Guaraguaçu, Bacia Litorânea, PR, Brasil. *Acta Botanica Brasilica*, **22** (4): 1101-1113. 10.1590/S0102-33062008000400021.

Van der Hammen, T. & Absy M. L. 1994. Amazonia during the last glacial. *Palaeogeography, palaeoclimatology, palaeoecology*, **109** (2-4): 247-261. https://doi.org/10.1016/0031-0182(94)90178-3.

Van Soelen E. E., Lammertsma E. I., Cremer H., Donders T. H., Sangiorgi F., Brooks G. R., Reichart G. J. 2010 Late Holocene sea-level rise in Tampa Bay: Integrated reconstruction using biomarkers, pollen, organic-walled dinoflagellate cysts, and diatoms. *Estuarine, Coastal and Shelf Science*, **86** (2): 216-224. https://doi.org/10.1016/j.ecss.2009.11.010.

Vale C.C. & Ferreira R.D. 1998. Os manguezais do litoral do Estado do Espírito Santo. *In*: Simpósio de Ecossistemas da Costa Brasileira, São Paulo, ACIESP, *Anais*[...] v. 1, p. 88-94.

Walker W. H., Meléndez-Fernández O. H., Nelson R. J., Reiter R. J. 2019. Global climate change and invariable photoperiods: A mismatch that jeopardizes animal fitness. *Ecology and Evolution*, **9** (17): 10044-10054. https://doi.org/10.1002/ece3.5537.

Wentworth C. K. 1922. A scale of grade and class terms for clastic sediments. *The Journal of Geology*, **30** (5): 377-392.

Woodroffe C.D., Grindrod J. 1991. Mangrove biogeography: the role of Quaternary environmental and Sea-Level Change. *J. Biogeogr*., **18**: 479–492. https://doi.org/10.2307/2845685.

Yao Q. & Liu Kam-Biu. 2017. Dynamics of marsh-mangrove ecotone since the mid-Holocene: a palynological study of mangrove encroachment and sea level rise in the Shark River Estuary, Florida., *PloS one*, **12** (3): e0173670. https://doi.org/10.1371/journal.pone.0173670.

Yao Q., Liu Kam-Biu, Aragón-Moreno A.A., Rodrigues E., Xu Y.J., Lam N.S. 2020. A 5200-year paleoecological and geochemical record of coastal environmental changes and shoreline fluctuations in southwestern Louisiana: implications for coastal sustainability. *Geomorphology* **365,** 107284. https://doi.org/10.1016/j.geomorph.2020.107284.

Yao Q., Liu Kam-Biu, Platt W.J., Rivera-Monroy V.H. 2015a. Palynological reconstruction of environmental changes in coastal wetlands of the Florida Everglades since the mid-Holocene. *Quat. Res.* (United States) **83:** 449–458. https://doi.org/10.1016/j.yqres.2015.03.005.

Zimmerman R. J., Wetzel R. G., Siemann E. H., Reed J. B., Miller R. L., Harwell M. A., Twilley R. B. 2001. *Confronting climate change in the Gulf region*: prospects for sustaining our ecological heritage. Union of Concerned Scientists: https://hdl.handle.net/1911/21940.

Zalasiewicz J., Waters C.N., Williams M., Summerhayes C. 2018. *The Anthropocene as a Geological Time Unit:* a guide to the scientific evidence and current debate. Cambridge, Cambridge University Press.

UNIVERSIDADE FEDERAL DO PARÁ
INSTITUTO DE GEOCIÊNCIAS
PROGRAMA DE PÓS-GRADUAÇÃO EM GEOLOGIA E GEOQUÍMICA

PARECER

Sobre a Defesa Pública da Tese de Doutorado de ÉRIKA DO SOCORRO FERREIRA RODRIGUES

A banca examinadora da Tese de Doutorado de **ÉRIKA DO SOCORRO FERREIRA RODRIGUES** orientanda do Prof. Dr. **Marcelo Cancela Lisboa** (**UFPA**), composta pelos professores doutores Nils Edvin Asp Neto (**Membro-UFPA**), **Paulo Eduardo de Oliveira** (**Membro-USP**), **Paulo César Fonseca Giannini** (**Membro-USP**), e **José Augusto Martins Corrêa** (**Membro-UFPA**), após apresentação da sua tese intitulada "**EFEITOS DAS MUDANÇAS CLIMÁTICAS NOS LIMITES AUSTRAL E BOREAL DOS MANGUEZAIS AMERICANOS DURANTE O HOLOCENO E ANTROPOCENO**", emite o seguinte parecer:

A candidata realizou sua apresentação de forma clara, bem organizada e segura no tempo estipulado. Na arguição mostrou domínio da temática abordada e respondeu às perguntas formuladas pela banca. O trabalho escrito foi apresentado na forma de cinco artigos, sendo um já publicado, um aceito e dois submetidos a periódicos de impacto internacional, sendo que o quinto artigo ainda não foi submetido. Dessa forma, todos os artigos atendem às exigências básicas para uma tese de doutorado.

Finalmente, a banca examinadora decidiu por unanimidade aprovar a tese de doutorado.

Belém, 08 de outubro de 2021.

Prof. Dr. Marcelo Cancela Lisboa (Orientador – UFPA)

Prof. Dr. Paulo Eduardo de Oliveira (Membro - USP)

Prof. Dr. Paulo César Fonseca Giannini (Membro - USP)

Prof. Dr. José Augusto Martins Corrêa (Membro - UFPA)

Prof. Dr. Nils Edvin Asp Neto (Membro – UFPA)